TESIS DE DOCTORADO

Novel approaches in local drug delivery systems for the treatment of Inflammatory Bowel Disease

Iria Seoane Viaño

ESCUELA DE DOCTORADO INTERNACIONAL
EN CIENCIAS DE LA SALUD DE LA USC

PROGRAMA DE DOCTORADO
EN INVESTIGACIÓN Y DESARROLLO DE MEDICAMENTOS

SANTIAGO DE COMPOSTELA

AÑO 2020

DECLARACIÓN DEL AUTOR DE LA TESIS

Novel approaches in local drug delivery systems for the treatment of Inflammatory Bowel Disease

Dña. Iria Seoane Viaño

Presento mi tesis, siguiendo el procedimiento adecuado al Reglamento, y declaro que:

1) *La tesis abarca los resultados de la elaboración de mi trabajo.*
2) *En su caso, en la tesis se hace referencia a las colaboraciones que tuvo este trabajo.*
3) *La tesis es la versión definitiva presentada para su defensa y coincide con la versión enviada en formato electrónico.*
4) *Confirmo que la tesis no incurre en ningún tipo de plagio de otros autores ni de trabajos presentados por mí para la obtención de otros títulos.*

En Santiago de Compostela, 25 de abril de 2020

Fdo………..

AUTORIZACIÓN DEL DIRECTOR / TUTOR DE LA TESIS

Novel approaches in local drug delivery systems for the treatment of Inflammatory Bowel Disease

D. Francisco Javier Otero Espinar

Dña. Asteria María Luzardo Álvarez

INFORMAN:

*Que la presente tesis, corresponde con el trabajo realizado por Dña. **Iria Seoane Viaño**, bajo mi dirección, y autorizo su presentación, considerando que reúne los requisitos exigidos en el Reglamento de Estudios de Doctorado de la USC, y que como director de ésta no incurre en las causas de abstención establecidas en Ley 40/2015.*

En Santiago de Compostela, 25 de abril de 2020

Fdo...   Fdo...

AGRADECEMENTOS

En primeiro lugar, quero agradecerlles aos meus directores de tese Dona Asteria Luzardo Álvarez e Don Francisco J. Otero Espinar o apoio e consellos recibidos durante estes anos, e especialmente pola confianza que depositaron en min dende un primeiro momento, brindándome a oportunidade de realizar a miña tese baixo a súa tutela. Non me esquezo tampouco dos grandes consellos de Don José Blanco Méndez, sempre disposto a compartir a súa experiencia e sabiduría connosco. O bo ambiente de grupo creado por eles, sen perder o bo humor nin nos momentos difíciles fixo que esta carrerira de fondo se convertise nun paseo.

En segundo lugar, gustaríame mostrarlle o meu agradecemento aos doutores Pablo Aguiar Fernández e Anxo Fernández Ferreiro por brindarme a oportunidade de realizar parte da miña tese en colaboración co grupo de imaxen molecular do IDIS. Durante as miñas estadías no servizo de medicina nuclear non só adquirín coñecementos, senón que tamén traballei nun grupo multidisciplinar cuns investigadores que se convertiron en amigos. Entre eles están Manuel, compañeiro infatigable de adestramentos de natación, David, sempre disposto a perder ao pádel, aínda que el diga que non, e especialmente Noemí, a miña compañeira de experimentos por excelencia e unha desas persoas que agradeces que se cruzasen na túa vida, sempre disposta a axudar cun sorriso na cara. Estou segura de que grazas a ela, estes anos, e especialmente as interminables horas de estudos no PET, fixéronse moito mais levadeiros.

Un especial agradecemento é o que lle debo ao doutor Álvaro Goyanes Goyanes por introducirme no mundo da impresión 3D e por compartir parte dos seus coñecementos conmigo. De igual maneira, quero agradecerlle os seus múltiples consellos e a súa infinita axuda nas distintas etapas dos proxectos que levamos a cabo. O entusiasmo que demostra polo seu traballo é contaxioso, o cal contribuíu sen dúbida a aumentar a miña ilusion de cara á investigación.

Non me podo esquecer da miña estancia no grupo de investigación do Inserm U1008 de Lille onde fun acollida como unha mais do grupo polos profesores Jurgen e Florence Siepmann, e onde tiven a oportunidade de traballar con persoas como Céline, Jeremy e Fabiana. Aínda que con esta última só coincidín brevemente, conseguíu que ese último mes de estancia fose o mellor.

E como non, unha mención especial merecen os meus pesados compañeiros de laboratorio, Carlos, Xurxo, Víctor, Victoria, Rubén, Guillermo, Elena, Andrea C. e Andrea L., polas innumerables horas compartidas dentro e fora do laboratorio non exentas de anécdotas, disputas e moitas gargalladas, pero sempre formando un grupo unido nun espazo moi reducido. Esta mesma mención especial tamén vai dirixida ao meu homólogo Iván, que a pesar de estar lonxe, sempre estivo disposto a compatir as súas perlas de sabiduría comigo durante todos estes anos. Así mesmo, quero agradecerlles aos nosos compañeiros do grupo I+D Farma os bos momentos que pasamos todos xuntos, así como a tódalas persoas que pasaron polo noso laboratorio e contribuiron na súa maneira a facer destes anos unha etapa para o recordo.

Finalmente, quero agradecerlle a miña familia a confianza e o apoio recibido durante esta etapa, especialmente o económico, así como aos meus amigos e amigas que me acompañaron

durante este periodo. Sería imposible citalos a todos, pero eles e elas saben quenes son; moitos os coñezo da miña etapa de natación, pero os cales tamén os atopei noutros ámbitos, como as miñas amigas da facultade e a miña veciña, e que, dalgunha forma, sempre estiveron ahí.

A todos, grazas.

Objectives

OBJECTIVES

Inflammatory bowel disease (IBD) is the term used to describe a group of chronic relapsing inflammatory diseases of the gastrointestinal (GI) tract, which encompasses two major phenotypes: Crohn´s disease (CD) and ulcerative colitis (UC). IBD is an idiopathic disease caused by an interplay of dysregulated immune responses to luminal microflora that together with environmental and genetic risk factors can trigger the onset of the illness in genetically predisposed individuals (1).

This multifactorial nature of IBD requires the development of animal models to shed light on the pathogenic mechanisms of the disease. Although these experimental animal models only partially reflect the complexity of the human disease, they allow us to control and define each interaction implicated in the pathogenesis of the illness. Moreover, the *in vivo* assessment of the safety and efficacy of novel therapeutic agents and treatments is a crucial step in the preclinical drug development pipeline, where animal models are essential to bridge the translational gap between preclinical and clinical research (2).

To accurately characterize IBD experimental models and assess the therapeutic activity of new drugs, imaging techniques commonly used in the clinical practice, can also be applied in preclinical studies. In particular, molecular imaging is especially promising in the characterization and quantification of biological processes at the cellular level detecting molecular alterations in living subjects, not limiting the investigations to the macroscopic field as it happens with diagnostic imaging (3).

To date, there is no curative therapy for IBD, so patients require life-long medications that can lead to frequent dosing, loss of response and severe side effects that can negatively affect patients' adherence to medication (4). Therefore, the discovery of new therapeutic agents to be added to the therapeutic arsenal, as well as the improvement of current treatments is still needed.

The aim of this thesis is the investigation of new therapeutic alternatives for the treatment of IBD. To achieve this aim the following specific objectives were envisaged:

1. To validate an experimental rat model of chemically-induced IBD described in the literature by the use of preclinical PET/CT (Positron emission tomography/computerized tomography) imaging technique (Chapter 1).

2. To assess the potential therapeutic activity of two antioxidant compounds, melatonin and resveratrol, in the previously validated animal model of IBD using preclinical PET/CT imaging technique (Chapter 2).

3. To explore the feasibility of preparing lipid-based suppositories loaded with tacrolimus using semisolid extrusion 3-dimensional printing (3DP) and subsequently characterize them in terms of printability, morphology, release profiles and self-emulsifying properties, among others (Chapter 3).

4. To combine preclinical PET/CT imaging with semisolid extrusion 3DP to prepare small suppositories loaded with tacrolimus and evaluate the feasibility of this approach to treat experimental IBD in the previously validated animal model (Chapter 4).

Introduction

INTRODUCTION

1.1. THE HUMAN GASTROINTESTINAL TRACT

The digestive system is composed by the organs of the gastrointestinal (GI) tract and accessory structures. The GI tract is a tubular-shaped organ that extends from the mouth to the anus. Most of foods and medicines are made up of molecules that are too large to be used by cells. Therefore, they must be broken down into smaller molecules in order to enter into cells. This process is known as digestion and the organs involved in it form the digestive system.

1.1.1. Anatomy of the Gastrointestinal Tract

The GI tract includes the mouth, the pharynx, the esophagus, the stomach, the small intestine, the large intestine, the rectum and the anus. The accessory digestive organs aids in the breakdown of food. The teeth and tongue begin mechanical digestion whereas the salivary glands begin chemical digestion. Liver, gallbladder and pancreas release secretions, such as bile and enzymes, which continue the digestion process (5) (Figure 1).

The **pharynx** is a funnel-shaped tube that extends from the choanae or posterior nasal apertures to the cricoid cartilage, where the pharynx continues as the esophagus. The pharynx is made up of skeletal muscle lined with a mucous membrane and comprises three parts: the nasopharynx, oropharynx and laryngopharynx. The nasopharynx is involved only in breathing, but the oropharynx and laryngopharynx have both digestive and respiratory functions (6).

The **esophagus** is a collapsible muscular tube located behind the trachea that serves as a passage between the pharynx and the upper stomach. The esophagus is divided into three regions: cervical esophagus, thoracic esophagus and abdominal esophagus (7).

The **stomach** is responsible for mechanical and enzymatic digestion of food. It is divided in four main parts: the cardia, fundus, body and pylorus. The cardia is the most proximal part and is histologically similar to the pylorus. Both parts protect the esophagus and the duodenum from the acid enzymes secreted in the stomach (7). The fundus is the rounded portion superior to and left of the cardias and the body is the large central portion inferior to the fundus. The pylorus is the most distal part and is divided in three parts. The first is the pyloric antrum, which is connected to the body of the stomach. The second is the pyloric canal, which is the narrower end that connects to the duodenum. Finally, the third part is the pyloric sphincter, which is a band of smooth muscle located at the latter point of connection with the duodenum that controls stomach emptying. Moreover, the long and convex border of

the stomach is called the greater curvature and the shorter and concave border is called the lesser curvature (8).

The **small intestine** is a long tubular organ where the most important processes of digestion and absorption occur. Its length provides a large area for nutrient absorption, which is further increased by the presence of circular folds, villi and microvilli (8). The small bowel is divided into three major sections: duodenum, jejunum and ileum. The duodenum is mostly retroperitoneal, whereas the jejunum and the ileum are intraperitoneal. The jejunum is formed by the proximal third of the intraperitoneal small intestine and narrows into the ileum. The ileum consists of the two distal thirds of the intraperitoneal small intestine and joins the large intestine at the ileocecal valve (7).

The **large intestine** extends from the ileum to the anus. It is attached to the posterior abdominal wall by a fold of peritoneum called mesocolon. The four main regions of the large intestine are the cecum, colon, rectum and anal canal. The cecum lies bellow the ileocecal valve in the right iliac fossa, and it is attached to the vermiform appendix, a worm-shaped blind tube that hangs down from the end of the cecum (9). The colon extends superiorly from the cecum and consists of the ascending, transverse, descending and sigmoid colon. The ascending and descending segments are retroperitoneal while the transverse and sigmoid segments are intraperitoneal (10).

The **rectum** is the final portion of the large intestine and extends from the sigmoid colon to the anal canal. It has three transverse folds called rectal valves. The last 2 or 3 cm of the rectum form the **anal canal**, which has two sphincters: an involuntary internal anal sphincter composed of smooth muscle and a voluntary external anal sphincter composed of skeletal muscle (8).
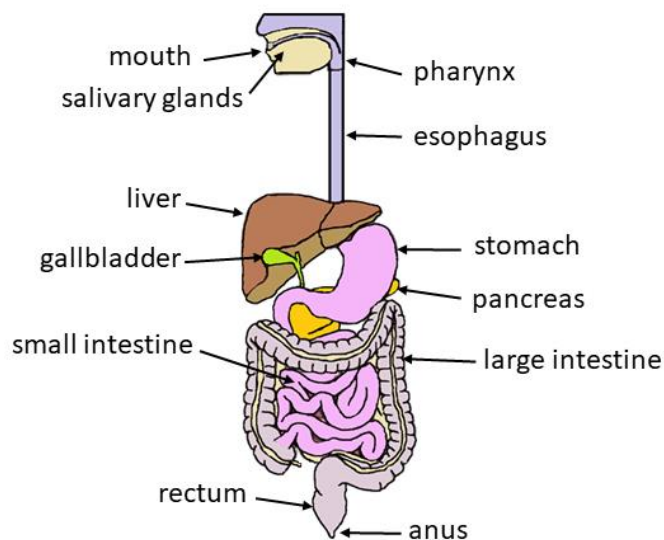
Figure 1. Squematic representation of the human gastrointestinal tract.

1.1.2. Histology of the Gastrointestinal Tract

From a histological point of view, throughout its length, the GI tract is composed of the same four tissue layers. Starting from the lumen and moving outwards, it can be distinguished the mucosa, submucosa, muscularis and serosa (5) (Figure 2).

1.1.2.1. Mucosa

The mucosa is the inner layer of the GI tract and consists of three concentric layers. From the lumen outward, these layers are: 1) an epithelial lining in direct contact with the luminal content; 2) an underlying connective tissue known as lamina propria; 3) a thin layer of smooth muscle cells known as muscularis mucosae, which separates the mucosa from the submucosa (5).

The **epithelium** of the esophagus is mainly constituted by nonkeratinized stratified squamous epithelium that has a protective function. The stomach, small intestine and colon have simple columnar epithelium that contains several cell types with secretion and absorption functions. Mucous secretory cells can be found as sheets of cells in the stomach and as Goblet cells in the small intestine and colon. Absorptive cells are also found in the small intestine and colon and take up metabolites, electrolytes and water. Enteroendocrine cells are present from the stomach to the rectum and secrete multiple regulatory factors, such as peptide hormones, which regulate digestive functions. Moreover, the epithelium of the GI tract is a regularly replicating tissue, with a renewal rate of epithelial cells between 5 and 7 days (11).

The **lamina propria** is connective tissue that consists of an abundant network of type I collagen fibers. In deeper layers, collagen type III and elastic fibers are also present. The lamina propria also contains blood capillaries and lymphatic vessels that allow the passage of absorbed nutrients to other tissues. This tissue includes mucosa-associated lymphoid tissue (MALT), which contains cells of the immune system that initiates immune responses to specific antigens encountered along mucosal surfaces (12).

The **muscularis mucosae** is a layer of smooth muscle fibers that fold the epithelium into finger-like projections or villi, which maximize the surface area of digestion and absorption. The movements of this layer ensure that all absorptive cells are exposed to the contents of the GI tract (13).

1.1.2.2. Submucosa

The submucosa is a layer of areolar connective tissue that binds the mucosa to the muscularis and contains blood and lymphatic vessels. In this layer there is also a neural network known as submucosal (Meissner's) nerve plexus (14).

1.1.2.3.Muscularis

The muscularis layer of the mouth, pharynx and esophagus contains skeletal muscle that allows voluntary swallowing. In the other parts of the GI tract, the muscularis consists of smooth muscle divided in an outer sheet of longitudinal fibers and an inner sheet of circular fibers. The involuntary contractions of smooth muscle help break down food and propel it along the GI tract. Between the layers of the muscularis is the myenteric (Auerbach's) nerve plexus (15).

1.1.2.4.Serosa

The serosa is the outer layer of the GI tract and is formed by mesothelium (simple squamous epithelium) and areolar connective tissue. In the esophagus, instead of serosa there is a single layer of areolar tissue called adventitia, which forms the superficial layer. The serosa helps to hold the organs of GI tract in place and reduce the frictional forces when the walls of the GI tract move. The serous layer that covers the viscera and other intraabdominal structures is known as the visceral peritoneum, while the parietal peritoneum lines the abdominal cavity. Between these two layers is the peritoneal cavity, which contains a serous fluid that prevents friction between the abdominal structures (16).

The double layer of peritoneum that surrounds a segment or a complete abdominal viscera and fixes it to the abdominal wall is known as mesentery. It contains nerves, blood and lymphatic vessels distributed throughout the intestinal wall. The omentum is a double-fold peritoneum that extends from the stomach to another organ. The lesser omentum attaches the stomach to the liver, while the greater omentum connects the stomach to the transverse colon. Moreover, the greater omentum moves in the peritoneal cavity with the peristaltic movements of the intestines. It can form adhesions (bands of fibrous scar tissue) adjacent to an inflamed organ to contain the infection and prevent its spread. The various amount of fat deposited in the greater omentum serve as a layer of insulation that prevent heat loss (17).
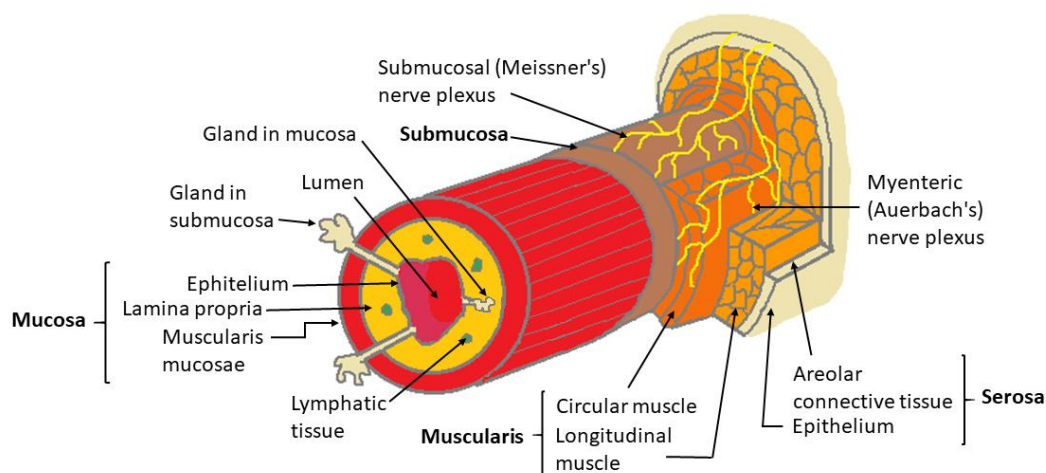
Figure 2. Schematic representation of the layers of the gastrointestinal tract (mucosa, submucosa, muscularis and serosa) and nerve plexus.

1.1.3. Physiology of the Gastrointestinal Tract

Oral route is the most common route for the administration of pharmaceuticals. The absorption of the drug from the GI tract into the bloodstream involves several phases, which can be divided broadly into three stages: the disintegration of the dosage form, dissolution of the active pharmaceutical ingredient and its passage through the intestinal wall. The efficiency of these processes is determined by the complex interplay between the dosage form, the drug and the GI tract. However, the GI tract physiology is complex and has a wide range of pH values, fluid volumes, luminal enzymes and transit times, which hindered the delivery of the drug to the target site (18).

1.1.3.1. Gastrointestinal pH

The human GI pH varies among the different regions of the GI tract, as well as between individuals and within them. Factors that affect pH values include the presence of food, systemic disease, circadian rhythms, age and drug administration (19). The different pH ranges directly impact drug absorption by affecting parameters such as stability and ionization. Healthy people in the fasted state exhibit a pH within the range from 1 to 3.5, which increases after the ingestion of a meal to less acidic pH values in the range from 3 to 7. Then, 2 or 3 hours after a meal, the gastric pH returns to the lower pH values of the fasting state. Therefore, dosage forms ingested shortly after a meal or with it will encounter a more acidic medium (20). The acidic gastric contents are buffered by alkaline pancreatic secretions as they emptied from the stomach, resulting in a gradual rise of pH values along the small

intestine. There are little differences between feed and fasted states, ranging from pH 5 in the mid part of the duodenum to pH 7.5 in the terminal ileum. The pH drops again in the colon to approximately 6.4 due to the action of colonic bacteria, which ferment carbohydrates generating the short chain fatty acids (SCAF) (21).

Changes in pH have been exploited for the purposes of drug delivery (22). Enteric coatings made of pH-responsive polymers prevent the release of the drug at the low pH of the stomach, but dissolve at the higher pH of the intestine (23). The same principle could be exploited for colonic drug delivery (24,25). The delivery of active substances directly into the colon could be specially challenging. Since the colon is located in the distal part of the GI tract, the dosage form must pass through the entire alimentary tube to reach its target site (4). Moreover, some gastrointestinal diseases such as UC and CD have been found to influence the colonic pH (21,26). These changes in intracolonic pH needs to be considered in the development of pH dependent colonic release formulations.

1.1.3.2. Fluid volume

Drug disintegration, dispersion, dissolution and absorption are highly dependent upon the volumes and distribution of gut fluids. The different fluid volumes along the GI tract should be taken into account in the design and testing of dosage forms. A study that used magnetic resonance imaging (MRI) to quantify the free fluid in the gut found that free water content is not homogeneously distributed along the gut. In fact, it exists as fluid pockets, which likely contribute to the individual variability of drug release and absorption in therapies with modified release dosage forms (27). Other study also employed MRI to quantify the volume and number of water pockets in the upper GI tract of fasted healthy humans following ingestion of 240 mL of water. The results showed that the fasted stomach contained 35 ± 7 mL of resting water whereas the small bowel contained 43 ± 14 mL. Some minutes after ingestion of water, small bowel water content rose to a value of 94 ± 24 mL divided in 15 ± 2 pockets of 6 ± 2 mL each (28). On the other hand, the fasted colon contained 11 ± 5 pockets of resting liquid with a total volume of 2 ± 1 mL. After drinking water, the colonic fluid peaked at 7 ± 4 mL distributed in 17 ± 7 liquid pockets. These liquid pockets were found primarily in ascending colon (29).

In the standardized protocols described in national pharmacopoeias, the possibility that the dosage form could pass through intestinal segments without fluid pockets is not considered (30). The transit of the dosage form through the dry segments may cause an erratic release that conventional *in vitro* dissolution tests are not suitable to predict. This variable should be taken into account in future *in vitro* tests together with pH gradients and luminal enzymes (27). As with intestinal pH, the *in vivo* fluids volume and its composition are affected by some pathologies. The active phase of IBD is linked with diarrhoea, which is the result of mucosal damage caused by persistent inflammation. The altered function of epithelial ion transporters and channels cause electrolyte retention and water accumulation in the

intestinal lumen, which accelerate the transit time of intestinal content through the GI tract (31).

1.1.3.3. Microbiota

Although bacteria are ubiquitous along the GI tract, their concentration increases steadily throughout it, being modest in the stomach and small bowel while very high in the colon. Moreover, microbiota is subject to permanent change during life and is highly variable between individuals. The microbial pattern is influenced by diet, age, hygiene, genetics and medication among others (32).

Intestinal bacteria ferment dietary fibre, are metabolically active and affect the pH of the large bowel. Thus, bacterial concentration could affect the luminal environment and the behaviour of the drug and the dosage form. However, this feature in combination with the fact that there are different bacterial concentrations in the upper and lower intestine could be exploited to trigger site-specific drug release in the colon (23). Several drug delivery strategies have been developed based on the high bacterial concentration in colon. For instance, fermentable polysaccharides can avoid degradation in the small intestine, but are used as a substrate by colonic bacteria. Drug-loaded tablets or pellets can be coated with a polysaccharide-based film, which is degraded by the microbiota once the dosage form reaches the colon (33).

Nevertheless, IBD can cause fluctuations in microbiota. Human gut bacteria belong to phyla Bacteroidetes, Firmicutes and Proteobacteria (34). The gut microbiota composition and activity of IBD patients is altered, with a decrease in prevalence of dominant members of the human commensal microbiota (e.g., *Clostridium* clusters IXa and IV) and an increase in detrimental bacteria (e.g., *Escherichia coli*) (35). In particular, CD patients showed higher concentrations of Bacteroides, Eubacteria and Peptostreptococcus, whereas Bifidobacteria numbers were reduced. On the other hand, UC patients showed higher concentrations of facultative anaerobic bacteria (36).

In preclinical evaluations of new drug delivery systems, is common to use animal models to simulate human GI tract conditions. However, intra- and inter- species differences in GI function lead to variations in drug delivery and absorption. For instance, rats are commonly used in preclinical studies and unlike human, bacterial microflora in these animals are present at high levels throughout the length of their GI tract (37). Therefore, polysaccharide fermentation and drug metabolism are inevitably higher in the rat gut, suggesting that the rat may otherwise not be a suitable model for predicting colonic drug stability or polysaccharide-based carriers (38).

1.2. INFLAMMATORY BOWEL DISEASE

Inflammatory bowel disease (IBD) is the term used to describe a group of chronic relapsing inflammatory diseases of the gastrointestinal (GI) tract, which encompasses two major phenotypes: Crohn´s disease (CD) and ulcerative colitis (UC). Both are long-term conditions that involve inflammation of the gut that have a natural course characterized by alternating periods of remission and relapse. The main symptoms of IBD include: weight loss, bloody diarrhoea, fever, vomiting and anaemia among others. Although there is currently no cure for IBD, treatment aims to relieve the symptoms and prevent new flares (39).

1.2.1. Ulcerative colitis

Ulcerative colitis is a relapsing inflammatory disease primarily affecting the mucosa of the large intestine in an uninterrupted pattern (Figure 4). Inflammation usually begins in the rectum extending proximally to cover all or part of the colon in a circumferential manner (40). The Montreal classification is a subclassification system for UC based on disease extent (Figure 3). This classification divides UC into three subgroups: ulcerative proctitis (disease limited to the rectum); left-sided colitis or distal UC (disease extending proximally beyond the rectum but no further than the splenic flexure); and extensive UC or pancolitis (involvement extends proximal to the splenic flexure) (41).
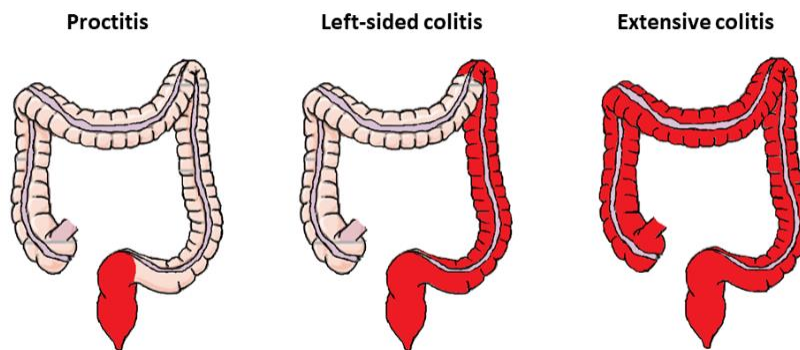
Figure 3. Clasification of ulcerative colitis based on disease extent according to the Montreal classification (41).

Moreover, the Montreal classification also classifies UC according to the severity of relapse made up of four categories: UC in remission or silent (no symptoms of the disease); mild UC (passage of four or fewer stools per day with or without blood, normal inflammatory markers); moderate UC (severity between mild and severe, with minimal signs of systemic toxicity); severe UC (passage of six or more bloody stools daily, tachycardia, anaemia and increased inflammatory markers, often with signs of serious systemic toxicity (41).

The macroscopic appearance varies with disease activity. In mild UC, the mucosa has an erythematous appearance with a fine granular surface that looks like sandpaper. In more severe cases, the mucosa has an oedematous and ulcerated appearance (42). Inflammatory pseudopolyps may also appear due to mucosal regeneration. In the case of fulminant colitis or toxic megacolon, the disease process may extend to the deeper muscular layers of the colon and even to the serosa, eventually leading to perforation (43).

In terms of histology, the process is limited to mucosa and submucosa, with the deepest layers undamaged except in fulminant disease. Characteristic histological features of intestinal biopsies during disease flares include crypt distortion, mucosal ulceration and inflammatory infiltrate consisting mainly of neutrophils, lymphocytes, macrophages and plasma cells appears. In particular, neutrophil transepithelial migration and crypt abscess are characteristic of active disease in individuals with IBD and strongly correlate with disease symptoms (44).

1.2.2. Crohn's disease

Crohn's disease is a relapsing inflammatory disease that can affect any segment of the GI tract, from the mouth to the anus (Figure 4). It is common to find affected areas surrounded by areas with healthy appearance. The most frequent affected regions are the terminal ileum and the proximal colon. Unlike UC, in CD the inflammation is transmural and extends through the entire thickness of the bowel wall from the mucosa to the serosa (45). In mild disease, superficial and small ulcers are observed, while in active disease, deep ulcers fuse transverse and longitudinally delimiting mucosa islets that can be histologically normal. The mucosa has a cobblestone appearance, this being a characteristic aspect of CD. As in UC, inflammatory polyps may also appear. CD is characterized by the inflammation of all the GI layers, submucosal oedema and deep ulcers that form fissures and fibrotic tissue (46).

Fistulae and stenosis are common complications in patients with CD. Stenotic lesions are caused by the combination of intestinal fibrosis and inflammation, resulting in a narrowing of the lumen that eventually causes intestinal obstruction. On the other hand, fistulas occur when the inflammation reaches the serosa and can result in the formation of adhesions between the inflamed intestinal segment and the adjacent organs. It is also possible to observe mesenteric fat surrounding the area of the affected intestine (47).
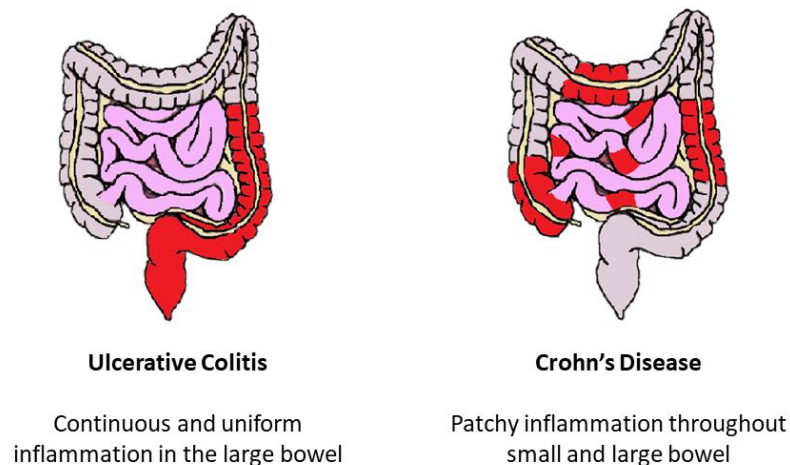
Figure 4. Differences between ulcerative colitis and Crohn's disease: Crohn's disease affects the entire gastrointestinal tract, whereas ulcerative colitis affects only the colon.

1.3. EPIDEMIOLOGY OF INFLAMMATORY BOWEL DISEASE

Epidemiological studies are of special interest in diseases of idiopathic nature such as IBD. They should not only focus on their incidence and prevalence, but also on their etiology and pathogenesis, as well as on the identification of possible environmental and genetic factors that could influence their appearance and development. The availability of quality epidemiological data will be useful to identify new risk factors and conduct studies on the efficacy of different therapies (48).

One example worth mentioning is the "hygiene hypothesis", a theory that emerged in the mid-twentieth century that tries to explain the increase in cases of IBD and other autoimmune diseases in developed countries. This theory postulates that the improvement of personal hygiene caused a loss of tolerance to organisms that normally come into contact during childhood. The lack of exposure prevents the development of a moderate immune response, which would avoid a disproportionate immune response if a new contact occurs in later ages (49).

The frequency of IBD varies greatly depending on geographic location. The highest rates are found in Europe, United Kingdom and North America, although the frequency has increased in in areas such as central and southern Europe, Asia, Africa and Latin America. In other regions, inflammatory enteropathies are considered rare, with the exception of Israel, Australia and South Africa (50).

The incidence rate is a measure of the frequency of new cases of disease during a span of time. In North America, incidence rates have fluctuated between 2.2 and 14.3 cases per 100,000 person-years for UC and between 3.1 and 14.6 cases per 100,000 person-years for CD. In Europe, the incidence rates recorded range between 1.5 and 20.3 cases per 100,000 person-years for UC and between 0.7 and 9.8 cases for CD (48,51).

The prevalence of a disease is the total number of disease cases in a population at any point during a given period of time. The prevalence of a chronic disease, such as IBD, will be considerably higher than its incidence. In North America, the prevalence fluctuates between 37 and 246 cases per 100,000 person-years for UC and between 26 and 199 cases per 100,000 person-years for CD. In Europe, the prevalence fluctuates between 21.4 and 243 cases for UC and between 8.3 and 214 cases per 100,000 person-years for CD (48,51).

Regarding to ethnic differences, the highest prevalence is found in the Jewish population, differing within the different Jewish populations, and decreases progressively in non-Jewish Caucasians, African Americans, Hispanics and Asians (52). Studies in emigrant populations suggest that differences in prevalence between different races may be related to a greater genetic predisposition to develop the disease, which could be hidden by environmental factors. For example, Asians born in the United Kingdom have a higher risk of developing IBD than the Europe's indigenous peoples (53). Moreover, rural areas and lower socioeconomic classes have a lower prevalence of IBD compared to their prevalence in cities and higher socioeconomic classes (54).

1.4. ETIOLOGY AND PATHOGENESIS OF INFLAMMATORY BOWEL DISEASE

Inflammation can be defined as a defensive reaction of a tissue and its vasculature triggered by any aetiological agent, whose main function is to dilute, destroy or wall off the pathogenic organism and repair the damage (55). Inflammation is predominantly a local form of protective response, while fever, for example, is a systemic response. In general, two types of inflammatory processes can be distinguished (5):

The **acute inflammatory reaction** is the most immediate response to an injurious agent of local tissues and blood vessels. It involves vasodilatation and extravasation of plasma and inflammatory cells to the damaged area. Neutrophils are the phagocytic leukocytes predominant in the inflammatory exudate, although other cell types such as macrophages, mast cells, basophils and eosinophils are also present.

The **chronic inflammatory reaction** is an inflammatory process prolonged in time due to the inability of the organism to eliminate the injurious agent, either due to an ineffective immune response or the difficulty in eliminating the inflammatory agent. The inflammatory infiltrate is made up of mononuclear cells (macrophages and lymphocytes) and vascular phenomena are less important. There is a greater proliferation of fibroblasts with the subsequent formation of scar tissue that replaces the functional tissues of the affected areas. The scar tissue derived from chronic inflammation of the intestine induces the narrowing of the intestinal lumen.

Furthermore, the generation, maintenance and resolution of the inflammatory response is controlled by regulatory molecules called mediators of inflammation, whose release is triggered after recognition of infection or injure (56). Depending on their origin, these chemical mediators could be divided in:

Plasma derived mediators, which are synthetized in the liver and circulate in the blood in the form of precursors and require a series of proteolytic processes for their activation. In this group are included the coagulation, fibrinolysis and complement systems (57).

Cell derived mediators, which are packaged in intracellular granules (histamine) or are synthesized de novo (cytosines) in response to inflammatory stimulus. In this group are also included vasoactive amines (histamine, serotonin), biolipids (eicosanoids, platelet-activating factor), oxygen free radicals, nitric oxide, lysosomal enzymes and proinflammatory cytokines (58).

The level of exposure to the injurious agent determines the severity and extent of the inflammatory response. In the case of the GI tract, its continuous exposure to luminal antigens keeps it in a constant state of controlled inflammation. The intestinal immune system has to distinguish between pathogenic antigens that must trigger an immune response from those that must be tolerated, such as intestinal microflora and food antigens (59).

There is an accumulating body of evidence suggesting that the chronic intestinal inflammation observed in IBD results from a dysregulated immune response to normal enteric antigens (60). Even though no unique bacterial abnormality has been identified as the cause of the inflammatory process, it is clear that bacteria play a major role in the pathogenesis of IBD (61). This fact is supported by animal models of IBD, in which the disease is not manifested as long as the animals are in a germ-free environment (62).

In both UC and CD, the activation of CD4^{+} T lymphocytes present in the lamina propria leads to increase secretion of inflammatory cytokines. Some of these T cells also activate other inflammatory cells, such as macrophages and B lymphocytes, which release proinflammatory cytokines (e.g., TNF-α, IL-1, IL-6) as well as other proinflammatory mediators that amplify the inflammatory response by recruiting and activating leukocytes and platelets. Fibrogenesis and collagen production is also promoted, and the coagulation cascade in local blood vessels is activated (63,64).

On the whole, IBD should be considered as the result of a dysregulated immune response to an undefined luminal antigen, which is probably part of the microflora. This alteration in the immune response together with the genetic predisposition of the individual and the environmental factors to which the individual is exposed, such as diet and smoking, results in an uncontrolled inflammatory process. In addition, the inflammation leads to mucosal injury and altered epithelial barrier function that increases the amount of bacteria that enter the intestinal wall, further aggravating the inflammatory response (65,66).

1.5. RISK FACTORS FOR INFLAMMATORY BOWEL DISEASE

Although the aetiology of IBD is not fully elucidated, multiple environmental and genetic factors have been associated with the development of the disease.

1.5.1. Environmental risk factors

Several environmental factors have been related to the development of IBD. Some of them have a different influence on UC and CD, which indicates that although both entities share many pathophysiological and clinical characteristics, they are two different entities. For instance, diet, tobacco, antibiotic exposure and oral contraceptives, among others, have been related to both the onset of the disease and its subsequent evolution (67). It is worth mentioning the relationship between smoking and IBD, since smoking seems to act as a protective factor in the development and clinical evolution of UC, while it is considered a risk factor directly associated with CD (68).

On the other hand, diet could be an explanation of the different risk of developing the disease depending on the geographical area. However, despite of the numerous studies that have been conducted on the subject, a consensus has not yet been reached. The most consistent association was the relationship between sugar consumption and the development of IBD, which acts as a risk factor (69). In the same way, the scarcity or overabundance of some nutrients could also disturb intestinal homeostasis and further exacerbate the disease (70).

Another hypothesis implies the possibility that the disease may be caused by certain infectious agents, although so far there is no clinical evidence of it. This infectious etiology is supported by epidemiological data such as the positive response to antibiotics of patients and the similarity between the symptoms of gastrointestinal infectious pathologies and IBD patients (71). Therefore, the influence of various microorganisms on the pathogenesis of IBD, including bacteria, mycobacteria and viruses, is not ruled out. It could be possible that some microorganisms from the genus *Salmonella*, *Shigella*, *Campylobacter* and *Clostridium difficile* could initiate an inflammatory response that the mucosal immune system would not control (72,73).

Furthermore, normal microflora could be perceived as pathogenic in IBD patients. In these patients, a sensitization of the immune system against elements of the microflora is found, which causes an excessive activation of lymphocytes and production of Immunoglobulin G (Ig G). Conversely, healthy individuals tolerate their microbiota and produce Immunoglobulin A (Ig A) (74). Moreover, faecal microbiota transplantation and probiotic agents have demonstrated to both reduce the dysbiotic environment and production of inflammatory mediators, achieving a significant remission in UC and CD (75).

1.5.2. Genetic risk factors

Family history is a risk factor for developing IBD. First-degree relatives have approximately 10% risk of developing the disease. Children whose both parents have CD have a higher risk, with approximately 36% likely to develop the disease. The anatomical site and the clinical type of the disease also usually coincide within the same family (76). Epidemiological evidence suggests some genes shared by UC and CD increase susceptibility

to develop the disease. Although the relationship between specific genes and disease development has not yet been fully elucidated, predisposing genes have been identified.

By the use of positional cloning techniques and fine mapping Hugo et al. (77) identified the CARD15 gene (also known as NOD2) in the IBD1 locus on chromosome 16 as a disease susceptibility gene. The NOD2 protein is expressed in monocytes, macrophages, dendritic cells, epithelial cells and Paneth cells. It consists of two N-terminal caspase recruitment domains (CARD), a central nucleotide-binding domain (NBD) and a series of C-terminal leucine-rich repeats (LRRs). NOD2 is a cytosolic molecule that acts as a pattern recognition receptor (PRR) and recognizes through its LRR terminal region the bacterial muramyl dipeptide (MDP). This recognition results in the secretion of antimicrobial peptides, such as α-defensins, to protect the host from bacterial invasion (78).

At least 30 mutations or polymorphisms in the NOD2/CARD15 gene associated with CD have been identified. Three of them are common (Arg702Trp, Gly908Arg and Leu1007insC) and represent approximately 82% of mutated alleles. Alleles related to CD allow excessive activation of nuclear factor kappa B (NF-κB) or a decrease in intestinal antimicrobial activity by reducing the production of defensins by Paneth cells (79). For example, the Leu1007 frameshift mutation of NOD2 produces a truncated protein that lacks 33 distal amino acids, whose association with an altered activation of NF-κB has been demonstrated *in vitro* (80). Inflammatory enteropathies have also been related to a second gene called DLG5 present on chromosome 10 (81) and with the interleukin receptor 23 (IL23R) (82), among others.

1.6. OXIDATIVE STRESS IN INFLAMMATORY BOWEL DISEASE

Oxidative stress arises when the balance between the production of reactive oxygen species (ROS) and antioxidant defences is disturbed. Various ROS arise as a consequence of metabolic processes in biological organisms, such as superoxide radicals ($O_2^{\bullet-}$), hydroxyl radicals ($^{\bullet}OH$), hydrogen peroxide (H_2O_2) and singlet oxygen ($^1O_2$) (83). ROS also act as second messengers in many intracellular signalling cascades or as safeguards against pathogens at moderate concentrations. However, ROS are highly reactive due their unstable conditions with unpaired electrons that could also attack any biological molecule, from lipids and proteins to DNA. To keep this attack in balance, a complex system of antioxidant defences has evolved. Situations in which ROS are inefficiently scavenged or overproduced lead to oxidative stress (84).

Oxidative stress is believed to play a pivotal role in IBD pathogenesis. For instance, one of the main histological features observed in IBD is neutrophil infiltration in the inflamed mucosa. Activated neutrophils are known potential sources of ROS production (85). Several studies indicated that increased systemic levels of oxidative stress and enhanced ROS production could contribute to chronic intestinal inflammation (86,87). As the incidence of IBD have increased, demands have grown for new therapeutic approaches for IBD. Considering the strong evidence that oxidative stress is increased in IBD, a medication plan that includes the

use of antioxidant compounds in conjunction with classical therapy may have fewer side effects and better treatment responses (88).

Several studies have suggested that the administration of antioxidants with additional anti-inflammatory activity may be beneficial in the treatment of IBD (88,89). For instance, melatonin, an endogenous hormone produced mainly in the pineal gland, and resveratrol, a natural (poly)phenol found in several species of berries, have been shown to ameliorate intestinal inflammation in animal models of the disease (90,91).

1.6.1. Melatonin

Melatonin (N-acetyl-5-methoxytryptamine) is the main hormone synthetized and secreted by the pineal gland under normal environmental conditions (Figure 5). The main physiological function of melatonin is to act as a neuroendocrine hormone involved in the regulation of circadian rhythms (92). Extrapineal sources of this hormone were reported in the retina, skin and bone marrow cells, among others, but especially in the GI tract of vertebrate species. The concentration of melatonin in the GI tract tissues surpasses the concentration in blood by 10-100 and there is at least 400 times more melatonin in the GI tract than in the pineal gland (93). Melatonin exerts its physiological effects through specific melatonin membrane receptors (MT1, MT2 and MT3) that can be found in the GI tract. Moreover, the levels of melatonin in the GI tract after a pinealectomy remain unchanged, suggesting a local synthesis of the hormone. This fact highlights the physiological importance of melatonin, which could regulate process such as GI motility and inflammation (94).

Melatonin is a potent ROS scavenger and displays antioxidative properties. Apart from directly scavenge ROS, melatonin increases the levels of antioxidative enzymes, such as superoxide dismutase, glutathione peroxidase and glutathione reductase (95). Considerable experimental evidence supporting the idea that oxidative stress plays a role in the pathogenesis of IBD, along with the high levels of melatonin found in the GI tract, have led to several investigations about the ability of melatonin to protect against intestinal inflammation. In animal models of IBD, melatonin has showed to reduce colonic inflammation through several mechanisms, such as the downregulation of proinflammatory molecules (96), the regulation of macrophage activity (97) or the local inhibition of iNOS and COX-2 expression in colonic mucosa (98).

1.6.2. Resveratrol

Resveratrol (3,5,4′-trihydroxystilbene) is a non-flavonoid polyphenolic compound produced by a wide variety of plants, such as grapes, peanuts and mulberries in response to stress, injury fungal infection or ultraviolet (UV) irradiation (99). Resveratrol possess two isomeric forms: *trans*-resveratrol and *cis*-resveratrol, being the *trans*-isomer the more sterically stable form (Figure 5). However, resveratrol is very sensitive against UV light and rapidly isomerizes from *trans*-resveratrol (active isomeric form) to *cis*-resveratrol (100).

Extensive research during the last decades has suggested that resveratrol possess cardioprotective and anticancer properties, as well as antiviral and antibacterial effects (99). The beneficial properties of resveratrol are attributed to its anti-inflammatory and antioxidant effects, which also makes this compound a potential therapeutic candidate in the treatment of IBD. Resveratrol can scavenge ROS in the intestine and improve antioxidant enzyme activity (101). In animal models of IBD, resveratrol has shown preventive effects when given as a pretreatment (102). This molecule also simulates apoptosis and reduces COX-2 expression thus reducing colon damage (103).

Melatonin   **trans-Resveratrol**
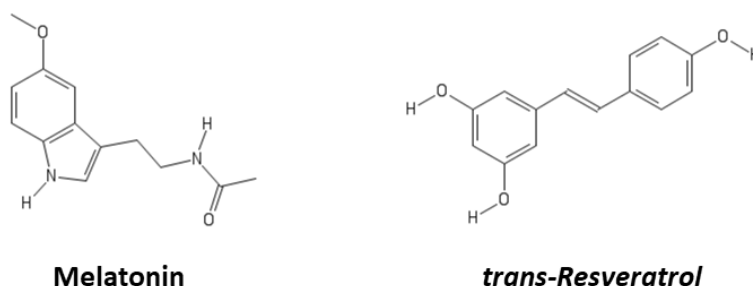
Figure 5. Chemical structures of melatonin and *trans*-resveratrol.

1.7. IN VIVO ANIMAL MODELS OF INFLAMMATORY BOWEL DISEASE

During the last years, a large number of animal models have been developed to provide a valuable insight into the different pathways involved in IBD pathogenesis. Moreover, these animal models enabled the preclinical development of a large number of new therapies. Depending on the mode of induction of intestinal inflammation, experimental IBD models can be divided into chemically induced models, genetically engineered models, spontaneous models and cell transfer models (104) (Table 1).

1.7.1. Chemically induced animal models

Chemically induced IBD animal models are commonly used because of the immediate inflammation, the high reproducibility and the simplicity of the induction process. Although they have limitations, they resemble in some histopathological and immunological aspects the human IBD.

1.7.1.1. TNBS colitis

Colitis can be induced in rats, mice and rabbits by intrarectal administration of 2,4,6-trinitrobenzenesulfonic acid (TNBS) diluted in varying concentrations of ethanol. TNBS is believed to haptenize colonic proteins rendering them immunogenic to the host immune

system, thereby triggering the host innate and adaptive immune responses. Ethanol is a prerequisite to break the mucosal barrier to allow penetration of TNBS in the lamina propria. The intrarectal administration of this reagent induces a transmural colitis driven by CD4$^+$ T cells, which makes it a valuable model to study T helper cell-dependent mucosal immune responses (105). In murine TNBS colitis, the genetic background is thought to influence the inmunopathogenesis with a predominant Th2 mediated immune response in BALB/c mice and a more Th1 response in SJL/J mice. Moreover, rats develop a distal colitis while mice often show a pancolitis. TNBS colitis initially cause injury to the epithelial barrier with infiltrations of lymphocytes and macrophages. In addition, a thickening of the colon wall can be appreciated with visible ulcers at the site of injection of the enema (106).

1.7.1.2. DSS colitis

The administration of dextran sulfate sodium (DSS) in drinking water for several days induces an acute colitis in mice, rats and hamsters characterized by bloody diarrhea, weight loss, ulcerations and neutrophilic infiltration. The mechanism by which DSS induces intestinal inflammation is unclear but it is believed to be toxic to epithelial cells of the basal crypts and to affect the integrity of the mucosal barrier (107). Chronic colitis can be induced by the administration of multiple cycles of DSS to some strains of mice (108). When administered to T- and B- cell deficient mice, they also developed acute intestinal inflammation, indicating that the adaptive immune system does not play an important role in this model, hence it is not well suited to address immunologic or therapeutic issues involving this immune response (109). Otherwise, the DSS model is particularly useful to study the contribution of the innate immune system to the development of colitis.

1.7.1.3. Oxazolone colitis

The rectal administration of the contact sensitizing agent oxazolone dissolved in ethanol induces colitis in rats and mice, manifested by weight loss and diarrhea with high death rates (105). In SJL/J mice, the inflammation affects only to the distal colon with neutrophil/lymphocyte infiltration limited to the superficial layer of the mucosa. Examination of the cytokine profiles of T cells isolated from the lamina propria demonstrated an elevated production of Th2 cytokines (IL-4, IL-5 and IL-13) in CD3/CD28-stimulated T cell cultures. The combination of histological features and the cytokine profile of this animal model resembles to characteristics that have been observed in human UC (110).

1.7.2. Genetically engineered animal models

More than 74 kinds of genetically engineered mouse strains have been developed since 1993 for studying IBD. Some of them carry the susceptibility genes identified in human IBD and other susceptibility genes have been discovered using these animal models. However, it is unlikely that these mutations represent the exact cause of human IBD due to the fact that IBD

involves a complex interaction of factors. Genetically engineered mice can be classified in transgenic models (Tg) and knockout models (KO), which are genetically engineered to overexpress or lack a gene of interest in all cell types, respectively (111).

1.7.2.1.Conventional knockout (KO) models

1.7.2.1.1. *Interleukin (IL-10) KO mice*

The regulatory cytokine IL-10 is a susceptibility gene for IBD. IL-10 KO mice are genetically engineered to lack IL-10 gene, developing a spontaneous colitis after 3 months of age (112). Development of colitis is inhibited if IL-10 deficient mice are raised under germ-free conditions (62) and the administration of probiotics and selective antibiotics can treat or prevent development of inflammation in mice colonized by bacteria (113). The CD4+ T cells mediate pathogenesis of colitis in IL-10 mice. Such enhanced Th1 response leads to macrophage activation and overproduction of inflammatory cytokines (62). Intestinal CX_3CR1^+ macrophages have been shown to be a major responder to IL-10 in the inflamed colon (114).

1.7.2.1.2. *Interleukin (IL-2) KO mice*

IL-2 deficient mice fail to maintain immune homeostasis and maintenance of self-tolerance, developing IBD after 4 weeks of age (115). IL-2 KO mice spontaneously develop a systemic autoimmune disease characterized by hepatitis, gastritis, pancreatitis and haemolytic anaemia among others. In this KO model, an unremitting colitis develops spontaneously in germ-free condition (116) resulting in progressive weight loss and death, also displaying a large variety of immune abnormalities (117).

1.7.2.1.3. *T cell receptor (TCR) α-chain-KO mice*

The T cell receptor (TCR) is required for the recognition of antigens by T cells. Spontaneous development of colitis has been observed in both TCRα and TCRβ-deficient mice, although only the 60 % of TCRα and none of TCRβ-deficient mice consistently develop a spontaneous colitis mediated by Th2 (118). By 4 months of age, unremitting chronic diarrhoea, consistent inflammation and rectal prolapse was observed in this model. Moreover, TCRα-deficient mice maintained in a germ-free environment do not develop colonic inflammation (119). In a B cell and TCRα-deficient mice, colitis is developed at an earlier age and of great severity than in mice B cell-competent and TCRα deficient, revealing a novel cell regulatory circuit in this model (120).

1.7.2.2.Conventional transgenic (Tg) models

1.7.2.2.1. *Interleukin (IL-7) Tg mice*

IL-7 is required for the development of mature T cells in the thymus and is implicated as a growth factor extrathymic T cell development in the intestine (121). IL-7 Tg mice spontaneously develop colitis between 4 and 12 weeks of age, which is manifested by anal bleeding and infiltration of monocytes, decrease in goblet cells and an increase in crypt abscesses in the lamina propria. In this chronic colitis model, the lack of IL-7 results in the apoptosis of the activated lymphocytes, which is suggested to be the cause of colitis (122).

1.7.2.2.2. *HLA-B27/β2M Tg rat*

Transgenic rats for human HLB-B27 and β2-microglobulin develop a spontaneous colitis manifested by chronic inflammation involving stomach, small and large intestine, being the colon the most affected site. It can be appreciated crypt hyperplasia and mucosal infiltration of mononuclear inflammatory cells (123) and CD4 T cells have been suggested to play a role in the pathogenesis of the disease (124). This model has been used to study the effect of normal luminal bacteria in the acute and chronic stages of inflammation by the colonization of germ-free B27 rats with groups of defined bacteria, showing that some resident enteric bacteria are more active than others inducing inflammation in this rat model (125).

1.7.2.2.3. *STAT-4 Tg mice*

Signal transducer and activator of transcription 4 (STAT-4) is a transcription factor that promotes Th1 development. The STAT-4 transgenic mice generated under the control of a cytomegalovirus (CMV) promoter overexpress this transcription factor developing a transmural colitis within 7-14 days after the activation of CMV promoter, also exhibiting a mediated $CD4^+$ Th1 T cells inflammation (126).

1.7.3. Spontaneous animal models

Although uncommon, IBD has been reported to occur spontaneously in animals, especially in some mice strains and in the Cotton-top Tamarin. In the last one, the exact pathogenesis still remains unknown (127). Disease in humans involves multiple pathways and the defects leading to IBD are more complex than those seen in genetically engineered animal models, therefore, spontaneous models may mimic better the complexity of human disease (62). Furthermore, novel models still been generated to explore the axis between different potential biomarkers and intestinal inflammation (128).

1.7.3.1.C3H/HeJBir mice

C3H/HeJBir mice develop spontaneous inflammation under certain housing conditions. Lesions occurred primarily in the cecum and proximal colon with acute and

chronic inflammation, crypt abscesses and ulceration (129). Disease appears early in life at 3-4 weeks and heals by 10-12 weeks. Moreover, C3H/HeJBir mice have no significant B or T cell reactivity to epithelial or food antigens whereas develop strong B cell and T cell responses to enteric bacterial antigen. This finding demonstrate that effector T cells reactive with conventional antigens of the enteric bacterial flora can mediate chronic IBD (130). The innate immunity of C3H/HeJBir mice exhibit defects that translate to increased T-cell responses to bacterial antigens. This approach has proven to be particularly useful in the identification of bacterial antigens that are recognized by pathogenic T cells and thus induce IBD (131), being a valuable resource for genetic and immunologic studies of the disease.

1.7.3.2. SAMP1/Yit mice

The SAMP1/Yit mice develop spontaneous inflammation that closely resembles to Crohn`s disease. In this model, the inflammation is primarily localized to the distal small intestine showing discontinuous lesions with transmural involvement, granulomas and alterations in the epithelial morphology (132). The inflammatory infiltrate is composed of mononuclear cells and neutrophils. Germ-free SAMP1/Yit mice do not develop intestinal inflammation whereas in contact with intestinal microflora develop disease by 15 weeks of age (133). Epithelial alterations may play a role in the pathogenesis in this model due to the activation of CD4$^+$ T cells reactive to bacterial antigens, which mediate the inflammation (134,135).

1.7.4. Adoptive transfer animal models

Among the animal models available to assess the contribution of T cells to the pathogenesis of IBD, the T cell transfer model of colitis is the most widely used to study the initiation, induction and regulation of immunopathology in chronic colitis mediated by T cells (136). Typically, naïve T-cells are transferred into immunocompromised mice and therefore develop intestinal inflammation because of inappropriate downregulation (137).

1.7.4.1. CD4+ /CD45RB^{high} T-cell transfer colitis

Normal CD4$^+$ T cells can be separated into naïve cells, which express high levels of CD45RB (CD4$^+$CD45RB^{hi}), and memory cells, which express low levels of CD45RB (CD4$^+$CD45RB^{lo}). The adoptive transfer of CD4$^+$CD45RB^{hi} T cells collected from the spleen and lymph nodes of wild-type mice into SCID and RAG-2-/- mice results in colitis and wasting (138,139). However, CD4$^+$CD45RB^{lo} T cells from germ-free mice are capable of supressing colitis induced by CD4$^+$CD45RB^{hi} (140), suggesting that regulatory T cells are considered a member of the CD4$^+$CD45RB^{lo} family and are believed to be involved in the regulation of inflammation (138). Therefore, colitis in models with transferred CD4$^+$CD45RB^{hi} can be caused by an impaired T-cell regulation (122). In sum, normal T cells

contain pathogenic cells that can cause intestinal inflammation, which is prevented by the action of regulatory cells.

1.7.4.2. Hsp60CD8+ T cells transfer colitis

In this mice model, intestinal inflammation is induced by the adoptive transfer of an hsp60-specific CD8$^+$ T-lymphocyte clone. The inflammatory lesions are concentrated on the small bowel and it is also developed in germ-free animals, without depending on the presence of normal intestinal flora. Immunocompetent mice usually do not develop disease after transfer of hsp60-specific T cells. This finding highlights the pathogenic potential of such T cells in a state of immunodeficiency or immune dysregulation (141).

Table 1. Classification of animal models of IBD.

Chemically induced	*Genetically engineered*		*Adoptive transfer*	*Spontaneous*
Enema	**Knockout**	**Transgenic**	*CD45RB^{high} cells*	*C3H/HeJBir*
TNBS	*IL-10*	*IL-7*	*CD62L^{high} cells*	*SAMP1/Yit*
DNBS	*IL-2*	*HLA-B27*	*Hsp60CD8$^+$T cells*	*Cotton-top*
Oxazolona	*IL-2R*	*STAT-4*		*tamarin*
Acetic acid	*TCRα*	*TGF-β*		
	Gαi2	*NOD2*		
Oral	*STAT-3*	*NF-κβ*		
DSS				
Indomethacin				
Carragenan				

1.7.5. Advantages and limitations of animal models

The knowledge obtained from the use of animal models in preclinical research is large, and there is no doubt about their contribution not only in defining the pathogenesis of IBD, but also in the inflammatory process itself. There has also been progress in understanding the complex interactions between the gut microbiota and the host, and how environmental and genetic factors could affect homeostasis.

Nowadays, there are many animal models available to study IBD. Each model has specific advantages over other models. For instance, the use of CD4$^+$ /CD45RB model has brought some information about the adaptive immune mechanism involved in the IBD pathogenesis. TNBS model has allowed the development of the monoclonal anti-IL-12p40 antibody that has demonstrated efficacy in the human CD treatment (142) and the mechanism of inflammation associated with epithelial homeostasis has been analysed using the DSS model. Furthermore, TCRα model shares etiological characteristics (smoking) with human UC (143). In addition, IL-10 KO model has contributed to the understanding of the probiotics mechanism in IBD (113,117).

Moreover, the possibility of being developed under certain conditions with a controlled microbial environment and with minimal differences in gut microbiota provides reproducible results. Also, the ability to control each stage of the inflammatory process and analyse the mechanisms from the beginning to the late events of the disease is an advantage of experimental models which cannot be done in patient studies. This allows to examine separately the events of the acute phase of the disease and those of the chronic phase, also distinguishing the underlying pathways of inflammation from the clinical features of the illness (2,144).

Nevertheless, these animal models can present some limitations. When interpreting data from experimental colitis, it must be taken into account the environmental influences that affect the pathophysiology of the intestinal mucosa in human IBD, which are not the same that in experimental colitis. This could be solved using specific microbial communities to evaluate their impact in the development of experimental colitis or even transplanting human faecal microbiota into germ-free mice for better simulate human IBD (145,146). Another disadvantage that could be mentioned is the different indexes usually used for evaluate the therapeutic efficacy of drugs between animal models and patients. The last ones are usually evaluated by activity scores of the disease, while IBD studies in animal models are normally assessed by histopathological scores of colonic tissue damage in combination with differences in the rate of weight loss between treated and non-treated animals (147).

Finally, when interpreting the treatment efficacy, it has to be taken into consideration the time of intervention. In experimental IBD, onset of inflammation occurs over defined time courses that enable a therapeutic intervention at specific time points. If a treatment is able to prevent the development of inflammation in an experimental model may not be equally effective in resolving stablished disease, it only proof the existence of a novel pathway of inflammation and will not be useful in patients with an established disease (104). Therefore, the development of new models that could better resemble human IBD and a more thorough interpretation of data obtained from them is still necessary.

1.7.6. Considerations for choosing a preclinical model

When choosing a preclinical IBD model, it is important to determine the model of greatest relevance to the particular scientific question to be addressed. For example, CD and UC usually occur in different anatomic regions of the GI tract. For this reason, to test a therapeutic candidate it must be taken into account if the inflammation will affect mainly the colon or the small intestine, since both differ in anatomical and cellular structure as well as bacterial diversity.

On the other hand, IBD models differ in the nature of the response that is evoked. Since pathological responses are different among animal models, it is necessary to take into consideration whether the therapeutic compound will target prevention of epithelium damage,

oxidative stress, inflammation mediated by an innate immune response or by an adaptive immune response, for example (148).

For instance, if research is focus on exploring therapeutics that may have protective properties for the intestinal epithelium, a chemically induced model such as the TNBS model could be more useful due to the acute damage it causes to the epithelial cells. One other example is the altered mucosal permeability that causes DSS or is present in mice with genetic deficiencies in permeability. Therapeutic compounds that maintain mucosal permeability will be protective in those types of colitis (149).

1.7.7. Relevance of animal models of IBD

Although none of the existent models are exact replicates of the human disease, the different subgroups of patients with IBD may be possibly reflected in the differences between animal models (150). With the development of personalized therapies, animal models will continue to play an important role in IBD research. In future studies, a specific model targeting a defined phenotype could provide a more relevant data. Furthermore, the identification of novel diagnostic biomarkers could be particularly beneficial, leading to a better classification of the illness and subsequent monitoring of the effectiveness of therapies (151).

In addition, to accurately characterize IBD models and evaluate the therapeutic efficacy of new compounds in preclinical studies, some diagnostic techniques such as diagnostic imaging have been applied in the preclinical field with a high translational potential to clinical practice. These innovative approaches may be of particular relevance in the management of IBD patients in combination with current diagnostic tools.

1.8. DIAGNOSTIC IMAGING TECHNIQUES IN INFLAMMATORY BOWEL DISEASE

In clinical practice, the standard diagnosis of IBD involves endoscopy and biopsy. Colonoscopy is the type of endoscopy most often performed to both monitor and diagnose the illness. Moreover, the biopsy tissue obtained during the colonoscopy is examined for specific features to help in the diagnosis (152). Nevertheless, this technique is very invasive and it is not able to evaluate the upper part of the small bowel as well as other areas outside the bowel. Furthermore, endoscopic imaging is restricted to the superficial mucosal layers of the intestine, so they do not allow a complete transmural view of the entire intestinal wall and thus do not reveal the extent and severity of the inflammatory process (153). For this reason, less invasive diagnostic imaging technologies such as barium X-rays, ultrasound, magnetic resonance imaging (MRI), computed tomography (CT), positron emission tomography (PET) and single photon emission computed tomography (SPECT), can play multiple roles not only in managing IBD in clinical patients, but also in preclinical research monitoring disease progression and treatment efficacy from its early stages.

1.9.IN VIVO IMAGING IN PRECLINICAL RESEARCH

In vivo imaging of small animals is increasingly being developed for the assessment of disease-specific animal models. These models are mainly rodents (mice and rats) that are too small to be managed accurately by the devices used in clinical practice, which raises problems such as low spatial resolution and low sensitivity. To overcome these limitations, miniaturized versions of clinical devices are currently available for small animal imaging in preclinical research (154).

1.9.1. Structural imaging techniques

1.9.1.1.Micro-computed tomography (µCT)

Computed tomography is an application of X-ray imaging that provides detailed images of organs, blood vessels, bones and soft tissue. A detector situated in opposition to the X-rays source sense those X-rays that are not absorbed by the tissues, which is inversely related to the density of the structure. The CT scan generate a 3D anatomical image, from which sectional or spatial images can be reconstructed (155). Computed tomography enterography (CTE) is a variation of standard abdominal CT scan that involves the use of small bowel distension in combination with the administration of an oral contrast agent (156). This technique is highly sensitive and specific for active small intestinal inflammation and therefore it is considered as a useful tool to assess CD patients (157,158).

In small animal studies, µCT has been used for the assessment of bone and soft-tissue tumour animal models, demonstrating the potential usefulness of µCT in cancer research (159). Furthermore, this technique allow the detection of colon wall thickening in DSS-induced colitis model in mice, thus serving as a non-invasive tool for monitoring colitis (160).

1.9.1.2.Micro-magnetic resonance imaging (µMRI)

Magnetic resonance imaging (MRI) is based on the interaction of nuclear spin with an external magnetic field. MRI produces spatial maps based on the properties of hydrogen nuclei (protons) contained in water molecules. This technique portrays anatomic details with high resolution in three dimensions (3D) and is especially useful for imaging soft tissues (155). MRI presents several advantages over CT for evaluating IBD, for example the lack of ionizing radiation exposure in patients, which allows the realization of numerous studies throughout their lives, and the better soft tissue contrast without the need for intravenous contrast (161). Furthermore, MRI offers a great opportunity to study the changes in the small intestine wall in patients with CD in combination with endoscopy, both in adults and paediatric patients (162,163). In particular, taking into consideration just the small bowel,

MRI can be performed using other approaches such as MR-enterography and MR-enteroclysis (158,164). Although in UC patients the extent of inflammation can be assessed by endoscopy since the extent of lesions are limited to the inner wall layers, MRI could also be important when endoscopy is not feasible (165).

In small animals, µMRI is frequently used to provide anatomic images and delineate tumours or areas of necrosis (166). Furthermore, MRI has been used to characterize potential disease biomarkers in DSS mice (167) and to perform a longitudinal study to investigate the evolution of IBD also in a DSS animal model (168), demonstrating the viability of this technique to monitor the development of colitis.

1.9.1.3. Micro-ultrasound (µUS)

Ultrasound represents an accurate and reproducible modality to assess disease activity in IBD patients since it can detect disease complications such as strictures and abscesses (169). This technique has been applied extensively in the follow-up of CD patients, providing prognostic information to the clinician (170). Ultrasound imaging is based on the differing acoustic properties of tissue and present some advantages such as high spatial and temporal resolutions without ionizing radiation (154). In preclinical research, micro-ultrasound represents a rapid, cost-efficient and non-invasive imaging tool for studying the development of model animals of human disease where high spatial resolution is needed. In mice cancer models, 3D high-frequency micro-ultrasound (3D-µUS) was used to perform measurements of colonic tumours (171).

A variant of ultrasound is the ultrasound molecular imaging that utilizes micron-sized, gas filled contrast microbubbles that are able to bind proteins on endothelial cells that are upregulated in the inflammation process. This modality was used for the assessment of acute inflammation in DSS-induced colitis model in mice (172). Another method is the ultrasound elasticity imaging, which allows to evaluate the changes in mechanical properties of the intestine due development of fibrosis after repeated cycles of inflammation. This technique was used in TNBS induced colitis in rats since it is known that this model develops fibrosis (173).

1.9.2. Functional imaging techniques

1.9.2.1. Micro-single photon emission computed tomography (µSPECT)

Single photon emission computed tomography is cross-sectional nuclear imaging using single photon emitting radionuclides. The most common radionuclides used in clinical practice are ^{99m}Tc, ^{67}Ga, ^{201}Tl, ^{111}In or ^{123}, ^{125}, ^{131}I, which have to be injected in the patient (174). ^{99m}Tc-labeled CXCL8 (interleukin-8) has used in IBD patients to detect an localize disease activity with good diagnostic accuracy (175). Also, ^{99m}Tc HMPAO-labelled white

blood cell (WBC) has been found to be useful in the assessment of disease extent without the need for colonoscopy (176). Nevertheless, SPECT alone is limited by low spatial resolution and it is not able to provide anatomical details, therefore this technique is usually used in combination with CT scan for an accurate lesion localization, avoiding erroneous interpretations (174). Although the molecular sensitivity of PET is higher than that of SPECT, it continues to be widely used in both preclinical research and clinical practice due to its lower cost and the longer half-life of its radionuclides that allow *in vivo* evaluations for a longer time (155).

SPECT imaging is highly valuable for study dynamic biological processes at the cellular and subcellular levels. Among other applications (177), μSPECT is useful to monitor disease activity in animal models of IBD. The monoclonal antibody infliximab radiolabelled with ^{99m}Tc has been able to detect inflammation in TNBS-induced colitis model in rats (178), demonstrating the target specificity of a clinical drug currently used in clinical practice. Other study injected superparamagnetic iron oxide (SPIO) nanoparticles and ^{111}In oxine–labelled macrophages in mice with DSS colitis. The SPECT/CT data provided information of pharmacokinetics and biodistribution of the macrophages in the IBD mice (179).

1.9.2.2.Micro-positron emission tomography (μPET)

Positron emission tomography is based on the detection of γ-photons emitted from a radiolabelled molecule with a positron-emitting radioisotope, mainly ^{11}C, ^{18}F and ^{64}Cu. A frequently used radiotracer is [^{18}F]Fluoro-2-deoxy-2-D-Glucose ([^{18}F]FDG), which is uptaked by tissues and emits positrons that react with electrons in the body. As a result, there is a production of photons that are detected by a PET scanner, which creates 3D images that show the distribution of the [^{18}F]FDG in the body. Areas with higher [^{18}F]FDG uptake appear more intense indicating a high level of metabolism occurring there due to inflammation or infection (180). PET is usually used in combination with CT, offering an anatomical reference to the physiological data obtained by PET scan with high resolution and sensitivity (181).

In clinical practice, [^{18}F]FDG PET/CT allows to visualize not only the mucosal layer, but also to get a full transmural view of the entire intestinal wall, revealing the extent and severity of the inflammatory process. [^{18}F]FDG PET/CT may be of particular value in the evaluation of a treatment effectiveness in a patient with CD, for whom a therapeutic decision has to be made on the basis of an objective assessment of the severity and extent of the inflammation. Pilot studies have shown good specificity and sensitivity for [^{18}F]FDG PET/CT in detecting and localize moderate to severe lesions in the bowel wall of patients with CD (182,183). Therefore, it is likely that PET/CT scan can be used as a complementary diagnostic tool and in the follow-up of IBD patients, especially in those in whom an invasive colonoscopy, such as children, is not desirable.

Nevertheless, the significant patient irradiation associated with PET/CT scan will impede frequent use (184). Moreover, the high cost of PET scanning will likely be a barrier

for its implementation in the clinical practice. Unless the cost of this technique decrease, PET/CT probably will not be a major or common tool for monitoring IBD. Due to the increasing demand for this technique, it is expected that in the coming years it will be available at more affordable prices.

In preclinical research, several works have been carried out to study its feasibility in the assessment intestinal inflammation in IBD animal models (Figure 6). This technique has been used to evaluate the disease activity in mice with DSS induced colitis (185) demonstrating its potential translational value. Moreover, longitudinal quantifications of inflammation have been carried out in both DSS (186) and TNBS (187) animal models showing that [18F]FDG PET/CT is a reliable tool to assess disease activity and remission over time. Therefore, this technique could have a major impact on preclinical *in vivo* imaging aiming to monitor the efficacy of new therapeutic compounds. Furthermore, white blood cells (WBC) radiolabelled with [18F]FDG have been proposed to serve as a quantitative marker of intestinal inflammation (188). This method could be useful to distinguish between non-malignant and malignant tissues where the inflammatory process could interfere in the accuracy of PET imaging. PET/CT technique has also demonstrated its usefulness to evaluate the *in vivo* behaviour of 3D printed devices, allowing the location and tracking of the device in the GI tract of the animal (189).

Currently, other radiotracers are available, such as the [18F]DPA-714, which is a radioligand of the translocator protein 18 kDa (TSPO) that has been used to study inflammation in IBD models. However, it has not yet been implemented in the clinical practice (190).

Figure 6. Image of a micro-PET/CT small animal imaging system (Albira PET/CT Preclinical Imaging System, Bruker Biospin, EEUU).

1.10. MEDICAL IMAGING IN INFLAMMATORY BOWEL DISEASE

Nowadays in clinical practice, endoscopy and biopsy are the gold standards for diagnosis and management of IBD patients. These two procedures are highly invasive and uncomfortable for patients, especially in those cases where evaluations over time are required. Moreover, it is not possible to evaluate the upper part of the small bowel as well as other areas outside the bowel (153).

Classical imaging modalities such as ultrasound, CT enterography and MRI enterography, have been implemented over the last few years as complementary tools that aim to get a solid diagnosis of IBD, especially CD. In addition, these techniques also help in the assessment of disease extent, activity and severity, influencing management decisions such as medication selection or the most appropriate type of surgery (191). Nevertheless, these imaging tools have some limitations. For instance, the difficulties encountered in distinguishing between active inflammatory disease and chronic fibrostenotic disease and the ionizing radiation to which patients are exposed with CT (192). Finally, there is still a need for technologies that provide more cellular level information to better understand the etiology of IBD that could lead to improve therapies aimed at specific biological targets.

Molecular imaging techniques are gaining a role of primary importance in preclinical research since it allows to characterize and quantify biological processes at the molecular and cellular level in living animals, and also to detect molecular alterations at the basis of the pathological pathway. Another asset of these techniques is that repeated evaluations can be carried out on each living animal, thus limiting the number of animals needed for individual measures of intestinal inflammation during the follow-up of the disease (193). Thereby, molecular imaging could help in the identification of biomarkers that will permit to more accurately assess the efficacy and mechanism of action of a new drug in preclinical models (3).

1.11. PHARMACEUTICAL APPROACHES IN INFLAMMATORY BOWEL DISEASE

The therapeutic management of IBD constitutes a special situation in drug delivery since most of its pathological manifestations are located in the gastrointestinal (GI) tract. Therefore, the main approaches have been focused on target formulations to deliver the drug directly in the intestine and retaining it in the intestinal lumen. These strategies are expected to reduce the adverse reactions derived from its systemic absorption and improve the pharmaceutical effect, mainly due to an increased contact time with the inflamed tissue (194).

IBD patients require lifelong treatment, whose two main goals are the induction and maintenance of remission and the prevention of disease flares. Conventional treatments are based on anti-inflammatory drugs (5-aminosalicylic acid and corticosteroids), immunosuppressives (azathioprine, 6-mercaptopurine), antibiotics and biologic agents (Infliximab and other anti-TNF agents). Because of the aim of this section is to review the main dosage forms from the point of view of novel drug delivery strategies, the reader is

referred to other works to obtain more information about pharmacological treatments of IBD (195–197).

Current drug-delivery strategies are focused on targeting the drug to the small intestine and colon. This goal can be achieved mainly through oral, rectal and parenteral administration approaches (198).

1.12. ORAL ROUTE OF ADMINISTRATION

Oral drug-delivery systems for the treatment of IBD have been developed to achieve a more effective drug delivery to the site of the disease. In UC, inflammation appears in a continuous manner in the large intestine, so most of oral dosage forms have been designed to target the colon. In CD, the inflammation is discontinuous and could appear in the entire GI tract, which makes its treatment by oral dosage forms more difficult. This fact has encouraged the research on pharmaceutical technology to develop innovative drug carrier systems, which are intended to deliver the drugs specifically to the inflamed intestinal areas (198).

Targeting drugs to the colon could improve pharmacological effects and reduce adverse reactions. However, several limitations related to biochemical, physical and environmental barriers must be taken into account when a new drug formulation is being developed, such as the different pH values and enzymatic barriers, mucus layer, epithelium, P-glycoprotein efflux pump and microbiota (199).

For instance, the solubility of the drug is affected by the low colonic fluid volume, the pH and the higher viscosity, which may represent a limiting factor for the colonic absorption. The colonic content and the colonic bacterial enzymes could also affect the stability of the drug, rendering it ineffective (4). The existing oral drug-delivery strategies can be divided based on the novelty of its approach.

1.12.1. Conventional pharmaceutical strategies

Several mechanisms have been developed to trigger drug release in the intestine, in particular from the distal ileum to the sigmoid colon. These mechanisms generally respond to variables, mainly time, pH, enzymatic activity and intraluminal pressure.

These conventional strategies have been extensively reviewed elsewhere (200,198). Although its use has been successful in IBD therapy, they may also have some disadvantages. The transit time of the drug through the GI tract is altered in IBD patients compared to the healthy population due to the typical symptoms, such as diarrhoea, which accelerate it. The colonic pH also differs from the normal value, which compromises the accuracy of pH-dependent formulations. In addition, in IBD patients the contractility is decreased, which reduces colonic pressure. The colonic flora is also altered, and in fact, variations in bacterial concentrations were observed, particularly in CD patients (201).

1.12.2. Novel pharmaceutical strategies

To overcome the limitations derived from the use of conventional drug release systems, micro- and nano- sized carriers have been developed to increase colonic residence time and provide additional benefits for IBD therapy. Of particular importance is their high surface-to-mass ratio, which make these carriers capable to bind to the mucous surface and carry many compounds (202).

1.12.2.1.   Micro- and nanoparticles

A size dependent accumulation of micro- and nanoparticles (MPs and NPs) can be observed in the inflamed intestinal tissues, particularly of those smaller than 1000 and 100 nm (203). These smaller drug carriers more effectively pass the mucus barrier due to the average pore size of the mucus, which is below 100 nm, in such a way that smaller particles can diffuse smoothly through it. The transport through the inflamed mucosa depends on particle size. MPs are retained in the superficial layers while NPs penetrate to greater depths. In CD patients, there is an increase in mucus production leading to thicker mucus layer, particularly in ulcerated areas. Therefore, strategies that modify the particle surface such as muco-adhesion, bio-adhesion and muco-penetration could improve targeting and retention of drug delivery systems (204).

The deposition of NPs in the inflamed tissue was evaluated in a TNBS-induced colitis animal model. NPs loaded with an anti-inflammatory were administered to the animals and compared with a control group to which the drug was administered in solution. When the animals were kept without treatment, the group that received NPs continued to show reduced inflammation levels whereas the other group displayed a strong relapse, demonstrating that the nanosized carrier provides a sustained drug release due to the retention of NPs in the inflamed area (205). Several studies such as the one mentioned above have been carried out in animal models of IBD with promising results and translational potential to the treatment of IBD patients (203).

1.12.2.2.   Liposomes

Liposomes are double-layer and sphere-shaped vesicle structures based on phospholipids that are enclosed in aqueous volumes. Due to their amphoteric properties, they are capable of carrying both hydrophilic and lipophilic compounds (206).

The activity of antioxidants encapsulated into negatively charged liposomes was tested in a DNBS-induced colitis animal model. Liposomal preparations were more effective than free molecules in the treatment of colitis, probably due to the binding of negatively charged liposomes to the inflamed mucosa, leading to the accumulation of the antioxidants in

the target area (207). Likewise, budesonide loaded liposomes showed a higher accumulation in the inflamed area due to its lipoidal nature compared to the free drug (208).

1.12.2.3. Self-microemulsifying drug delivery systems

Self-microemulsifying drug delivery systems (SMEDDS) are isotropic mixtures of oil, surfactants, co-surfactants and drug which in contact with aqueous media, spontaneously form oil-in-water (o/w) microemulsion under conditions of agitation. The agitation required for the self-emulsification is provided by the digestive motility of stomach and intestine (209). The nanosized droplets have thermodynamic stability and high surface area, which ensures an effective absorption and delivery of the drug. SMEDDS are particularly useful to enhance oral bioavailability of poorly water soluble drugs by keeping them solubilized in the small oil globules during their transit through the GI tract (210).

SMEDDS formulations containing prednisolone were developed for colon-specific delivery and tested in rats with acetic acid-induced colitis. The results showed a lower histological disease score and a decreased activity of myeloperoxidase (MPO) compared with the group that received standard prednisolone treatment due to the higher accumulation of prednisolone SMEDDS in the inflamed area (210). Likewise, SMEDDS as a carrier of curcumin, a poorly water-soluble drug, were designed and its bioavailability was evaluated in mice, resulting in an increase in the drug dissolution *in vitro* and bioavailability *in vivo* (211).

1.12.2.4. Self-assembled polymer systems: hydrogels

Hydrogels are cross-linked networks of hydrophobic polymeric materials physically or chemically linked to each other. This structure is capable of holding large amounts of water in the 2D or 3D network and release the drug immediately or in a sustained way by mechanisms such as diffusion or erosion (212).

The efficacy of a hydrogel loaded with NPs containing an anti-inflammatory was evaluated in a DSS-induced colitis animal model. Due to the protection of the hydrogel, the NPs were able to pass through the stomach and small intestine without damage and being degraded in the inflamed colon. As a result, there was a reduction in the colitis symptoms accompanied by a reduction in MPO activity and a lower histological disease score (213).

1.13. RECTAL ROUTE OF ADMINISTRATION

Although the oral route is the most convenient route for drug administration, there are circumstances under which it may be preferable to give drugs rectally rather than orally. These special circumstances include the administration of drugs to patients who are unwilling to take drugs orally, with nausea or vomiting and unconscious (214). In these cases, rectal route represents an alternative to administer treatments intended to have both local (215) and systemic effects (216).

Moreover, rectal route has a number of advantages, such as the minimization of first-pass effect, which could be useful for drugs that undergo high hepatic first-pass metabolism. Drugs administered in the lower part of the rectum are firstly delivered into the venous circulation before their pass through the liver and, therefore, avoid the first-pass effect. However, complete avoidance of first-pass metabolism cannot be guaranteed by rectal administration since the superior rectal vein empties in the portal venous system (217). This route could be also useful for drugs with limited absorption in the upper GI tract, unstable in gastric medium or those that cause irritation to gastric mucosa. Furthermore, this route is commonly used for the administration of drugs that exert a local action on the rectum or distal colon, such as some drugs used in IBD therapy. As a consequence of the local administration of the drug, systemic absorption decreases and, therefore, adverse effects are also reduced (215,218).

The main rectal formulations for drug delivery to the rectum and lower parts of the distal colon are liquid dosage forms (e.g., enemas), semi-solid dosage forms (e.g., foams, gels and creams) and solid dosage forms (e.g., suppositories and capsules).

1.13.1. Liquid dosage forms

Enemas are the main liquid dosage form for rectal drug delivery and are commonly administered from disposable squeeze bottles with an extended tip for rectal insertion. The drug contained on them is typically in the form of solution, suspension or emulsion (218). Enemas extend from rectum to the sigmoid colon and even the transverse colon, depending on the volume administered (219). Moreover, the composition of the enema could promote its systemic absorption or, on the contrary, its local effect. A study showed that strongly hypotonic or hypertonic enemas caused rapid systemic drug absorption, whereas moderately hypotonic enemas showed minimal systemic drug absorption and high local tissue levels (220). Enemas are commonly used for the localized treatment of IBD (221), to stimulate defecation before operative procedures (222) or as a medium to deliver contrast agent before radiographic examination (223).

1.13.2. Semi-solid dosage forms

Foams and gels are common rectal semi-solid dosage forms in which the drug is dispersed in either hydrophilic or lipophilic base together with other excipients. These formulations are usually packed in a collapsible tube with an applicator (224). In particular, rectal foams extend form the rectum to the sigmoid colon and overcome some inconveniences of enemas, such as the difficulty some patients experience in retaining the liquid enema after administration. Compared to liquid formulations, rectal foams are characterized by a higher viscosity, a finer dispersion on the colonic mucosa and a greater adhesiveness to the colonic mucosa (225).

On the other hand, rectal gels could be formulated using thermosensitive polymers (e.g., poloxamers) that are in a liquid state at room temperature and convert into a gel at body

temperature, which provides them with improved contact with the rectal mucosal surface reducing leakage (218). To improve the strength and adhesion properties of thermosensitive polymers, they can be used in combination with mucoadhesive polymers, such as hydroxypropyl methylcellulose and sodium alginate (226). Rectal gels (227) and foams (228) are used for the localized treatment of IBD or to be delivered to systemic circulation for the treatment of some medical conditions, such as seizures (229).

1.13.3. Solid dosage forms

Suppositories are the most common solid dosage form in which the drug is solubilized or suspended in a suppository base. Suppositories can be formulated using lipophilic or hydrophilic bases to form a homogeneous system with the drug (224). Lipophilic bases, such as coconut oil, cocoa butter and hydrogenated vegetable oils, melt at body temperature and do not require fluids to spread and release the drug, making them ideal for the rectum. On the other hand, hydrophilic bases, such as polyethylene glycols and glycerinated gelatin, are unaffected by body temperature and need to dissolve in the physiological fluids for drug release, which make them a more appropriate vehicle for vaginal application (230).

Moreover, it is possible to modulate drug release rate from suppositories. For instance, the release of drugs that are soluble in the suppository base occurs as the suppository melts, whereas drugs that are poorly soluble in the suppository base leave the dosage form more easily and begin to solubilize in the physiological fluid. These means that hydrophobic drugs will show faster release form lipophilic bases and lipophilic drugs will show faster release from hydrophilic ones (218,231). As an example of clinical applications, it could be mentioned the use of rectal suppositories loaded with mesalazine (232) or tacrolimus (233) for the topical treatment of UC.

1.14. PARENTERAL ROUTE OF ADMINISTRATION

The parenteral route is used for a systemic immune suppressive therapy in case of a severe exacerbation or severe extra-intestinal disease. Solutions, suspensions and emulsions mainly of corticosteroids and anti-TNF agents, are administered by an intravenous, subcutaneous or intramuscular injection. This route has some advantages, such as fast drug reaction and no first-pass effect, obtaining a bioavailability of almost 100%. Conversely, this kind of administration has the potential risk of adverse reactions (198).

1.15. 3D PRINTING IN PHARMACEUTICALS

Current pharmaceutical manufacturing is based on the mass production of medicines with a limited number of dose-strengths of each drug. This traditional approach has been successful providing good-quality drug products to the patients and reducing the overall per unit production cost. The most common medicines are solid dosage forms for oral drug delivery,

being tablets the most widely used. These formulations consist of a mixture of one or more drugs (active pharmaceutical ingredient) and excipients (inactive ingredients), showing different shapes (cylindrical, oblong, etc.) and designed to fulfil specific drug delivery requirements (234).

Although this conventional approach offers advantages for both patients and manufacturers, it also presents some drawbacks, such as limitations in the range of doses and dose combinations in marketed products. With the advent of digital technologies, significant opportunities have emerged to improve the development and manufacture of pharmaceutical products. In this sense, three-dimensional printing (3DP) technology has represented a major breakthrough in the pharmaceutical sector since it constitutes an effective strategy to overcome some challenges of current pharmaceutical manufacturing. 3DP is an additive manufacturing method that enables the production of bespoke objects in a layer-by-layer fashion. The physical object to be printed can be designed by a computer-aided design (CAD) software and the 3D model exported to be printed layer-by-layer, creating an individualized object with the desired shape and size. These unique manufacturing process could make 3DP a revolutionary technology to prepare formulations and medical devices that could be tailored to meet the individual needs of each patient (235). As an example, printlets (3D printed tablets) can be prepared with a defined drug dose, size and shape combining one or more drugs into a single formulation, improving the efficacy of the treatment and reducing side effects (236). It is forecasted that these innovative printlets will be prepared on-demand, close to the patient, at the dispensing point (237).

3D printing of medicines has become a hot topic in the pharmaceutical industry since the US Food and Drug Administration (FDA) approved Spritam, the first 3D printed tablet in 2015 (238). The formulation created by Aprecia Pharmaceuticals for the treatment of epilepsy is an oral medicine that rapidly disintegrates in the mouth with a sip of liquid to facilitate swallowing. Spritam includes high dose of drug so it is especially useful for patients who have swallowing difficulties, such as children, the elderly and people with neurological disorders. However, this medicine is manufactured in industrial facilities and it is not an example of personalized dose medicines.

The big pharmaceutical companies and regulatory authorities like the Food and Drug Administration (FDA) in US or the European Medicines Agency (EMA) in EU are in the process of evaluating the 3DP technology and adopting it for the manufacture of medicines.

1.16. PHARMACEUTICAL 3D PRINTING TECHNOLOGIES

3D printing, otherwise known as additive manufacturing, is a generic term that encompasses a range of different printing technologies, which have in common the construction of objects in a layer-by-layer manner. Independently of used technique; the whole process starts by designing the object to be printed with a CAD software package. Afterwards, the 3D design is divided into a series of layers and exported to the 3D printer. As a result, a bespoke object of

virtually any shape and size can be produced. Since the entire manufacturing process is a computer-controlled procedure, any desired change in the final object can be achieved by a modification of the CAD file. Based on the American Society for Testing and Materials (ASTM) scheme, the different 3DP technologies can be classified into seven main categories (239). Since three of the technologies are not very suitable for drug products, in this chapter, the pharmaceutical application of only four of them is described: binder jetting, material extrusion, power bed fusion and vat polymerization.

1.16.1. Binder jetting

Binder jetting was first invented and patented in 1989 by Sachs et al. (240) at the Massachusetts Institute of Technology (MIT). In this type of printing a liquid binding solution is selectively deposited with a printer nozzle over a thin layer of powder (powder bed). The powder particles wetted by the binder solution adhere together, causing layer solidification. Once the layer is printed, a new layer of powder is spread over the bed, often employing a blade or a roller, and the process is repeated sequentially to produce successive layers of selected regions of bonded powder until the printing process is completed. Finally, the 3D printed object is extracted from the powder bed and excess unbound powder is removed (241).

The applications of binder jetting in healthcare were licensed to Therics Inc., trademarked as TheriForm in 1994 (242). The initial pharmaceutical development of TheriForm focused primarily on the deposition of drug loaded liquids onto powder bed made of pharmaceutical excipients to form immediate, extended, or multi release tablets. The main disadvantage of this approach is the limited options to obtain drug loaded inks that could perform consistent jetting. An alternative approach involves the deposition of liquid binder onto a powder beds incorporating not only excipients but also the drug. This technique is the basis of ZipDose technology, which was used to manufacture the first FDA approved 3D printed tablet (Spritam by Aprecia Pharmaceuticals) in 2015 (243). Spritam tablets are specially designed to quickly dissolve in the mouth, in less than 11 s, needing only small amount of saliva. This technology allows the production of high dose medications, up to 1000 mg, which is a very high dose for an orodispersible tablet. ZipDose technology was scaled up using multiple nozzles that deposit the binding solution onto a powder bed transported on a conveyor belt. Tablets are gradually built layer-by-layer until they are completed, then, the tablets are removed from the powder bed, dried and packed (244). ZipDose technology represents an alternative to manufacture dosage forms that cannot be manufactured by conventional processes.

Other examples of fast dissolving tablets developed using binder jetting include drug delivery devices with a predefined inner structure of unbound powder surrounded by an external region of bound powder (245). Binder jetting has also been used to create zero-order drug release formulations composed of an immediate release core and a shell that control the drug release (246). Other types of delayed release tablets were also developed with excellent

content uniformity and also demonstrating that 3DP is capable of accurately construct dosage forms containing a few micrograms of drug (247).

The main commercial application of this technique in the pharma field is its ability to formulate highly porous, fast dissolving tablets with high drug loadings, as in Spritam. However, multiple tablet structures could be produced, enabling the creation of 3DP objects with highly complex geometries. Binder jetting also has some drawbacks, for instance, the high porosity of the tablet could affect the mechanical strength and friability of the formulation. Another limitation is that it is not possible to print hollow objects as the powder is filling all the spaces. Furthermore, additional excess powder removal and drying steps are required to obtain tablets without lose particles and to evaporate any residual solvent (248).

1.16.2. Material extrusion

1.16.2.1.   Fused deposition modelling
Fused deposition modelling (FDM), also known as fused filament fabrication (FFF), is possibly one of the most common and affordable printing technologies. In this 3DP technique, a polymer filament is heated and extruded through a small heated tip. The soften polymer is deposited onto a building plate to harden, creating one layer of the object to be fabricated, subsequently, the build plate moves down and the next layer is deposited and so on until finally create the 3D printed object (249).

Goyanes et al. (249) were one of the first researchers to demonstrate the feasibility of FDM to fabricate drug loaded tablets. Polyvinyl alcohol (PVA) filaments were loaded with fluorescein (used as a model drug) by placing them into an ethanolic solution of fluorescein. It is possible to print tablets with different drug release profiles by modifying printer parameters like the infill percentage of the formulations. PVA filaments were loaded by diffusion using different model drugs including prednisolone and aminosalicylates (250,251). During the printing process of PVA filaments loaded with two aminosalicylate isomers used in the treatment of colonic conditions (5-ASA and 4-ASA), 4-ASA (thermally labile) was significant degraded, while 5-ASA (nonthermally labile) did not suffer degradation (251). This show that FDM may not be suitable for the manufacture of drugs with degradation temperatures lower than the printing temperature. This finding lead to the search of new excipients that can print at lower temperatures that PVA to avoid degradation of the drug (252–254).

The drug loaded filaments are currently manufactured by hot melt extrusion (HME), which involves the mixing excipients and/or drugs together and the application of heat and pressure to force the mixture to pass through a die (255). This highly versatile technology is widely used within the pharmaceutical sector and the FDA has already approved several hot melt extruded products (256). First time combination of HME and FDM was used to fabricate printlets with different shapes (cube, pyramid, cylinder, sphere and torus) and sizes. Drug release was dependent on the surface area to volume ratio of the formulations, so changing the

shape and/or the size of printlets will result in a different drug release profile (257). The shape of the formulations can change drug release from the printlets but also modify medicine acceptability, as shown in the first patient acceptability study in humans, conducted with 3D printed tablets manufactured by FDM 3DP (258). The results showed that patients have preference for torus shape printlets, and other factors, such as colour and size, could affect the willingness of people to shallow the printlets. This fact gains importance in certain age groups such as paediatric patients or the elderly, where a more attractive dosage form could improve patients' acceptability of medications and adherence to the treatment.

HME and FDM was combined with fluid bed coating to create a new modified release dosage form loaded with budesonide, also used in the treatment of colonic conditions (259). The 3D printed cores were coated with an enteric polymer to provide them with enteric properties. The resultant capsule shaped tablets (caplets) were compared with commercial budesonide products, demonstrating the potential of FDM combined with established pharmaceutical processes to manufacture oral dosage forms. In order to avoid the need for a separate coating process, different alternatives were processed like printing a shell using a dual 3D printer (260,261) or the use of 3D printed capsular devices made with different excipients (262–264). The manufacturing process was also improved by developing a single filament that incorporates different grades of drug loading, enteric polymer and infill, obtaining printlets (3D-printed tablets) with different delayed release patterns, making it possible to target different regions of the gastrointestinal tract (236). The effect of the microstructure of the extruded filament and the 3D printed tablets on drug dissolution rate was also investigated (265), concluding that the porosity of the tablets did not affect the drug release, which could ultimately be controlled by diffusion/erosion mechanisms.

Another asset of FDM is the possibility of incorporating different drugs in the same 3D printed tablet (polypill). This could be achieved through the construction of tablets containing distinct regions, where multiple combinations of drugs and polymers are possible. The same drug could be incorporated in different polymers, or different drugs could be incorporated in the same polymer, so that the drug release profiles could be modulated (266,267). Furthermore, it is possible to develop 3D printed tablets loaded with polymeric nanocapsules by soaking the printed devices in a nanoparticle liquid suspension. This strategy offers a useful approach to convert nanocapsules liquid suspensions into solid drug dosage forms with tailored dose and drug release profiles (268). Apart from tablets, another FDM application that is worth mentioning is the manufacture of personalized wound dressings through the combination of 3D scanning and 3D printing (269). In this work, metal ions were incorporated into PCL filaments to print dressings against scanned templates of a target wound, creating anatomically adaptable dressings that can be tailored to the particular needs of each patient.

In the pharmaceutical field, FDM is one of the most feasible 3DP technologies due to the low cost of the printers and the high range of usable materials. The 3D printed devices show high mechanical strength, which makes them stable throughout different forms of

processing. Moreover, several materials could be integrated into the same printing layer, making FDM a highly efficient process. Nevertheless, FDM also has some limitations, such as the heat needed for the extrusion and printing. This could be partially avoided by the selection of polymers with lower melting temperatures and, if possible, polymers with melting temperatures lower than the melting temperature of the drugs (270,271). Another limitation is the need for the preparation of drug loaded filaments as previous step for 3D printing.

1.16.2.2. Direct powder extrusion

Direct powder extrusion involves the extrusion of material in the form of powder through the nozzle of the printer, which uses a single screw extruder. Unlike FDM, direct powder extrusion is a single step technology that does not require the preparation of filaments using HME. Since the HME step is avoided, this technique may be especially useful for preparing formulations as amorphous dispersions using small amounts of drugs and excipients. This could be advantageous for preclinical and clinical studies, where the quantity of drugs is often limited. By using a direct powder extruder 3D printer, sustained release printlets containing a poorly soluble drug were prepared, and the effect of different hydroxypropylcellulose (HPC) grades on the final printlets was also evaluated (272).

1.16.3. Gel/paste extrusion

Gel extrusion, also known as semisolid extrusion (SSE), is a manufacturing technique that employs a syringe-like system to deposit semisolids, such as gel or pastes, onto a build plate to create a solid object. As in FDM, the extruded material hardens following cooling or by solvent evaporation, which allows the material to support the weight of subsequent layers (273).

Semisolids commonly used in pharmaceuticals can be formulated by mixing the polymers, drugs and solvents in the correct ratio to produce formulations of an adequate viscosity for printing. The viscosity of the material to be extruded and the position of the extrusion head with respect to the bedplate can significantly impact the printing process. Moreover, to facilitate the removal of the object from the printing bed, the surface of the bed could be heated to minimize the adherence of the base layers thereto (273).

SSE technique has been used to produce a number of formulations, such as bilayer tablets (274) and polypills capable of delivering multiple drugs in an immediate or sustained release manner through different release mechanisms, such as osmosis and diffusion (275,276). Another application of SSE technology is found in the fabrication of fast dissolving tablets. As an example, it could be mentioned the manufacture of high drug loading paracetamol oral tablets with an immediate release profile that achieve disintegration in less than 60 s and almost complete release of paracetamol within 5 min (277). One interesting approach in this field of orodispersible printlets is the use of cyclodextrins as excipients in the fabrication of printlets loaded with poorly soluble drugs. This is the case of the rapid release formulations of

the hydrophobic drug carbamazepine prepared with hydroxypropil-β-cyclodextrin (HPβCD), which acts as a soluble filler and forms drug- HPβCD complexes (278). This technology was used to fabricate chewable formulations in a hospital setting for patients with a rare metabolic disease (237). This was the first clinical study using 3D printing to prepare personalized dose medicines. The printlets had a good acceptance among patients and were able to maintain the optimum range of isoleucine levels in the blood of the patients.

Furthermore, this technology has also been applied to prepare lipid-based formulations, including suppositories. Self-microemulsifying drug delivery systems (SMEDDS) are liquid formulations that form oil-in-water (O/W) emulsions in the gastrointestinal tract allowing the solubilization of lipophilic drugs in the small lipid droplets (279). SSE technique have made possible the transformation of these liquid formulations into solid self-microemulsifying drug delivery systems (S-SMEDDS) with different geometrical shapes (cylindrical, prism, cube and torus) (280). These printlets with different geometries were evaluated under simulated gastric conditions and the obtained results indicated that geometry affects the dispersion time, obtaining the shortest dispersion time for torus shapes (Figure 7).
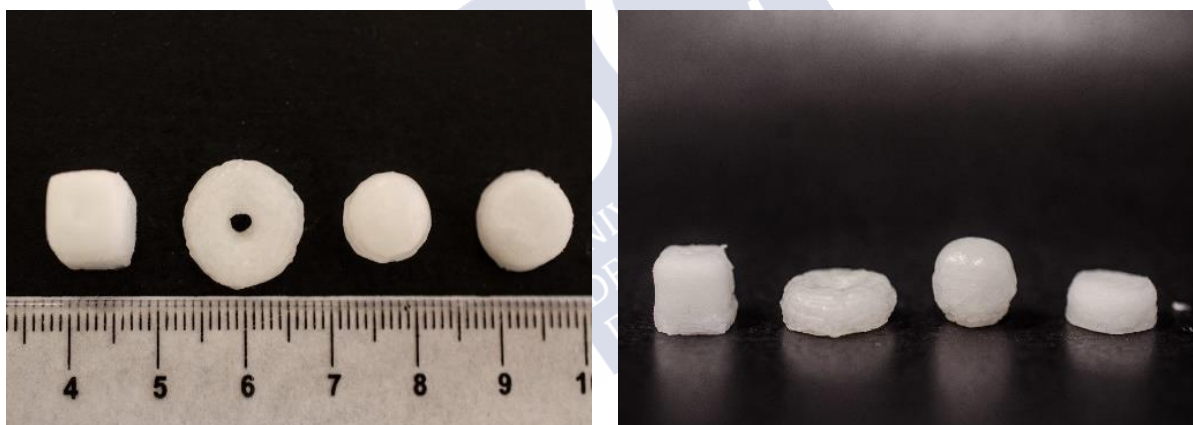
Figure 7. Printlets with different geometries fabricated by semisolid extrusion 3D printing.

SSE stands out for its simplicity, since drugs and excipients can be mixed directly forming the gel/paste base for printing. Moreover, the heat applied to obtain a suitable viscosity of the feedstock (if any needed) is much lower than in other 3DP techniques, being thus possible to utilize thermolabile drugs. Due to the necessity to accommodate the viscous material, the nozzle heads need wider orifices, which affects the resolution of the printer. However, this low resolution allows to achieve higher printing speed rates than other 3DP technologies (273).

1.16.4. Powder bed fusion
Power bed fusion is a selective thermal process that involves the fusion of powder particles by the application of a heat source, such as a laser. This technology includes

selective laser sintering (SLS), which employs a laser to build up a 3D printed object from a powder bed. The laser binds the powder particles together forming a solid structure with a specific pattern. Once the first layer is completed, a new layer of powder is deposited on top of the previous one and the process is repeated sequentially, building the object in a layer-wise manner. Finally, the object is recovered from underneath the powder bed (281).

SLS technique has been used in a variety of medical applications including the production of patient-specific anatomical models (282), implantable devices (283) and in the field of tissue engineering (284). Commonly used materials for SLS are polymeric powdered forms of plastics, metal alloys and ceramics that require high temperatures to be sintered, which may cause drug or excipient degradation. Because of these harsh printing conditions, the entry of SLS technology in the pharmaceutical field has been hampered for years (285).

In 2017, oral printlets were first manufactured using a SLS 3D printer (281). The printlets were prepared using pharmaceutical grade polymers and no degradation of the drug was observed. The 3D printer used in the study contained a diode laser with emits a lower intensity laser compared to the more potent infrared CO_2 lasers, that have been tested before to prepare drug delivery systems (283–286). This initial work led to the development of printlets with orally disintegrating properties and accelerated drug release (286), as well as printlets with gyroid lattice structures having customisable drug release characteristics (287). SLS technique was also used to produce small 3D printed pellets (miniprintlets) containing two different drugs with customized drug release patterns (288). These studies demonstrate that by simply changing the 3D design, the drug release profiles of different polymers can be modified, which allows to tailor the dosage form to the individual needs of each patient.

SLS technology offers some advantages over other printing techniques. For instance, SLS is a solvent free process and offers faster production as compared to binder jetting, which may require around 48 h post manufacture to allow the solvent to evaporate (289). Moreover, SLS does not require the prior production of drug loaded filaments as in the case of FDM, only a suitable powder mixture is required (252).

In addition, SLS produces objects of higher resolution due the precision of the laser compared to those produced by other methods, such as FDM or semisolid extrusion.

1.16.5. Vat polymerization

Vat polymerization process selectively cures a vat of liquid photopolymer, transforming it into a solid through the application of a light source. In this technology is included the technology called stereolithography (SLA), which uses a laser to induce the solidification of a liquid resin by photopolymerization. In this process the photoinitiator and the photopolimerizable resin are placed in a build tank exposed to a high energy light source focused to a particular depth. The photoinitiator undergoes a reaction producing initiating species, such as free radicals, which attack the monomer units of the resin adding more monomers/oligomers and, consequently, crosslinking takes place. When the first layer of the

object is solidified, the build plate moves up to a defined distance according to the desired thickness of each layer and more liquid resin is redistributed on the top of the previous layer. The process is repeated until the object is built layer-by-layer and, finally, the 3D printed object is washed to remove any excess liquid resin (290).

The possibilities for using SLA in the biomedical area are numerous (291). For instance, SLA can be applied to tissue engineering for fabricating very precise moulds using 3D models obtained by micro-computed tomography (CT), as well as scaffolds (292,293) and 3D-printed biomimetic hydrogels that simulate tissues with detoxification properties (294) due to its high accuracy for manufacturing complex structures. Moreover, SLA printing can be used to produce medical devices, such as personalised anti-acne masks loaded with drugs like salicylic acid (295).

In the field of oral drug delivery, the use of SLA is more recent. This printing technique has been used to produce oral modified release dosage forms loaded with paracetamol and 4-aminosalicylic acid (4-ASA) (296). The drug 4-ASA is known to be thermally labile, however, no drug degradation occurred during the printing process, which makes SLA an interesting alternative to print objects loaded with thermolabile drugs. SLA was also used to fabricate ibuprofen loaded hydrogels with different water content using riboflavin as a non-toxic photo-initiator. Hydrogels with higher water content showed faster drug release rates (297). Other study investigated the effect of geometric parameters on the drug release kinetics of SLA printlets, having the greatest influence on them the constant surface area/volume ratio (SA/V). This implies that the specific drug release profile can be maintained by changing the SA/V ratio (298). One limitation of SLA is the production of polypills due to the difficulty of printing spatially separated layers, although some printlets incorporating up to 6 drugs were prepared (299).

Among the advantages of this technology, it could be mentioned the possibility of dissolving or dispersing the drugs directly in the resin to incorporate them into the printing object. Moreover, SLA is capable of producing objects with complex geometries and allows to achieve higher accuracy and resolution than other printing technologies (300). The photopolymerization reactions are considered to be a green technology since they are solvent-free and require low electrical input and low temperature of operation. Nevertheless, the use of SLA for biomedical and pharmaceutical purposes has some limitations, mainly due to the appreciable toxicity that photopolimerizable chemicals tend to have, along with the limited number of biocompatible resins that are commercially available for SLA (290). Another drawback is that some drugs may chemically react with the monomers during the printing process preventing any drug release from the printlets (301).

1.17. 3D PRINTING: A NEW ERA OF PERSONALIZED MEDICINE

The numerous applications of 3DP to pharmaceuticals are evident. The advent of personalized medicine involves a shift away from the traditional one-size-fits-all approach, to one in which

the management of a patient´s health is based on the individual patient´s specific characteristics. But to make this possible, it is essential to understand how a person´s unique genetic profile makes them susceptible to a certain disease (302). Since the first draft of the human sequence has been announced in 2000 (303), there has been a dramatic drop in DNA sequencing costs, mainly due to the new sequencing technology and the development of high speed computing needed for analysis, which has allowed this technology to be considered as part of routine healthcare. The integration of genetic information and other clinical data results in the discovery of new pathways involved in diseases, and in extension, helps to understand the mode of action of the pharmaceutical products (304).

Based on this approach, different subtypes of patients within a given condition can be identified, and treatment can be tailored to match an individual´s underlying cause. However, this tailoring of medical treatment to the patient´s unique genetic make-up has not yet been fully achieved, and one of the major issues that have contributed to this delay is manufacturing technology. Traditional pharmaceutical manufacturing processes are unsuitable for the production of personalized medicines, since they are based on mass production of fixed dose medicines, which limits the commercial availability of doses or dose combinations (244). Therefore, it is evident that before this new era of personalized medicine can truly begin, the pharmaceutical industry has to adapt and embrace new innovative technologies for tailored therapy production. 3DP technologies have the potential to reshape the way that medicines are designed and manufactured. This technology is forecast to play a major role in the production of highly flexible and customized dosage forms on-demand, overcoming the limitations of conventional manufacturing processes.

1.18. THE UNLIMITED POSSIBILITIES OF 3D PRINTING IN HEALTHCARE

The therapeutic doses of the drugs that are used in clinical practice are selected in early phase clinical trials based on the doses that exerted a therapeutic effect in the majority of patients. This dosing approach focuses on the average patient and, to certain extent, does not normally take into account the variability between patients based on their genetic profiles, disease state and other factors such as age, weight and gender (305). Hence, it is expected that the response to drug therapy and the susceptibility to side effects may differ between each patient. This is of particular importance for drugs with narrow therapeutic index where the interindividual variability of the response increases the likelihood of serious adverse effects or otherwise inadequate therapeutic levels (306). This understanding laid the foundations for the development of personalized medicine, which aims to tailor the treatment according to each patient´s individual characteristics, needs and preferences. The ideal dosing method for personalization should be accurate, simple, cheap and suitable for the maximum number of patients, starting from young children to the elderly (307).

3DP technologies have the potential to lead the way for this era of personalized medicine, revolutionizing the way medicines are made. Instead of using conventional large batches processes, 3DP offers the opportunity to produce customized 3D-printed tablets (printlets)

with a tailored dose, shape, size and release characteristics, far from the traditional "one-size-fits-all" approach. In a digital pharmacy era, the specific prescription for a particular patient could be sent directly to the compounding pharmacy or the hospital pharmacy setting and small batches of individualized printlets could be produced with the appropriate dosage, drugs combinations and formulation type specially designed to suit the patient (308,309). Furthermore, the high automation of the printing process and the lower number of production steps reduce the possibility of human errors, for example weighting errors, increasing the safety of the formulations prepared in pharmacies and hospitals.

Quality control analysis in solid oral dosage forms is commonly performed by high performance liquid chromatography (HPLC) and UV spectroscopy, which are destructive methods that require sample preparation and are not suitable for small batches produced by 3DP. In this regard, analytical alternatives to test content uniformity and dose verification in 3D printed dosage forms have been explored. For instance, near infrared (NIR) and Raman spectroscopy have shown to be capable of performing quality control measures of medicines in a non-destructive manner (310,311). In particular, NIR spectroscopy was used as non-destructive method for quality control tests in printlets, obtaining a sensitivity comparable to that of chromatographic and UV spectroscopy methods (312). Other interesting technique is terahertz pulsing imaging (TPI), which allows the acquisition of single depth-resolved scans in a few milliseconds. Terahertz radiation penetrates through polymeric materials, which makes it an attractive tool for the non-destructive analysis of 3D printed products (313). Moreover, inkjet printing has been used to produce dosage forms in the pattern of a quick response (QR) codes. This edible printed pattern contains the drug itself and information relevant for the patient or healthcare professionals readable by a smartphone (314). The tracking of printlets through the supply chain is also possible by printing quick response (QR) codes and data matrices onto the surface of the printlet. Anticounterfeiting strategies could be also implemented through the deposition in the printlet of inks detectable by Raman spectroscopy (315).

Overall, the digitalization of the printing process together with the new analytical approaches and tracking methods can make a significant contribution to the safety of 3D printed medicines. However, the combined efforts of industry, pharmacies and regulatory agencies are necessary to set a path to full 3DP implementation in clinical practice.

1.18.1. Manufacturing of personalized printlets on-demand

The demand for personalized medicines is expected to increase in the coming years, especially for paediatric and geriatric patients. These patients differ in many aspects from the "standard patient", in which pharmaceutical industry focuses during the drug development process. Dose requirements in children and older patients can be markedly different compared to the average patient, mainly due to physiological changes, differences in physical characteristics (e.g., age, body weight and surface area) and pharmacokinetics (e.g., changes in metabolic functions and in renal clearance) (316).

Drug dosing in children is commonly extrapolated linearly from adult doses with adjustments based on body weight, length and age (317). They receive medicines initially designed for adults despite the important differences in pharmacokinetics and pharmacodynamics. This practice is called "unlicensed" or "off label use", and may result in serious toxicity and inadequate clinical responses (318). In the case of the elderly, it is common to find patients aged 65 years or more who are prescribed more than one medicine and also have comorbidities that further complicate the situation (319). The high rate of prescribed drugs increases the likelihood of drugs interaction and thus the risk of drug-related hospitalizations. According to a systematic review, up to 10% of hospitalizations in adults are drug-related (320). Older adults reported a higher prevalence, comprising around 30% of all hospitalizations (321).

Another problem arises in the case of medicines with few available strengths or in a single type formulation. It is common among patients and carers to achieve the target dose by means of splitting the tablets, which results in variations in the drug content of each part (305). Moreover, when there are no suitable dosage forms available for specific patients, they must be extemporaneously compounded by pharmacists or clinical staff, for example by crushing the tablets or using the contents of the capsules. This lead to a number of risks, such as compounding errors and inaccurate dosing (322).

The majority of these challenges could be easily overcome by the implementation of 3DP in clinical practice (Figure 8). Pharmacists and clinical staff could design a personalized printlet containing an exact dosage of drug or drug combination for each patient (308). A great example of the benefits derived from the use of this technology is found in the first clinical study using 3D printed medicines in paediatric patients (237). In this study, a pharmaceutical 3D printer was integrated into the Pharmacy Department of the Clinic University Hospital of Santiago de Compostela (Spain), to produce chewable printlets containing personalized dosages of isoleucine intended to treat children with maple syrup urine disease (MSUD). The dosage forms were printed in a variety of colours and flavours that were well accepted amongst all patients. The results shown that a tighter control over target blood levels is obtained compared to the extemporaneous formulations prepared by clinical staff, which were the standard therapy. Other examples of the potential applicability of 3DP could be found in the manufacture of liquid capsules (260) or immediate release tablets (254) containing individualized doses of theophylline (a narrow therapeutic index drug), as well as controlled release tablets loaded with the corticosteroids prednisolone (250) and budesonide (259).

Figure 8. Image of a 3D printer suitable for the manufacture of pharmaceutical products (M3DIMAKER ™, FabRx Ltd., UK).

1.18.2. Patient-friendly formulations

An appropriate pharmaceutical design of a dosage form is a key aspect to improve acceptability and patient outcomes. This is of especial importance in paediatric and geriatric populations, as they differ in many aspects from the other age subsets of population and, therefore, require particular considerations regarding the physical characteristics of formulations intended for them (323). For instance, the ability to swallow the dosage form intact (e.g., capsules or tablets) largely determine the acceptability of medicines in older patients, whereas formulation factors such as taste, smell and viscosity are important features for paediatric medicines. Dysphagia (difficulty in swallowing) can occur in both populations, being associated with an age-related decline in swallowing function in the elderly, and with developmental, behavioural and psychological disorders in children (323).

Oral liquid formulations are regarded as appropriated dosage forms for children and the geriatric patients due to advantages such as dose flexibility and ease of swallowing. Nevertheless, palatability is a critical factor for the acceptance of these formulations. Many drugs and excipients are known to have an aversive taste, and other attributes such as viscosity, particle size and smell also affect the acceptability of the product (324). In this regard, orally disintegrating tablets (ODTs) and chewable tablets represent an interesting approach especially if they could be administered without water. For instance, 3D printed orodispersible films (ODFs) for children were successfully prepared in a hospital pharmacy setting (325) as an alternative to the established method of producing patient-tailored warfarin doses. The 3D printed ODFs displayed improved drug content along with other advantages, such as the administration directly into the patient´s mouth without the need for water. On the contrary, the unit dose sachets prepared by the conventional method need to be dissolved in a liquid prior to administration. Moreover, 3D printed ODTs could be especially useful for

patients who are purposely non-adherent, such as patients with psychiatric disorders, since it is more difficult to hide the formulation in the mouth or to split it out (326).

Apart from palatability and size (327), other characteristics of oral drug products, such as the shape and colour of the dosage form, could strongly affect the end user willingness to take their medication. One study found that patients consider polypills to be an adequate way to reduce the number of medicines. Moreover, acceptability of 3D printed medicines was determined based on whether patients relied on 3DP technology (328). Another study investigated the influence of shape of different printlets on patient acceptability regarding picking and swallowing (258). Among the different printed shapes (sphere, torus, disc, tilted, capsule, pentagon, diamond, heart, triangle and cube), torus shape was found to be an acceptable novel shape together with capsule and disc shapes, which were found to be acceptable mainly due to their familiar geometry associated with conventional medicines.

1.18.3. 3D printed polypills for complex dosage regimes

Printing technologies could make a significant contribution to treatment adherence and safety of patients with complex dosage regimes. Polypharmacy (the concurrent use of multiple medicines) is a common problem among elderly and hospitalized patients, which are affected by high tablet burdens with different dosing regimens. 3DP offers the possibility of loading different drugs in a single tablet, called polypill (329) (Figure 9). These polypills offer an innovative approach for personalized medicine, designing multiple drug containing devices with specific pharmacokinetics characteristics that would not otherwise be created using conventional manufacturing methods. Different 3DP technologies have already been used to manufacture polypills with varying designs and release profiles (276,299,330). In the same way, safety issues arising from the use of narrow therapeutic index (TI) drugs could also be overcome through the use of 3DP. Narrow TI drugs show a small range between their effective and toxic dose (306), which could lead to an increased risk of adverse effects. By the use of 3DP, printlets with an exact dose of the drug could be created, thus reducing the risk of medication errors arising from the incorrect manipulation of conventional fixed-strength tablets in order to create the customized formulation (261). Furthermore, conventional fabrication techniques are ineffective in controlling the release of two or more drugs independently in different areas of the GI tract. However, through the use of 3DP techniques, the manufacture of polypills containing multiple drugs accommodated in multiple polymers becomes possible. These formulations could be tailored to the specific characteristics of each patient, adjusting the formulation to the individual´s gastric transit time, pH and even microflora depending on the disease state (331,332).
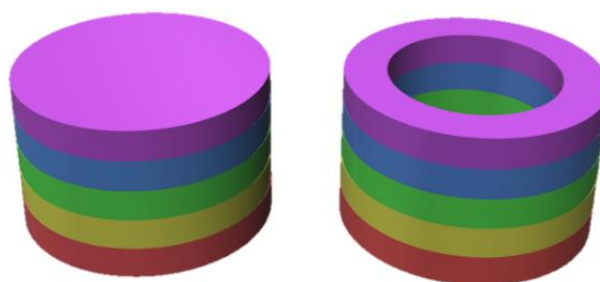
Figure 9. 3D design of polypills containing multiple drugs. On the left a cylinder design and on the right a ring design. In both cases, each layer corresponds to a different drug.

1.18.4. 4D printing

4D printing (4DP) is a relatively new concept originated by integrating a new dimension to 3DP technology; namely time. 4DP involves the use of smart materials with the ability to change their configuration over time in response to an external stimulus such as pH, light, heat, moisture and magnetic or electric forces (333). In the field of bioengineering, the production of dynamic 3D printed structures by 4DP has been applied in tissue engineering, for example in constructing patient specific scaffolds (334). Moreover, medical devices such as stents can be printed, deformed into its temporary shape, inserted in the body and then deployed back into its permanent shape through the use of a thermal stimulus. These 4D printed stents better match the particular structure, improving the prognosis of the patients (335). Despite the high potential of 4DP, this technique has not yet been fully exploited in the pharmaceutical field. One study explored the viability of 4DP approach to fabricate retentive intravesical delivery systems (336). The devices have water-induced shape memory, which allows them to be retained in the bladder with no need for being removed due to its erosion/dissolution over time. In addition, the release rate of the drug could be modified by changing the molecular weight of the polymer. Future applications of 4DP within pharmaceuticals could help to manufacture medicines that were previously challenging to produce, opening new perspectives in personalized drug manufacturing.

1.19. THE POTENTIAL ROLE OF 3D PRINTING IN DRUG DEVELOPMENT

Early phase drug development comprises several stages, from drug discovery and preclinical studies in animals to first-in-human (FIH) clinical trials. At the end of this timeline, the financial burden for the pharmaceutical industry created by the cost of bringing a new compound into commercialisation is really high, while the clinical approval success rate is very low (337). For this reason, the development of innovative technologies that could optimize the drug development process becomes essential, allowing the identification of new drug candidates as early as possible at a minimal cost (338). When a compound with therapeutic potential is discovered, a series of steps must be followed until the final formulation is obtained (339). The selection of an appropriate formulation and its optimization

is one of the main steps in the development process. It is at this stage where 3DP could play a major role by enabling the production of small batches of formulations with unique characteristics at low cost. These requirements are not often meet by traditional manufacturing methods based on mass production of, for example, oral dosage forms (340). The implementation of 3DP as an alternative manufacturing tool could be the solution to overcome the current challenges in manufacturing formulations for the early stages of drug development.

1.19.1. 3D printing in preclinical studies

The drug discovery process begins with the identification of an unmet medical need, that is, a medical condition whose treatment is not satisfactorily addressed with currently available treatments or these are non-existent. Broadly, the drug development process can be segregated into preclinical and clinical development stages. In preclinical development, a molecular target is selected and validated, with a high throughput screening of compound libraries performed to identify potential drug candidates. The candidates are subsequently optimized to exhibit adequate potency and selectivity towards the molecular target *in vitro* before testing its efficacy *in vivo* (341). Preclinical studies are designed to assess the efficacy and safety of the new compounds in relevant animal models to select suitable drug candidates to be tested in humans (342,343). Apart from safety pharmacology and toxicology studies in animals, the preclinical development program includes other activities, such as formulation development and quality control measures. If the candidate successfully completes the preclinical phase, its clinical development begins after requesting permission from the drug regulatory agencies (344).

Oral dosage forms, such as tablets and capsules, are commonly used in preclinical research to administer drugs to animals. However, the manufacture of tablets is a lengthy process and the tablets are often produced in a fixed dose. Capsules also have some disadvantages, such as the need for staff to manually fill the capsules with the exact dose of drug, which is a time-consuming task (340). On the other hand, liquid formulations permit a higher degree of dose flexibility, but their use is limited since the solubility and stability of the drug could be compromised (343). Technological advances have led to a sharp drop in the price of 3D printers over the past years, which made 3DP an affordable technology that could be easily integrated into a laboratory setting. With a small and compact 3D printer, researchers could produce printlets with different sizes and geometries adapted to meet the animal requirements (Figure 10). In preclinical studies, small devices such as capsules (size 9 and 9h), minitablets and pellets are often used to administer drugs to rodents (345). With a 3D printer, these devices could be manufactured on demand in a rapid manner and containing the exact dosage for the animal model, from rodents to larger animals, such as primates (346). Moreover, 3D printed devices could be filled with contrast agents or radiotracers to investigate their pass through the gastrointestinal tract of rats using imaging techniques (347). The size could be rapidly modified to improve the gastric emptying of the devices (189). A

study in beagle dogs modified the release of a drug form 3D printed capsules by modulating the wall thickness (348).
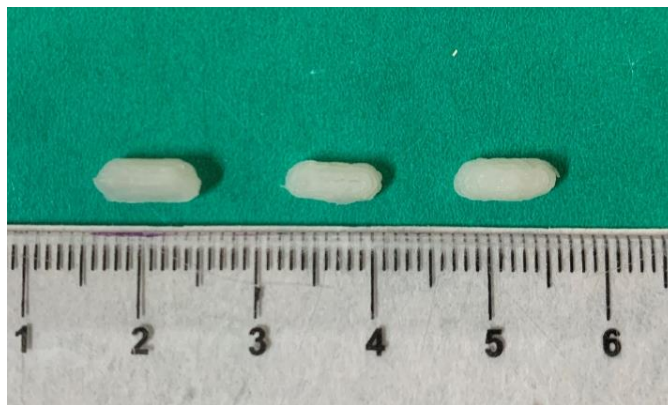

Figure 10. Small 3D printed devices adapted in size for rectal administration to small animals.

1.19.2. 3D printing in first-in-human (FIH) clinical trials

Clinical drug development consists of four temporal phases (I-IV). First-in-human (FIH) trials are performed as part of phase I and represent the first opportunity to investigate the drug in humans (349). The investigated substance is sequentially administered to a small group of healthy volunteers with an appropriate interval of observation between dosing of individual subjects (350). The study begins with the administration of the drug at low doses based on preclinical toxicological data (351), which are then escalated incrementally following different schemes (commonly single ascending dose studies and multiple ascending dose studies) (350). The primary goal of FIH trials is the identification of an appropriate dose and dosing interval for testing efficacy in phase II trials, based on the safety and tolerability of the drug (352).

In light of the schemes commonly followed by FIH trials, it is evident that multiple dose strengths are required, especially in multiple ascending dose studies. Traditional manufacturing processes are lengthy and multi-step processes that require expensive equipment and large workspaces (353). The implementation of 3D printing in the early phase drug development could allow the production of small batches of printlets with any desired drug dose (340). Dosage forms with varying sizes and many geometrical outlines could be produced to increase the acceptance and make the administration easier (354,355).

In the case of poorly soluble drugs, HME coupled with FDM could be used to create a solid dispersion of the poor soluble drug within a polymer matrix, thereby increasing drug bioavailability (356,357). In blinded trials, printlets could be designed to meet the requirements of the study (358) by masking the presence of the drug using, for example, a DuoCaplet design (267), which is a two compartment device where the drug core is embedded within a larger tablet. Moreover, the possibility of manufacturing printlets on demand immediately before administration avoids the need for long term stability studies. Stability

studies are necessary for long storage and usually delay the beginning of the clinical trial, being only necessary a short term evaluation (359).

It is likely that the integration of 3DP in the field of early phase drug development is easily attainable under current regulatory pathways. However, both its use in later phases of drug development, such as phase II and III trials, and its implementation in clinical practice are not currently possible. Current 3DP platforms are not suitable for scale-up and do not meet the standards required by good manufacturing practice (GMP) guidelines (308). Regulatory initiatives are needed to move this innovative technology from the research level to its application as a manufacturing tool to support the pharmaceutical industry.

REFERENCES

1. Abraham BP, Ahmed T, Ali T. Inflammatory Bowel Disease: Pathophysiology and Current Therapeutic Approaches. Handb Exp Pharmacol. 2017;239:115-46.

2. Kolios G. Animal models of inflammatory bowel disease: how useful are they really? Curr Opin Gastroenterol. 2016;32(4):251-7.

3. Kaaru E, Bianchi A, Wunder A, Rasche V, Stiller D. Molecular Imaging in Preclinical Models of IBD with Nuclear Imaging Techniques: State-of-the-Art and Perspectives. Inflamm Bowel Dis. 1 de octubre de 2016;22(10):2491-8.

4. Amidon S, Brown JE, Dave VS. Colon-Targeted Oral Drug Delivery Systems: Design Trends and Approaches. AAPS PharmSciTech. 13 de junio de 2015;16(4):731-41.

5. Grossman S, Porth CM. Porth. Fisiopatología: Alteraciones de la salud. Conceptos básicos. 9ª. Lippincott Williams & Wilkins; 2014.

6. Bruss DM, Sajjad H. Anatomy, Head and Neck, Laryngopharynx. En: StatPearls [Internet]. Treasure Island (FL): StatPearls Publishing; 2020 [citado 26 de febrero de 2020]. Disponible en: http://www.ncbi.nlm.nih.gov/books/NBK549913/

7. Reinus JF, Simon D. Gastrointestinal Anatomy and Physiology: The Essentials. John Wiley & Sons; 2014. 200 p.

8. Tortora GJ, Derrickson B. Principios de Anatomía y Fisiología. 13ª Edición. Panamericana; 2013.

9. PhD EPS. Introduction to Human Anatomy and Physiology. Elsevier Health Sciences; 2015. 340 p.

10. Drake R, Vogl AW, Mitchell AWM. Gray's Anatomy for Students E-Book. Elsevier Health Sciences; 2014. 1191 p.

11. Eastwood GL. Gastrointestinal Epithelial Renewal. Gastroenterology. 1 de mayo de 1977;72(5):962-75.

12. Moharamzadeh K. 14 - Oral mucosa tissue engineering. En: Tayebi L, Moharamzadeh K, editores. Biomaterials for Oral and Dental Tissue Engineering [Internet]. Woodhead Publishing; 2017 [citado 18 de febrero de 2020]. p. 223-44. Disponible en: http://www.sciencedirect.com/science/article/pii/B9780081009611000141

13. Feher J. 8.3 - Intestinal and Colonic Chemoreception and Motility. En: Feher J, editor. Quantitative Human Physiology (Second Edition) [Internet]. Boston: Academic Press; 2017 [citado 18 de febrero de 2020]. p. 796-809. Disponible en: http://www.sciencedirect.com/science/article/pii/B9780128008836000793

14. Zhang S. Digestive System. En: Zhang S, editor. An Atlas of Histology [Internet]. New York, NY: Springer; 1999 [citado 18 de febrero de 2020]. p. 187-251. Disponible en: https://doi.org/10.1007/978-0-387-21760-4_10

15. Liao D-H, Zhao J-B, Gregersen H. Gastrointestinal tract modelling in health and disease. World J Gastroenterol WJG. 14 de enero de 2009;15(2):169-76.

16. Welcome MO. Gastrointestinal Physiology: Development, Principles and Mechanisms of Regulation. Springer; 2018. 1037 p.

17. Bontrager KL, Lampignano J. Textbook of Radiographic Positioning & Related Anatomy - Pageburst E-Book on VitalSource8: Textbook of Radiographic Positioning & Related Anatomy - Pageburst E-Book on VitalSource. Elsevier Health Sciences; 2013. 847 p.

18. Vertzoni M, Augustijns P, Grimm M, Koziolek M, Lemmens G, Parrott N, et al. Impact of regional differences along the gastrointestinal tract of healthy adults on oral drug absorption: An UNGAP review. Eur J Pharm Sci Off J Eur Fed Pharm Sci. 15 de junio de 2019;134:153-75.

19.   Abuhelwa AY, Williams DB, Upton RN, Foster DJR. Food, gastrointestinal pH, and models of oral drug absorption. Eur J Pharm Biopharm Off J Arbeitsgemeinschaft Pharm Verfahrenstechnik EV. marzo de 2017;112:234-48.

20.   Aulton ME, Taylor KMG. Aulton's Pharmaceutics E-Book: The Design and Manufacture of Medicines. Elsevier Health Sciences; 2017. 933 p.

21.   Nugent SG, Kumar D, Rampton DS, Evans DF. Intestinal luminal pH in inflammatory bowel disease: possible determinants and implications for therapy with aminosalicylates and other drugs. Gut. abril de 2001;48(4):571-7.

22.   Liu L, Yao W, Rao Y, Lu X, Gao J. pH-Responsive carriers for oral drug delivery: challenges and opportunities of current platforms. Drug Deliv. 1 de enero de 2017;24(1):569-81.

23.   McConnell EL, Fadda HM, Basit AW. Gut instincts: Explorations in intestinal physiology and drug delivery. Int J Pharm. diciembre de 2008;364(2):213-26.

24.   Woraphatphadung T, Sajomsang W, Rojanarata T, Ngawhirunpat T, Tonglairoum P, Opanasopit P. Development of Chitosan-Based pH-Sensitive Polymeric Micelles Containing Curcumin for Colon-Targeted Drug Delivery. AAPS PharmSciTech. 1 de abril de 2018;19(3):991-1000.

25.   Ibekwe VC, Khela MK, Evans DF, Basit AW. A new concept in colonic drug targeting: a combined pH-responsive and bacterially-triggered drug delivery technology. Aliment Pharmacol Ther. 1 de octubre de 2008;28(7):911-6.

26.   Sasaki Y, Hada R, Nakajima H, Fukuda S, Munakata A. Improved localizing method of radiopill in measurement of entire gastrointestinal pH profiles: colonic luminal pH in normal subjects and patients with Crohn's disease. Am J Gastroenterol. enero de 1997;92(1):114-8.

27.   Schiller C, Fröhlich CP, Giessmann T, Siegmund W, Mönnikes H, Hosten N, et al. Intestinal fluid volumes and transit of dosage forms as assessed by magnetic resonance imaging. Aliment Pharmacol Ther. 15 de noviembre de 2005;22(10):971-9.

28.   Mudie DM, Murray K, Hoad CL, Pritchard SE, Garnett MC, Amidon GL, et al. Quantification of gastrointestinal liquid volumes and distribution following a 240 mL dose of water in the fasted state. Mol Pharm. 2 de septiembre de 2014;11(9):3039-47.

29.   Murray K, Hoad CL, Mudie DM, Wright J, Heissam K, Abrehart N, et al. Magnetic Resonance Imaging Quantification of Fasted State Colonic Liquid Pockets in Healthy Humans. Mol Pharm. 7 de agosto de 2017;14(8):2629-38.

30.   Markl D, Zeitler JA. A Review of Disintegration Mechanisms and Measurement Techniques. Pharm Res. 2017;34(5):890-917.

31.   Anbazhagan AN, Priyamvada S, Alrefai WA, Dudeja PK. Pathophysiology of IBD associated diarrhea. Tissue Barriers. 2018;6(2):e1463897.

32.   Eckburg PB, Bik EM, Bernstein CN, Purdom E, Dethlefsen L, Sargent M, et al. Diversity of the Human Intestinal Microbial Flora. Science. 10 de junio de 2005;308(5728):1635-8.

33.   Villar-López ME, Nieto-Reyes L, Anguiano-Igea S, Otero-Espinar FJ, Blanco-Méndez J. Formulation of triamcinolone acetonide pellets suitable for coating and colon targeting. Int J Pharm. 15 de marzo de 1999;179(2):229-35.

34.   Dieterich W, Schink M, Zopf Y. Microbiota in the Gastrointestinal Tract. Med Sci [Internet]. 14 de diciembre de 2018 [citado 23 de febrero de 2020];6(4). Disponible en: https://www.ncbi.nlm.nih.gov/pmc/articles/PMC6313343/

35.   Fava F, Danese S. Intestinal microbiota in inflammatory bowel disease: friend of foe? World J Gastroenterol. 7 de febrero de 2011;17(5):557-66.

36.   Linskens RK, Huijsdens XW, Savelkoul PH, Vandenbroucke-Grauls CM, Meuwissen SG. The bacterial flora in inflammatory bowel disease: current insights in pathogenesis and the influence of antibiotics and probiotics. Scand J Gastroenterol Suppl. 2001;(234):29-40.

37.   Hatton GB, Yadav V, Basit AW, Merchant HA. Animal Farm: Considerations in Animal Gastrointestinal Physiology and Relevance to Drug Delivery in Humans. J Pharm Sci. septiembre de 2015;104(9):2747-76.

38.   Karrout Y, Dubuquoy L, Piveteau C, Siepmann F, Moussa E, Wils D, et al. In vivo efficacy of microbiota-sensitive coatings for colon targeting: a promising tool for IBD therapy. J Control Release. 10 de enero de 2015;197:121-30.

39.   Hendrickson BA, Gokhale R, Cho JH. Clinical Aspects and Pathophysiology of Inflammatory Bowel Disease. Clin Microbiol Rev. enero de 2002;15(1):79-94.

40.   Walsh AJ, Radford-Smith GL. Ulcerative Colitis and Ulcerative Proctitis: Clinical Course and Complications. En: Inflammatory Bowel Disease [Internet]. John Wiley & Sons, Ltd; 2010 [citado 9 de febrero de 2020]. p. 212-27. Disponible en: https://onlinelibrary.wiley.com/doi/abs/10.1002/9781444318418.ch15

41.   Silverberg MS, Satsangi J, Ahmad T, Arnott ID, Bernstein CN, Brant SR, et al. Toward an Integrated Clinical, Molecular and Serological Classification of Inflammatory Bowel Disease: Report of a Working Party of the 2005 Montreal World Congress of Gastroenterology [Internet]. Canadian Journal of Gastroenterology and Hepatology. 2005 [citado 5 de abril de 2018]. Disponible en: https://www.hindawi.com/journals/cjgh/2005/269076/abs/

42.   Jung S-A. Differential Diagnosis of Inflammatory Bowel Disease: What Is the Role of Colonoscopy? Clin Endosc. septiembre de 2012;45(3):254-62.

43.   Parray FQ, Wani ML, Malik AA, Wani SN, Bijli AH, Irshad I, et al. Ulcerative Colitis: A Challenge to Surgeons. Int J Prev Med. noviembre de 2012;3(11):749-63.

44.   DeRoche TC, Xiao S-Y, Liu X. Histological evaluation in ulcerative colitis. Gastroenterol Rep. agosto de 2014;2(3):178-92.

45.   Baumgart DC, Sandborn WJ. Crohn's disease. Lancet. noviembre de 2012;380(9853):1590-605.

46.   Lee JM, Lee K-M. Endoscopic Diagnosis and Differentiation of Inflammatory Bowel Disease. Clin Endosc. julio de 2016;49(4):370-5.

47.   Zeitz J, Fournier N, Labenz C, Biedermann L, Frei P, Misselwitz B, et al. Risk Factors for the Development of Fistulae and Stenoses in Crohn Disease Patients in the Swiss Inflammatory Bowel Disease Cohort. Inflamm Intest Dis. 2016;1(4):172-81.

48.   Loftus EV Jr. Clinical epidemiology of inflammatory bowel disease: incidence, prevalence, and environmental influences. Gastroenterology. 126(6):1504-17.

49.   Visan I. The hygiene hypothesis. Nat Immunol. 18 de abril de 2012;13:437.

50.   Alatab S, Sepanlou SG, Ikuta K, Vahedi H, Bisignano C, Safiri S, et al. The global, regional, and national burden of inflammatory bowel disease in 195 countries and territories, 1990–2017: a systematic analysis for the Global Burden of Disease Study 2017. Lancet Gastroenterol Hepatol. 1 de enero de 2020;5(1):17-30.

51.   Friedman S, Blumberg RS. Capítulo 295. Enfermedad Intestinal Inflamatoria. En: Harrison Principios de Medicina Interna. 18.ª ed. McGraw-Hill; 2012.

52.   Roth M-P, Petersen GM, McElree C, Feldman E, Rotter JI. Geographic origins of Jewish patients with inflammatory bowel disease. Gastroenterology. 1989;97(4):900-4.

53.   M Montgomery S, L Morris D, E Pounder R, Wakefield A. Asian ethnic origin and the risk of inflammatory bowel disease. Eur J Gastroenterol Hepatol. 1999;11:543-6.

54.   M'Koma AE. Inflammatory Bowel Disease: An Expanding Global Health Problem. Clin Med Insights Gastroenterol. 14 de agosto de 2013;6:33-47.

55.   Grisham MB, Kevil CG, Harris NR, Granger DN. The Role of the Vasculature in Chronic Intestinal Inflammation. En: Inflammatory Bowel Disease [Internet]. John Wiley & Sons, Ltd; 2010 [citado 30 de enero de 2020]. p. 157-69. Disponible en: https://onlinelibrary.wiley.com/doi/abs/10.1002/9781444318418.ch11

56.   Abdulkhaleq LA, Assi MA, Abdullah R, Zamri-Saad M, Taufiq-Yap YH, Hezmee MNM. The crucial roles of inflammatory mediators in inflammation: A review. Vet World. mayo de 2018;11(5):627-35.

57.   Esmon CT, Taylor FB, Snow TR. Inflammation and coagulation: linked processes potentially regulated through a common pathway mediated by protein C. Thromb Haemost. 12 de julio de 1991;66(1):160-5.

58.   Doener F, Michel A, Reuter S, Friedrich P, Böhm L, Relle M, et al. Mast cell-derived mediators promote murine neutrophil effector functions. Int Immunol. 1 de octubre de 2013;25(10):553-61.

59.   Bamias G, Nyce MR, De La Rue SA, Cominelli F, American College of Physicians, American Physiological Society. New concepts in the pathophysiology of inflammatory bowel disease. Ann Intern Med. 20 de diciembre de 2005;143(12):895-904.

60.   Monteleone G, Fina D, Caruso R, Pallone F. New mediators of immunity and inflammation in inflammatory bowel disease. Curr Opin Gastroenterol. julio de 2006;22(4):361-4.

61.   Stoller JK, Michota FA, Mandell BF. The Cleveland Clinic Foundation Intensive Review of Internal Medicine. Lippincott Williams & Wilkins; 2009. 1010 p.

62.   Elson CO, Cong Y, McCracken VJ, Dimmitt RA, Lorenz RG, Weaver CT. Experimental models of inflammatory bowel disease reveal innate, adaptive, and regulatory mechanisms of host dialogue with the microbiota. Immunol Rev. 1 de agosto de 2005;206(1):260-76.

63.   Strober W, Fuss IJ. Pro-Inflammatory Cytokines in the Pathogenesis of IBD. Gastroenterology. mayo de 2011;140(6):1756-67.

64.   Granger DN, Senchenkova E. Leukocyte–Endothelial Cell Adhesion [Internet]. Morgan & Claypool Life Sciences; 2010 [citado 3 de febrero de 2020]. Disponible en: https://www.ncbi.nlm.nih.gov/books/NBK53380/

65.   Zhang Y-Z, Li Y-Y. Inflammatory bowel disease: Pathogenesis. World J Gastroenterol WJG. 7 de enero de 2014;20(1):91-9.

66.   Ko JK, Auyeung KK. Inflammatory bowel disease: etiology, pathogenesis and current therapy. Curr Pharm Des. 2014;20(7):1082-96.

67.   Piovani D, Danese S, Peyrin-Biroulet L, Nikolopoulos GK, Lytras T, Bonovas S. Environmental Risk Factors for Inflammatory Bowel Diseases: An Umbrella Review of Meta-analyses. Gastroenterology. 2019;157(3):647-659.e4.

68.   Mahid SS, Minor KS, Soto RE, Hornung CA, Galandiuk S. Smoking and Inflammatory Bowel Disease: A Meta-analysis. Mayo Clin Proc. 81(11):1462-71.

69.   Reif S, Klein I, Lubin F, Farbstein M, Hallak A, Gilat T. Pre-illness dietary factors in inflammatory bowel disease. Gut. junio de 1997;40(6):754-60.

70.   Sugihara K, Morhardt TL, Kamada N. The Role of Dietary Nutrients in Inflammatory Bowel Disease. Front Immunol [Internet]. 2019 [citado 4 de febrero de 2020];9. Disponible en: https://www.frontiersin.org/articles/10.3389/fimmu.2018.03183/full

71.   Schultz BM, Paduro CA, Salazar GA, Salazar-Echegarai FJ, Sebastián VP, Riedel CA, et al. A Potential Role of Salmonella Infection in the Onset of Inflammatory Bowel Diseases. Front Immunol [Internet]. 28 de febrero de 2017 [citado 4 de febrero de 2020];8. Disponible en: https://www.ncbi.nlm.nih.gov/pmc/articles/PMC5329042/

72.   Darfeuille-Michaud A, Boudeau J, Bulois P, Neut C, Glasser A-L, Barnich N, et al. High prevalence of adherent-invasive Escherichia coli associated with ileal mucosa in Crohn's disease. Gastroenterology. 127(2):412-21.

73.   N Bernstein C, F Blanchard J, Rawsthorne P, T Collins M. Population-Based Case Control Study of Seroprevalence of Mycobacterium paratuberculosis in Patients with Crohn's Disease and Ulcerative Colitis. J Clin Microbiol. 2004;42:1129-35.

74.   Pirzer U, Schönhaar A, Fleischer B, Hermann E, Meyer zum Büschenfelde KH. Reactivity of infiltrating T lymphocytes with microbial antigens in Crohn's disease. Lancet Lond Engl. 16 de noviembre de 1991;338(8777):1238-9.

75.   Basso PJ, Câmara NOS, Sales-Campos H. Microbial-Based Therapies in the Treatment of Inflammatory Bowel Disease – An Overview of Human Studies. Front Pharmacol [Internet]. 10 de enero de 2019 [citado 4 de febrero de 2020];9. Disponible en: https://www.ncbi.nlm.nih.gov/pmc/articles/PMC6335320/

76.   Kevans D, Silverberg MS, Borowski K, Griffiths A, Xu W, Onay V, et al. IBD Genetic Risk Profile in Healthy First-Degree Relatives of Crohn's Disease Patients. J Crohns Colitis. febrero de 2016;10(2):209-15.

77.   Hugot J-P, Chamaillard M, Zouali H, Lesage S, Cézard J-P, Belaiche J, et al. Association of NOD2 leucine-rich repeat variants with susceptibility to Crohn's disease. Nature. 31 de mayo de 2001;411:599.

78.   Hedin C, Rioux JD, D'Amato M. Molecular Genetics of Inflammatory Bowel Disease. Springer Nature; 2019. 399 p.

79.   Tan G, Zeng B, Zhi F-C. Regulation of human enteric α-defensins by NOD2 in the Paneth cell lineage. Eur J Cell Biol. enero de 2015;94(1):60-6.

80.   Ogura Y, Bonen DK, Inohara N, Nicolae DL, Chen FF, Ramos R, et al. A frameshift mutation in NOD2 associated with susceptibility to Crohn's disease. Nature. 31 de mayo de 2001;411(6837):603-6.

81.   Hampe J, Schreiber S, Shaw SH, Lau KF, Bridger S, Macpherson AJS, et al. A Genomewide Analysis Provides Evidence for Novel Linkages in Inflammatory Bowel Disease in a Large European Cohort. Am J Hum Genet. marzo de 1999;64(3):808-16.

82.   Duerr RH, Taylor KD, Brant SR, Rioux JD, Silverberg MS, Daly MJ, et al. A Genome-Wide Association Study Identifies IL23R as an Inflammatory Bowel Disease Gene. Science. 1 de diciembre de 2006;314(5804):1461-3.

83.   Guan G, Lan S. Implications of Antioxidant Systems in Inflammatory Bowel Disease [Internet]. BioMed Research International. 2018 [citado 7 de noviembre de 2018]. Disponible en: https://www.hindawi.com/journals/bmri/2018/1290179/

84.   Burton GJ, Jauniaux E. Oxidative stress. Best Pract Res Clin Obstet Gynaecol. junio de 2011;25(3):287-99.

85.   Takagi T, Naito Y, Yoshikawa T. Free Radicals in Inflammatory Bowel Disease. Free Radic Biol Dig Dis. 2011;29:128-36.

86.   Rezaie A, Parker RD, Abdollahi M. Oxidative Stress and Pathogenesis of Inflammatory Bowel Disease: An Epiphenomenon or the Cause? Dig Dis Sci. 1 de septiembre de 2007;52(9):2015-21.

87.   Bourgonje AR, von Martels JZH, Bulthuis MLC, van Londen M, Faber KN, Dijkstra G, et al. Crohn's Disease in Clinical Remission Is Marked by Systemic Oxidative Stress. Front Physiol [Internet]. 2019 [citado 29 de febrero de 2020];10. Disponible en: https://www.frontiersin.org/articles/10.3389/fphys.2019.00499/full

88.   Tian T, Wang Z, Zhang J. Pathomechanisms of Oxidative Stress in Inflammatory Bowel Disease and Potential Antioxidant Therapies. Oxid Med Cell Longev [Internet]. 2017 [citado 1 de marzo de 2020];2017. Disponible en: https://www.ncbi.nlm.nih.gov/pmc/articles/PMC5506473/

89.   Moura FA, de Andrade KQ, dos Santos JCF, Araújo ORP, Goulart MOF. Antioxidant therapy for treatment of inflammatory bowel disease: Does it work? Redox Biol. 23 de octubre de 2015;6:617-39.

90.   Cuzzocrea S, Mazzon E, Serraino I, Lepore V, Terranova ML, Ciccolo A, et al. Melatonin reduces dinitrobenzene sulfonic acid-induced colitis. J Pineal Res. 1 de enero de 2001;30(1):1-12.

91.   Martín AR, Villegas I, Sánchez-Hidalgo M, de la Lastra CA. The effects of resveratrol, a phytoalexin derived from red wines, on chronic inflammation induced in an experimentally induced colitis model. Br J Pharmacol. abril de 2006;147(8):873-85.

92.   Hardeland R, Pandi-Perumal SR, Cardinali DP. Melatonin. Int J Biochem Cell Biol. marzo de 2006;38(3):313-6.

93.   Bubenik GA. Gastrointestinal melatonin: localization, function, and clinical relevance. Dig Dis Sci. octubre de 2002;47(10):2336-48.

94.   Chen C-Q, Fichna J, Bashashati M, Li Y-Y, Storr M. Distribution, function and physiological role of melatonin in the lower gut. World J Gastroenterol WJG. 14 de septiembre de 2011;17(34):3888-98.

95.   Claustrat B, Brun J, Chazot G. The basic physiology and pathophysiology of melatonin. Sleep Med Rev. 1 de febrero de 2005;9(1):11-24.

96.   Li J-H, Yu J-P, Yu H-G, Xu X-M, Yu L-L, Liu J, et al. Melatonin Reduces Inflammatory Injury Through Inhibiting   NF-κB Activation in Rats With Colitis. Mediators Inflamm. 31 de agosto de 2005;2005(4):185-93.

97.   Mei Q, Yu J-P, Xu J-M, Wei W, Xiang L, Yue L. Melatonin reduces colon immunological injury in rats by regulating activity of macrophages. Acta Pharmacol Sin. octubre de 2002;23(10):882-6.

98.   Dong W-G. Effects of melatonin on the expression of iNOS and COX-2 in rat models of colitis. World J Gastroenterol. 2003;9(6):1307.

99.   Aggarwal BB, Bhardwaj A, Aggarwal RS, Seeram NP, Shishodia S, Takada Y. Role of resveratrol in prevention and therapy of cancer: preclinical and clinical studies. Anticancer Res. octubre de 2004;24(5A):2783-840.

100.   Luzardo-Álvarez A, Lamela-Gómez I, Otero-Espinar F, Blanco-Méndez J. Development, Characterization, and In Vitro Evaluation of Resveratrol-Loaded Poly-(ε-caprolactone) Microcapsules Prepared by Ultrasonic Atomization for Intra-Articular Administration. Pharmaceutics. junio de 2019;11(6):249.

101.   Shi Y, Zhou J, Jiang B, Miao M. Resveratrol and inflammatory bowel disease. Ann N Y Acad Sci. 2017;1403(1):38-47.

102.   Yildiz G, Yildiz Y, Ulutas PA, Yaylali A, Ural M. Resveratrol Pretreatment Ameliorates TNBS Colitis in Rats. Recent Pat Endocr Metab Immune Drug Discov. 2015;9(2):134-40.

103.   Martín AR, Villegas I, La Casa C, de la Lastra CA. Resveratrol, a polyphenol found in grapes, suppresses oxidative damage and stimulates apoptosis during early colonic inflammation in rats. Biochem Pharmacol. 1 de abril de 2004;67(7):1399-410.

104.   Valatas V, Vakas M, Kolios G. The value of experimental models of colitis in predicting efficacy of biological therapies for inflammatory bowel diseases. Am J Physiol Gastrointest Liver Physiol. diciembre de 2013;305(11):G763-785.

105.   Wirtz S, Neufert C, Weigmann B, Neurath MF. Chemically induced mouse models of intestinal inflammation. Nat Protoc. 2007;2(3):541-6.

106.   Hoffmann JC, Pawlowski NN, Kühl AA, Höhne W, Zeitz M. Animal models of inflammatory bowel disease: an overview. Pathobiol J Immunopathol Mol Cell Biol. 2003 de 2002;70(3):121-30.

107.   Chassaing B, Aitken JD, Malleshappa M, Vijay-Kumar M. Dextran Sulfate Sodium (DSS)-Induced Colitis in Mice. Curr Protoc Immunol Ed John E Coligan Al. 4 de febrero de 2014;104:Unit-15.25.

108.   Cooper HS, Murthy SN, Shah RS, Sedergran DJ. Clinicopathologic study of dextran sulfate sodium experimental murine colitis. Lab Investig J Tech Methods Pathol. agosto de 1993;69(2):238-49.

109.   Dieleman LA, Ridwan BU, Tennyson GS, Beagley KW, Bucy RP, Elson CO. Dextran sulfate sodium-induced colitis occurs in severe combined immunodeficient mice. Gastroenterology. diciembre de 1994;107(6):1643-52.

110.   Boirivant M, Fuss IJ, Chu A, Strober W. Oxazolone Colitis: A Murine Model of T Helper Cell Type 2 Colitis Treatable with Antibodies to Interleukin 4. J Exp Med. 16 de noviembre de 1998;188(10):1929-39.

111.   Mizoguchi A, Takeuchi T, Himuro H, Okada T, Mizoguchi E. Genetically Engineered Mouse Models for Studying Inflammatory Bowel Disease. J Pathol. enero de 2016;238(2):205-19.

112.   Kühn R, Löhler J, Rennick D, Rajewsky K, Müller W. Interleukin-10-deficient mice develop chronic enterocolitis. Cell. 22 de octubre de 1993;75(2):263-74.

113.   Hoentjen F, Harmsen HJM, Braat H, Torrice CD, Mann BA, Sartor RB, et al. Antibiotics with a selective aerobic or anaerobic spectrum have different therapeutic activities in various regions of the colon in interleukin 10 gene deficient mice. Gut. diciembre de 2003;52(12):1721-7.

114.   Zigmond E, Bernshtein B, Friedlander G, Walker CR, Yona S, Kim K-W, et al. Macrophage-restricted interleukin-10 receptor deficiency, but not IL-10 deficiency, causes severe spontaneous colitis. Immunity. 15 de mayo de 2014;40(5):720-33.

115.   Sadlack B, Merz H, Schorle H, Schimpl A, Feller AC, Horak I. Ulcerative colitis-like disease in mice with a disrupted interleukin-2 gene. Cell. 22 de octubre de 1993;75(2):253-61.

116.   Contractor NV, Bassiri H, Reya T, Park AY, Baumgart DC, Wasik MA, et al. Lymphoid hyperplasia, autoimmunity, and compromised intestinal intraepithelial lymphocyte development in

colitis-free gnotobiotic IL-2-deficient mice. J Immunol Baltim Md 1950. 1 de enero de 1998;160(1):385-94.

117.   Mizoguchi A. Animal Models of Inflammatory Bowel Disease. En: Conn PM, editor. Progress in Molecular Biology and Translational Science [Internet]. Academic Press; 2012 [citado 10 de octubre de 2018]. p. 263-320. (Animal Models of Molecular Pathology; vol. 105). Disponible en: http://www.sciencedirect.com/science/article/pii/B9780123945969000093

118.   Mombaerts P, Mizoguchi E, Grusby MJ, Glimcher LH, Bhan AK, Tonegawa S. Spontaneous development of inflammatory bowel disease in T cell receptor mutant mice. Cell. 22 de octubre de 1993;75(2):275-82.

119.   Dianda L, Hanby AM, Wright NA, Sebesteny A, Hayday AC, Owen MJ. T cell receptor-alpha beta-deficient mice fail to develop colitis in the absence of a microbial environment. Am J Pathol. enero de 1997;150(1):91-7.

120.   Mizoguchi A, Mizoguchi E, Smith RN, Preffer FI, Bhan AK. Suppressive role of B cells in chronic colitis of T cell receptor alpha mutant mice. J Exp Med. 17 de noviembre de 1997;186(10):1749-56.

121.   Watanabe M, Watanabe N, Iwao Y, Ogata H, Kanai T, Ueno Y, et al. The Serum Factor from Patients with Ulcerative Colitis that Induces T Cell Proliferation in the Mouse Thymus Is Interleukin-7. J Clin Immunol. 1 de julio de 1997;17(4):282-92.

122.   HIBI T, OGATA H, SAKURABA A. Animal models of inflammatory bowel disease. J Gastroenterol. junio de 2002;37(6):409-17.

123.   Hammer RE, Maika SD, Richardson JA, Tang J-P, Taurog JD. Spontaneous inflammatory disease in transgenic rats expressing HLA-B27 and human β2m: An animal model of HLA-B27-associated human disorders. Cell. 30 de noviembre de 1990;63(5):1099-112.

124.   Breban M, Fernández-Sueiro JL, Richardson JA, Hadavand RR, Maika SD, Hammer RE, et al. T cells, but not thymic exposure to HLA-B27, are required for the inflammatory disease of HLA-B27 transgenic rats. J Immunol. 15 de enero de 1996;156(2):794-803.

125.   Rath HC, Herfarth HH, Ikeda JS, Grenther WB, Hamm TE, Balish E, et al. Normal luminal bacteria, especially Bacteroides species, mediate chronic colitis, gastritis, and arthritis in HLA-B27/human beta2 microglobulin transgenic rats. J Clin Invest. 15 de agosto de 1996;98(4):945-53.

126.   Wirtz S, Finotto S, Kanzler S, Lohse AW, Blessing M, Lehr HA, et al. Cutting edge: chronic intestinal inflammation in STAT-4 transgenic mice: characterization of disease and adoptive transfer by TNF- plus IFN-gamma-producing CD4+ T cells that respond to bacterial antigens. J Immunol Baltim Md 1950. 15 de febrero de 1999;162(4):1884-8.

127.   Madara JL, Podolsky DK, King NW, Sehgal PK, Moore R, Winter HS. Characterization of spontaneous colitis in cotton-top tamarins (Saguinus oedipus) and its response to sulfasalazine. Gastroenterology. enero de 1985;88(1 Pt 1):13-9.

128.   De Santis S, Kunde D, Galleggiante V, Liso M, Scandiffio L, Serino G, et al. TNFα deficiency results in increased IL-1β in an early onset of spontaneous murine colitis. Cell Death Dis. 10 de 2017;8(8):e2993.

129.   Sundberg JP, Elson CO, Bedigian H, Birkenmeier EH. Spontaneous, heritable colitis in a new substrain of C3H/HeJ mice. Gastroenterology. diciembre de 1994;107(6):1726-35.

130.   Cong Y, Brandwein SL, McCabe RP, Lazenby A, Birkenmeier EH, Sundberg JP, et al. CD4+ T cells reactive to enteric bacterial antigens in spontaneously colitic C3H/HeJBir mice: increased T helper cell type 1 response and ability to transfer disease. J Exp Med. 16 de marzo de 1998;187(6):855-64.

131.   Brandwein SL, McCabe RP, Cong Y, Waites KB, Ridwan BU, Dean PA, et al. Spontaneously colitic C3H/HeJBir mice demonstrate selective antibody reactivity to antigens of the enteric bacterial flora. J Immunol. 1 de julio de 1997;159(1):44-52.

132.   Matsumoto S, Okabe Y, Setoyama H, Takayama K, Ohtsuka J, Funahashi H, et al. Inflammatory bowel disease-like enteritis and caecitis in a senescence accelerated mouse P1/Yit strain. Gut. julio de 1998;43(1):71-8.

133.   Strober W, Nakamura K, Kitani A. The SAMP1/Yit mouse: another step closer to modeling human inflammatory bowel disease. J Clin Invest. 15 de marzo de 2001;107(6):667-70.

134. Kosiewicz MM, Nast CC, Krishnan A, Rivera-Nieves J, Moskaluk CA, Matsumoto S, et al. Th1-type responses mediate spontaneous ileitis in a novel murine model of Crohn's disease. J Clin Invest. marzo de 2001;107(6):695-702.

135. Vidrich A, Buzan JM, Barnes S, Reuter BK, Skaar K, Ilo C, et al. Altered epithelial cell lineage allocation and global expansion of the crypt epithelial stem cell population are associated with ileitis in SAMP1/YitFc mice. Am J Pathol. abril de 2005;166(4):1055-67.

136. Eri R, McGuckin MA, Wadley R. T cell transfer model of colitis: a great tool to assess the contribution of T cells in chronic intestinal inflammation. Methods Mol Biol Clifton NJ. 2012;844:261-75.

137. Weigmann B. Induction of colitis in mice (T-cell transfer model). Methods Mol Biol Clifton NJ. 2014;1193:143-51.

138. Powrie F, Correa-Oliveira R, Mauze S, Coffman RL. Regulatory interactions between CD45RBhigh and CD45RBlow CD4+ T cells are important for the balance between protective and pathogenic cell-mediated immunity. J Exp Med. 1 de febrero de 1994;179(2):589-600.

139. Powrie F, Leach MW, Mauze S, Caddle LB, Coffman RL. Phenotypically distinct subsets of CD4+ T cells induce or protect from chronic intestinal inflammation in C. B-17 scid mice. Int Immunol. noviembre de 1993;5(11):1461-71.

140. Annacker O, Burlen-Defranoux O, Pimenta-Araujo R, Cumano A, Bandeira A. Regulatory CD4 T Cells Control the Size of the Peripheral Activated/Memory CD4 T Cell Compartment. J Immunol. 1 de abril de 2000;164(7):3573-80.

141. Steinhoff U, Brinkmann V, Klemm U, Aichele P, Seiler P, Brandt U, et al. Autoimmune intestinal pathology induced by hsp60-specific CD8 T cells. Immunity. septiembre de 1999;11(3):349-58.

142. Niederreiter L, Adolph TE, Kaser A. Anti-IL-12/23 in Crohn's disease: bench and bedside. Curr Drug Targets. noviembre de 2013;14(12):1379-84.

143. Sheikh SZ, Hegazi RA, Kobayashi T, Onyiah JC, Russo SM, Matsuoka K, et al. An anti-inflammatory role for carbon monoxide and heme oxygenase-1 in chronic Th2-mediated murine colitis. J Immunol Baltim Md 1950. 1 de mayo de 2011;186(9):5506-13.

144. Khanna PV, Shih DQ, Haritunians T, McGovern DP, Targan S. Use of animal models in elucidating disease pathogenesis in IBD. Semin Immunopathol. septiembre de 2014;36(5):541-51.

145. Umesaki Y. Use of gnotobiotic mice to identify and characterize key microbes responsible for the development of the intestinal immune system. Proc Jpn Acad Ser B Phys Biol Sci. 2014;90(9):313-32.

146. Nguyen TLA, Vieira-Silva S, Liston A, Raes J. How informative is the mouse for human gut microbiota research? Dis Model Mech. enero de 2015;8(1):1-16.

147. Schoeb TR, Bullard DC. Microbial and histopathologic considerations in the use of mouse models of inflammatory bowel diseases. Inflamm Bowel Dis. agosto de 2012;18(8):1558-65.

148. DeVoss J, Diehl L. Murine models of inflammatory bowel disease (IBD): challenges of modeling human disease. Toxicol Pathol. enero de 2014;42(1):99-110.

149. Perše M, Cerar A. Dextran sodium sulphate colitis mouse model: traps and tricks. J Biomed Biotechnol. 2012;2012:718617.

150. Jurjus AR, Khoury NN, Reimund J-M. Animal models of inflammatory bowel disease. J Pharmacol Toxicol Methods. 1 de septiembre de 2004;50(2):81-92.

151. Fraser MB and A. Animal Models of Colitis: Lessons Learned, and Their Relevance to the Clinic. Ulcerative Colitis - Treat Spec Popul Future [Internet]. 2011 [citado 14 de octubre de 2018]; Disponible en: https://www.intechopen.com/books/ulcerative-colitis-treatments-special-populations-and-the-future/animal-models-of-colitis-lessons-learned-and-their-relevance-to-the-clinic

152. Bharadwaj S, Narula N, Tandon P, Yaghoobi M. Role of endoscopy in inflammatory bowel disease. Gastroenterol Rep. 1 de mayo de 2018;6(2):75-82.

153. Dmochowska N, Wardill H, Hughes P, Dmochowska N, Wardill HR, Hughes PA. Advances in Imaging Specific Mediators of Inflammatory Bowel Disease. Int J Mol Sci. 21 de agosto de 2018;19(9):2471.

154. Lauber DT, Fülöp A, Kovács T, Szigeti K, Máthé D, Szijártó A. State of the art in vivo imaging techniques for laboratory animals. Lab Anim. octubre de 2017;51(5):465-78.

155. Wang ZJ, Chang T-TA, Slauter R. Chapter 35 - Use of Imaging for Preclinical Evaluation. En: Faqi AS, editor. A Comprehensive Guide to Toxicology in Nonclinical Drug Development (Second Edition) [Internet]. Boston: Academic Press; 2017 [citado 17 de octubre de 2018]. p. 921-38. Disponible en: http://www.sciencedirect.com/science/article/pii/B9780128036204000359

156. Kim SH. Computed Tomography Enterography and Magnetic Resonance Enterography in the Diagnosis of Crohn's Disease. Intest Res. enero de 2015;13(1):27-38.

157. Bruining DH, Loftus EV, Ehman EC, Siddiki HA, Nguyen DL, Fidler JL, et al. Computed tomography enterography detects intestinal wall changes and effects of treatment in patients with Crohn's disease. Clin Gastroenterol Hepatol Off Clin Pract J Am Gastroenterol Assoc. agosto de 2011;9(8):679-683.e1.

158. Siddiki HA, Fidler JL, Fletcher JG, Burton SS, Huprich JE, Hough DM, et al. Prospective comparison of state-of-the-art MR enterography and CT enterography in small-bowel Crohn's disease. AJR Am J Roentgenol. julio de 2009;193(1):113-21.

159. Paulus MJ, Gleason SS, Kennel SJ, Hunsicker PR, Johnson DK. High Resolution X-ray Computed Tomography: An Emerging Tool for Small Animal Cancer Research. Neoplasia N Y N. enero de 2000;2(1-2):62-70.

160. Fredin MF, Hultin L, Hyberg G, Rehnström E, Hultgren Hörnquist E, Melgar S, et al. Predicting and monitoring colitis development in mice by micro-computed tomography. Inflamm Bowel Dis. abril de 2008;14(4):491-9.

161. Gee MS, Harisinghani MG. MRI in patients with inflammatory bowel disease. J Magn Reson Imaging JMRI. 1 de marzo de 2011;33(3):527-34.

162. Paolantonio P, Ferrari R, Vecchietti F, Cucchiara S, Laghi A. Current status of MR imaging in the evaluation of IBD in a pediatric population of patients. Eur J Radiol. marzo de 2009;69(3):418-24.

163. Rimola J, Ordás I, Rodriguez S, García-Bosch O, Aceituno M, Llach J, et al. Magnetic resonance imaging for evaluation of Crohn's disease: validation of parameters of severity and quantitative index of activity. Inflamm Bowel Dis. agosto de 2011;17(8):1759-68.

164. Fidler JL, Guimaraes L, Einstein DM. MR imaging of the small bowel. Radiogr Rev Publ Radiol Soc N Am Inc. octubre de 2009;29(6):1811-25.

165. Maccioni F, Colaiacomo MC, Parlanti S. Ulcerative colitis: value of MR imaging. Abdom Imaging. octubre de 2005;30(5):584-92.

166. He Q, Xu RZ, Shkarin P, Pizzorno G, Lee-French CH, Rothman DL, et al. Magnetic resonance spectroscopic imaging of tumor metabolic markers for cancer diagnosis, metabolic phenotyping, and characterization of tumor microenvironment. Dis Markers. 2004 de 2003;19(2-3):69-94.

167. Larsson AE, Melgar S, Rehnström E, Michaëlsson E, Svensson L, Hockings P, et al. Magnetic resonance imaging of experimental mouse colitis and association with inflammatory activity. Inflamm Bowel Dis. junio de 2006;12(6):478-85.

168. Bianchi A, Bluhmki T, Schönberger T, Kaaru E, Beltzer A, Raymond E, et al. Noninvasive Longitudinal Study of a Magnetic Resonance Imaging Biomarker for the Quantification of Colon Inflammation in a Mouse Model of Colitis. Inflamm Bowel Dis. 2016;22(6):1286-95.

169. Bryant RV, Friedman AB, Wright EK, Taylor KM, Begun J, Maconi G, et al. Gastrointestinal ultrasound in inflammatory bowel disease: an underused resource with potential paradigm-changing application. Gut. 1 de mayo de 2018;67(5):973-85.

170. Carnevale Maffè G, Brunetti L, Formagnana P, Corazza GR. Ultrasonographic findings in Crohn's disease. J Ultrasound. 24 de mayo de 2014;18(1):37-49.

171. Nania S, Blaas L, Gerling M. 3D high-frequency ultrasound of the mouse colon to monitor tumor development. 7 de julio de 2017 [citado 17 de octubre de 2018]; Disponible en: https://www.nature.com/protocolexchange/protocols/5475#/introduction

172. Machtaler S, Knieling F, Luong R, Tian L, Willmann JK. Assessment of Inflammation in an Acute on Chronic Model of Inflammatory Bowel Disease with Ultrasound Molecular Imaging. Theranostics. 8 de agosto de 2015;5(11):1175-86.

173.   Kim K, Johnson LA, Jia C, Joyce JC, Rangwalla S, Higgins PDR, et al. Noninvasive ultrasound elasticity imaging (UEI) of Crohn's disease: animal model. Ultrasound Med Biol. junio de 2008;34(6):902-12.

174.   Jacene HA, Goetze S, Patel H, Wahl RL, Ziessman HA. Advantages of Hybrid SPECT/CT vs SPECT Alone. Open Med Imaging J [Internet]. 1 de agosto de 2008 [citado 17 de octubre de 2018];2(1). Disponible en: https://benthamopen.com/ABSTRACT/TOMIJ-2-67

175.   Aarntzen EHJG, Hermsen R, Drenth JPH, Boerman OC, Oyen WJG. 99mTc-CXCL8 SPECT to Monitor Disease Activity in Inflammatory Bowel Disease. J Nucl Med Off Publ Soc Nucl Med. marzo de 2016;57(3):398-403.

176.   Bennink R, Peeters M, D'Haens G, Rutgeerts P, Mortelmans L. Tc-99m HMPAO white blood cell scintigraphy in the assessment of the extent and severity of an acute exacerbation of ulcerative colitis. Clin Nucl Med. febrero de 2001;26(2):99-104.

177.   Khalil MM, Tremoleda JL, Bayomy TB, Gsell W. Molecular SPECT Imaging: An Overview [Internet]. International Journal of Molecular Imaging. 2011 [citado 17 de octubre de 2018]. Disponible en: https://www.hindawi.com/journals/ijmi/2011/796025/

178.   Tsopelas C, Penglis S, Ruskiewicz A, Bartholomeusz DL. Scintigraphic imaging of experimental colitis with technetium-99m-infliximab in the rat. Hell J Nucl Med. agosto de 2006;9(2):85-9.

179.   Wu Y, Briley-Saebo K, Xie J, Zhang R, Wang Z, He C, et al. Inflammatory bowel disease: MR- and SPECT/CT-based macrophage imaging for monitoring and evaluating disease activity in experimental mouse model--pilot study. Radiology. mayo de 2014;271(2):400-7.

180.   James ML, Gambhir SS. A molecular imaging primer: modalities, imaging agents, and applications. Physiol Rev. abril de 2012;92(2):897-965.

181.   Perlman SB, Hall BS, Reichelderfer M. PET/CT Imaging of Inflammatory Bowel Disease. Semin Nucl Med. 1 de noviembre de 2013;43(6):420-6.

182.   Louis E, Ancion G, Colard A, Spote V, Belaiche J, Hustinx R. Noninvasive Assessment of Crohn's Disease Intestinal Lesions with 18F-FDG PET/CT. J Nucl Med. 1 de julio de 2007;48(7):1053-9.

183.   Neurath MF, Vehling D, Schunk K, Holtmann M, Brockmann H, Helisch A, et al. Noninvasive assessment of Crohn's disease activity: a comparison of ^{18}F-fluorodeoxyglucose positron emission tomography, hydromagnetic resonance imaging, and granulocyte scintigraphy with labeled antibodies. Am J Gastroenterol. agosto de 2002;97(8):1978-85.

184.   Lemberg DA, Issenman RM, Cawdron R, Green T, Mernagh J, Skehan SJ, et al. Positron emission tomography in the investigation of pediatric inflammatory bowel disease. Inflamm Bowel Dis. agosto de 2005;11(8):733-8.

185.   Bettenworth D, Reuter S, Hermann S, Weckesser M, Kerstiens L, Stratis A, et al. Translational 18F-FDG PET/CT imaging to monitor lesion activity in intestinal inflammation. J Nucl Med Off Publ Soc Nucl Med. mayo de 2013;54(5):748-55.

186.   Hindryckx P, Staelens S, Devisscher L, Deleye S, De Vos F, Delrue L, et al. Longitudinal quantification of inflammation in the murine dextran sodium sulfate-induced colitis model using µPET/CT. Inflamm Bowel Dis. octubre de 2011;17(10):2058-64.

187.   Seoane-Viaño I, Gómez-Lado N, Lázare-Iglesias H, Barreiro-de Acosta M, Silva-Rodríguez J, Luzardo-Álvarez A, et al. Longitudinal PET/CT evaluation of TNBS-induced inflammatory bowel disease rat model. Int J Pharm. 5 de octubre de 2018;549(1-2):335-42.

188.   Pio BS, Byrne FR, Aranda R, Boulay G, Spicher K, Song MH, et al. Noninvasive quantification of bowel inflammation through positron emission tomography imaging of 2-deoxy-2-[18F]fluoro-D-glucose-labeled white blood cells. Mol Imaging Biol. 1 de julio de 2003;5(4):271-7.

189.   Goyanes A, Fernández-Ferreiro A, Majeed A, Gomez-Lado N, Awad A, Luaces-Rodríguez A, et al. PET/CT imaging of 3D printed devices in the gastrointestinal tract of rodents. Int J Pharm. 30 de enero de 2018;536(1):158-64.

190.   Bernards N, Pottier G, Thézé B, Dollé F, Boisgard R. In vivo evaluation of inflammatory bowel disease with the aid of µPET and the translocator protein 18 kDa radioligand [18F]DPA-714. Mol Imaging Biol MIB Off Publ Acad Mol Imaging. febrero de 2015;17(1):67-75.

191.   Loftus EV. Imaging in Inflammatory Bowel Disease: Computed Tomography and Magnetic Resonance Enterography, Ultrasound and Enteroscopy. En: Inflammatory Bowel Disease [Internet]. Wiley-Blackwell; 2010 [citado 20 de octubre de 2018]. p. 266-78. Disponible en: https://onlinelibrary.wiley.com/doi/abs/10.1002/9781444318418.ch19

192.   Pita I, Magro F. Advanced imaging techniques for small bowel Crohn's disease: what does the future hold? Ther Adv Gastroenterol. 2018;11:1756283X18757185.

193.   Phelps ME. Positron emission tomography provides molecular imaging of biological processes. Proc Natl Acad Sci U S A. 1 de agosto de 2000;97(16):9226-33.

194.   Wolk O, Epstein S, Ioffe-Dahan V, Ben-Shabat S, Dahan A. New targeting strategies in drug therapy of inflammatory bowel disease: mechanistic approaches and opportunities. Expert Opin Drug Deliv. septiembre de 2013;10(9):1275-86.

195.   Blonski W, Buchner AM, Lichtenstein GR. Inflammatory bowel disease therapy: current state-of-the-art. Curr Opin Gastroenterol. julio de 2011;27(4):346-57.

196.   Paramsothy S, Rosenstein AK, Mehandru S, Colombel J-F. The current state of the art for biological therapies and new small molecules in inflammatory bowel disease. Mucosal Immunol. 15 de junio de 2018;

197.   Neurath MF. Current and emerging therapeutic targets for IBD. Nat Rev Gastroenterol Hepatol. mayo de 2017;14(5):269-78.

198.   Lautenschläger C, Schmidt C, Fischer D, Stallmach A. Drug delivery strategies in the therapy of inflammatory bowel disease. Adv Drug Deliv Rev. 1 de mayo de 2014;71:58-76.

199.   Zhang M, Merlin D. Nanoparticle-Based Oral Drug Delivery Systems Targeting the Colon for Treatment of Ulcerative Colitis. Inflamm Bowel Dis. 8 de junio de 2018;24(7):1401-15.

200.   Kotla NG, Rana S, Sivaraman G, Sunnapu O, Vemula PK, Pandit A, et al. Bioresponsive drug delivery systems in intestinal inflammation: State-of-the-art and future perspectives. Adv Drug Deliv Rev. 29 de junio de 2018;

201.   Xiao B, Merlin D. Oral colon-specific therapeutic approaches toward treatment of inflammatory bowel disease. Expert Opin Drug Deliv. noviembre de 2012;9(11):1393-407.

202.   Hua S, Marks E, Schneider JJ, Keely S. Advances in oral nano-delivery systems for colon targeted drug delivery in inflammatory bowel disease: Selective targeting to diseased versus healthy tissue. Nanomedicine Nanotechnol Biol Med. 1 de julio de 2015;11(5):1117-32.

203.   Viscido A, Capannolo A, Latella G, Caprilli R, Frieri G. Nanotechnology in the treatment of inflammatory bowel diseases. J Crohns Colitis. septiembre de 2014;8(9):903-18.

204.   Collnot E-M, Ali H, Lehr C-M. Nano- and microparticulate drug carriers for targeting of the inflamed intestinal mucosa. J Controlled Release. julio de 2012;161(2):235-46.

205.   Lamprecht A, Ubrich N, Yamamoto H, Schäfer U, Takeuchi H, Maincent P, et al. Biodegradable nanoparticles for targeted drug delivery in treatment of inflammatory bowel disease. J Pharmacol Exp Ther. noviembre de 2001;299(2):775-81.

206.   Zhang J-X, Wang K, Mao Z-F, Fan X, Jiang D-L, Chen M, et al. Application of liposomes in drug development--focus on gastroenterological targets. Int J Nanomedicine. 2013;8:1325-34.

207.   Jubeh TT, Nadler-Milbauer M, Barenholz Y, Rubinstein A. Local treatment of experimental colitis in the rat by negatively charged liposomes of catalase, TMN and SOD. J Drug Target. 1 de enero de 2006;14(3):155-63.

208.   Gupta AS, Kshirsagar SJ, Bhalekar MR, Saldanha T. Design and development of liposomes for colon targeted drug delivery. J Drug Target. febrero de 2013;21(2):146-60.

209.   Talegaonkar S, Azeem A, Ahmad FJ, Khar RK, Pathan SA, Khan ZI. Microemulsions: a novel approach to enhanced drug delivery. Recent Pat Drug Deliv Formul. 2008;2(3):238-57.

210.   Bansode ST, Kshirsagar SJ, Madgulkar AR, Bhalekar MR, Bandivadekar MM. Design and development of SMEDDS for colon-specific drug delivery. Drug Dev Ind Pharm. 2016;42(4):611-23.

211.   Wu X, Xu J, Huang X, Wen C. Self-microemulsifying drug delivery system improves curcumin dissolution and bioavailability. Drug Dev Ind Pharm. enero de 2011;37(1):15-23.

212.   Siemoneit U, Schmitt C, Alvarez-Lorenzo C, Luzardo A, Otero-Espinar F, Concheiro A, et al. Acrylic/cyclodextrin hydrogels with enhanced drug loading and sustained release capability. Int J Pharm. 7 de abril de 2006;312(1):66-74.

213. Laroui H, Dalmasso G, Nguyen HTT, Yan Y, Sitaraman SV, Merlin D. Drug-Loaded Nanoparticles Targeted to the Colon With Polysaccharide Hydrogel Reduce Colitis in a Mouse Model. Gastroenterology. 1 de marzo de 2010;138(3):843-853.e2.

214. Malamed SF, editor. Chapter 8 - Rectal Sedation. En: Sedation (Sixth Edition) [Internet]. Mosby; 2018 [citado 24 de febrero de 2020]. p. 120-4. Disponible en: http://www.sciencedirect.com/science/article/pii/B9780323400534000081

215. Klotz U, Schwab M. Topical delivery of therapeutic agents in the treatment of inflammatory bowel disease. Adv Drug Deliv Rev. 6 de enero de 2005;57(2):267-79.

216. Choonara IA. Giving drugs per rectum for systemic effect. Arch Dis Child. 1 de agosto de 1987;62(8):771-2.

217. Klein S. Rectal Dosage Forms. En: In Vitro Drug Release Testing of Special Dosage Forms [Internet]. John Wiley & Sons, Ltd; 2019 [citado 24 de febrero de 2020]. p. 211-33. Disponible en: https://onlinelibrary.wiley.com/doi/abs/10.1002/9781118675748.ch8

218. Hua S. Physiological and Pharmaceutical Considerations for Rectal Drug Formulations. Front Pharmacol [Internet]. 2019 [citado 24 de febrero de 2020];10. Disponible en: https://www.frontiersin.org/articles/10.3389/fphar.2019.01196/full

219. Brown J, Haines S, Wilding IR. Colonic spread of three rectally administered mesalazine (Pentasa) dosage forms in healthy volunteers as assessed by gamma scintigraphy. Aliment Pharmacol Ther. agosto de 1997;11(4):685-91.

220. Maisel K, Chattopadhyay S, Moench T, Hendrix C, Cone R, Ensign LM, et al. Enema ion compositions for enhancing colorectal drug delivery. J Control Release Off J Control Release Soc. 10 de julio de 2015;209:280-7.

221. Sutherland LR, Martin F, Greer S, Robinson M, Greenberger N, Saibil F, et al. 5-Aminosalicylic acid enema in the treatment of distal ulcerative colitis, proctosigmoiditis, and proctitis. Gastroenterology. 1 de junio de 1987;92(6):1894-8.

222. Pittet O, Nocito A, Balke H, Duvoisin C, Clavien PA, Demartines N, et al. Rectal enema is an alternative to full mechanical bowel preparation for primary rectal cancer surgery. Colorectal Dis Off J Assoc Coloproctology G B Irel. noviembre de 2015;17(11):1007-10.

223. Giordano S. Examination Review for Radiography. Lippincott Williams & Wilkins; 2013. 281 p.

224. Purohit TJ, Hanning SM, Wu Z. Advances in rectal drug delivery systems. Pharm Dev Technol. diciembre de 2018;23(10):942-52.

225. Loew BJ, Siegel CA. Foam preparations for the treatment of ulcerative colitis. Curr Drug Deliv. julio de 2012;9(4):338-44.

226. Reanmongkol W, Kaewnopparat N, Ratanajamit C. Development of tramadol hydrochloride rectal gel preparations and evaluation of analgesic activity in experimental animals. J Drug Deliv Sci Technol. 1 de enero de 2011;21(6):503-7.

227. Garcia-del Rio L, Diaz-Rodriguez P, Landin M. New tools to design smart thermosensitive hydrogels for protein rectal delivery in IBD. Mater Sci Eng C. 1 de enero de 2020;106:110252.

228. Christophi GP, Rengarajan A, Ciorba MA. Rectal budesonide and mesalamine formulations in active ulcerative proctosigmoiditis: efficacy, tolerance, and treatment approach. Clin Exp Gastroenterol. 19 de mayo de 2016;9:125-30.

229. Fitzgerald BJ, Okos AJ, Miller JW. Treatment of out-of-hospital status epilepticus with diazepam rectal gel. Seizure. enero de 2003;12(1):52-5.

230. Ham AS, Buckheit RW. Designing and developing suppository formulations for anti-HIV drug delivery. Ther Deliv. 2017;8(9):805-17.

231. Schmitt M, Guentert TW. Influence of the hydrophilicity of suppository bases on rectal absorption of carprofen, a lipophilic nonsteroidal anti-inflammatory drug. J Pharm Sci. 1990;79(4):359-63.

232. Watanabe M, Nishino H, Sameshima Y, Ota A, Nakamura S, Hibi T. Randomised clinical trial: evaluation of the efficacy of mesalazine (mesalamine) suppositories in patients with ulcerative colitis and active rectal inflammation – a placebo-controlled study. Aliment Pharmacol Ther. 2013;38(3):264-73.

233. Jaeger SU, Klag T, Hoeger K, Klumpp S, Escher M, Malek N, et al. Tacrolimus Suppositories in Therapy-Resistant Ulcerative Proctitis. Inflamm Intest Dis. 2018;3(3):116-24.

234. Pacheco RM. Tratado de Tecnología Farmacéutica. Pacheco RM, editor. Síntesis; 2017. 458 p. (Pacheco RM. Formas de Dosificación; vol. 3).

235. Norman J, Madurawe RD, Moore CMV, Khan MA, Khairuzzaman A. A new chapter in pharmaceutical manufacturing: 3D-printed drug products. Adv Drug Deliv Rev. Enero 1;108:39-50.

236. Goyanes A, Fina F, Martorana A, Sedough D, Gaisford S, Basit AW. Development of modified release 3D printed tablets (printlets) with pharmaceutical excipients using additive manufacturing. Int J Pharm. 7;527(1–2):21-30.

237. Goyanes A, Madla CM, Umerji A, Piñeiro GD, Montero JMG, Diaz MJL, et al. Automated therapy preparation of isoleucine formulations using 3D printing for the treatment of MSUD: first single-centre, prospective, crossover study in patients. Int J Pharm. 4 de julio de 2019;118497.

238. Pharmaceutials A. Manufactured Using 3D Printing [Internet]. 2015. Disponible en: http://www.spritam.com/ - /hcp/zipdose-technology/manufactured-using-3d-printing.

239. Madla CM, Trenfield SJ, Goyanes A, Gaisford S, Basit AW. 3D Printing Technologies, Implementation and Regulation: An Overview. En: Basit AW, Gaisford S, editores. 3D Printing of Pharmaceuticals [Internet]. Springer International Publishing; 2018. p. 21-40. Disponible en: https://doi.org/10.1007/978-3-319-90755-0_2

240. Sachs E. M. Haggerty JS; C MJ Williams, PA. Three dimensional printing techniques. 20 de abril de 1993;(U.S. Patent 5,204,055).

241. Trenfield SJ, Madla CM, Basit AW, Gaisford S. Binder Jet Printing in Pharmaceutical Manufacturing. En: Basit AW, Gaisford S, editores. 3D Printing of Pharmaceuticals [Internet]. Cham: Springer International Publishing; 2018. p. 41-54. Disponible en: https://doi.org/10.1007/978-3-319-90755-0_3

242. Goole J, Amighi K. 3D printing in pharmaceutics: A new tool for designing customized drug delivery systems. Int J Pharm. 3 de enero de 2016;499(1-2):376-94.

243. Hsiao W-K, Lorber B, Reitsamer H, Khinast J. 3D printing of oral drugs: A new reality or hype? Expert Opin Drug Deliv. 2017;null-null.

244. Gaisford S. 3D printed pharmaceutical products. En: Kalaskar D, editor. 3D Printing in Medicine. 1st ed. Woodhead Publishing; 2017. p. 155-65.

245. Yu DG, Branford-White C, Y.C. Y, Zhu LM, Welbeck EW, Yang XL. A novel fast disintegrating tablet fabricated by three-dimensional printing. Drug Dev Ind Pharm. 2009;35(12):1530-6.

246. Wang CC, Tejwani MR, Roach WJ, Kay JL, Yoo J, Surprenant HL, et al. Development of near zero-order release dosage forms using three-dimensional printing (3-DP (TM)) technology. Drug Dev Ind Pharm. 2006;32(3):367-76.

247. Katstra WE, Palazzolo RD, Rowe CW, Giritlioglu B, Teung P, Cima MJ. Oral dosage forms fabricated by three dimensional printing. J Control Release. 3 de mayo de 2000;66(1):1-9.

248. Yu DG, Zhu LM, Branford-White CJ, Yang XL. Three-dimensional printing in pharmaceutics: Promises and problems. J Pharm Sci. septiembre de 2008;97(9):3666-90.

249. Goyanes A, Buanz AB, Basit AW, Gaisford S. Fused-filament 3D printing (3DP) for fabrication of tablets. Int J Pharm. 30 de septiembre de 2014;476(1-2):88-92.

250. Skowyra J, Pietrzak K, Alhnan MA. Fabrication of extended-release patient-tailored prednisolone tablets via fused deposition modelling (FDM) 3D printing. Eur J Pharm Sci. 20 de febrero de 2015;68:11-7.

251. Goyanes A, Buanz AB, Hatton GB, Gaisford S, Basit AW. 3D printing of modified-release aminosalicylate (4-ASA and 5-ASA) tablets. Eur J Pharm Biopharm. 9 de diciembre de 2015;89:157-62.

252. Kollamaram G, Croker DM, Walker GM, Goyanes A, Basit AW, Gaisford S. Low temperature fused deposition modeling (FDM) 3D printing of thermolabile drugs. Int J Pharm. 10 de julio de 2018;545(1):144-52.

253. Kempin W, Domsta V, Grathoff G, Brecht I, Semmling B, Tillmann S, et al. Immediate Release 3D-Printed Tablets Produced Via Fused Deposition Modeling of a Thermo-Sensitive Drug. Pharm Res. 20 de abril de 2018;35(6):124.

254. Okwuosa TC, Stefaniak D, Arafat B, Isreb A, Wan K-W, Alhnan MA. A lower temperature FDM 3D printing for the manufacture of patient-specific immediate release tablets. Pharm Res. 2016;33(11):2704-12.

255. Wilson M, Williams MA, Jones DS, Andrews GP. Hot-melt extrusion technology and pharmaceutical application. Ther Deliv. 2012;3(6):787-97.

256. Lang B, McGinity JW, Williams I Robert O. Hot-melt extrusion – basic principles and pharmaceutical applications. Drug Dev Ind Pharm. septiembre de 2014;40(9):1133-55.

257. Goyanes A, Martinez PR, Buanz A, Basit A, Gaisford S. Effect of geometry on drug release from 3D printed tablets. Int J Pharm. 28 de abril de 2015;494(2):657-63.

258. Goyanes A, Scarpa M, Kamlow M, Gaisford S, Basit AW, Orlu M. Patient acceptability of 3D printed medicines. Int J Pharm. 15 de septiembre de 2017;530(1):71-8.

259. Goyanes A, Chang H, Sedough D, Hatton GB, Wang J, Buanz A, et al. Fabrication of controlled-release budesonide tablets via desktop (FDM) 3D printing. Int J Pharm. 2015;496(2):414-20.

260. Okwuosa TC, Soares C, Gollwitzer V, Habashy R, Timmins P, Alhnan MA. On demand manufacturing of patient-specific liquid capsules via co-ordinated 3D printing and liquid dispensing. Eur J Pharm Sci. 15 de junio de 2018;118:134-43.

261. Okwuosa TC, Pereira BC, Arafat B, Cieszynska M, Isreb A, Alhnan MA. Fabricating a Shell-Core Delayed Release Tablet Using Dual FDM 3D Printing for Patient-Centred Therapy. Pharm Res. 2017;34(2):427-37.

262. Melocchi A, Parietti F, Maccagnan S, Ortenzi MA, Antenucci S, Briatico-Vangosa F, et al. Industrial Development of a 3D-Printed Nutraceutical Delivery Platform in the Form of a Multicompartment HPC Capsule. AAPS PharmSciTech [Internet]. junio de 2018; Disponible en: https://doi.org/10.1208/s12249-018-1029-9263. Melocchi A, Parietti F, Maroni A, Foppoli A, Gazzaniga A, Zema L. Hot-melt extruded filaments based on pharmaceutical grade polymers for 3D printing by fused deposition modeling. Int J Pharm. 7;509(1–2):255-63.

264. Melocchi A, Parietti F, Loreti G, Maroni A, Gazzaniga A, Zema L. 3D printing by fused deposition modeling (FDM) of a swellable/erodible capsular device for oral pulsatile release of drugs. J Drug Deliv Sci Technol. 2015;30(B):360-7.

265. Goyanes A, Kobayashi M, Martinez-Pacheco R, Gaisford S, Basit AW. Fused-filament 3D printing of drug products: Microstructure analysis and drug release characteristics of PVA-based caplets. Int J Pharm. 30 de noviembre de 2016;514(1):290-5.

266. Xu X, Zhao J, Wang M, Wang L, Yang J. 3D Printed Polyvinyl Alcohol Tablets with Multiple Release Profiles. Sci Rep. 28 de agosto de 2019;9(1):12487.

267. Goyanes A, Wang J, Buanz A, Martinez-Pacheco R, Telford R, Gaisford S, et al. 3D Printing of Medicines: Engineering Novel Oral Devices with Unique Design and Drug Release Characteristics. Mol Pharm. 2 de noviembre de 2015;12(11):4077-84.

268. Beck RCR, Chaves PS, Goyanes A, Vukosavljevic B, Buanz A, Windbergs M, et al. 3D printed tablets loaded with polymeric nanocapsules: An innovative approach to produce customized drug delivery systems. Int J Pharm. 2017;528(1–2):268-79.

269. Muwaffak Z, Goyanes A, Clark V, Basit AW, Hilton ST, Gaisford S. Patient-specific 3D scanned and 3D printed antimicrobial polycaprolactone wound dressings. Int J Pharm. 2017;527(1):161-70.

270. Awad A, Gaisford S, Basit AW. Fused Deposition Modelling: Advances in Engineering and Medicine. En: Basit AW, Gaisford S, editores. 3D Printing of Pharmaceuticals [Internet]. Cham: Springer International Publishing; 2018. p. 107-32. Disponible en: https://doi.org/10.1007/978-3-319-90755-0_6

271. Fuenmayor E, Forde M, Healy A, Devine D, Lyons J, McConville C, et al. Material Considerations for Fused-Filament Fabrication of Solid Dosage Forms. Pharmaceutics. 2018;10(2):44.

272.   Goyanes A, Allahham N, Trenfield SJ, Stoyanov E, Gaisford S, Basit AW. Direct powder extrusion 3D printing: Fabrication of drug products using a novel single-step process. Int J Pharm. 15 de agosto de 2019;567:118471.

273.   Firth J, Basit AW, Gaisford S. The Role of Semi-Solid Extrusion Printing in Clinical Practice. En: Basit AW, Gaisford S, editores. 3D Printing of Pharmaceuticals [Internet]. Springer International Publishing; 2018. p. 133-51. Disponible en: https://doi.org/10.1007/978-3-319-90755-0_7

274.   Khaled SA, Burley JC, Alexander MR, Roberts CJ. Desktop 3D printing of controlled release pharmaceutical bilayer tablets. Int J Pharm. 30 de enero de 2014;461(1-2):105-11.

275.   Khaled SA, Burley JC, Alexander MR, Yang J, Roberts CJ. 3D printing of tablets containing multiple drugs with defined release profiles. Int J Pharm. 30 de octubre de 2015;494(2):643-50.

276.   Khaled SA, Burley JC, Alexander MR, Yang J, Roberts CJ. 3D printing of five-in-one dose combination polypill with defined immediate and sustained release profiles. J Controlled Release. 10 de noviembre de 2015;217:308-14.

277.   Khaled SA, Alexander MR, Wildman RD, Wallace MJ, Sharpe S, Yoo J, et al. 3D extrusion printing of high drug loading immediate release paracetamol tablets. Int J Pharm. Enero 3;538(1–2):223-30.

278.   Conceição J, Farto-Vaamonde X, Goyanes A, Adeoye O, Concheiro A, Cabral-Marques H, et al. Hydroxypropyl-β-cyclodextrin-based fast dissolving carbamazepine printlets prepared by semisolid extrusion 3D printing. Carbohydr Polym [Internet]. 29 de mayo de 2019; Disponible en: http://www.sciencedirect.com/science/article/pii/S0144861719305570

279.   Vithani K, Goyanes A, Jannin V, Basit AW, Gaisford S, Boyd BJ. An Overview of 3D Printing Technologies for Soft Materials and Potential Opportunities for Lipid-based Drug Delivery Systems. Pharm Res. 7 de noviembre de 2018;36(1):4.

280.   Vithani K, Goyanes A, Jannin V, Basit AW, Gaisford S, Boyd BJ. A Proof of Concept for 3D Printing of Solid Lipid-Based Formulations of Poorly Water-Soluble Drugs to Control Formulation Dispersion Kinetics. Pharm Res. 16 de mayo de 2019;36(7):102.

281.   Fina F, Goyanes A, Gaisford S, Basit AW. Selective laser sintering (SLS) 3D printing of medicines. Int J Pharm. 30 de agosto de 2017;529(1):285-93.

282.   Silva D, Gerhardt De Oliveira M, Meurer E, Meurer M, Silva J, santa barbara A. Dimensional error in selective laser sintering and 3D-printing of models for craniomaxillary anatomy reconstruction. Vol. 36. 2008. 443-9 p.

283.   Leong KF, Chua CK, Gui WS, Verani. Building Porous Biopolymeric Microstructures for Controlled Drug Delivery Devices Using Selective Laser Sintering. Int J Adv Manuf Technol. 2006;31(5):483-9.

284.   Du Y, Liu H, Yang Q, Wang S, Wang J, Ma J, et al. Selective laser sintering scaffold with hierarchical architecture and gradient composition for osteochondral repair in rabbits. Biomaterials. agosto de 2017;137:37-48.

285.   Alhnan MA, Okwuosa TC, Sadia M, Wan KW, Ahmed W, Arafat B. Emergence of 3D Printed Dosage Forms: Opportunities and Challenges. Pharm Res. 18 de mayo de 2016;33(8):1817-32.

286.   Fina F, Madla CM, Goyanes A, Zhang J, Gaisford S, Basit AW. Fabricating 3D printed orally disintegrating printlets using selective laser sintering. Int J Pharm. 14 de febrero de 2018;541(1-2):101-7.

287.   Fina F, Goyanes A, Madla CM, Awad A, Trenfield SJ, Kuek JM, et al. 3D printing of drug-loaded gyroid lattices using selective laser sintering. Int J Pharm [Internet]. 19 de mayo de 2018; Disponible en: http://www.sciencedirect.com/science/article/pii/S0378517318303545

288.   Awad A, Fina F, Trenfield SJ, Patel P, Goyanes A, Gaisford S, et al. 3D Printed Pellets (Miniprintlets): A Novel, Multi-Drug, Controlled Release Platform Technology. Pharmaceutics. 29 de marzo de 2019;11(4).

289.   Rowe CW, Katstra WE, Palazzolo RD, Giritlioglu B, Teung P, Cima MJ. Multimechanism oral dosage forms fabricated by three dimensional printing. J Controlled Release. mayo de 2000;66(1):11-7.

290.   Robles Martinez P, Basit AW, Gaisford S. The History, Developments and Opportunities of Stereolithography. En: Basit AW, Gaisford S, editores. 3D Printing of Pharmaceuticals [Internet].

Springer International Publishing; 2018. p. 55-79. Disponible en: https://doi.org/10.1007/978-3-319-90755-0_4

291. Derakhshanfar S, Mbeleck R, Xu K, Zhang X, Zhong W, Xing M. 3D bioprinting for biomedical devices and tissue engineering: A review of recent trends and advances. Bioact Mater. 1 de junio de 2018;3(2):144-56.

292. Melchels FP, Feijen J, Grijpma DW. A poly(D,L-lactide) resin for the preparation of tissue engineering scaffolds by stereolithography. Biomaterials. agosto de 2009;30(23-24):3801-9.

293. Elomaa L, Teixeira S, Hakala R, Korhonen H, Grijpma DW, Seppälä JV. Preparation of poly(ε-caprolactone)-based tissue engineering scaffolds by stereolithography. Acta Biomater. 1 de noviembre de 2011;7(11):3850-6.

294. Gou M, Qu X, Zhu W, Xiang M, Yang J, Zhang K, et al. Bio-inspired detoxification using 3D-printed hydrogel nanocomposites. Nat Commun. 8 de mayo de 2014;5:3774.

295. Goyanes A, Det-Amornrat U, Wang J, Basit AW, Gaisford S. 3D scanning and 3D printing as innovative technologies for fabricating personalized topical drug delivery systems. J Control Release. 14 de mayo de 2016;234:41-8.

296. Wang J, Goyanes A, Gaisford S, Basit AW. Stereolithographic (SLA) 3D printing of oral modified-release dosage forms. Int J Pharm. 4;503(1–2):207-12.

297. Martinez PR, Goyanes A, Basit AW, Gaisford S. Fabrication of drug-loaded hydrogels with stereolithographic 3D printing. Int J Pharm. 30 de octubre de 2017;532(1):313-7.

298. Martinez PR, Goyanes A, Basit AW, Gaisford S. Influence of Geometry on the Drug Release Profiles of Stereolithographic (SLA) 3D-Printed Tablets. AAPS PharmSciTech. noviembre de 2018;19(8):3355-61.

299. Robles-Martinez P, Xu X, Trenfield SJ, Awad A, Goyanes A, Telford R, et al. 3D Printing of a Multi-Layered Polypill Containing Six Drugs Using a Novel Stereolithographic Method. Pharmaceutics. 11 de junio de 2019;11(6).

300. Melchels FP, Feijen J, Grijpma DW. A review on stereolithography and its applications in biomedical engineering. Biomaterials. 2010;31(24):6121-30.

301. Xu X, Robles-Martinez P, Madla CM, Goyanes A, Joubert F, Basit AW, et al. Stereolithography (SLA) 3D printing of an antihypertensive polyprintlet: Case study of an unexpected photopolymer-drug reaction. Addit Manuf. 13 de enero de 2020;101071.

302. Brittain HK, Scott R, Thomas E. The rise of the genome and personalised medicine. Clin Med Lond. diciembre de 2017;17(6):545-51.

303. Lander ES, Linton LM, Birren B, Nusbaum C, Zody MC, Baldwin J, et al. Initial sequencing and analysis of the human genome. Nature. 1 de febrero de 2001;409(6822):860-921.

304. Seyhan AA, Carini C. Are innovation and new technologies in precision medicine paving a new era in patients centric care? J Transl Med. 5 de abril de 2019;17(1):114.

305. Alomari M, Mohamed FH, Basit AW, Gaisford S. Personalised dosing: Printing a dose of one's own medicine. Int J Pharm. 30 de octubre de 2015;494(2):568-77.

306. Blix HS, Viktil KK, Moger TA, Reikvam A. Drugs with narrow therapeutic index as indicators in the risk management of hospitalised patients. Pharm Pract. 2010;8(1):50-5.

307. Wening K, Breitkreutz J. Oral drug delivery in personalized medicine: unmet needs and novel approaches. Int J Pharm. 14 de febrero de 2011;404(1-2):1-9.

308. Trenfield SJ, Awad A, Goyanes A, Gaisford S, Basit AW. 3D Printing Pharmaceuticals: Drug Development to Frontline Care. Trends Pharmacol Sci. 2018;39(5):440-51.

309. Araujo MRP, Sa-Barreto LL, Gratieri T, Gelfuso GM, Cunha-Filho M. The Digital Pharmacies Era: How 3D Printing Technology Using Fused Deposition Modeling Can Become a Reality. Pharmaceutics. 19 de marzo de 2019;11(3).

310. Edinger M, Bar-Shalom D, Rantanen J, Genina N. Visualization and Non-Destructive Quantification of Inkjet-Printed Pharmaceuticals on Different Substrates Using Raman Spectroscopy and Raman Chemical Imaging. Pharm Res. mayo de 2017;34(5):1023-36.

311. Cournoyer A, Simard JS, Cartilier L, Abatzoglou N. Quality Control of Multi-Component, Intact Pharmaceutical Tablets with Three Different Near-Infrared Apparatuses. Pharm Dev Technol. 1 de enero de 2008;13(5):333-43.

312. Trenfield SJ, Goyanes A, Telford R, Wilsdon D, Rowland M, Gaisford S, et al. 3D printed drug products: Non-destructive dose verification using a rapid point-and-shoot approach. Int J Pharm. 5 de octubre de 2018;549(1):283-92.

313. Markl D, Zeitler JA, Rasch C, Michaelsen MH, Mullertz A, Rantanen J, et al. Analysis of 3D Prints by X-ray Computed Microtomography and Terahertz Pulsed Imaging. Pharm Res. mayo de 2017;34(5):1037-52.

314. Edinger M, Bar-Shalom D, Sandler N, Rantanen J, Genina N. QR encoded smart oral dosage forms by inkjet printing. Int J Pharm. 30 de enero de 2018;536(1):138-45.

315. Trenfield SJ, Xian Tan H, Awad A, Buanz A, Gaisford S, Basit AW, et al. Track-and-trace: Novel anti-counterfeit measures for 3D printed personalized drug products using smart material inks. Int J Pharm. 15 de agosto de 2019;567:118443.

316. Breitkreutz J, Boos J. Paediatric and geriatric drug delivery. Expert Opin Drug Deliv. enero de 2007;4(1):37-45.

317. Al-Metwali B, Mulla H. Personalised dosing of medicines for children. J Pharm Pharmacol. mayo de 2017;69(5):514-24.

318. Visser JC, Woerdenbag HJ, Hanff LM, Frijlink HW. Personalized Medicine in Pediatrics: The Clinical Potential of Orodispersible Films. AAPS PharmSciTech. febrero de 2017;18(2):267-72.

319. Cascorbi I. Drug interactions--principles, examples and clinical consequences. Dtsch Arzteblatt Int. 2012;109(33-34):546-56.

320. Al Hamid A, Ghaleb M, Aljadhey H, Aslanpour Z. A systematic review of hospitalization resulting from medicine-related problems in adult patients. Br J Clin Pharmacol. 1 de agosto de 2014;78(2):202-17.

321. Oscanoa TJ, Lizaraso F, Carvajal A. Hospital admissions due to adverse drug reactions in the elderly. A meta-analysis. Eur J Clin Pharmacol. junio de 2017;73(6):759-70.

322. Kairuz TE, Gargiulo D, Bunt C, Garg S. Quality, safety and efficacy in the «off-label» use of medicines. Curr Drug Saf. enero de 2007;2(1):89-95.

323. Liu F, Ranmal S, Batchelor HK, Orlu-Gul M, Ernest TB, Thomas IW, et al. Patient-centred pharmaceutical design to improve acceptability of medicines: similarities and differences in paediatric and geriatric populations. Drugs. octubre de 2014;74(16):1871-89.

324. Walsh J, Ranmal SR, Ernest TB, Liu F. Patient acceptability, safety and access: A balancing act for selecting age-appropriate oral dosage forms for paediatric and geriatric populations. Int J Pharm. 5 de febrero de 2018;536(2):547-62.

325. Oblom H, Sjoholm E, Rautamo M, Sandler N. Towards Printed Pediatric Medicines in Hospital Pharmacies: Comparison of 2D and 3D-Printed Orodispersible Warfarin Films with Conventional Oral Powders in Unit Dose Sachets. Pharmaceutics. 14 de julio de 2019;11(7).

326. Jamróz W, Kurek M, Łyszczarz E, Szafraniec J, Knapik-Kowalczuk J, Syrek K, et al. 3D printed orodispersible films with Aripiprazole. Int J Pharm. 30 de noviembre de 2017;533(2):413-20.

327. Liu F, Ghaffur A, Bains J, Hamdy S. Acceptability of oral solid medicines in older adults with and without dysphagia: A nested pilot validation questionnaire based observational study. Int J Pharm. 2016;512(2):374-81.

328. Fasto MM, Genina N, Kaae S, Kalvemark Sporrong S. Perceptions, preferences and acceptability of patient designed 3D printed medicine by polypharmacy patients: a pilot study. Int J Clin Pharm. octubre de 2019;41(5):1290-8.

329. Park BJ, Choi HJ, Moon SJ, Kim SJ, Bajracharya R, Min JY, et al. Pharmaceutical applications of 3D printing technology: current understanding and future perspectives. J Pharm Investig. 1 de noviembre de 2019;49(6):575-85.

330. Haring AP, Tong Y, Halper J, Johnson BN. Programming of Multicomponent Temporal Release Profiles in 3D Printed Polypills via Core–Shell, Multilayer, and Gradient Concentration Profiles. Adv Healthc Mater. 1 de agosto de 2018;7(16):1800213.

331. Charbe NB, McCarron PA, Lane ME, Tambuwala MM. Application of three-dimensional printing for colon targeted drug delivery systems. Int J Pharm Investig. abril de 2017;7(2):47-59.

332.   Linares V, Casas M, Caraballo I. Printfills: 3D printed systems combining fused deposition modeling and injection volume filling. Application to colon-specific drug delivery. Eur J Pharm Biopharm. enero de 2019;134:138-43.

333.   Trenfield SJ, Awad A, Madla CM, Hatton GB, Firth J, Goyanes A, et al. Shaping the future: recent advances of 3D printing in drug delivery and healthcare. Expert Opin Drug Deliv. 3 de octubre de 2019;16(10):1081-94.

334.   Miao S, Zhu W, Castro NJ, Leng J, Zhang LG. Four-Dimensional Printing Hierarchy Scaffolds with Highly Biocompatible Smart Polymers for Tissue Engineering Applications. Tissue Eng Part C Methods. octubre de 2016;22(10):952-63.

335.   Zarek M, Mansour N, Shapira S, Cohn D. 4D Printing of Shape Memory-Based Personalized Endoluminal Medical Devices. Macromol Rapid Commun. enero de 2017;38(2).

336.   Melocchi A, Inverardi N, Uboldi M, Baldi F, Maroni A, Pandini S, et al. Retentive device for intravesical drug delivery based on water-induced shape memory response of poly(vinyl alcohol): design concept and 4D printing feasibility. Int J Pharm. 25 de marzo de 2019;559:299-311.

337.   Wong CH, Siah KW, Lo AW. Estimation of clinical trial success rates and related parameters. Biostatistics. 1 de abril de 2019;20(2):273-86.

338.   Awad A, Trenfield SJ, Goyanes A, Gaisford S, Basit AW. Reshaping drug development using 3D printing. Drug Discov Today. 24 de mayo de 2018;23(8):1547-55.

339.   Shah N, Sandhu H, Choi DS, Kalb O, Page S, Wyttenbach N. Structured Development Approach for Amorphous Systems. En: Williams Iii RO, Watts AB, Miller DA, editores. Formulating Poorly Water Soluble Drugs [Internet]. New York, NY: Springer New York; 2012. p. 267-310. Disponible en: https://doi.org/10.1007/978-1-4614-1144-4_8

340.   Trenfield S, Madla C, Basit A, Gaisford S. The Shape of Things to Come: Emerging Applications of 3D Printing in Healthcare. En 2018. p. 1-19.

341.   Sinha S, Vohora D. Chapter 2 - Drug Discovery and Development: An Overview. En: Vohora D, Singh G, editores. Pharmaceutical Medicine and Translational Clinical Research [Internet]. Boston: Academic Press; 2018. p. 19-32. Disponible en: http://www.sciencedirect.com/science/article/pii/B978012802103300002X

342.   Seoane-Viaño I, Gómez-Lado N, Lázare-Iglesias H, Rey-Bretal D, Lamela-Gómez I, Otero-Espinar F, et al. Evaluation of the therapeutic activity of Melatonin and Resveratrol in Inflammatory Bowel Disease: a longitudinal PET/CT study in an animal model. Int J Pharm. 5 de octubre de 2019;118713.

343.   Gao Y, Gesenberg C, Zheng W. Chapter 17 - Oral Formulations for Preclinical Studies: Principle, Design, and Development Considerations. En: Qiu Y, Chen Y, Zhang GGZ, Yu L, Mantri RV, editores. Developing Solid Oral Dosage Forms (Second Edition) [Internet]. Boston: Academic Press; 2017. p. 455-95. Disponible en: http://www.sciencedirect.com/science/article/pii/B9780128024478000170

344.   Singh G. Chapter 4 - Preclinical Drug Development. En: Vohora D, Singh G, editores. Pharmaceutical Medicine and Translational Clinical Research [Internet]. Boston: Academic Press; 2018. p. 47-63. Disponible en: http://www.sciencedirect.com/science/article/pii/B9780128021033000043

345.   Saphier S, Rosner A, Brandeis R, Karton Y. Gastro intestinal tracking and gastric emptying of solid dosage forms in rats using X-ray imaging. Int J Pharm. 30 de marzo de 2010;388(1-2):190-5.

346.   Pietrzak K, Isreb A, Alhnan MA. A flexible-dose dispenser for immediate and extended release 3D printed tablets. Eur J Pharm Biopharm. 2015;96:380-7.

347.   Gómez-Lado N, Seoane-Viaño I, Matiz S, Madla MC, Yadav V, Aguiar P, et al. Gastrointestinal Tracking and Gastric Emptying of Coated Capsules in Rats with or without Sedation Using CT imaging. Pharmaceutics. 2020;12(1).

348.   Smith D, Kapoor Y, Hermans A, Nofsinger R, Kesisoglou F, Gustafson TP, et al. 3D printed capsules for quantitative regional absorption studies in the GI tract. Int J Pharm. 25 de octubre de 2018;550(1):418-28.

349.   Buoen C, Bjerrum OJ, Thomsen MS. How first-time-in-human studies are being performed: a survey of phase I dose-escalation trials in healthy volunteers published between 1995 and 2004. J Clin Pharmacol. octubre de 2005;45(10):1123-36.

350.   Derhaschnig U, Jilma B. Phase-I studies and first-in-human trials. En: Müller M, editor. Clinical Pharmacology: Current Topics and Case Studies [Internet]. Vienna: Springer Vienna; 2010. p. 89-99. Disponible en: https://doi.org/10.1007/978-3-7091-0144-5_7

351.   FDA. Estimating the maximum safe starting dose in initial clinical trials for therapeutics in adult healthy volunteers. [Internet]. 2005. Disponible en: https://www.fda.gov/regulatory-information/search-fda-guidance-documents/estimating-maximum-safe-starting-dose-initial-clinical-trials-therapeutics-adult-healthy-volunteers

352.   Shen J, Swift B, Mamelok R, Pine S, Sinclair J, Attar M. Design and Conduct Considerations for First-in-Human Trials. Clin Transl Sci. enero de 2019;12(1):6-19.

353.   Bittorf KJ, Sanghvi T, Katstra JP. Design of Solid Dosage Formulations. En: Chemical Engineering in the Pharmaceutical Industry [Internet]. John Wiley & Sons, Ltd; 2019 [citado 29 de enero de 2020]. p. 19-52. Disponible en: https://onlinelibrary.wiley.com/doi/abs/10.1002/9781119600800.ch52

354.   Yang Y, Wang H, Li H, Ou Z, Yang G. 3D printed tablets with internal scaffold structure using ethyl cellulose to achieve sustained ibuprofen release. Eur J Pharm Sci. 30 de marzo de 2018;115:11-8.

355.   Isreb A, Baj K, Wojsz M, Isreb M, Peak M, Alhnan MA. 3D printed oral theophylline doses with innovative «radiator-like» design: Impact of polyethylene oxide (PEO) molecular weight. Int J Pharm. 10 de junio de 2019;564:98-105.

356.   Zhang J, Feng X, Patil H, Tiwari RV, Repka MA. Coupling 3D printing with hot-melt extrusion to produce controlled-release tablets. Int J Pharm. 3;519(1–2):186-97.

357.   Solanki NG, Tahsin M, Shah AV, Serajuddin ATM. Formulation of 3D Printed Tablet for Rapid Drug Release by Fused Deposition Modeling: Screening Polymers for Drug Release, Drug-Polymer Miscibility and Printability. J Pharm Sci. enero de 2018;107(1):390-401.

358.   Page SJ, Persch AC. Recruitment, retention, and blinding in clinical trials. Am J Occup Ther. marzo de 2013;67(2):154-61.

359.   EMA. ICH Q1A (R2) Stability testing of new drug sustances and drug products [Internet]. 2003. Disponible en: https://www.ema.europa.eu/en/ich-q1a-r2-stability-testing-new-drug-substances-drug-products
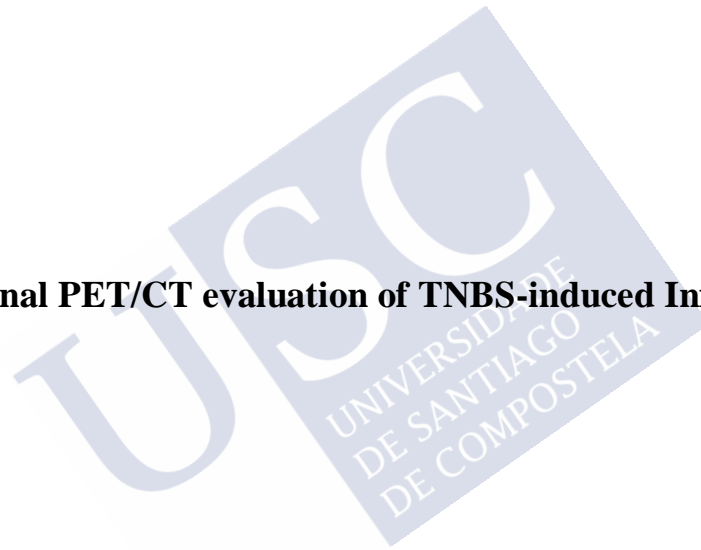
Chapter I.

Longitudinal PET/CT evaluation of TNBS-induced Inflammatory Bowel Disease rat model

CHAPTER I

ABSTRACT

Inflammatory bowel disease (IBD) is a group of chronic disorders of the gastrointestinal tract, which two main types are Crohn´s disease and ulcerative colitis. It has multifactorial etiologies, being essential the use of animal models and disease activity measures to develop new therapies. With this aim, the use of animal models in combination with non-invasive molecular imaging can play an important role in the development of new treatments. In this study, IBD was induced in rats using 2,4,6-trinitrobenzenesulfonic acid (TNBS) and longitudinal [18F]FDG PET/CT scans were conducted to assess disease progression post-TNBS administration. Afterwards, [18F]FDG PET/CT scans were carried out after treatment with methylprednisolone to validate the model. In non-treated rats, SUV_{max} (Standardized Uptake Value) rapidly increased after IBD induction, being particularly significant ($p<0.01$) on days 7-13 after induction. There were no significant differences between non-treated and treated IBD rats from days 0-3. Nevertheless, treated IBD rats showed a significant decrease in SUV_{max} between days 7-13 ($p<0.01$). Histological examination showed descending and transverse colon as the most affected regions. There was a moderate ($R^2=0.61$) and strong ($R^2=0.82$) correlation of SUV_{max} with Nancy grade (parameter for histological assessment of disease activity) and weight changes, respectively. In this study, we have performed the first longitudinal [18F]FDG PET/CT assessment of TNBS-induced IBD in rats, demonstrating the potential role of preclinical molecular imaging for the evaluation of new therapies in combination with IBD rat models.

Keywords: inflammatory bowel disease, colitis, TNBS-induced, [18F]FDG PET, rat model.

INTRODUCTION

Inflammatory bowel disease (IBD) represents a group of chronic relapsing inflammatory diseases of the gastrointestinal tract which can be presented under two major entities, ulcerative colitis and Crohn's disease (1). Crohn´s disease is a transmural disease that can affect the whole gastrointestinal tract, while ulcerative colitis affects mainly the mucosa of the large bowel. The exact etiology of the illness still remain unknown but several factors such as luminal microflora, external environment, genetic susceptibility and disturbances in the immune responses have been suggested to play a role in the pathogenesis of IBD. The clinical symptoms of IBD may range from mild to severe, with a very heterogenic presentation regarding to behaviour and disease location. Furthermore, the course of the disease can change over time, alternating remission periods and others with severe exacerbations. During the outbreaks, the main symptoms of both major types are very similar and roughly consist of abdominal pain, bloody diarrhea, decreased body weight, fever and leucocytosis (2,3).

Conventional treatment of IBD has been based on anti-inflammatory drugs such as corticosteroids and a variety of immunosuppressants which involve a non-specific suppression of the immune response, leading to undesirable side effects. Other therapeutic approach is based on biological agents, such as monoclonal antibodies and recombinant proteins. The success of the monoclonal antibody Infliximab, which target the mediator TNF-α has encouraged the development of agents targeting the mechanisms involved in the inflammatory process. In addition, each patient shows their own combination of factors underlying the inflammatory process, which means that the response to therapy is different among patients, being often ineffective. For this reason, further work needs to be done in order to determine whether a patient will respond properly to the treatment, taking into account symptoms, site and behaviour of disease (4). Therefore, the search for novel biomarkers that enable a treatment planning is an emerging field that will play a promising role in the development of future personalized therapies, first through the choice of an adequate therapy to treat the active disease and later, monitoring the efficacy of a treatment in its earliest stages. (5).

Over the last decades, multiple preclinical IBD animal models have been developed to investigate the immunopathogenic mechanisms involved in the illness in order to develop specific therapeutic compounds for IBD, rather than the generic drugs currently used. The most commonly used animal models are those chemically induced or obtained from transgenic models (6-9). Among these preclinical models of IBD, most of the current preclinical studies have been performed using chemically induced models, such as the TNBS model. The chemically induced intestinal inflammation is achieved by a topical administration of 2,4,6-trinitrobenzenesulfonic acid (TNBS) in 50% ethanol which involves both chemical damage and T cell immune reactivity (10, 11). This reagent is a hapten which causes a T-cell mediated immunity against haptenized proteins and luminal antigens. It administration results in acute necrosis of the colon wall due to oxidative damage, along with transmural inflammation that closely resembles the histopathological lesions developed in human Crohn's disease (8, 12, 13). The ethanol breaks the mucosal barrier allowing the penetration of the

reagent. The main symptoms of animals with TNBS-induced colitis are bloody diarrhea, weight loss and intestinal wall thickening. The advantages of this animal model include rapid development of the illness, localized damage to the colon and low cost. Some drawbacks are the requirement of technical expertise and the need of anaesthesia for rectal administration. It has to be mentioned that although IBD animal models allow us to approach the complex mechanisms involved in chronic intestinal inflammation, they only partially reflect the complexity of the human disease (14). Therefore, a detailed study of the pathological characteristics and the disease progression should be carried out for each experiment (15).

The medical imaging techniques most commonly used in the clinical routine, such as PET, SPECT, CT and MRI, can also be applied in the field of preclinical research in order to accurately characterize IBD models and evaluate the potential and effectiveness of new therapies. In particular, molecular imaging has a promising future due to its applicability in the characterization and quantification of biological processes at the cellular level, thus detecting the existing metabolic and functional changes in the pathological pathway (16).

In addition, several works have been focused on the identification of non-invasive preclinical imaging biomarkers that can strongly help in the characterization of IBD. SPECT imaging was initially employed in IBD murine models induced with TNBS by using [^{111}In]labelled white blood cells (17, 18) and more recently [^{67}Ga]citrate (19). These techniques showed serial measurements of radiotracer uptake to assess the disease activity over time. Moreover, several works showed that MRI easily distinguishes between rats with IBD and controls based on anatomical measurements of the colon wall thickness (20, 21). MRI also can be used as SPECT imaging for disease activity assessment by the use of contrast agents such as macrophages labelled with superparamagnetic iron oxide nanoparticles (SPIONs) (22). These works were based on longitudinal assessments on the same animal over time and thereby the number of animals was drastically reduced (23, 24). Furthermore, pathological characteristics and disease progression obtained from each IBD model can be compared to the human disease and the biomarkers identified can be directly transferred to clinical practice. Nevertheless, the translational value of SPECT and MRI imaging biomarkers is limited for IBD due to the standard clinical methods used to assess the patient's disease activity. These are based on indirect methods, such as blood and stool tests, or direct methods such as colonoscopy and recently PET/CT (Positron emission tomography/Computed tomography) (25).

The clinical use of PET/CT with the radiotracer [^{18}F]Fluoro-2-deoxy-2-D-Glucose ([^{18}F]FDG), has been shown to be highly sensitive in the identification of severe to moderate inflammatory involvement in the digestive tract. PET/CT integrates the physiological information obtained by PET with the anatomic information of CT. Consequently, it may be a useful tool for the noninvasive quantification of inflammation in patients with IBD (26-28). The radiotracer [^{18}F]FDG is a glucose metabolism marker used to identify areas where there is abnormally high glucose metabolism due to inflammation or infection. When compared with other radiotracers, it has the advantage of being widely available at a reasonable cost.

In particular, an evaluation of genetic murine models of IBD with [18F]FDG PET was used to provide a strong basis for its use during the follow-up. This study showed a significant correlation between increased [18F]FDG uptake in colon wall with increased expression of Glut-1 in CD4+T cells, which reflects the disease-associated intestinal activity that precedes clinical inflammation (29). Furthermore, [18F]FDG PET was also used for longitudinal assessments of disease activity in IBD mice induced with dextran sodium sulfate (DSS), a reagent that induces high diffuse inflammation in the colon (30, 31). This study showed that PET is a reliable technique to monitor murine DSS-induced models over time. More recently, [18F]FDG PET was used for the evaluation of TNBS-induced models, but without longitudinal assessment of disease activity. This study concluded that TNBS models provide a spatial pattern of local inflammation substantially different from the global inflammation obtained from DSS models (32). Therefore, it would be interesting to carry out longitudinal and extensive assessments of disease progression in TNBS models such as those previously carried out for DSS models.

Our work is focused on conducting longitudinal [18F]FDG PET/CT studies over the time for the assessment of spatial inflammation patterns and disease progression in a TNBS-induced IBD rat model. Furthermore, the aim of this work is to validate the use of this technique in combination with an animal model for the development of new medicines and therapies for IBD through the assessment of disease progression and subsequent remission in rats systematically treated with corticosteroids. To our knowledge, this is the first longitudinal [18F]FDG PET/CT study performed in TNBS-induced IBD rats, as well as the first assessment of inflammation remission in treated IBD rats.

METHODS

Inflammatory Bowel Disease (IBD) models

These studies were carried out on male Sprague-Dawley rats (average weight of 300±25g) supplied by the animal facilities at the University of Santiago de Compostela. During the experiments, animals were kept in individual cages under controlled temperature (22±1ºC) and humidity (60±5%) conditions, with day-night cycles regulated by artificial light (12/12 hours) and fed *ad libitum*. All animal experiments complied the ARRIVE guidelines (33) and were carried out in accordance with the Spanish and European Union (UE) directive for animal experiments RD53/2013 and 2010/63/EU. Experiments were approved by the University of Santiago de Compostela (USC) Bioethics Comitte, (Ref. 15007AE/12/FUN01FARM03/MRLF1), Xunta de Galicia. Experiments were performed at the Research Imaging Unit (UNIME) of the Health Research Institute of Santiago de Compostela (IDIS) (REGA number: ES1507802928 01) with the authorization of the research center management.

TNBS-induced IBD models were obtained by using the method previously described by Morris *et al.* (11). Briefly, all animals were fasted for 18 h before rectal administration of

TNBS (50 mg/kg body weight) dissolved in ethanol 50% (v/v), via a catheter inserted 8 cm proximal to the anus, under isoflurane anaesthesia (2%). The animals were positioned face up and kept in vertical position during 1-2 min to avoid that the administered reagent comes back out. Finally, animals were returned to their cages with free access to food and water.

Experimental design

In this study, 84 PET/CT scans were performed in rats in order to study the colonic disease physiology. In the first experiment, some of these studies were carried out in 10 rats (8 IBD rats and 2 control rats receiving 0,9% saline per day) before the IBD induction (basal condition) and 1, 3, 7, 10, 13 and 15 days post-TNBS administration.

In the second experiment, a new study was designed in order to evaluate the efficacy of the treatment with corticosteroids and to confirm the reproducibility of this experimental model. With this aim, some PET/CT scans were carried out in 10 rats (8 rats daily treated after day 3 with methylprednisolone 0.5 mg/kg intraperitoneally and 2 control rats receiving 0,9% saline per day) before the IBD induction (basal condition) and 1, 3, 7, 10, 13 and 15 days post-TNBS administration.

Animals of both experimental groups were sacrificed at either days 3, 7, 13 and 15 post-TNBS induction to carry out the histopathological assays and the macroscopic evaluation of the colon.

PET/CT acquisition

PET/CT images were acquired using an Albira PET/CT Preclinical Imaging System (Bruker Biospin, Woodbridge, Connecticut, United States). The PET subsystem comprises three rings of eight compact modules based on monolithic crystals coupled to multi-anode photomultiplier tubes (MAPMTs), forming an octagon with an axial FOV of 14.8 cm and a transaxial FOV of 8 cm in diameter. This system can create PET images with a spatial resolution of 1.2 mm and a sensitivity around 10%. The CT subsystem consists of a microfocus x-ray tube of 50 kVp and a CsI scintillator 2D pixelated flat panel detector that can generate images around 90 μm with a FOV of 7 cm.

Before the images acquisition, the animals were placed in a gas chamber containing 3% isoflurane in oxygen until they were unconscious. Afterwards, the animals were removed from the chamber and 12 ± 1 MBq of [^{18}F]FDG was injected in the tail vein of each animal under the effects of anaesthesia (2% of isoflurane). The animals woke up few minutes later and they remained at rest during 40 minutes with access to food and water. After that time, the animals were again anesthetized and a rectal administration of 2 mL of Iopromide Ultravist® 300 mg/mL via a catheter inserted 8 cm proximal to the anus was used as CT contrast agent. Finally, PET/CT static acquisitions were performed, consisting of 20 minutes PET scan

followed by 20 minutes CT scan. PET images were reconstructed using the maximum likelihood expectation maximization (MLEM) algorithm with 12 iterations and image pixel size of $0.4 \times 0.4 \times 0.4$ mm^3, including scatter and random coincidences and no attenuation correction. The CT was centred in the abdominal region of each animal and the acquisition parameters were 35 kV for a tube current of 200 µA with a 250 projections per bed.

All images were analysed using AMIDE software (amide.sourceforge.net). Fused [^{18}F]FDG PET/CT images were used to define three different regions of the rat colon (ascending, transverse and descending regions). Then, quantitative analysis was carried out by using circularly delineated Regions of Interest (ROIs) on CT images following longitudinal colon sections at ascending, transverse and descending regions in the CT images (Figure 1.1). The cylindrical ROIs dimensions ranged from 5 mm to 15 mm in diameter (fitting to the diameter of the colon section) and 1 mm in length. Subsequently, the ROIs were transferred to PET images in order to calculate the maximum [^{18}F]FDG uptake value. Finally, Standardized Uptake Value (SUV$_{max}$) were calculated as the maximum [^{18}F]FDG uptake value normalized by the injected activity and the body weight of the animal. The injected [^{18}F]FDG activity was estimated by subtracting the extravasated activity in tail. Body weight was measured daily on all animals until day 15 post-TNBS administration.

Statistical analysis was carried out using a two-way analysis of the variance (ANOVA) including as factors the time after TNBS administration, weight and treatment (non-treated IBD and treated IBD). Furthermore, Tukey multiple comparisons test was carried out for comparing SUV$_{max}$ over time.
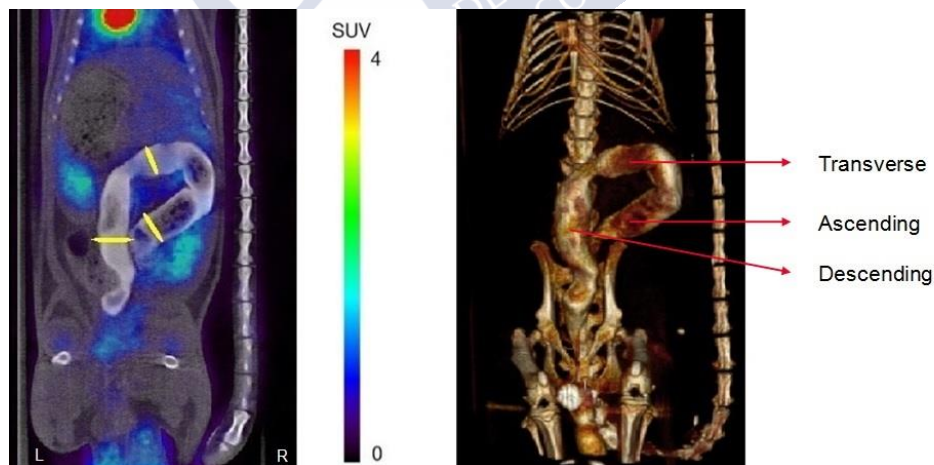

Figure 1.1. On the left, cylindrical ROIs drawn on fused PET/CT images of a control rat in the ascending, transverse and descending colon. On the right, CT image in 3D of the same animal, showing the different sections of the colon. Reproduced with permission from Elsevier.

Macroscopic evaluation and histopathology

The animals were sacrificed by an intracardiac injection of 5 ml of potassium chloride (Braun 1 mEq/ml) at 3, 7, 10 and 15 days post-TNBS administration. Colons were removed, macroscopically examined and subsequently photographed. Afterwards, they were individually fixed in 10% formalin and dehydrated, paraffin embedded, sectioned in slices with 4 μm thickness and stained with H&E (haematoxylin and eosin). The samples were blindly evaluated by a digestive pathologist using a Zeiss® microscope. Histological disease activity was scored in five grades using the Nancy histological index as follows: Ulceration of colonic mucosa with inflamed granulation tissue (Grade 4). Presence of multiple clusters of neutrophils in lamina propria and epithelium and the acute inflammatory cells infiltrate is moderate to severe (Grade 3). Presence of few neutrophils in lamina propria and in epithelium and mild acute inflammatory cells infiltrate (Grade 2). Chronic inflammatory infiltrate with no acute inflammatory infiltrate (Grade 1). No increase in chronic inflammatory cell number or absence of histological significant disease (Grade 0) (34, 35).

Statistical analysis was carried out using the Kruskal-Wallis nonparametric test between Nancy histological index obtained at ascending, transverse and descending regions from different groups (non-treated IBD, treated and controls).

RESULTS

PET/CT studies in non-treated IBD rats

The quantification of [18F]FDG PET/CT images from non-treated IBD rats provided longitudinal SUV_{max} values in the colon wall over time. Figure 1.2 shows that SUV_{max} rapidly increase after IBD induction, being particularly significant on days 7-13 after IBD induction. Two-way ANOVA analysis of SUV_{max} data shows significant influence of colon section and time after IBD induction with a significance of $p<0.01$ for both parameters. The increase in SUV_{max} is clearer in descending and transverse colon, where SUV_{max} is increased 2-3 times from baseline values and seems to be decreased on day 15, which is interpreted as a spontaneous remission of the inflammation.

The Tukey multiple comparison test ($p<0.01$) showed the following results:

Ascending: $\underline{0 = 15} < \underline{1 = 3 = 10 = 13 = 7}$

Transverse: $0 < \underline{15 = 1 = 3} < \underline{7 = 10 = 13}$

Descending: $\underline{0 = 15} < 7 < 3 < \underline{1 = 10} < 13$

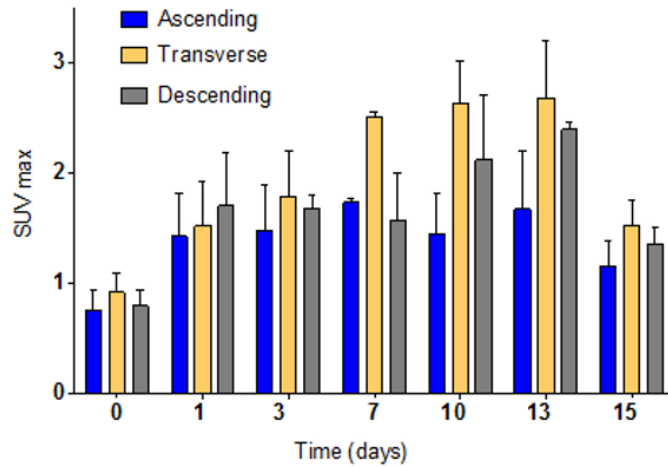Underlines grouped the homogeneous samples (not significant).

Figure 1.2. Longitudinal SUV$_{max}$ values in ascending, transverse and descending colon wall over time in the non-treated group. Notice the increase of the SUV$_{max}$ after the induction (day o) and its spontaneous recovery at day 15. Reproduced with permission from Elsevier.

PET/CT studies in treated IBD rats

Previous SUV$_{max}$ values were compared to those obtained in rats treated with methylprednisolone. Figure 1.3 shows separately the results for ascending (A), transverse (B) and descending (C) colon. A significant decrease in SUV$_{max}$ values is noticed after the corticosteroid administration. The obtained SUV$_{max}$ values are similar for non-treated and treated IBD rats from days 0-3, but SUV$_{max}$ values are significantly decreased for treated rats between days 7-13. The corticosteroid treatment caused a remission of the inflammation after day 3, whereas for non-treated rats the remission is only achieved on day 15.
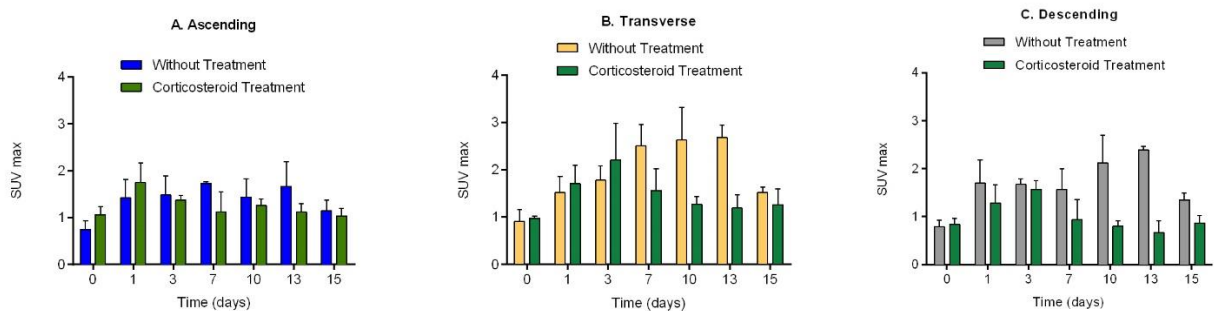
Figure 1.3. Longitudinal SUV$_{max}$ values in ascending, transverse and descending colon wall over time for treated and non-treated rats. Observe significant differences between groups on days 7-13 post-TNBS in all the regions. Reproduced with permission from Elsevier.

Figure 1.4 shows fused PET/CT images over time for non-treated and treated rats. The colon can be identified on the CT images through the contrast agent (white color). Furthermore, the colon wall inflammation can be visualized in PET images as areas with high [^{18}F]FDG accumulation, especially on days 7-13. This high [^{18}F]FDG uptake can be clearly detected in PET images from non-treated rats but it does not appear on treated ones, showing only a slight [^{18}F]FDG uptake around the colon.
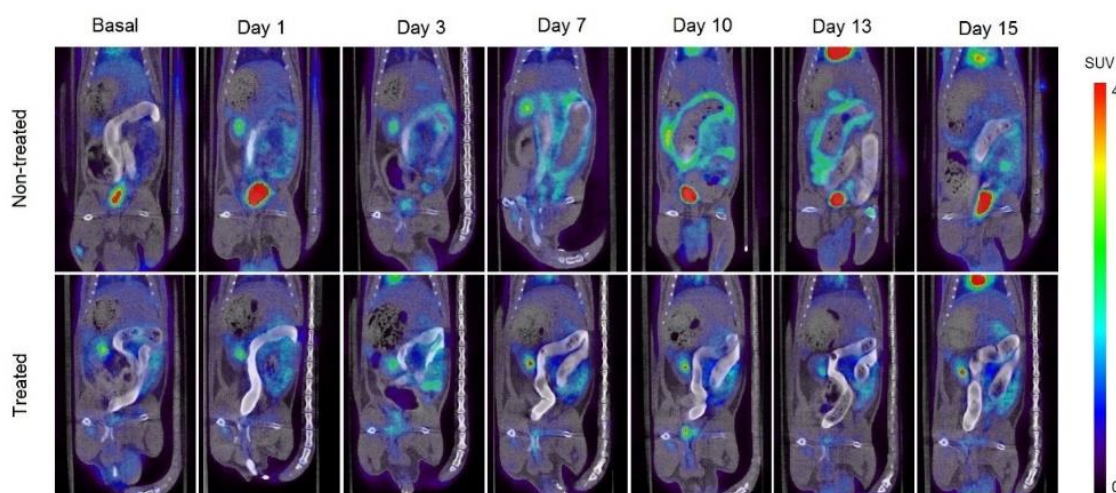
Figure 1.4. Longitudinal fused PET/CT images over time from treated and non-treated rats. The metabolic activity is coded on a color scale from blue (low radioactive tracer uptake) to red (high uptake). Realize the high FDG uptake around the colon wall at days 7-13 in the non-treated rat. Reproduced with permission from Elsevier.

Body weight, macroscopic examination and histology

The progression of the disease model was assessed through longitudinal weight changes from the baseline weight, macroscopic examination of the entire colon and histological analysis of the colon wall at ascending, transverse and descending areas.

Figure 1.5 shows changes in body weight over time for treated and non-treated rats. The group of non-treated rats showed a sustained decrease in body weight until day 13, with values of body weight loss close to 20% compared to the baseline weight. Instead, the group of treated rats showed a weight decrease on day 1 and 3, but the animals recovered the initial weight on day 7 and even the weight was increased with respect to the baseline weight on days 10-15.
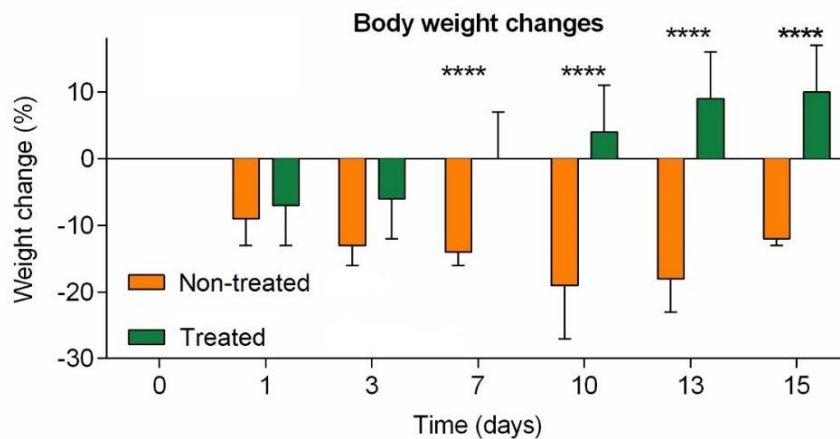
Figure 1.5. Body weight changes (%) of treated and non-treated rats over time from the baseline value. Notice the significant changes in the treated group compared with the non-treated one from day 7. Reproduced with permission from Elsevier.

The macroscopic evaluation of *ex vivo* colons showed clear thickening areas in the descending colon wall. Figure 1.6 shows the macroscopic images of *ex-vivo* colons along 15 days. It can be seen clear lesions in those colon samples obtained from days 7-15 from non-treated rats, but no lesions were found after day 7 in colons from the treated ones.

Figure 1.6. Macroscopic evaluation of ex-vivo colons. Observe the recovery of the treated group from day 7 compared with the non-treated one that has visible and several damage around the colon wall. Reproduced with permission from Elsevier.

Figure 1.7 shows the results of the histological evaluation for ascending, transverse and descending colon wall. As expected, the histological analysis shows that the inflammation is clearly located in the descending and transverse regions of the colon. Thus, descending colon wall was scored as Grade 4 in 8/8 colon samples from non-treated rats, only in 3/8 samples from treated animals and in 0/4 samples from control animals (Kruskal-Wallis test gives a p-value over 0.5 for differences between groups). Similarly, transverse colon samples were scored as Grade 4 in 5/8 from non-treated rats, 4/8 from treated ones and in 0/4 from controls. Finally, ascending colon samples were scored as Grade 4 in 1/8 from non-treated animals and in none from the treated and control rats.
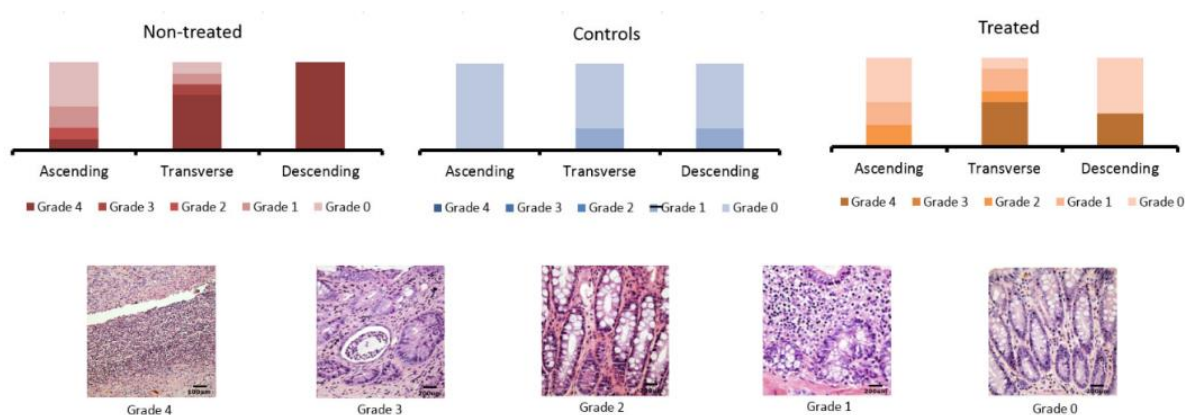

Figure 1.7. At the top, Nancy histological index for ascending, transverse and descending colon wall obtained from non-treated, control and treated animals. At the bottom, representative images of every Nancy index took from the experimental groups. Reproduced with permission from Elsevier.

Correlation between PET, histological analysis and body weight

Figure 1.8 shows the correlation of SUV_{max} with Nancy grade and weight changes. The statistic parameter R^2 was 0.61 and 0.82 respectively, indicating a high correlation between the variables. The p-value for the lack of adjustment in the ANOVA table is greater than 0.05 so the model seems to be adequate for the observed data. Thereby, the results show that Grade 0 is associated with an averaged SUV_{max} of 0.95±0.23, Grade 1 with an averaged SUV_{max} of 1.03±0.30, Grade 2 with an averaged SUV_{max} of 1.46±0.21, Grade 3 with an averaged SUV_{max} of 1.70±0.29 and finally Grade 4 with an averaged SUV_{max} of 2.02±0.67. Similarly, weight changes with respect to baseline weight are clearly associated with SUV_{max} in the colon wall. $SUV_{max} <1$ can only be found for positive weight changes, mainly in treated rats. Instead, weight loss is always related with increased SUV_{max} values, which are found in non-treated rats.
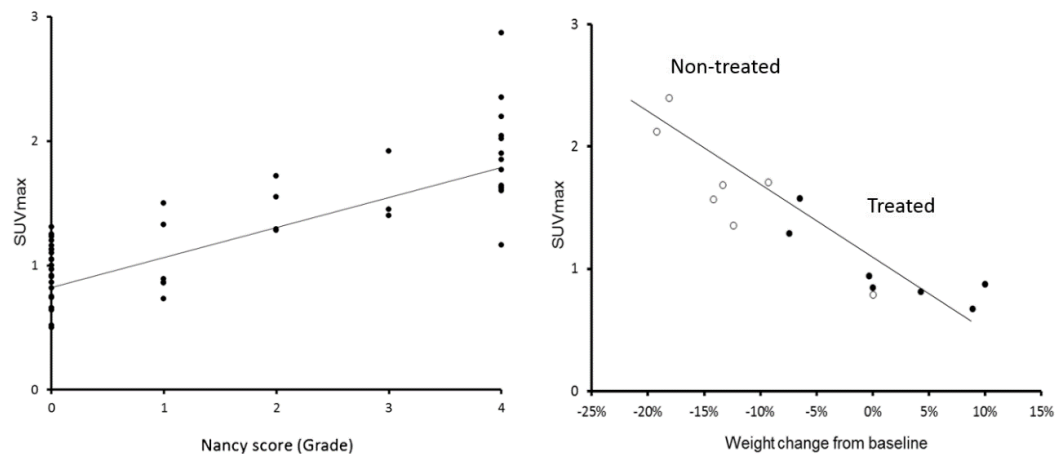
Figure 1.8: Correlation of SUV$_{max}$ with Nancy indexes (left) and body weight changes (right). Notice a good correlation between each parameter (R^2 of 0.61 and 0.82, respectively). In the correlation of SUV$_{max}$ with body weight changes, white points correspond to non-treated animals and black points to the treated ones. Reproduced with permission from Elsevier.

DISCUSSION

[^{18}F]FDG PET/CT studies were carried out for the assessment of spatial inflammation patterns and disease progression in a TNBS-induced IBD rat model and the subsequently follow-up of rats treated with corticosteroids. PET/CT images showed extensive spatial patterns of inflammation, mainly affecting the wall of descending and transverse colon. The quantification of longitudinal PET images in terms of SUV$_{max}$ and the standardized measurement of metabolism obtained from the images showed early signs of inflammation just one day after induction and also significant differences in disease progression once the corticosteroid treatment was administered. Our results showed that TNBS-induced IBD rat model has a positive response to corticosteroids, a commonly used treatment in IBD patients, thus praising the translational value of TNBS models. Furthermore, our findings provided significant associations between SUV$_{max}$ and Nancy grades, which are validated indexes to assess histological disease activity in IBD patients (35), showing excellent correlations on ascending, transverse and descending colon wall. Also, SUV$_{max}$ was correlated with longitudinal weight changes from the baseline weight, showing significant differences between non-treated and treated animals. In summary, our findings support the usefulness of SUV$_{max}$ value in the colon wall as al quantitative biomarker for longitudinal assessment of disease progression and treatment response evaluation.

Although our work is the first longitudinal PET/CT study on TNBS-induced IBD rats, the findings can be compared to those obtained from DSS-induced IBD rats. A study carried out in DSS mice proposed a quantitative biomarker for longitudinal assessment of disease progression based on the colonic/brain [^{18}F]FDG-signal ratio over time (0-14 days) (30). They found significant associations with histological inflammation scores and also provided differences between non-treated and treated mice. Nevertheless, as mentioned by the authors,

DSS is rapidly converted to glucose, resulting in competitive [^{18}F]FDG displacement that has to be considered. This only can be solved using the brain as a reference region, which could induce additional variability.

Other study proposed a different parameter to evaluate proximal, medial and distal colon separately of DSS-induced IBD in mice (31). This parameter is similar to the one we have proposed in our work. Given this fact, interesting conclusions can be drawn comparing TNBS and DSS models. It seems that the spontaneous remission of inflammation in DSS-induced animals is achieved after day 7, while our results showed that such remission in TNBS-induced animals is achieved on day 15. Furthermore, a similar spatial pattern was found in DSS-induced animals showing that the most severe inflammation was also found in transverse and descending colon. In any case, several points must be mentioned. Firstly, the evaluation of DSS-induced model was only based on three longitudinal PET studies, making it difficult to determine the day on which the spontaneous remission occurs. In addition, the DSS evaluation was carried out in mice, while our work was performed in rats. Only a recent study used [^{18}F]FDG PET for evaluating TNBS-induced rat models on day 7 after induction (32). The increase in SUV_{max} on day 7 was about 2-3 times from baseline values, consistent with our results.

It has to be mentioned that the assessment of the inflammatory process through PET/CT allows repeated investigations on each living animal, thereby limiting the number of rats needed for individual measures of inflammation during the follow-up. In addition, molecular imaging allows to locally quantify the inflammation in specific anatomic areas of the intestine avoiding histological examinations and therefore the sacrifice of the animals. This quantification could be used together with surrogate markers such as weight loss and diarrhea.

Overall, our findings showed that PET/CT and in particular the SUV_{max} parameter obtained from the quantification of longitudinal PET images is a reliable biomarker to monitor TNBS-induced IBD model over time and for the assessment of the response to the current therapies. Also, this study has an added clinical value due to its ability to assess a treatment efficacy in its earliest stages. Furthermore, SUV_{max} is commonly used in clinical routine, so it is a completely translational parameter that can be considered as a promising biomarker with high-throughput screening of new drugs in preclinical research.

CONCLUSIONS

[^{18}F]FDG PET studies were performed for the assessment of spatial inflammation patterns and disease progression on TNBS-induced IBD rat model and the evaluation of inflammation in rats treated with corticosteroids. To our knowledge, this is the first longitudinal PET study performed in TNBS-induced IBD models, as well as the first assessment of the remission of inflammation in IBD rats treated with conventional treatments. The results demonstrate the potential of this technique to address the preclinical evaluation of

anti-inflammatory formulations for new therapies and further to serve as useful tool to evaluate the progression of IBD in clinical practice.

ACKNOWLEDGEMENTS

CONFLIT OF INTEREST

The authors declare no conflit of interest.

REFERENCES

1.   Vermeire S, Van Assche G, Rutgeerts P. Classification of inflammatory bowel disease: the old and the new. Curr Opin Gastroenterol. julio de 2012;28(4):321-6.

2.   Hatton GB, Madla CM, Rabbie SC, Basit AW. All disease begins in the gut: Influence of gastrointestinal disorders and surgery on oral drug performance. Int J Pharm. 30 de junio de 2018;548(1):408-22.

3.   Yadav V, Varum F, Bravo R, Furrer E, Bojic D, Basit AW. Inflammatory bowel disease: exploring gut pathophysiology for novel therapeutic targets. Transl Res J Lab Clin Med. 2016;176:38-68.

4.   Duijvestein M, Battat R, Vande Casteele N, D'Haens GR, Sandborn WJ, Khanna R, et al. Novel Therapies and Treatment Strategies for Patients with Inflammatory Bowel Disease. Curr Treat Options Gastroenterol. marzo de 2018;16(1):129-46.

5.   Sandborn WJ. The Present and Future of Inflammatory Bowel Disease Treatment. Gastroenterol Hepatol. julio de 2016;12(7):438-41.

6.   Wirtz S, Neurath MF. Mouse models of inflammatory bowel disease. Adv Drug Deliv Rev. 30 de septiembre de 2007;59(11):1073-83.

7.   Randhawa PK, Singh K, Singh N, Jaggi AS. A Review on Chemical-Induced Inflammatory Bowel Disease Models in Rodents. Korean J Physiol Pharmacol. 1 de agosto de 2014;18(4):279-88.

8.   Antoniou E, Margonis GA, Angelou A, Pikouli A, Argiri P, Karavokyros I, et al. The TNBS-induced colitis animal model: An overview. Ann Med Surg. 19 de agosto de 2016;11:9-15.

9.   Jiminez JA, Uwiera TC, Douglas Inglis G, Uwiera RRE. Animal models to study acute and chronic intestinal inflammation in mammals. Gut Pathog [Internet]. 10 de noviembre de 2015 [citado 9 de noviembre de 2017];7. Disponible en: https://www.ncbi.nlm.nih.gov/pmc/articles/PMC4641401/

10.   Wirtz S, Popp V, Kindermann M, Gerlach K, Weigmann B, Fichtner-Feigl S, et al. Chemically induced mouse models of acute and chronic intestinal inflammation. Nat Protoc. julio de 2017;12(7):1295-309.

11.   Morris GP, Beck PL, Herridge MS, Depew WT, Szewczuk MR, Wallace JL. Hapten-induced model of chronic inflammation and ulceration in the rat colon. Gastroenterology. marzo de 1989;96(3):795-803.

12.   Motavallian-Naeini A, Andalib S, Rabbani M, Mahzouni P, Afsharipour M, Minaiyan M. Validation and optimization of experimental colitis induction in rats using 2, 4, 6-trinitrobenzene sulfonic acid. Res Pharm Sci. 2012;7(3):159-69.

13.   El-Salhy M, Hatlebakk JG. Changes in enteroendocrine and immune cells following colitis induction by TNBS in rats. Mol Med Rep. diciembre de 2016;14(6):4967-74.

14.   Hatton GB, Yadav V, Basit AW, Merchant HA. Animal Farm: Considerations in Animal Gastrointestinal Physiology and Relevance to Drug Delivery in Humans. J Pharm Sci. septiembre de 2015;104(9):2747-76.

15.   Siegel CA, Whitman CB, Spiegel BMR, Feagan B, Sands B, Loftus EV, et al. Development of an index to define overall disease severity in IBD. Gut. 1 de febrero de 2018;67(2):244-54.

16.   Kaaru E, Bianchi A, Wunder A, Rasche V, Stiller D. Molecular Imaging in Preclinical Models of IBD with Nuclear Imaging Techniques: State-of-the-Art and Perspectives. Inflamm Bowel Dis. 1 de octubre de 2016;22(10):2491-8.

17.   van Montfrans C, Bennink RJ, de Bruin K, de Jonge W, Verberne HJ, Ten Kate FJW, et al. In vivo evaluation of 111In-labeled T-lymphocyte homing in experimental colitis. J Nucl Med Off Publ Soc Nucl Med. octubre de 2004;45(10):1759-65.

18.   Bennink RJ, van Montfrans C, de Jonge WJ, de Bruin K, van Deventer SJ, te Velde AA. Imaging of intestinal lymphocyte homing by means of pinhole SPECT in a TNBS colitis mouse model. Nucl Med Biol. enero de 2004;31(1):93-101.

19.   Marion-Letellier R, Bohn P, Modzelewski R, Vera P, Aziz M, Guérin C, et al. SPECT-computed tomography in rats with TNBS-induced colitis: A first step toward functional imaging. World J Gastroenterol. 14 de enero de 2017;23(2):216-23.

20.   Charpentier C, Marion-Letellier R, Savoye G, Nicol L, Mulder P, Aziz M, et al. Magnetic resonance colonography in rats with TNBS-induced colitis: A feasibility and validation study. Inflamm Bowel Dis. 1 de octubre de 2012;18(10):1940-9.

21.   Melchior C, Loeuillard E, Marion-Letellier R, Nicol L, Mulder P, Guerin C, et al. Magnetic Resonance Colonography for Fibrosis Assessment in Rats with Chronic Colitis. PLOS ONE. 7 de julio de 2014;9(7):e100921.

22.   Wu Y, Briley-Saebo K, Xie J, Zhang R, Wang Z, He C, et al. Inflammatory bowel disease: MR- and SPECT/CT-based macrophage imaging for monitoring and evaluating disease activity in experimental mouse model--pilot study. Radiology. mayo de 2014;271(2):400-7.

23.   Cunha L, Szigeti K, Mathé D, Metello LF. The role of molecular imaging in modern drug development. Drug Discov Today. julio de 2014;19(7):936-48.

24.   Capozzi ME, Gordon AY, Penn JS, Jayagopal A. Molecular Imaging of Retinal Disease. J Ocul Pharmacol Ther. marzo de 2013;29(2):275-86.

25.   D'Haens G, Ferrante M, Vermeire S, Baert F, Noman M, Moortgat L, et al. Fecal calprotectin is a surrogate marker for endoscopic lesions in inflammatory bowel disease. Inflamm Bowel Dis. 1 de diciembre de 2012;18(12):2218-24.

26.   Perlman SB, Hall BS, Reichelderfer M. PET/CT imaging of inflammatory bowel disease. Semin Nucl Med. noviembre de 2013;43(6):420-6.

27.   Spier BJ, Perlman SB, Reichelderfer M. FDG-PET in inflammatory bowel disease. Q J Nucl Med Mol Imaging Off Publ Ital Assoc Nucl Med AIMN Int Assoc Radiopharmacol IAR Sect Soc Of. febrero de 2009;53(1):64-71.

28.   Hustinx R. The Utility of FDG PET/CT in Inflammatory Bowel Disease. PET Clin. abril de 2012;7(2):219-25.

29.   Brewer S, McPherson M, Fujiwara D, Turovskaya O, Ziring D, Chen L, et al. Molecular imaging of murine intestinal inflammation with 2-deoxy-2-[18F]fluoro-D-glucose and positron emission tomography. Gastroenterology. septiembre de 2008;135(3):744-55.

30.   Hindryckx P, Staelens S, Devisscher L, Deleye S, De Vos F, Delrue L, et al. Longitudinal quantification of inflammation in the murine dextran sodium sulfate-induced colitis model using μPET/CT. Inflamm Bowel Dis. octubre de 2011;17(10):2058-64.

31.   Bettenworth D, Reuter S, Hermann S, Weckesser M, Kerstiens L, Stratis A, et al. Translational 18F-FDG PET/CT imaging to monitor lesion activity in intestinal inflammation. J Nucl Med Off Publ Soc Nucl Med. mayo de 2013;54(5):748-55.

32.   Bernards N, Pottier G, Thézé B, Dollé F, Boisgard R. In vivo evaluation of inflammatory bowel disease with the aid of μPET and the translocator protein 18 kDa radioligand [18F]DPA-714. Mol Imaging Biol MIB Off Publ Acad Mol Imaging. febrero de 2015;17(1):67-75.

33.   Kilkenny C, Browne W, Cuthill IC, Emerson M, Altman DG, NC3Rs Reporting Guidelines Working Group. Animal research: reporting in vivo experiments: the ARRIVE guidelines. Br J Pharmacol. agosto de 2010;160(7):1577-9.

34.   Marchal-Bressenot A, Salleron J, Boulagnon-Rombi C, Bastien C, Cahn V, Cadiot G, et al. Development and validation of the Nancy histological index for UC. Gut. enero de 2017;66(1):43-9.

35.   Marchal-Bressenot A, Scherl A, Salleron J, Peyrin-Biroulet L. A practical guide to assess the Nancy histological index for UC. Gut. noviembre de 2016;65(11):1919-20.

Chapter II.

Evaluation of the therapeutic activity of Melatonin and Resveratrol in Inflammatory Bowel Disease: a longitudinal PET/CT study in an animal model

CHAPTER II

ABSTRACT

Inflammatory Bowel Disease (IBD) is a group of chronic disorders of the gastrointestinal tract, which two main types are Crohn's disease and ulcerative colitis. Although conventional therapeutic strategies have demonstrated to be effective in the IBD treatment, it is necessary to incorporate novel therapeutic agents that target other mechanisms involved in the pathogenesis of the disease, such as oxidative stress. For this reason, the efficacy *in vivo* of two antioxidant compounds, melatonin and resveratrol, has been investigated in an animal model of TNBS (2, 4, 6 - trinitrobenzenesulfonic acid) induced colitis. PET/CT (Positron emission tomography / Computer Tomography) scans were performed to assess disease activity and evaluate treatment response. SUV_{max} (Standardized Uptake Value) values, body weight changes and histological evaluation were used as inflammatory indices to measure the efficacy of both treatments. SUV_{max} values increased rapidly after induction of colitis, but after the beginning of the treatment (day 3) a statistically significant decrease was observed on days 7 and 10 in treated animals compared to the non-treated group. This remission of the disease was also confirmed by histological analysis of the colon tissue using the Nancy histological index (p value < 0.05 for differences between non-treated and both groups of treated animals). Moreover, statistical analysis showed a correlation ($R^2 = 65.52\%$) between SUV_{max} values and weight changes throughout the treatment. Overall, this study demonstrates the potential of resveratrol, and melatonin in lower extent, as therapeutic agents in the IBD treatment.

INTRODUCTION

Inflammatory Bowel Disease (IBD) is the term used to describe a group of chronic relapsing inflammatory diseases of the gastrointestinal (GI) tract of unknown aetiology. Although it is an idiopathic disease, an interplay of luminal microflora, external environment and disturbances in the immune responses are hypothesized to trigger the onset of the disease in a genetically susceptible host (1). The two main pathophysiological forms of IBD are Crohn´s disease (CD) and ulcerative colitis (UC), being highly heterogenic with regard to activity, site and behaviour of the disease. Furthermore, the anatomic involvement of the gastrointestinal tract differs between the both pathologies. CD is known to be transmural and can affect the whole GI tract with no particular location, whereas UC is limited mainly to the mucosa of the large bowel (2).

The primary goals of medical therapy are to treat active disease, induce and maintain remission resulting in a reduction of the clinical symptoms. The conventional treatment of IBD has been based on the use of anti-inflammatory drugs, corticosteroids, immunosuppressants and antibiotics (3). Emerging therapies include the use of biological agents, which can target specific cytokines. The first monoclonal antibody incorporated into clinical practice was infliximab, which inhibits the biological activity of TNF by binding to it with high affinity (4). The success of this therapy promoted the development of additional anti-TNF agents structurally different from infliximab (5) which have demonstrated to be effective in the treatment of the disease. Nevertheless, some works have suggested that IBD is associated with oxidative stress in the inflamed mucosa, which could contribute to chronic tissue damage (6) mainly caused by an imbalance derived from ROS (reactive oxygen species) overproduction and decreased antioxidant activity. Due to this, it could be interesting to incorporate antioxidant agents with additional anti-inflammatory activity in order to be used as adjuvant therapies. In this context, melatonin, an endogenous hormone, and resveratrol, a natural polyphenol, have been proposed as promising antioxidant agents due to their relatively high anti-inflammatory activity.

The development of rectal dosage forms for localized drug delivery in the colon represents a useful approach for IBD treatment. Rectal drug administration protects enzymatically unstable drugs and when the dosage form is administered at an appropriate distance in the rectum, the first-pass effect is minimized (7). The low oral bioavailability of melatonin and resveratrol make them suitable candidates for inclusion in a rectal dosage form. On the other hand, resistant starches and other dietary fibers are substrates for microbial fermentation that produces short chain fatty acids (SCFAs), which play important roles in maintaining intestinal homeostasis (8). Moreover, starches could form gels through a process called gelatinization. These gels display bioadhesive properties that could be exploited for increase the residence time of drugs in the colon (9). Preclinical animal models such as the TNBS (2, 4, 6 - trinitrobenzenesulfonic acid) (10–12), could be used to demonstrate efficacy

of treatments and the ability of rectally administered pharmaceutical products to reach the area of interest for the treatment (13).

Melatonin (N-acetyl-5-methoxytryptamine) is a pineal gland secretory product with multiple neurohormonal functions, such as the regulation of the circadian rhythm. However, it is also released from extrapineal sources, being the GI tract a major source of this hormone. The melatonin secreted in the GI tract is 400 times higher than that secreted from the pineal gland, suggesting that the melatonin synthesized in the GI tract may have direct effect on the GI physiology, such as the regulation of the epithelium function and its regeneration, modulation of the immune response in the gut and reducing the tone of GI muscles through specific membrane receptors in smooth muscle cells (14). Thus, melatonin has been shown to target multiple molecules involved in the inflammatory processes caused by UC and CD, which are associated with elevated production of free oxygen radicals.

In this regard, several works have reported the beneficial and protective effect of melatonin, although the exact mechanism of these effects still remains unknown (15,16). In animal models of colitis and in humans suffering from IBD, the release of serotonin (5-HT) and melatonin from the mucosa is altered. In a DSS-induced colitis mouse model, the availability of 5-HT is increased whereas the availability of melatonin is decreased, which induces inflammation and exacerbates colitis. This supports the fact that melatonin could restore the ratio between the two molecules (17) and therefore it can be used as an adjuvant therapy to achieve a more efficient remission in patients with UC (18). Others studies in animal models showed a positive effect of melatonin when administered intracolonically or intraperitoneally, reducing colonic lesions and decreasing colitis symptoms through the inhibition of inflammatory mediators such as inducible nitric oxide synthase (iNOS) and cyclooxygenase-2 (COX-2) (19,20) and by the suppression of the nuclear factor kappa B (NF-Kb) activation, also implicated in the expression of pro-inflammatory cytokines in the inflamed mucosa (21).

Resveratrol (3, 4´, 5 - trihydroxystilbene) is produced by a variety of plant species, for example, grapes (*Vitis vinifera*), peanuts (*Arachis hypogaea*) and several species of berries. *Trans*-resveratrol was found for the first time in grapevines where it is synthesized in response to exogenous stress factors such as UV light and fungal damage (22). This compound exists as *trans*- and *cis*- isomeric forms, being the *trans*- isomer the most stable form. It is also highly photosensitive and the *trans*-resveratrol is converted to the *cis*-isomer when is exposed to UV irradiation (23). The anti-inflammatory activity of the resveratrol is only produced by the *trans*-resveratrol, whereas the *cis*-isomer presents no significant biological activity (24).

Resveratrol possesses many beneficial effects because of its antioxidant and anti-inflammatory properties. Hence, these beneficial properties could be interesting in the development of therapies for IBD (25,26). *In vivo* protective effects of resveratrol have been tested in animal models. As an example, if resveratrol is administered daily to DSS-induced colitis rat model, not only an anti-inflammatory effect is observed but also an increase in the

beneficial microbiota (27). Furthermore, resveratrol can also improve inflammation score and suppress markers of inflammatory stress (28). In a TNBS-induced colitis rat model, resveratrol attenuated intestinal mucosal damage and decreased the production of inflammatory mediators such as TNF-α when administered by oral gavage (29) and intraperitoneally (30). Other beneficial effects of resveratrol involve the inhibition of NF-κB, the decrease in the COX-2 expression and the reduction of proinflammatory cytokines (31).

Although the anti-inflammatory and antioxidant activities of both molecules have been tested in previous works, there is still no consistent works on the activity of both molecules in animal models over time and none of the previous studies has longitudinally assessed the disease progression using quantitative, non-invasive and reproducible biomarkers potentially useful for clinical translation. Non-invasive imaging techniques such as PET/CT (Positron emission tomography / Computer Tomography) commonly used in clinical practice, have been used to accurately characterize preclinical IBD models (32,33). In this regard, our group recently showed the utility of longitudinal PET/CT using the radiotracer [18F]Fluoro-2-deoxy-2-D-Glucose ([18F]FDG) for the assessment of disease extent and activity in a TNBS animal model of colitis. This study has also demonstrated that the SUV_{max} (Standardized Uptake Value), a common biomarker used in current clinical practice for the assessment of inflammatory processes (34), can be considered as a translational biomarker for evaluating disease progression and treatment response.

The present work is focused on conducting longitudinal [18F]FDG PET/CT studies to assess the therapeutic efficacy of melatonin and resveratrol in a TNBS-induced IBD animal model.

MATERIALS AND METHODS

Materials

Reagents and chemicals

TNBS (2, 4, 6 - trinitrobenzenesulfonic acid) was purchased from Sigma-Aldrich Company Ltd, Madrid, Spain. Ethanol absolute was obtained from VWR International S.A.S., France. High-amylose maize starch (Novelose 240) was purchased from National Starch & Chemical Ltd, Manchester, UK. Polyethene glycol 400 (PEG 400) was obtained from Acofarma Company, Madrid, Spain. Methanol (MeOH) of analytical grade was supplied by Merck, Darmstad, Germany. Trolox (6-hidroxy-2,5,7,8-tetramethylchroman-2-carboxylic acid), 2,2´-azinobis(3-ethylbenzothialozinesulfonicacid) (ABTS) and Potassium persulfate ($K_2S_2O_8$) were purchased from Sigma, Madrid, Spain. NaCl 0.9% B. Braun was purchased from Braun Medical Inc. Barcelona, Spain. Ultravist ® 300 mg / mL was purchased from Bayer Hispania S.L. Barcelona, Spain. Melatonin (N-acetyl-5-methoxytryptamine) was purchased from Acofarma Company Ltd, Madrid, Spain and *Trans*-resveratrol (3, 4´, 5 - trihydroxystilbene) was obtained from Sigma-Aldrich Company Ltd, Madrid, Spain.

Methods

General methods

In this work, an experimental study was carried out in a TNBS animal model of colitis using Sprague-Dawley rats. Animals were treated with rectal formulations of resveratrol and melatonin. Firstly, a formulation study was performed in order to select the most adequate carrier for both compounds. Then, the compounds were included in the optimized vehicle and administered intracolonically to animals. PET/CT scans were performed for evaluation of disease activity and treatment efficacy in the colitis animal model.

Preparation of melatonin and resveratrol formulations

Melatonin was dissolved in water at a concentration of 10 mg / mL. Resveratrol was first dissolved in PEG 400 (40% of the total volume) due to its poor solubility in water and then added to a volume of water (pH 5.5), obtaining a final concentration of 10 mg / mL.

Inflammatory Bowel Disease (IBD) animal model

These studies were carried out on male Sprague-Dawley rats (average weight of 250 ± 25g) supplied by the animal facility at the University of Santiago de Compostela. During the experiments, animals were kept in individual cages under controlled temperature (22 ± 1ºC) and humidity (60 ± 5%) conditions, with day-night cycles regulated by artificial light (12/12 hours) and fed *ad libitum*. All animal experiments complied the ARRIVE guidelines (35) and were carried out in accordance with the Spanish and European Union (UE) directive for animal experiments RD53/2013 and 2010/63/EU. Experiments were approved by the University of Santiago de Compostela (USC) Bioethics Comitte, (Ref. 15007AE/12/FUN01FARM03/MRLF1), Xunta de Galicia. Experiments were performed at the Research Imaging Unit (UNIME) of the Health Research Institute of Santiago de Compostela (IDIS) (REGA number: ES1507802928 01) with the authorization of the research center management.

The TNBS-induced IBD animal model was obtained following the method previously described by Morris *et al.* (10). All animals were fasted for 18 h before rectal administration of TNBS in a dose of 50 mg / kg body weight dissolved in ethanol 50% (v / v), through a catheter inserted rectally into the colon until reaching 8 cm proximal to the anus, under isoflurane anaesthesia (2%). Then, they were kept in a vertical position for 1 min to prevent leakage of the intracolonic instillation. Finally, animals were returned to their cages with free access to food and water.

Experimental design

In this study, 168 [^{18}F]FDG PET/CT scans were performed to follow-up the disease in 24 IBD rats (7 scans/rat). Each animal was weighted daily. Three additional rats were used to determine the colonic residence time of different formulations.

Determination of colonic residence time

Two different formulations were investigated in order to determine the residence time of the dosage form in the colon, selecting the most suitable one as vehicle for the incorporation of the active substances. Thus, a gel-based vehicle and a water-based vehicle were prepared to compare their colonic biodistribution by PET/CT. Firstly, a high-amylose maize starch (Novelose 240) suspension (10% w / v) in water was heated at 95 ºC for 10 min and then allowed to cool to room temperature. The starch-based gel formed after this procedure was mixed with [^{18}F]FDG dissolved in 0.9% saline solution (NaCl 0.9% B. Braun®) and the contrast agent (Iopromide Ultravist® 300 mg / mL). Similarly, [^{18}F]FDG dissolved in 0.9% saline solution and the contrast agent were also mixed with distilled water to obtain the water-based vehicle.

The starch-based vehicle was administered to three different animals in a total volume of 1 mL and the water-based vehicle was administered in a total volume of 1 and 2 mL to the same three animals. PET/CT scans were carried out 1 and 2 hours' post-administration.

Assessment of the efficacy of resveratrol and melatonin treatments

Melatonin was administered intrarectally to 12 rats in a single daily dose of 10 mg / kg. The total volume of solution administered was 1 mL per animal. The treatment was started 3 days after induction of colitis, and the [^{18}F]FDG PET/CT scans were carried out before the IBD induction (basal condition) and 1, 3, 7, 10, 13 and 15 days post-TNBS administration. Resveratrol was administered in a separate group of 12 rats using the same scheme. All animals were sacrificed at day 15 post-TNBS induction (Scheme 2.1).
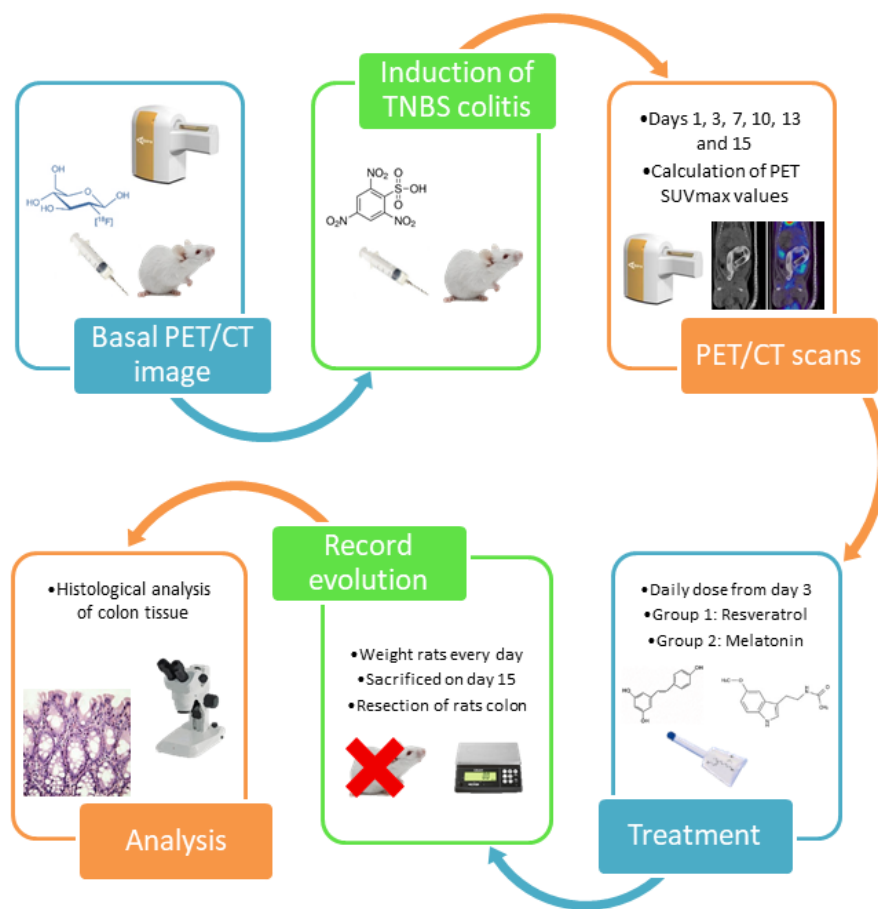
Scheme 2.1. Protocol of [¹⁸F]FDG PET/CT studies and treatment in the TNBS animal model. Reproduced with permission from Elsevier.

PET/CT acquisition and evaluation

PET/CT images were acquired using an Albira PET/CT Preclinical Imaging System (Bruker Biospin, Woodbridge, Connecticut, United States). The PET subsystem comprises three rings of eight compact modules based on monolithic crystals coupled to multi-anode photomultiplier tubes (MAPMTs), forming an octagon with an axial FOV of 8x14.8 cm (transaxial and axial directions respectively). This subsystem generates PET images with spatial resolution of 1.2 mm and a sensitivity of 10%. The CT subsystem consists of a microfocus x-ray tube of 50 kVp, a CsI scintillator 2D pixelated flat panel detector and a FOV of 5.2x5.2 cm, generating images of 90 µm spatial resolution.

The animals were placed in a gas chamber (2% isoflurane) until they were unconscious. Afterwards, the animals were removed from the chamber and 12±1 MBq of [¹⁸F]FDG were injected in the tail vein of each animal under anaesthesia (2% of isoflurane). The animals woke up a few minutes later and they were kept at rest for 40 minutes with access to food and water. After that time, the animals were again anaesthetized and 2 mL of Iopromide Ultravist®

300 mg / mL (CT contrast agent) was administered intrarectally via a catheter inserted 8 cm proximal to the anus. Finally, PET/CT static acquisitions were performed, consisting of 20 min PET scan followed by 20 min CT scan. PET images were reconstructed using the maximum likelihood expectation maximization (MLEM) algorithm with 12 iterations and image pixel size of $0.4 \times 0.4 \times 0.4$ mm^3, including scatter and random coincidences and no attenuation correction. The CT acquisition parameters were 35 kV for a tube current of 200 μA with 250 projections per bed The FOV of PET scan was centred in animal encompassing from the upper part of the lungs to the lower extremities and the FOV of CT scan was centred in the abdominal region.

All images were analyzed using AMIDE software (amide.sourceforge.net). Fused [^{18}F]FDG PET/CT images were used to define three different regions of the rat colon (ascending, transverse and descending regions). Then, quantitative analysis was carried out by using circularly delineated Regions of Interest (ROIs) on CT images following longitudinal colon sections at ascending, transverse and descending regions (Figure 2.1). The cylindrical ROIs dimensions ranged from 5 mm to 15 mm in diameter (fitting to the diameter of the colon section) and 1 mm in length. Subsequently, the ROIs were transferred to PET images in order to calculate the maximum [^{18}F]FDG uptake value. Finally, Standardized Uptake Value (SUV$_{max}$) was calculated as the maximum [^{18}F]FDG uptake value normalized by the injected activity and the body weight of the animal. The injected [^{18}F]FDG activity was estimated by subtracting the extravasated activity in the tail.
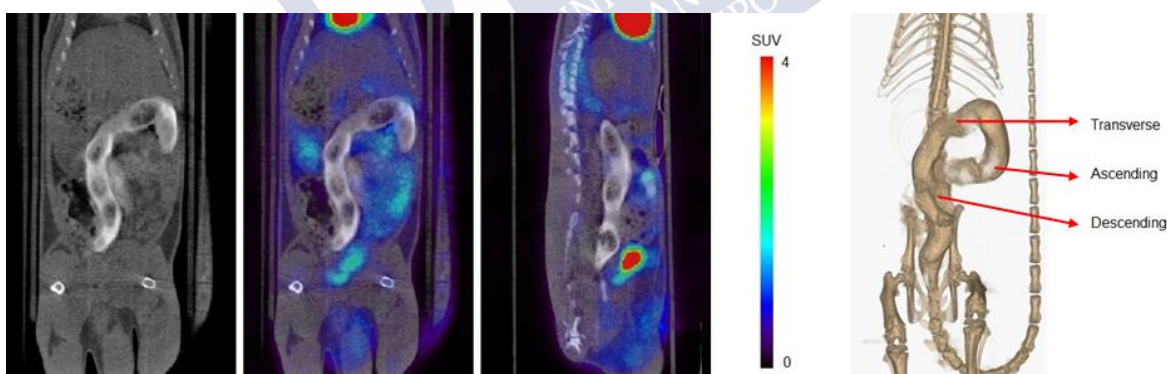

Figure 2.1. On the left, gastrointestinal tract CT scan in coronal plane of a healthy rat. A contrast agent was used for enhancing contrast in the colon of the animal (white colour). In the middle, [^{18}F]FDG PET/CT fusion images for the coronal and sagittal planes of the same animal. Notice the normal [^{18}F]FDG uptake in the heart, bladder and kidneys. On the right, 3D colon reconstruction from CT images where can be seen the three colon sections (ascending, transverse and descending). Reproduced with permission from Elsevier.

Statistical analysis was carried out using a two-way analysis of the variance (ANOVA) including as factors time after TNBS administration, weight and treatment. The data for non-treated animals were obtained from the previous work of this group (34) to compare the

previous results with those obtained in the present study for animals treated with melatonin and resveratrol. Furthermore, Tukey multiple comparisons test was carried out for comparing SUV_{max} values over time. Significant differences between groups were indicated in the figures as follows: $p < 0.05$(*), $p < 0.01$(**), $p < 0.001$(***) and $p < 0.0001$(****).

Macroscopic evaluation and histopathology

The animals were sacrificed by CO_2 inhalation (60-70%) in a euthanasia chamber on day 15 post-TNBS administration. Colons were removed, macroscopically examined and subsequently photographed. Afterwards, they were individually fixed in 10% formalin and dehydrated, paraffin embedded, sectioned in slices with 4 μm thickness and stained with H&E (haematoxylin and eosin). The samples were blindly evaluated by a digestive pathologist using a Zeiss® microscope.

Nancy histological index was used as a reference score for the histological disease activity. The activity was scored in five grades as follows: (Grade 4) - Ulceration of colonic mucosa with inflamed granulation tissue. (Grade 3) - Presence of multiple clusters of neutrophils in lamina propria and epithelium and the acute inflammatory cells infiltrate is moderate to severe. (Grade 2) - Presence of few neutrophils in lamina propria and in epithelium and mild acute inflammatory cells infiltrate. (Grade 1) - Chronic inflammatory infiltrate with no acute inflammatory infiltrate. (Grade 0) - No increase in chronic inflammatory cell number or absence of histological significant disease (36).

Statistical analysis was carried out using the Kruskal-Wallis nonparametric test and Dunn´s multiple comparisons test to evaluate the differences between Nancy scores obtained in the ascending, transverse and descending regions of melatonin, resveratrol and non-treated groups.

Determination of antioxidant activity of resveratrol and melatonin

The antioxidant activity of resveratrol and melatonin was determined by using ABTS radical cation (ABTS$^{\bullet+}$). This method is based on the ability of an antioxidant to reduce ABTS$^{\bullet+}$ into its colourless form. ABTS$^{\bullet+}$ was produced according to a procedure described previously with some modifications (37). Briefly, ABTS radical cation was generated by the reaction between ABTS dissolved in water to a 7 mM concentration and a 2.45 mM $K_2S_2O_8$ aqueous solution. The mixture was allowed to stand in the dark at room temperature for 16 h before use. The ABTS$^{\bullet+}$ solution was then diluted with ethanol absolute to obtain an initial absorbance of 0.80 (± 0.1) at 730 nm, using a Thermo Fisher Evolution 60s spectrophotometer.

A calibration curve of Trolox, the reference antioxidant compound, was prepared for a calibration range of 5 - 32 μM in methanol-water (1:1). Each concentration of the standard was reacted with 3.9 mL of ABTS$^{\bullet+}$ solution ($A_{730nm} = 0.80 \pm 0.1$) and the absorbance was read at a wavelength of 730 nm. Afterwards, different concentrations of resveratrol (21 – 131 μM) and melatonin (21 – 131 μM) in ethanol were added to 3.9 mL of ABTS$^{\bullet+}$ solution and also read at a wavelength of 730 nm. Subsequently, the percentage of inhibition of absorbance at 730 nm was calculated as a function of the concentration of resveratrol and Trolox. Finally, the antioxidant capacity of resveratrol expressed in TEAC (Trolox equivalent antioxidant capacity values) was calculated by linear regression between Trolox and *trans*-resveratrol and melatonin concentrations that produce the same percentage on ABTS$^{\bullet+}$ radical reduction.

RESULTS

Determination of the most adequate vehicle of administration

As can be seen in Figure 2.2., PET/CT images showed that the gel only covers the descending colon while the liquid enema also reaches the transverse and part of the ascending colon. Furthermore, the liquid showed the longest residence time in the colon; 2 hours' post-administration there was still liquid enema, while the gel had already been expelled. Finally, the most appropriate volume of administration was determined by comparing the biodistribution of 1 and 2 mL of the liquid enema in the same animal. PET/CT images after administration showed that both liquid enemas had the same residence time. Also, the 2 mL enema reached the ascending colon but also other upper parts of the GI tract that are not of interest for the treatment. Therefore, the 1 mL liquid enema was selected as the most appropriate for treatment administration. Each formulation was tested in three different animals, obtaining the same results regarding to gastrointestinal biodistribution and residence time.
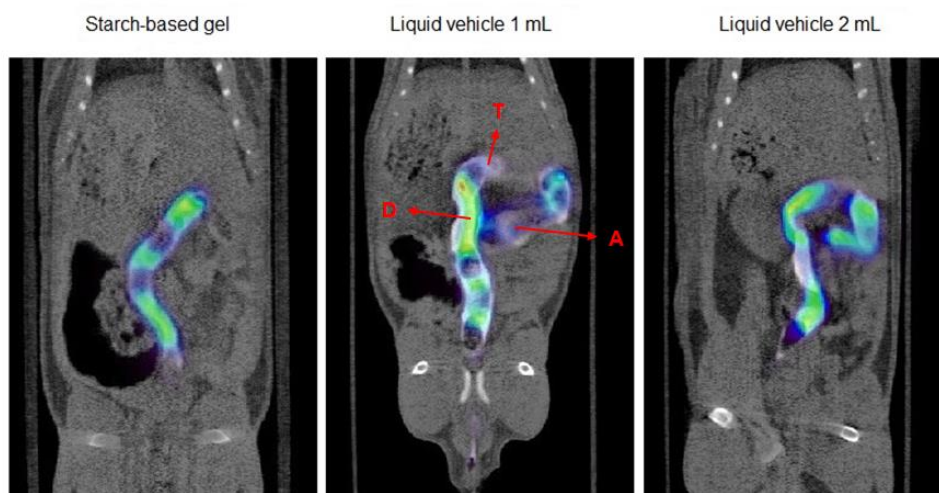
Figure 2.2. Colonic biodistribution of two different formulations administered intrarectally in different volumes. The images of the colonic spread of the starch-based and liquid-based vehicles were obtained immediately after the administration of the formulations. The animal on the left received 1 mL of a starch-based gel mixed with the radiotracer [^{18}F]FDG and the contrast agent. In the middle, the same animal received 1 mL of [^{18}F]FDG diluted in 0,9% saline solution and the contrast agent in distilled water. On the right, the same mixture of [^{18}F]FDG diluted in 0,9% saline solution and the contrast agent in distilled water was administered but in a total volume of 2 mL. Notice that the formulations include the contrast agent to be visualized in the CT images. (D: descending, T: transverse, A: ascending). Reproduced with permission from Elsevier.

PET/CT studies in IBD rats treated with melatonin and resveratrol

Figure 2.3. presents separately the obtained SUV$_{max}$ values for ascending, transverse and descending colon (SUV$_{max}$ values of animals without treatment were extracted from our previous work (34)). All values were very similar for non-treated and treated IBD rats on days 0-3. Nevertheless, a significant decrease in SUV$_{max}$ was observed after the beginning of treatment administration on day 3. This decrease was more remarkable in the resveratrol group, showing significant differences between non-treated and resveratrol-treated groups on days 7 and 10 for ascending and descending colon, and on days 7, 10 and 13 for descending colon. Instead, significant decrease for melatonin-treated group was only found for descending colon, which is the most affected area in the TNBS model. The remission in non-treated rats is only achieved on day 15.
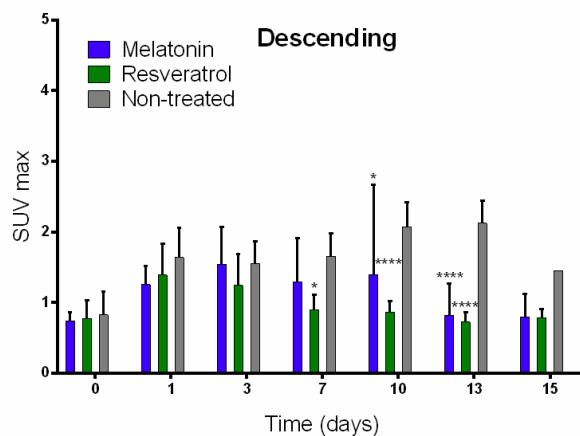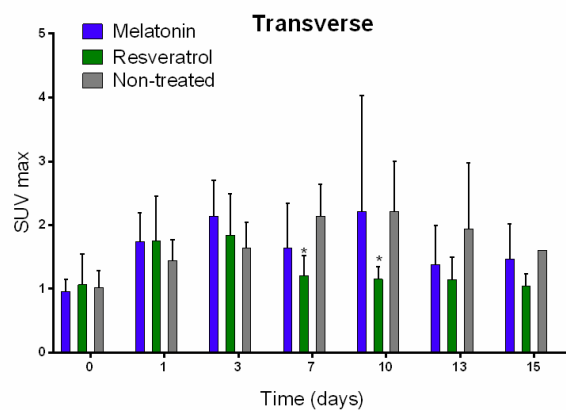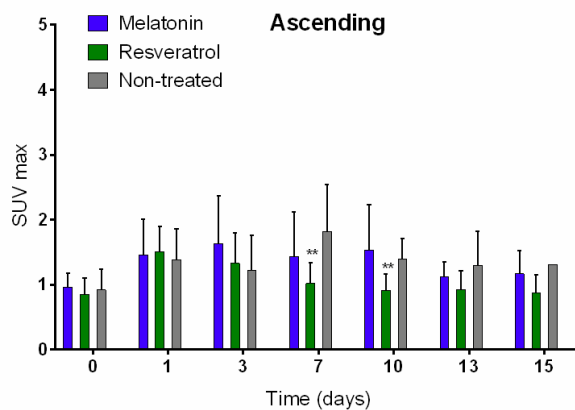
Figure 2.3. Longitudinal SUV$_{max}$ values for ascending, transverse and descending colonic segments over time for non-treated rats and animals treated with melatonin and resveratrol. Significant differences can be noticed between non-treated and treated animals on days 7-13 post-induction of colitis in the three regions. Reproduced with permission from Elsevier.

Figure 2.4 shows fused PET/CT images over time for non-treated and treated rats (melatonin and resveratrol groups). The anatomical location of the colon is given by the CT images through the contrast agent (white colour). The inflamed colon wall can be visualized in PET images through [^{18}F]FDG accumulation, especially on days 7-13. This [^{18}F]FDG accumulation can be clearly visualized in non-treated rats and only a slight [^{18}F]FDG accumulation can be appreciated in treated rats.
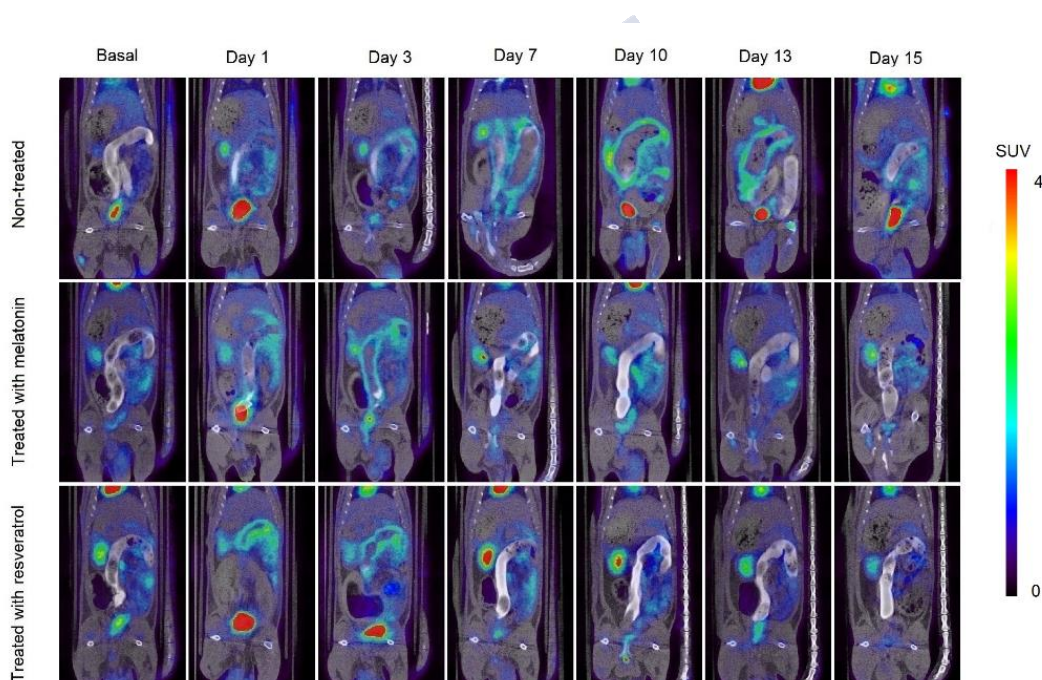

Figure 2.4. Longitudinal fused PET/CT images over time obtained from rats without treatment after the colitis induction and treated with melatonin and resveratrol. The metabolic activity is coded on a colour scale ranging from blue (low [^{18}F]FDG uptake) to red (high [^{18}F]FDG uptake). In the groups of treated animals, it can be clearly noticed the high [^{18}F]FDG uptake around the colon on days 1-3 and its subsequent reduction when the treatments administration begins on day 3. On the contrary, the non-treated group does not achieve a reduction in the [^{18}F]FDG uptake until day 15, when the spontaneous remission of the disease occurs. Reproduced with permission from Elsevier.

Body weight, macroscopic examination and histology

Figure 2.5 shows the body weight changes over time of rats treated with melatonin and resveratrol (body weight changes of non-treated rats were obtained from our previous work

(34)). After the initial decrease in body weight before treatment, melatonin and resveratrol groups showed an early recovery of the initial weight on day 7 (non-treated rats showed a sustained decrease in body weight until day 13). It is worthwhile to mention that the resveratrol group showed the best recovery rates.
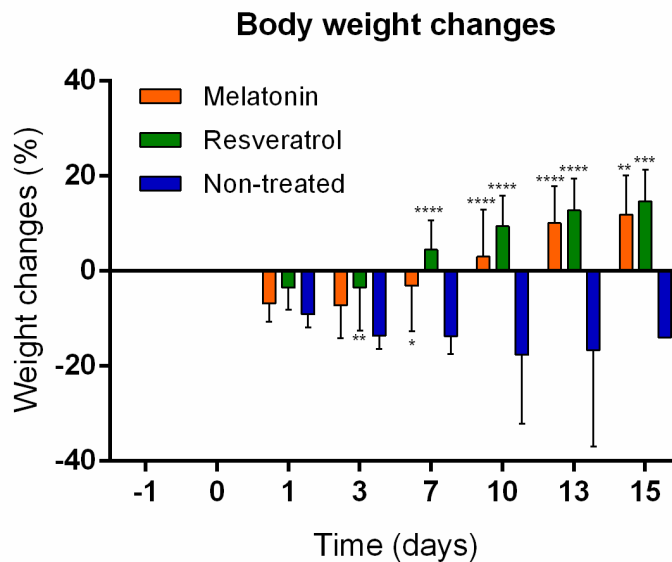

Figure 2.5. Body weight changes (%) of treated and non-treated animals over time from the baseline value. Significant differences can be appreciated for treated animals compared to those non-treated from day 7 post-induction of colitis. Reproduced with permission from Elsevier.

Figure 2.6 shows the macroscopic images of *ex vivo* colons on day 15 of rats treated with melatonin and resveratrol (images of non-treated and control rats were obtained from our previous work (34)). The sample from the melatonin-treated and resveratrol-treated animals were free from lesions, wall thickening and necrosis that was clearly observed in non-treated animals. Particularly, the resveratrol-treated image closely resembles the sample of the control animal.

Figure 2.6. Macroscopic evaluation of *ex-vivo* colons at day 15 post-TNBS induction in a) control group (healthy animals), b) non-treated group, c) melatonin-treated group and d) resveratrol-treated group. Observe the recovery in both treated groups compared with the non-treated one that has visible damage such as wall thickening and areas of necrosis. The colon of the control group shows no sign of damage. Reproduced with permission from Elsevier.

Figure 2.7 represents the images of the histological examination of colon tissue samples from rats treated with melatonin and resveratrol. They showed regenerative changes in the epithelium with increased mitotic figures in crypt epithelial cells and even in some parts normal mucosal structure. The images from non-treated animals (34) are also represented for comparison, showing neutrophilic infiltration of crypts accompanied by crypt abscesses, eroded mucosa and relevant ulceration. Figure 2.8 provides the results of the histological evaluation of ascending, transverse and descending colon on day 15 using the Nancy histological index. The melatonin group provided improved Nancy scores compared with non-treated group, showing grade 0 in 2/12 descending colon, in 9/12 transverse colon and in 11/12 ascending colon samples. This improvement was much more prominent in the resveratrol group, showing grade 0 in 9/12 descending colon, in 11/12 transverse colon and in 11/12 ascending colon samples, and grade 4 in 1/12 transverse colon samples and none of the descending and ascending colon samples.
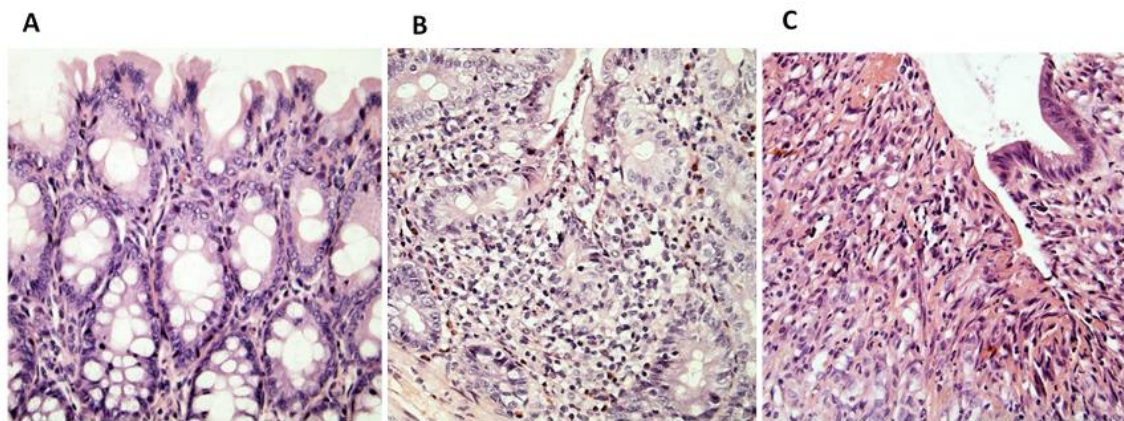
Figure 2.7. Representative optical microscopy images at 40X magnification of the Nancy index obtained from the different experimental groups: A) grade 0 image showing a normal mucosa structure, B) grade 2 image showing crypt abscesses and polymorphonuclear infiltration and C) grade 4 image showing intense inflammation with loss of goblet cells. The shape of the crypts is distorted and inflammatory cells are present. Reproduced with permission from Elsevier.
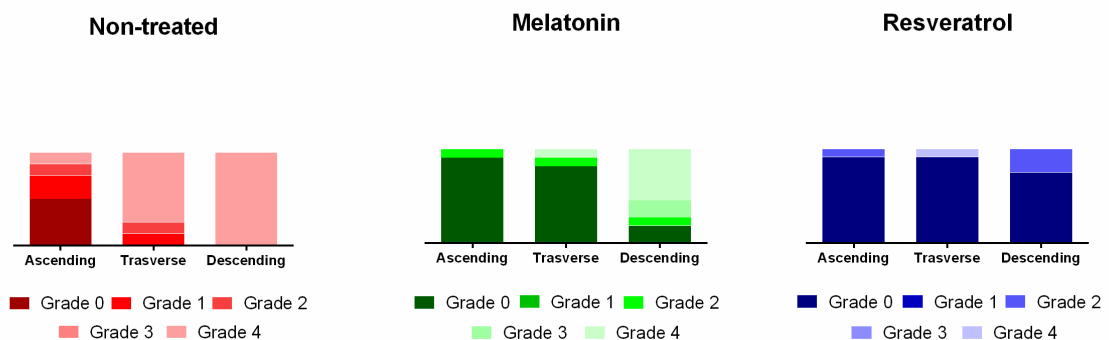

Figure 2.8. Nancy histological index for ascending, transverse and descending colon sections of the non-treated group, melatonin-treated group and resveratrol-treated group. Reproduced with permission from Elsevier.

Kruskal-Wallis test gives a p value < 0.05 for differences between groups. For ascending and transverse colon, Dunn´s multiple comparisons test gives a p-value < 0.05 for differences between non-treated animals and both groups of treated animals. For descending colon, the test gave a p-value < 0.05 for differences between non-treated and resveratrol-treated animals, and also between resveratrol-treated animals and melatonin-treated animals, highlighting the positive outcome of resveratrol treatment.

Correlation between SUV_{max} values and body weight

Figure 2.9 shows the correlation of the average SUV_{max} values for the ascending, transverse and descending regions of the colon with weight changes for each day on which PET/CT studies were performed. The Pearson coefficient R^2 was 66.41%, which indicates a correlation between the variables. As shown by the graph, weight changes with respect to baseline are clearly associated with SUV_{max} values. Positive weight changes are found mainly in the treated groups, whose SUV_{max} values are mostly less than 1. On the contrary, weight loss is always linked to an increase in SUV_{max} values, which are related to the non-treated group.
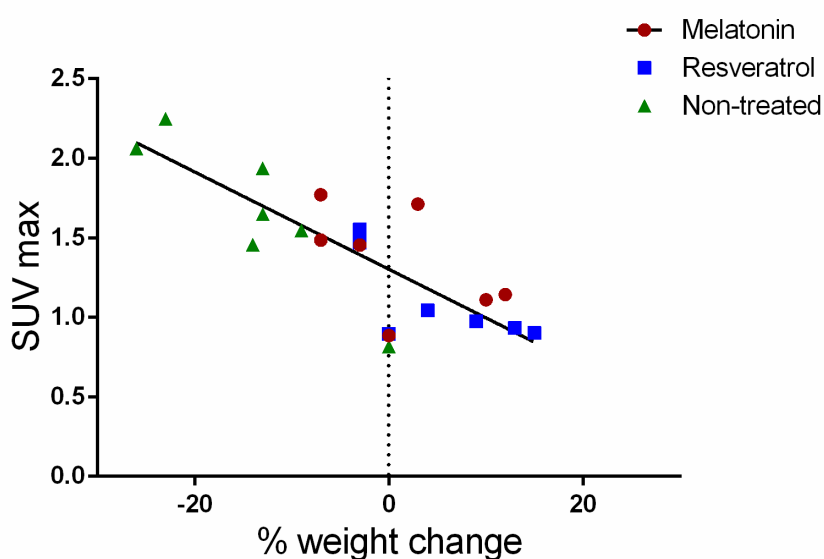

Figure 2.9. Correlation of average SUV_{max} values with body weight changes from baseline (%). Notice a correlation between both parameters (R^2 = 65.52 %). In addition, higher values of SUVmax and weight loss can be clearly differentiated for the non-treated group in comparison with those treated with melatonin and resveratrol. Reproduced with permission from Elsevier.

Antioxidant capacity of resveratrol and melatonin

ABTS assay was performed to investigate the antioxidant effect of resveratrol and melatonin. The results obtained from the ABTS assay showed that resveratrol had a substantially high antioxidant effect compared to Trolox. A linear relationship was found between the antioxidant activity and the antioxidant concentration of both compounds when used at different concentrations in the ABTS assay. As can be seen in Figure 2.10, the regression analysis points to the linear response between Trolox´s and resveratrol´s concentration and the percentage of inhibition of $ABTS^{\bullet+}$ absorbance yielding the following equations:

Trolox: $y = 0.0043x + 0.2566 \quad R^2 = 0.9998$

Resveratrol: y = 0.023x + 0.0743 $R^2 = 0.9986$

Then, the antioxidant activity of *trans*-resveratrol was calculated. The slope of the equation resulting from the representation of μM of Trolox vs. μM of resveratrol (y = 2.3623x + 121.04) ($R^2 = 0.9998$) represents the antioxidant capacity of resveratrol expressed in TEAC values (Figure 2.10). These results indicated that 1 μM of resveratrol provides the same antioxidant capacity of 2.36 μM of Trolox, being, therefore, the antioxidant capacity of resveratrol 2.36 times higher than that of Trolox.

On the other hand, it has not been possible to obtain a linear response between melatonin concentration and the percentage of inhibition of ABTS$^{\bullet+}$ and, therefore, its antioxidant capacity could not be calculated through the ABTS assay. For this reason, the results for the melatonin assay are not shown here.
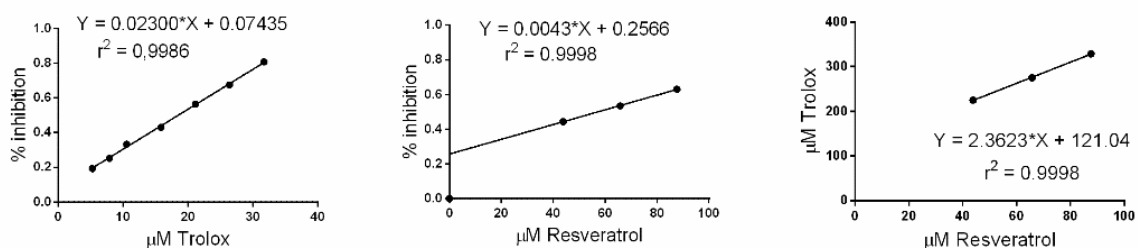

Figure 2.10. A linear relationship was found between Trolox (left)and resveratrol (middle), and the percentage of inhibition of ABTS$^{\bullet+}$ absorbance. On the right, a linear regression was performed between the concentrations of Trolox and *trans*-resveratrol that produce the same percentage of ABTS$^{\bullet+}$ radical reduction to calculate the antioxidant capacity of resveratrol expressed in TEAC. Reproduced with permission from Elsevier.

DISCUSSION

We have carried out [^{18}F]FDG PET/CT scans in a TNBS-induced IBD rat model to assess the efficacy of melatonin and resveratrol as potential therapies for IBD. We used a novel PET-based quantitative measurement previously developed by our group (34) in order to evaluate the disease activity and the response of melatonin and resveratrol therapies over mid-time, unlike previous reports only developed in the short-term. Our methodology was particularly focused on ensuring the arrival of the drugs to the area to be treated after being administered intrarectally. It has to be mentioned that melatonin and resveratrol could be metabolized or degraded quickly when given orally due to their pass through the GI tract, which leads to a limited concentration of drug in the inflamed colon.

First, we evaluated the suitability of two different vehicles and their residence time, concluding that the liquid enema of 1 mL was the most appropriate since it reached the

colonic areas of interest. The gel formulation was easily expelled with the faecal material due to its higher viscosity, which limits its spreadability and favours its expulsion among with the faeces. Our approach enabled the accurate prediction of the *in vivo* residence time of the formulation in the application area, which is a common drawback that arises when developing a mucoadhesive system (38). Once selected the most appropriate vehicle, PET/CT images over time showed that the administration of melatonin and resveratrol intrarectally can deliver the compounds directly into the inflamed mucosa, thereby avoiding the disadvantages of other routes of administration and attaining an effective level to treat the disease.

IBD is associated with increased permeability of the epithelial lining of the intestine, which results in a continuous stimulation of the mucosal immune system. Luminal bacteria contributes to maintain the permeability defect, establishing a self-sustaining cycle of mucosal inflammation (16). One study in animals found that luminal melatonin reduces the mucosal permeability, and this effect was compared to that of ethanol, which produces a robust increase in mucosal permeability. In addition, a pre-treatment with melatonin showed to strongly reduce the response to ethanol. These results suggest a mucosal protective mode of action of melatonin (39). Another study found that resveratrol activity is related to its interaction with the gut endocannabinoid system (ECS), resulting in a reduction of the intestinal permeability. Thus, resveratrol contributes to the maintenance of gut barrier integrity and helps in the inhibition of gut inflammation (40).

Furthermore, melatonin administered intrarectally could inhibit the action of macrophages in inflamed tissues and thus the secretion of pro-inflammatory cytokines such as IL-1, IL-6 and TNF-α in a TNBS animal model (41). The role of pro-inflammatory cytokines and free radicals and the effect of melatonin on its expression have been extensively studied in TNBS animal models of IBD. In these works, melatonin was administered intrarectally and in the same doses (10 mg / kg) as those used in the present study (20,21,42). The protective effects of melatonin have been also observed in other animal models, such as the acetic acid colitis model, playing a role in the preservation of the endogenous antioxidant reserve and the inhibition of the enhanced MPO activity (43).

On the other hand, the effects of resveratrol on chronic colonic injury have also been investigated by several authors. The administration of oral resveratrol in a TNBS animal model has shown anti-inflammatory effects in colitis treatment, due to a reduction in the production of inflammatory mediators (29). Other work has evaluated the antioxidant properties of resveratrol when it is given intraperitoneally as a pre-treatment before induction of TNBS colitis. With the same dose (10 mg / kg) as the one used in the present study, the malondialdehyde (MDA) levels were significantly reduced, while those of glutathione peroxidase (GSH Px) were increased (30).

Chemical assays currently used to assess the antioxidant activity of a compound are based on the ability to scavenge free radicals. A variety of radical scavenging methods, such as ABTS assay, are common spectrophotometric procedures for determining the antioxidant

capacity of a substance. In this study, ABTS assay was performed to evaluate the antioxidant properties of resveratrol and melatonin. Phenolic compounds such as resveratrol are known as high-level antioxidants due to their radical-scavenging activity, which is attributed to the aromatic ring systems (44), while the antioxidant activity of melatonin lies mainly in its electron-rich indole ring. The reducing capacity of a compound may serve as an indicator of its potential antioxidant activity. Therefore, the phenolic hydroxyl group of resveratrol has higher radical scavenging and reducing activity than melatonin since resveratrol with the phenolic group can easily transfer a hydrogen atom to $ABTS^{\bullet+}$ (45). These findings are consistent with the results obtained in the present study. When comparing the antioxidant capacity of resveratrol with the values obtained for reference antioxidant Trolox, resveratrol proved to be several times higher. However, melatonin did not show enough antioxidant activity by this method in achieving a linear response between melatonin concentration and the percentage of inhibition of $ABTS^{\bullet+}$ absorbance. Although it exists evidence supporting the role of melatonin and its metabolites as antioxidant agents *in vivo* (46), the *in vitro* ABTS assay has shown only limited antioxidant activity of melatonin compared to resveratrol. Further studies may be needed to investigate other mechanisms involved in antioxidant activity, such as the antioxidant effect produced by scavenging free radicals or inhibiting their production, or alternatively, by upregulating endogenous antioxidant defences *in vivo* (such as enzymatic systems). The use of other models of colitis or even other animal models could be useful for this purpose.

Our approach based on [^{18}F]FDG PET/CT imaging allows repeated investigations on each living animals, thereby limiting the number of animals needed for individual measures during the follow-up. In particular, PET imaging allows to locally quantify the inflammation in specific anatomic areas of the intestine avoiding histological examinations and therefore the sacrifice of the animals. This quantification could be used together with surrogate markers such as weight loss and diarrhoea. Moreover, PET/CT has an added clinical value since it allows to evaluate the treatment efficacy from its earliest stages. In our study, we have found that just one day after the induction of colitis, PET/CT images showed extensive spatial patterns of inflammation mainly affecting the transverse and descending colon. The subsequent quantification of PET images in terms of the SUV_{max} parameter showed significant differences in disease progression once both treatments were administered to both groups of animals. This follow-up of the disease through the standardized measurement of metabolism obtained from the images exhibited a clear remission of the inflammation throughout the days. This remission could be explained by the antioxidant and anti-inflammatory activity of melatonin and resveratrol since TNBS inflammation is due to the generation of transmural oxidative stress and release of proinflammatory cytokines (47).

After the IBD induction, animals showed different degrees of weight loss and diarrhoea. From day 3 when the treatment began, these clinical symptoms improved significantly and on day 7 almost all the treated animals reached their basal weight again. When sacrificed 15 days after colitis induction, most of melatonin-treated animals and all of resveratrol-treated animals did not show bowel wall thickening or areas of necrosis. In non-treated animals (34), the

macroscopic evaluation of *ex vivo* colons showed significant bowel wall thickening with areas of necrosis. The deposition of fibrotic tissue, which is part of the healing process, may explain the obstruction observed in some animals. This obstruction may arise from swelling and the formation of scar tissue that creates a narrowed bowel passage.

In the previous work of our group, it has been demonstrated that TNBS-induced IBD rat model has a positive response to corticosteroids, a commonly used treatment in clinical practice, which validates it for the evaluation of the efficacy of new compounds. Moreover, the longitudinal assessment of the inflammatory process performed through PET/CT highlighted the translational potential of this technique for monitoring patients in clinical practice (34). Our present work is the first longitudinal PET/CT study to our knowledge to investigate the therapeutic effects of melatonin and resveratrol in a TNBS animal model. Although several works, such as those mentioned above, have already reported the beneficial properties and the potential use of both compounds as therapeutic agents in IBD treatment, none of these studies has used a non-invasive method for the assessment of novel drugs activity and disease progression after the administration of those new compounds.

Overall, our findings showed that the SUV_{max} parameter obtained from the quantification of longitudinal PET images is a reliable biomarker to monitor the disease progression and the treatment response in a TNBS animal model. Furthermore, SUV_{max} is commonly used in clinical routine, so it represents a completely translational parameter and a promising biomarker with a high-throughput screening of new drugs in preclinical research. In addition, our results provide compelling evidence for the implementation of melatonin and resveratrol as therapies for IBD and suggest that this approach appears to be effective in the treatment of gastrointestinal pathologies whose pathogenesis is in part due to oxidative stress, such as IBD.

Future work should focus on the development of a rectal dosage form for melatonin and resveratrol with longer residence time and mucoadhesive properties, which allows a sustained release of both compounds in the colonic mucosa.

CONCLUSIONS

[^{18}F]FDG PET/CT studies were performed to evaluate the efficacy of melatonin and resveratrol in the treatment of experimental IBD. To our knowledge, this is the first longitudinal PET/CT study performed with the aim of assessing the therapeutic effects of both compounds in a TNBS-induced IBD animal model. Our findings showed that melatonin and to a greater extent, resveratrol, have shown to serve as potential therapeutic agents in IBD treatment. In addition, PET/CT technique has demonstrated its value in the preclinical research of new drugs, also providing additional data that could help in the assessment of disease activity. In the near future, this method could be a useful tool for follow-up IBD patients in a non-invasive way and monitor the treatment efficacy.

ACKNOWLEDGEMENTS

CONFLIT OF INTEREST

The authors declare no conflit of interest.

REFERENCES

1.   Hanauer SB. Inflammatory Bowel Disease: Epidemiology, Pathogenesis, and Therapeutic Opportunities. Inflamm Bowel Dis. 1 de enero de 2006;12(suppl_1):S3-9.

2.   Yadav V, Varum F, Bravo R, Furrer E, Bojic D, Basit AW. Inflammatory bowel disease: exploring gut pathophysiology for novel therapeutic targets. Transl Res J Lab Clin Med. 2016;176:38-68.

3.   Burger D, Travis S. Conventional medical management of inflammatory bowel disease. Gastroenterology. mayo de 2011;140(6):1827-1837.e2.

4.   Adegbola SO, Sahnan K, Warusavitarne J, Hart A, Tozer P. Anti-TNF Therapy in Crohn's Disease. Int J Mol Sci. agosto de 2018;19(8):2244.

5.   Levin AD, Wildenberg ME, van den Brink GR. Mechanism of Action of Anti-TNF Therapy in Inflammatory Bowel Disease. J Crohns Colitis. agosto de 2016;10(8):989-97.

6.   Dudzińska E, Gryzinska M, Ognik K, Gil-Kulik P, Kocki J. Oxidative Stress and Effect of Treatment on the Oxidation Product Decomposition Processes in IBD [Internet]. Oxidative Medicine and Cellular Longevity. 2018 [citado 23 de abril de 2019]. Disponible en: https://www.hindawi.com/journals/omcl/2018/7918261/

7.   Purohit TJ, Hanning SM, Wu Z. Advances in rectal drug delivery systems. Pharm Dev Technol. diciembre de 2018;23(10):942-52.

8.   Parada Venegas D, De la Fuente MK, Landskron G, González MJ, Quera R, Dijkstra G, et al. Short Chain Fatty Acids (SCFAs)-Mediated Gut Epithelial and Immune Regulation and Its Relevance for Inflammatory Bowel Diseases. Front Immunol [Internet]. 2019 [citado 9 de septiembre de 2019];10. Disponible en: https://www.frontiersin.org/articles/10.3389/fimmu.2019.00277/full

9.   Mulhbacher J, Ispas-Szabo P, Ouellet M, Alex S, Mateescu MA. Mucoadhesive properties of cross-linked high amylose starch derivatives. Int J Biol Macromol. 15 de diciembre de 2006;40(1):9-14.

10.   Morris GP, Beck PL, Herridge MS, Depew WT, Szewczuk MR, Wallace JL. Hapten-Induced Model of Chronic Inflammation and Ulceration in the Rat Colon. Gastroenterology. 1 de febrero de 1989;96(2):795-803.

11.   Seoane-Viaño I, Gómez-Lado N, Otero-Espinar F, Fernández-Ferreiro A, Aguiar P, Ruibal Á, et al. Preclinical Models of Inflammatory Bowel Disease and Colonic Treatments. Inflamm Bowel Dis. 2019;26.

12.   Wirtz S, Popp V, Kindermann M, Gerlach K, Weigmann B, Fichtner-Feigl S, et al. Chemically induced mouse models of acute and chronic intestinal inflammation. Nat Protoc. julio de 2017;12(7):1295-309.

13.   Ferri D, Costero AM, Gaviña P, Parra M, Merino V, Teruel AH, et al. Efficacy of budesonide-loaded mesoporous silica microparticles capped with a bulky azo derivative in rats with TNBS-induced colitis. Int J Pharm. 20 de abril de 2019;561:93-101.

14.   Terry PD, Villinger F, Bubenik GA, Sitaraman SV. Melatonin and ulcerative colitis: evidence, biological mechanisms, and future research. Inflamm Bowel Dis. enero de 2009;15(1):134-40.

15.   Jena G, Trivedi PP. A review of the use of melatonin in ulcerative colitis: experimental evidence and new approaches. Inflamm Bowel Dis. marzo de 2014;20(3):553-63.

16.   Motilva V, García-Mauriño S, Talero E, Illanes M. New paradigms in chronic intestinal inflammation and colon cancer: role of melatonin. J Pineal Res. 1 de agosto de 2011;51(1):44-60.

17.   MacEachern SJ, Keenan CM, Papakonstantinou E, Sharkey KA, Patel BA. Alterations in melatonin and 5-HT signalling in the colonic mucosa of mice with dextran-sodium sulfate-induced colitis. Br J Pharmacol. mayo de 2018;175(9):1535-47.

18.   Mozaffari S, Abdollahi M. Melatonin, a promising supplement in inflammatory bowel disease: a comprehensive review of evidences. Curr Pharm Des. diciembre de 2011;17(38):4372-8.

19.   Cuzzocrea S, Mazzon E, Serraino I, Lepore V, Terranova ML, Ciccolo A, et al. Melatonin reduces dinitrobenzene sulfonic acid-induced colitis. J Pineal Res. 1 de enero de 2001;30(1):1-12.

20.   Mei Q. Change of nitric oxide in experimental colitis and its inhibition by melatonin in vivo and in vitro. Postgrad Med J. 1 de octubre de 2005;81(960):667-72.

21.   Li J-H, Yu J-P, Yu H-G, Xu X-M, Yu L-L, Liu J, et al. Melatonin Reduces Inflammatory Injury Through Inhibiting   NF-κB Activation in Rats With Colitis. Mediators Inflamm. 31 de agosto de 2005;2005(4):185-93.

22.   Langcake P, Pryce RJ. The production of resveratrol by Vitis vinifera and other members of the Vitaceae as a response to infection or injury. Physiol Plant Pathol. 1 de julio de 1976;9(1):77-86.

23.   Luzardo-Álvarez A, Lamela-Gómez I, Otero-Espinar F, Blanco-Méndez J. Development, Characterization, and In Vitro Evaluation of Resveratrol-Loaded Poly-(ε-caprolactone) Microcapsules Prepared by Ultrasonic Atomization for Intra-Articular Administration. Pharmaceutics. junio de 2019;11(6):249.

24.   Rius C, Abu-Taha M, Hermenegildo C, Piqueras L, Cerda-Nicolas J-M, Issekutz AC, et al. Trans- but not cis-resveratrol impairs angiotensin-II-mediated vascular inflammation through inhibition of NF-κB activation and peroxisome proliferator-activated receptor-gamma upregulation. J Immunol Baltim Md 1950. 15 de septiembre de 2010;185(6):3718-27.

25.   Salehi B, Mishra A, Nigam M, Sener B, Kilic M, Sharifi-Rad M, et al. Resveratrol: A Double-Edged Sword in Health Benefits. Biomedicines. 9 de septiembre de 2018;6(3):91.

26.   Shi Y, Zhou J, Jiang B, Miao M. Resveratrol and inflammatory bowel disease. Ann N Y Acad Sci. 2017;1403(1):38-47.

27.   Larrosa M, Yañéz-Gascón MJ, Selma MV, González-Sarrías A, Toti S, Cerón JJ, et al. Effect of a low dose of dietary resveratrol on colon microbiota, inflammation and tissue damage in a DSS-induced colitis rat model. J Agric Food Chem. 25 de marzo de 2009;57(6):2211-20.

28.   Cui X, Jin Y, Hofseth AB, Pena E, Habiger J, Chumanevich A, et al. Resveratrol Suppresses Colitis and Colon Cancer Associated with Colitis. Cancer Prev Res (Phila Pa). 1 de abril de 2010;3(4):549-59.

29.   Martín AR, Villegas I, Sánchez-Hidalgo M, de la Lastra CA. The effects of resveratrol, a phytoalexin derived from red wines, on chronic inflammation induced in an experimentally induced colitis model. Br J Pharmacol. abril de 2006;147(8):873-85.

30.   Yildiz G, Yildiz Y, Ulutas PA, Yaylali A, Ural M. Resveratrol Pretreatment Ameliorates TNBS Colitis in Rats. Recent Pat Endocr Metab Immune Drug Discov. 2015;9(2):134-40.

31.   Nunes S, Danesi F, Del Rio D, Silva P. Resveratrol and inflammatory bowel disease: the evidence so far. Nutr Res Rev. junio de 2018;31(01):85-97.

32.   Kaaru E, Bianchi A, Wunder A, Rasche V, Stiller D. Molecular Imaging in Preclinical Models of IBD with Nuclear Imaging Techniques: State-of-the-Art and Perspectives. Inflamm Bowel Dis. 1 de octubre de 2016;22(10):2491-8.

33.   Goyanes A, Fernández-Ferreiro A, Majeed A, Gomez-Lado N, Awad A, Luaces-Rodríguez A, et al. PET/CT imaging of 3D printed devices in the gastrointestinal tract of rodents. Int J Pharm. 30 de enero de 2018;536(1):158-64.

34.   Seoane-Viaño I, Gómez-Lado N, Lázare-Iglesias H, Barreiro-de Acosta M, Silva-Rodriguez J, Luzardo-Álvarez A, et al. Longitudinal PET/CT evaluation of TNBS-induced Inflammatory Bowel Disease rat model. Int J Pharm. 1 de agosto de 2018;549.

35.   Kilkenny C, Browne W, Cuthill IC, Emerson M, Altman DG, NC3Rs Reporting Guidelines Working Group. Animal research: reporting in vivo experiments: the ARRIVE guidelines. Br J Pharmacol. agosto de 2010;160(7):1577-9.

36.   Marchal-Bressenot A, Salleron J, Boulagnon-Rombi C, Bastien C, Cahn V, Cadiot G, et al. Development and validation of the Nancy histological index for UC. Gut. 2017;66(1):43-9.

37.   Re R, Pellegrini N, Proteggente A, Pannala A, Yang M, Rice-Evans C. Antioxidant activity applying an improved ABTS radical cation decolorization assay. Free Radic Biol Med. mayo de 1999;26(9-10):1231-7.

38.   Campaña-Seoane M, Pérez-Gago A, Vázquez G, Conde N, González P, Martinez A, et al. Vaginal residence and pharmacokinetic preclinical study of topical vaginal mucoadhesive W/S emulsions containing ciprofloxacin. Int J Pharm. 10 de enero de 2019;554:276-83.

39.   Sommansson A, Saudi WSW, Nylander O, Sjöblom M. Melatonin inhibits alcohol-induced increases in duodenal mucosal permeability in rats in vivo. Am J Physiol Gastrointest Liver Physiol. 1 de julio de 2013;305(1):G95-105.

40.   Chen M, Hou P, Zhou M, Ren Q, Wang X, Huang L, et al. Resveratrol attenuates high-fat diet-induced non-alcoholic steatohepatitis by maintaining gut barrier integrity and inhibiting gut inflammation through regulation of the endocannabinoid system. Clin Nutr Edinb Scotl. 30 de mayo de 2019;

41.   Mei Q, Yu J-P, Xu J-M, Wei W, Xiang L, Yue L. Melatonin reduces colon immunological injury in rats by regulating activity of macrophages. Acta Pharmacol Sin. octubre de 2002;23(10):882-6.

42.   Dong W-G. Effects of melatonin on the expression of iNOS and COX-2 in rat models of colitis. World J Gastroenterol. 2003;9(6):1307.

43.   Nosál'ová V, Zeman M, Cerná S, Navarová J, Zakálová M. Protective effect of melatonin in acetic acid induced colitis in rats. J Pineal Res. abril de 2007;42(4):364-70.

44.   Gülçin İ. Antioxidant properties of resveratrol: A structure-activity insight. Innov Food Sci Emerg Technol [Internet]. 2010 [citado 10 de mayo de 2019]; Disponible en: http://agris.fao.org/agris-search/search.do?recordID=US201301726871

45.   Gülçin I. Measurement of antioxidant ability of melatonin and serotonin by the DMPD and CUPRAC methods as trolox equivalent. J Enzyme Inhib Med Chem. enero de 2008;23(6):871-6.

46.   Reiter RJ, Tan D-X, Manchester SR-C and LC. The Universal Nature, Unequal Distribution and Antioxidant Functions of Melatonin and Its Derivatives [Internet]. Mini-Reviews in Medicinal Chemistry. 2013 [citado 10 de mayo de 2019]. Disponible en: http://www.eurekaselect.com/106807/article

47.   Shi X-Z, Winston JH, Sarna SK. Differential immune and genetic responses in rat models of Crohn's colitis and ulcerative colitis. Am J Physiol-Gastrointest Liver Physiol. 14 de octubre de 2010;300(1):G41-51.
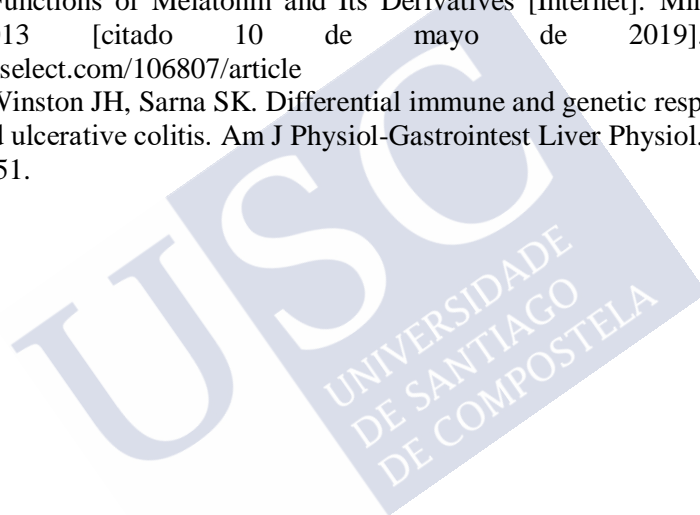
Chapter III.

3D printed tacrolimus suppositories for the treatment of ulcerative colitis.

CHAPTER III

ABSTRACT

Ulcerative colitis is a global health problem, affecting over 2 million individuals worldwide. As it is an inflammatory condition localised in the large intestine, rectal delivery of immunosuppressive therapies such as tacrolimus is a promising strategy to maximise drug concentration at the site of action whilst minimising systemic side effects. Here, for the first time, self-supporting 3D-printed tacrolimus suppositories were prepared without the aid of moulds using a pharmaceutical semi-solid extrusion (SSE) 3D printer. The suppositories were printed vertically in three different sizes using combinations of two lipid pharmaceutical excipients (Gelucire 44/14 or Gelucire 48/16) and coconut oil. Although both formulations had the appropriate viscosity characteristics for printing, the Gelucire 44/14 formulation required less energy and force for extrusion compared to the Gelucire 48/16 formulation. The Gelucire 44/14 suppositories disintegrated more rapidly but released tacrolimus more slowly than the Gelucire 48/16 suppositories. Although the tacrolimus release profiles were significantly different, both suppository types released more than 80% drug within 120 minutes. DSC and XRPD data were inconclusive to determine the solid-state properties of the drug in the matrix due to the low concentration of tacrolimus present. Overall, this article reports the feasibility of fabricating 3D printed self-supporting suppositories to deliver personalised doses of a narrow therapeutic index drug, with potential benefits for treatment outcomes in patients with ulcerative colitis.

Keywords: 3D printing, semi-solid extrusion, suppository, pressure assisted syringe, 3D printed drug products, self-emulsifying system.

INTRODUCTION

Inflammatory bowel disease (IBD) is a group of incurable chronic inflammatory disorders of the gastrointestinal tract, of which Crohn's disease and ulcerative colitis are the most common (1, 2). Specifically, ulcerative colitis is characterised by inflammation of the colon and the rectum. Despite being an inflammatory condition of the distal gastrointestinal tract, the majority of efforts for new treatments have revolved around the development of oral therapies (3). However, oral delivery in ulcerative colitis is challenging as potentially only a fraction of the administered drug might reach the intended site of action. In contrast, rectal delivery can enhance therapeutic efficacy and safety by maximising drug concentrations at the disease site, reduce systemic side effects, and increase the rate of response (4).

Studies have previously reported the use of tacrolimus suppositories as a treatment in therapy-resistant ulcerative proctitis (ulcerative colitis limited to the rectum) (5-7). Tacrolimus is a calcineurim inhibitor widely used as an immunosuppressive agent (8). Treatment with tacrolimus induces a rapid clinical response and mucosal healing in hospitalized patients with steroid-refractory ulcerative colitis, and its use is also supported in patients with Crohn's disease refractory to conventional therapies (9-11). The administration of oral tacrolimus is related with long-term toxicity (especially hypertension and renal dysfunction) and the higher the serum trough levels, the more likely it is that a patient will suffer an adverse effect (therapeutic range $5 - 20$ μg/L) (12). This fact, together with the low oral bioavailability of tacrolimus, makes it a suitable candidate for inclusion in a rectal dosage form. However, there are currently no commercially available tacrolimus suppositories, warranting their extemporaneous compounding in pharmaceutical services.

In current practice, suppositories are prepared by a moulding technique, which requires several steps and a relatively long time for hardening. Additionally, it is common for hospital pharmacists to compound suppository formulations from tablets designed for oral administration when a suppository formulation is not available. This leads to a number of risks, such as compounding errors and inaccurate dosing (13).

In light of these issues, three-dimensional printing (3DP) has been explored as a novel manufacturing technology for the manufacture of bespoke formulations including suppositories. 3DP is an additive manufacturing technology that enables the production of individualised objects in a layer-by-layer manner. In the pharmaceutical field, 3DP offers the opportunity to make a significant technological contribution in the design and manufacture of medicines (14). When compared to conventional manufacturing processes, this technology offers unique benefits for the manufacture of solid drug products, such as patient-tailored medicines (15), retentive devices (16, 17), and customised drug release formulations (18, 19). Within the pharmaceutical field five main 3DP technologies are currently used; powder bed ink jet printing (20), fused deposition modelling (FDM) (21), selective laser sintering (SLS) (22), stereolithography (SLA) (23), and semi-solid extrusion (SSE) (24, 25).

Semi-solid extrusion 3DP is based on the deposition of semisolids (gel or paste) in sequential layers through a syringe-based tool-head nozzle to create the 3D object, and it is highly relevant to print objects using soft materials (26, 27). Compared to other 3DP techniques, SSE is suitable for thermolabile compounds since the printing process does not require high temperatures (28). Moreover, the excipients and drugs can be added directly to the gel base without the need for intermediate steps, such as the preparation of drug-loaded filaments in FDM (29). This technique has been used to manufacture polypills with well-defined and separate controlled release profiles for the different drugs incorporated into the multi-active tablet (30), as well as immediate release tablets with high drug loading (31). Moreover, SSE 3DP was the first 3D printing technology used to prepare personalised printlets (3D printed tablets) in a hospital setting. The dosage forms were chewable printlets used for the treatment of a rare metabolic disease, and they were well accepted by paediatric patients, demonstrating the feasibility of this approach to prepare oral tailored-dose therapies (32).

The ability of SSE 3DP to print soft materials could be exploited to prepare lipid based formulations (26). The use of self-emulsifying drug delivery systems (SEDDS) and self-microemulsifying drug delivery systems (SMEDDS) is one of the most popular approaches for enhancing the solubility of poorly water-soluble drugs (33). SEDDS and SMEDDS are isotropic mixtures of an oil, a surfactant, cosurfactant and a drug which form kinetically stable oil-in-water (O/W) emulsions. The lipophilic drugs are solubilized in the small lipid droplets, which have a large interfacial surface area for drug absorption (34). In this regard, drug-loaded solid SMEDDS (S-SMEDDS) intended for oral administration were successfully prepared using SSE 3DP (35). This approach could allow for the preparation of novel lipid-based formulations with a defined dose, shape, size and drug release profile tailored to the needs of each patient.

As such, by implementing SSE 3D printers in hospital settings, different suppository sizes may be printed to suit the patient's comfort. Given that discomfort was the main reason for non-adherence to suppositories in ulcerative colitis treatment, the ability to tailor suppositories according to the patient's comfort can enhance adherence and consequently treatment outcomes (36). Additionally, pharmacists could design a personalized suppository containing a precise dose of drug for each patient. This is especially useful in the case of narrow therapeutic index drugs, such as tacrolimus. Previous work has described the fabrication of suppository moulds and shells with different shapes and geometries (37-39), but to date no study has directly printed the suppositories without the need for a mould or a cover. Enabling the direct preparation of self-supporting suppositories would obviate the need for a mould, reducing both the time and material costs required to prepare the suppositories. Additionally, since a reason for the poor and variable oral bioavailability of tacrolimus is its low water solubility (4-12 µg/mL in water) (40), the preparation of tacrolimus suppositories via SSE 3DP with the drug solubilized within SEDDS, would increase its water solubility and consequently its effectiveness.

Therefore, this study reports, for the first time, the use of a SSE 3D printer to fabricate self-supporting and self-emulsifying suppositories loaded with the immunosuppressant drug tacrolimus for the treatment of ulcerative colitis to produce patient-tailored suppositories. Moreover, the versatility of lipid excipients was exploited to modulate the melting range of the suppositories, as well as their disintegration times and drug release kinetics.

MATERIALS AND METHODS

Materials

Tacrolimus was purchased from Guinama S.L.U., Spain. Coconut oil was obtained from Acofarma, Spain. Gelucire 44/14 and Gelucire 44/16 were kindly donated by Gattefosse España SA, Spain.

Methods

Design of the 3D models

The software 123D Design (Autodesk Inc., USA) was used to design the templates of the suppositories with three different sizes. The smallest size was 8 mm diameter x 24.77 mm height, the medium size was 9 mm × 27.87 mm (Figure 3.1) and the biggest size was 12 mm x 36 mm.
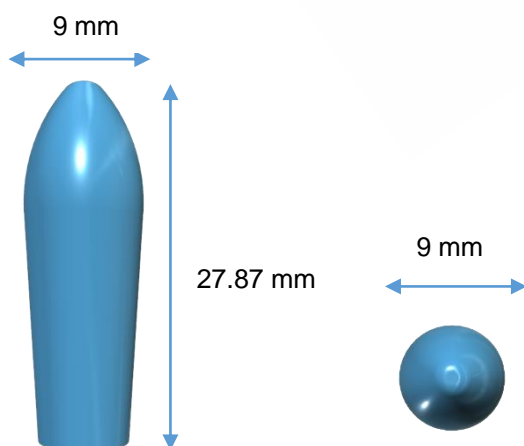

Figure 3.1. 3D model of a suppository from two different views: a side view (left) and a top view (right).

Semisolid extrusion 3D printing

Pre-selected ratios of lipid excipients and drug were mixed in a glass beaker and placed on a heating plate (Table 1). The tacrolimus dose was selected according to published literature (5). The mixtures were heated until the mixtures were melted and they remained under magnetic stirring until complete solubilization of the drug in the lipid excipients occurred. The masses were immediately transferred to a 20 mL extrusion syringe with a tapered extrusion tip (0.58 mm orifice) and allowed to solidify at room temperature. Then, the syringe was placed into the pharmaceutical 3D printer with the semisolid extrusion tool (M3DIMAKER, FabRx Ltd, UK). The previously prepared 3D models of the suppositories were transformed into .gcode files using Cura software (v 15.04.6, Ultimaker Utrecht, Netherlands) using the following printing parameters: 0.5mm layer height; 2.4mm shell thickness; 25 mm/s flow speed; 1.2 mm nozzle size, room temperature of build plate and chamber, printing temperature (Table 1). in two different positions, vertical and horizontal. Finally, 3D printed suppositories were allowed to solidify at room temperature and subsequently stored in the fridge at 4 ºC.

Table 1. Formulation composition and printing temperature.

Formulation	Gelucire 44/14 (% w/w)	Gelucire 48/16 (% w/w)	Coconut oil (% w/w)	Tacrolimus (% w/w)	Printing temperature (°C)
Gel 44	79.94	0	19.94	0.12	42
Gel 48	0	79.94	19.94	0.12	48

Characterization of the 3D printed suppositories

Scanning Electron Microscopy (SEM)

Scanning Electron Microscopy (SEM) images of the suppositories surface were taken in the horizontal position with a scanning electron microscope ZEISS EVO LS15 at 20Kv using a BSD detector (backscattered electron detector) / SE (secondary electron detector), under conditions of variable pressure (VP).

Syringe Extrusion Force Studies

The syringe extrusion force studies were performed in sextuplicate by using Shimazdu´s Autograph AGS-X universal tester with a load cell (SSM-DAM-1000N) with a maximum capacity of 1 kN. Each extrusion syringe loaded with the mixture of drug and lipid excipients was heated up at the printing temperature (42 ºC for Gel 44 and 48 ºC for Gel 48), placed in a

physical support and immobilized. A ram (15 mm diameter) was moved to apply pressure at a displacement rate of 10 mm/min on the plunger of the syringe and the load cell was utilized to measure extrusion force during each extrusion run. TRAPEZIUM X Materials Testing Software in compression mode was used for collecting extrusion force data. Statistical analysis of the results was carried out using the Mann-Whitney non-parametric test to evaluate the differences in the energy and extrusion force required to extrude each formulation.

Drug loading

The content uniformity of the drug in the suppositories was determined in triplicate using high performance liquid chromatography (HPLC). Approximately 1.7g of the drug-loaded suppositories was dissolved in 50 mL of ethanol absolute at 37°C under magnetic stirring until a clear transparent solution was obtained. The resulting solution was centrifuged for 30 min at 12500 rpm and the supernatant was collected and analysed by HPLC.

The amount of drug in solution was determined using a Hewlett Packard 1050 Series HPLC system (Agilent Technologies, UK). The validated high-performance liquid chromatographic assay entailed injecting 20 μL samples for analysis using a mobile phase, consisting of water-acetonitrile (35:65 v/v) through a Poroshell 120, EC-C18 (4.6x100 mm 4 μm) and at a temperature of 60ºC. The mobile phase was pumped at a flow rate of 1 mL/min. A wavelength of 210 nm was employed for the quantification of tacrolimus. All measurements were made in triplicate.

Fourier transform-infrared spectroscopy (FT-IR)

FT-IR spectroscopy was performed using FT-IR model Varian 670-IR attached to an attenuated total reflectance (ATR) accessory (GladiATR, PIKE Technologies). ATR was fitted with a single monolithic diamond at 45º internally reflected incident light providing a sampling area of 1.5 mm in diameter with a sampling depth of several microns. Drug, lipid excipients and suppository formulations were analysed. A small amount of the sample was directly placed on the diamond disk. Sample was scanned for absorbance over the wavenumber range of 4000 to 400 (cm^{-1}) at a resolution of 4 cm^{-1}.

Differential Scanning Calorimetry (DSC)

The thermal properties of raw materials (drug and lipid excipients) and suppository formulations were determined by Differential Scanning Calorimetry (DSC Q100, TA Instruments, New Castle, DE, USA). Samples were heated from room temperature to 300ºC at 10 °C/min under nitrogen flow (50 mL / min). The calibration for cell constant and enthalpy was done with indium (Tm = 156.6ºC, ΔHf = 28.71 J/g) according to the manufacturer's

instructions. Aluminium (TA) pans and lids (Tzero) were used with an average sample mass of 7–9 mg. TA Advantage software (version 2.8.394) and TA Instruments Universal Analysis 2000 were used to collect and analyse the data, respectively.

X-ray Diffraction Analysis (XRD)

X-ray diffraction measurements of the powdered samples were performed using a Philips diffractometer (Almelo, The Netherlands) fitted with a Philips PW1710 control unit, a Vertical Philips PW1820/00 goniometer, and an Enraf Nonius FR590 generator operating at 40 Kv and 30 mA. The X-ray were obtained from a Cu sealed tube and the radiation was monochromated with a monochromator of graphite (λ ($K_{\alpha 1}$) = 1.5406 Å). The diffractograms were obtained in the 2θ angle range $2^{\circ} – 50^{\circ}$ with a step of 0.04° and a counting time of 6s per step. The samples were mounted into a sample holder substrate (Silicon single crystal) to skip the dispersion that could be produced by a glass substrate.

Determination of Disintegration Time

The test was performed in distilled water at 37 ºC using the U.S.P. disintegration apparatus slightly modified to meet the requirements of the method described in the European Pharmacopeia (41). Each suppository was placed between the two perforated plates of the basket, which was inserted into a transparent plastic sleeve. The suppository disintegration rig was then placed in the glass beaker containing 1 L of distilled water at 37 ºC. The mean values were calculated from three parallel measurements.

Determination of Self-Emulsification Time

The emulsification time of SEDDS suppositories was determined according to USP XXIII, dissolution apparatus type II. Each formulation was melted and then added dropwise to 500 mL of purified water at 37°C. Gentle agitation was provided by a standard stainless-steel dissolution paddle at 50 rpm. Self-microemulsification time was recorded as the time taken by the formulation to form a clear solution in water.

Determination of Droplet Size and ζ Potential

Solid formulations (50 mg) were added to 100 mL of ultrapure water under constant stirring until the emulsion was formed. Droplet size distribution (mean diameter of lipid droplets and polydispersity index) and ζ potential (the charge of droplets) were determined using a Zetasizer Nano (Malvern Instrument Limited, Worcestershire, UK. All measurements were performed in triplicate.

Transmission Electron Microscopy (TEM)

Transmission Electron Microscopy (TEM) images of microemulsion droplets were taken using a transmission electron microscope JEOL JEM-1011. First, 50 mg of SEDDS suppositories were placed in 100 mL of distilled water under magnetic stirring until the emulsion was formed. Then, a drop of diluted SEDDS was then deposited on the holey film grid, stained by 1% aqueous solution of Phosphotungstic acid and observed after drying.

In Vitro Drug Release

In vitro drug release profiles of the 3DP suppositories were obtained using a USP-II mini paddle apparatus (Model PTWS, Pharmatest, Hainburg, Germany). The studies were conducted in 100 mL pH 8 phosphate buffer (0.1 M) and the paddle speed was set at 100 rpm with a temperature of 37 ±0.5 ℃ (n=3). At pre-determined time points (20, 40, 60, 80, 100, 120 min), 1 mL aliquots were withdrawn and 0.5 mL of ethanol absolute were added to the samples to solubilize the tacrolimus that could be trapped inside the lipid droplets. Then, the samples were centrifuged for 30 min at 12500 rpm and the supernatant was collected and analysed by HPLC as described in section 2.3.3.

Tacrolimus release profiles from the suppositories were fitted to the Gompertz growth model (equation 1).

$$\% \; released = \% \max \left(\frac{\%_{min}}{\%_{max}} \right)^{e^{-kt}} \tag{1}$$

where $\%\max$ is the maximum percentage of drug released, $\%\min$ is the minimum percentage of drug released and k is a constant. Gompertz growth model was fitted to drug release profile by non-linear regression analysis using the program GraphPad Prism (version 7.0).

Furthermore, the dissolution profiles of Gel 44 and Gel 48 formulations were compared using an f_2 similarity test, which is calculated using equation (2) (42). The similarity factor f_2 is a logarithmic transformation of the sum-squared error of differences between T_t and R_t over all the considered time points:

$$f^2 = 50 \times \log \left\{ \left[1 + \frac{1}{n} \sum_{t=1}^{n} (R_t - T_t)^2 \right]^{-\frac{1}{2}} \times 100 \right\} \tag{2}$$

Where R_t and T_t are the release profiles of the reference and test formulations at time point t respectively, and n the number of dissolution time points considered. The $f2$ value ranges from 0 to 100 and, in general, $f2$ values higher than 50 indicate similarity of the dissolution profiles (43). Moreover, as the $f2$ value decreases below 50, the variation between

the dissolution profiles increases, indicating that the formulations have different release profiles (44).

RESULTS AND DISCUSSION

This study proved that it was feasible to prepare drug-loaded suppositories without a mould or other physical support using 3DP technology. The printed suppositories were well-defined and with acceptable consistency for normal handling. No material slumping was observed during the printing process, and it was not necessary to use a refrigerated build plate to facilitate the solidification of the printed layers. During the printing process, the suppositories quickly solidified in less than 1 minute without the need for additional cooling or drying steps. Two different compositions of printing material were tested (Table 1).

The suppositories were printed in two positions, vertically (Figure 3.2a) and horizontally (Figure 3.2b) The printing time for the suppositories printed vertically was around 4 min 30 s and 2 min 16 s for those printed horizontally. Although printing the suppositories in the horizontal plane was faster due to the lower number of layers, the shape and resolution of the suppositories was better when they were printed vertically (Figure 3.2a).
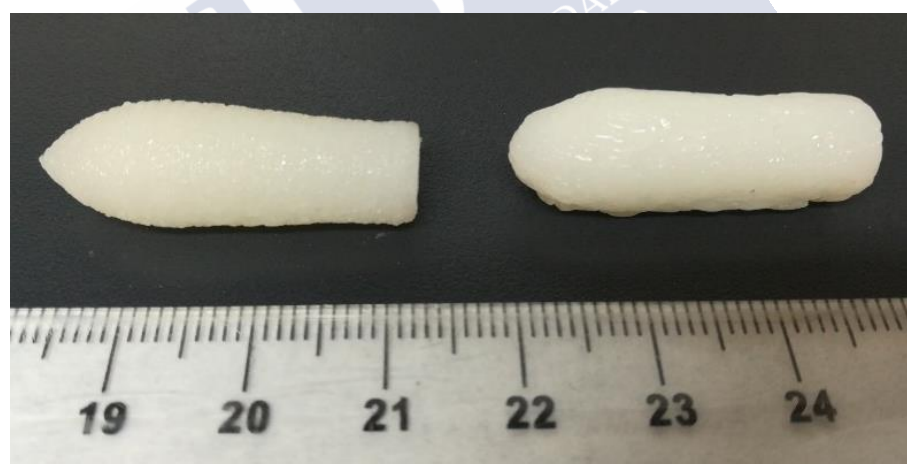

Figure 3.2. Gel 44 suppositories printed in (a) vertical position and (b) horizontal position (scale is in cm).

The scanning electron microscopy images indicate that the deposition of the individual layers are connected to each other forming a solid low porosity object (Figure 3.3). However, SEM images also showed that the deposition of layers when printing the suppository in vertical position was better than when printing horizontally (Figure 3.3). This is because when printing horizontally, some layers of material have no support underneath due to the convex shape of the suppository and are partially deposited in the air. Thus, some layers have irregularities that affect the final shape of the suppository.
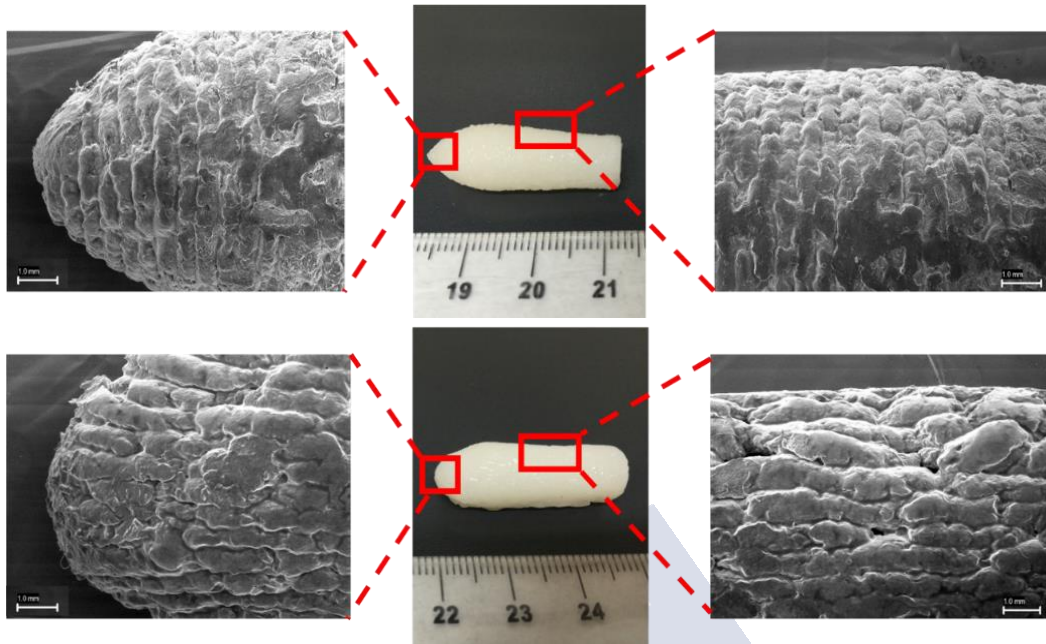
Figure 3.3. SEM images of different sections of Gel 44 self-emulsifying suppositories printed in (above) vertical position and (bellow) horizontal position.

Therefore, for the rest of the studies, all the suppositories were printed vertically. Suppositories with two different compositions were printed in three different sizes to demonstrate that it is possible to produce personalized suppositories containing different doses (Figure 3.4).
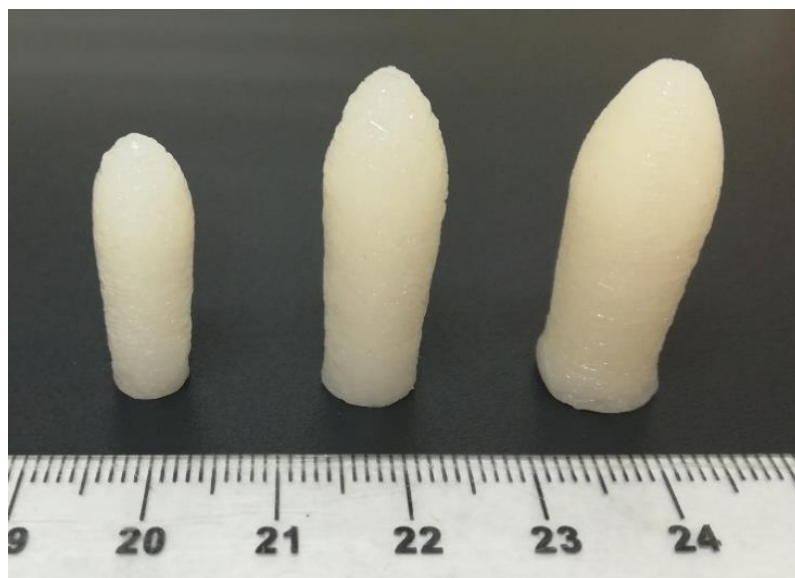
Figure 3.4. Picture of Gel 44 suppositories printed in three different sizes (from left to right: small, medium and large) as an example of personalization.

Preliminary studies were performed using only Gelucire 44/14 or Gelucire 48/16, but these excipients alone did not have adequate properties, such as the appropriate viscosity, for printing. To improve the printability properties of both Gelucire, coconut oil was employed as a plasticizer. Both Gelucire 44/14 and Gelucire 48/16 were completely miscible with coconut oil when melted.

The printing temperature was set at 42 ºC for Gel 44 formulation and to 48 ºC for Gel 48, being adequately controlled by the 3D printer avoiding solidification of the material in the nozzle tip. The mixtures from the syringes were heated until they reached a viscosity low enough to extrude through the tip of the nozzle. If the material was too extensively melted, the 3D printed suppository structure would not be able to hold its shape. But if it was too viscous, the nozzle would clog and the material would not flow. Extrusion force studies, interpreted as the force required to make the material pass through the extrusion tip at the printing temperature, were performed to obtain the energy and maximum extrusion force in order to evaluate the ease of extrusion of the mixtures at printing temperatures. Statistical analysis showed that the extrusion force and energy required to extrude Gel 48 was significantly higher ($p < 0.05$) than that required to extrude Gel 44 even though the printing temperature was higher for Gel 48 (Table 2).

The mean weight of suppositories was between 1.7 to 1.81 g (Table 2). The drug loading values of the suppositories represented 98.03% of the to the theoretical drug loading value for Gel 44 and 108.53% for Gel 48 (Table 2). The values suggest that tacrolimus did not undergo any degradation either during the mixture preparation or the printing process. The difference could be attributable to inadequate mixing of drug and excipients; however, the values differless than 10% from theoretical values.

Table 2. Characterization of the 3D printed suppositories.

Formulation	Extrusion energy (J) ± SD	Maximum extrusion force (N) ± SD	Mean weight (g) ± SD	Drug loading (mg) ± SD	Theoretical drug loading (mg) ± SD
Gel 44	0.070 ±0.017	18.3 ±0.6	1.70 ±0.05	2.00 ±0.34	2.04 ±0.04
Gel 48	0.139 ±0.014	36.0 ±3.5	1.81 ±0.03	2.29 ±0.15	2.11 ±0.06

Table 2.1. Continuation of Table 2.

Formulation	Disintegration time (min) ± SD	Self-emulsifying time (min) ± SD	Droplet Size (nm) ± SD	ζ Potential (mV) ±SD	PdI ± SD
Gel 44	33 ±3.9	1.2 ±0.2	1213 ±12	14.0 ±0.5	0.190 ± 0.04
Gel 48	43.5 ±5.4	2.4 ±0.2	1317 ±23	20.2 ±0.6	0.345 ± 0.36

FT-IR spectroscopy was performed to investigate possible interactions between the drug and the selected lipid excipients in their formulations (Figure 3.5). The IR patterns of Gel 44 and Gel 48 are practically the same as Gelucire 44/14 and Gelucire 48/16. The proportion of Gelucire in both formulations is around 80% w/w, and tacrolimus is only 0.12% w/w so the IR peaks of the drug practically disappear and cannot be detected in the final Gel 44 and Gel 48 formulations.
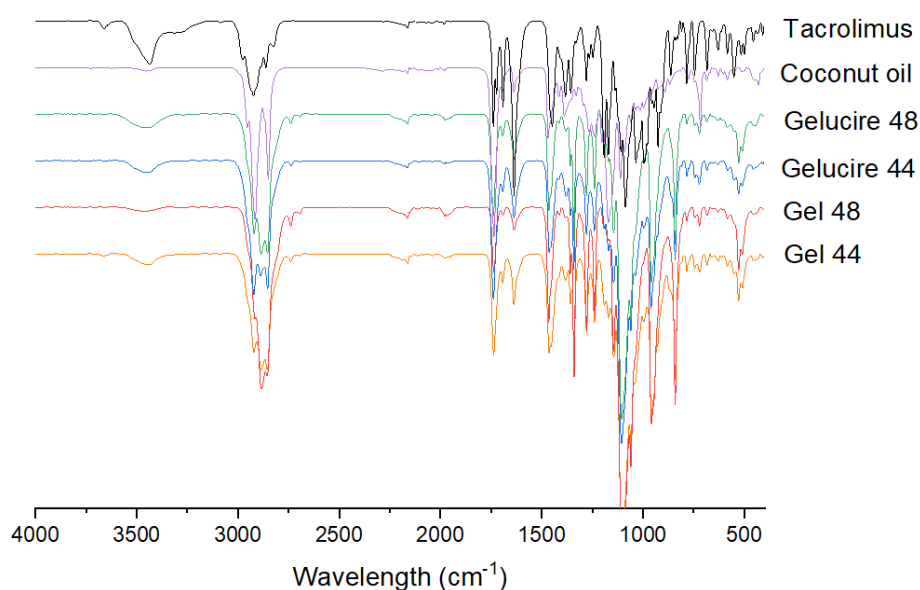
Figure 3.5. FT-IR spectra of the drug (tacrolimus), the lipid excipients (coconut oil, Gelucire 44 and Gelucire 48) and the formulations (Gel 44 and Gel 48).

DSC and X-ray analysis were employed to investigate the physical state of the drug in the final formulations. The DSC thermographs show that tacrolimus raw material melts around 130ºC while the melting point of both Gelucire 44/14 and 48/16 is between 40-50ºC (Figure 3.6). The melting peaks for Gelucire 44/14 and Gelucire 48/16 are almost the same as their respective Gel 44 and Gel 48 formulations. It was not possible to determine the melting point of tacrolimus in the formulations which indicates that the drug may be forming a solid solution with the lipid excipients. Other explanations are that during the DSC study while the temperature increases the drug is completely dissolved in the melted polymer or that the drug content is below the detection limit of the DSC equipment.
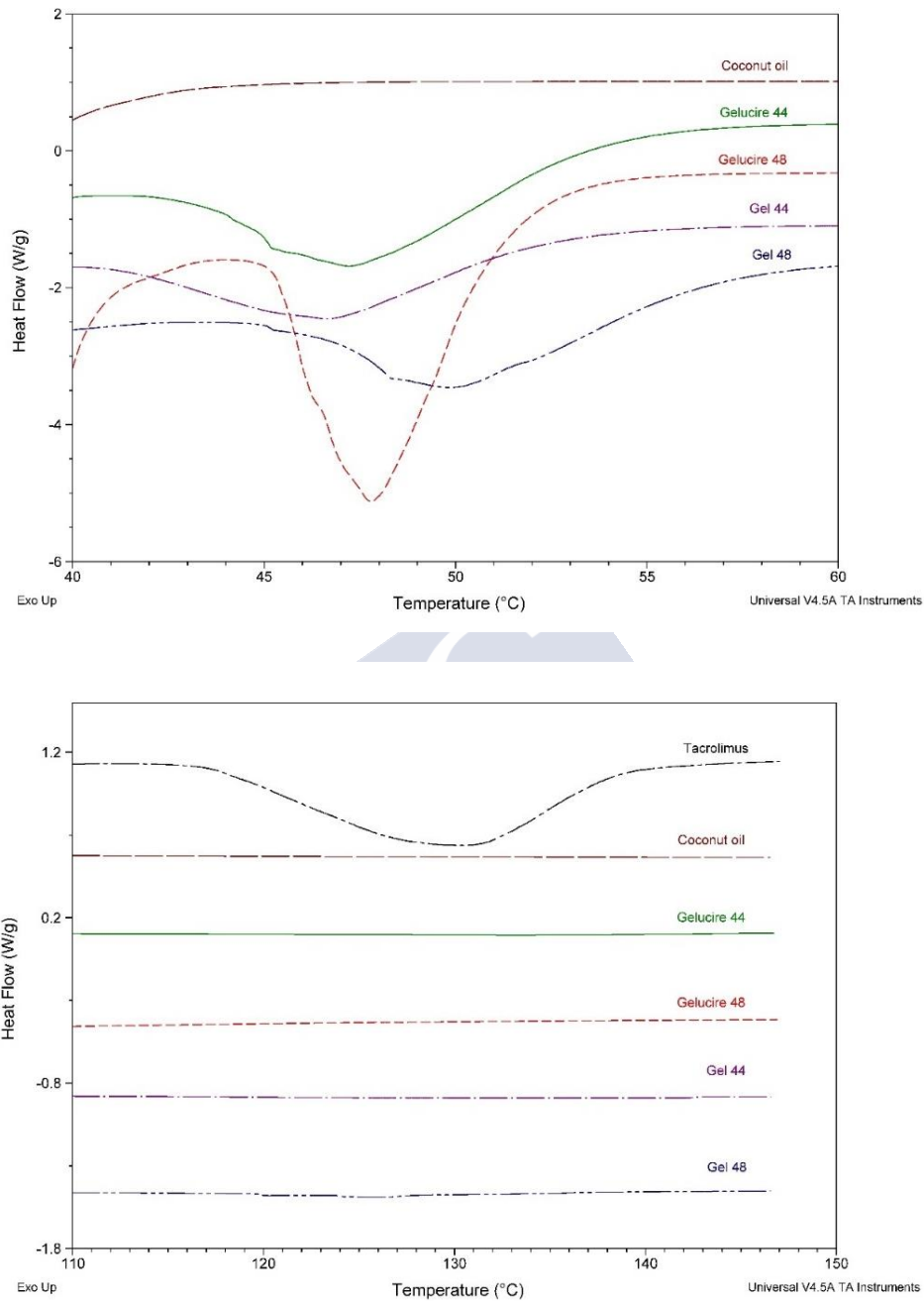
Figure 3.6. DSC curves for the drug (tacrolimus), the lipid excipients (coconut oil, Gelucire 44 and Gelucire 48) and the formulations (Gel 44 and Gel 48).

The X-ray diffractograms of Gelucire 44/14, Gelucire 48/16, Gel 44 and Gel 48 showed very similar structural behaviours. In particular, the peaks of Gelucire 48/16 and Gel 48 are sharper than those of Gelucire 44/14 and Gel 44, which may be due to the higher degree of crystallinity of Gelucire 48/16 and Gel 48. Tacrolimus showed the characteristic peaks of crystalline structures. The absence of the sharp peaks of tacrolimus in the diffractograms of

the formulations suggests that the drug content is below the detection limit of the XRD instrument. (Figure 3.7).
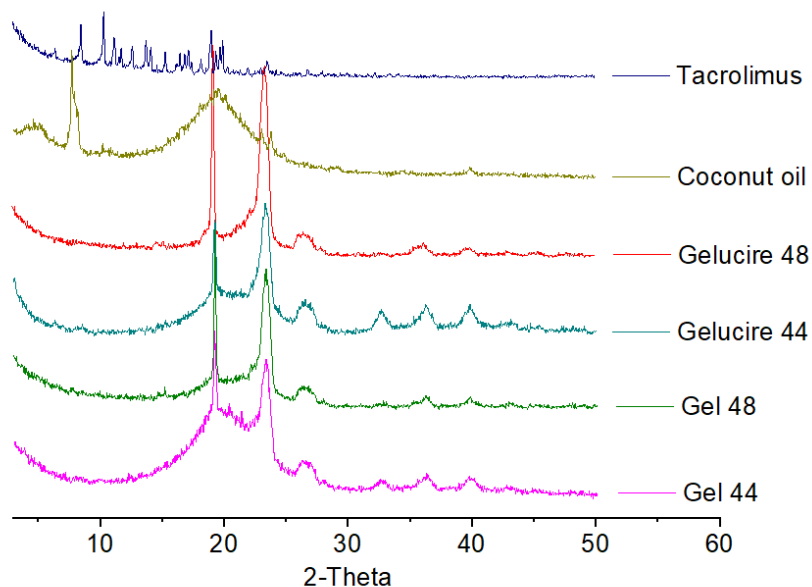

Figure 3.7. X-ray spectra of the drug, the excipients (coconut oil, Gelucire 44 and Gelucire 48) and the formulations (Gel 44 and Gel 48).

The disintegration time was determined following the method described in the European Pharmacopeia (41) to evaluate the time required to disintegrate the suppository formulations. Gel 48 suppositories took a longer than Gel 44 suppositories to disintegrate, which may be attributed to the higher melting points of the material (Table 1). In the same line, when the self-emulsification time was evaluated, Gel 44 showed a faster emulsification time compared to Gel 48 (Table 2.1), which also justifies its shorter disintegration time.

To characterize the formed system, the globule size of both self-emulsifying suppository formulations and the ζ potential of the emulsion droplets were measured (Table 2.1). The mean size of lipid droplets of both formulations was between 1-1.5 μm, and the stability of the system was given by ζ potential of lipid droplets, this being – 14 mV for Gel 44 and – 20 mV for Gel 48, which means that the system formed by Gel 48 was more stable due to its higher charge. Although it is reported in the literature that Gelucire 44/14 forms microemulsions and Gelucire 48/16 forms micellar systems in aqueous media (45, 46), the larger particle sizes obtained in this study may be due to the inclusion of coconut oil as a plasticizer to facilitate the printing process. Moreover, the low polydispersity index of Gel 44 (0.190±0.04) is indicative of a homogeneous monodisperse population, whereas the polydispersity index value for Gel 48 (0.345±0.36) is representative of a more heterogeneous population. Regarding the globule morphology and structure, TEM microphotographs were obtained to

directly visualize the lipid droplets (Figure 3.8), The images show globules with spherical shapes and sizes consistent with the dynamic light scattering measurements.
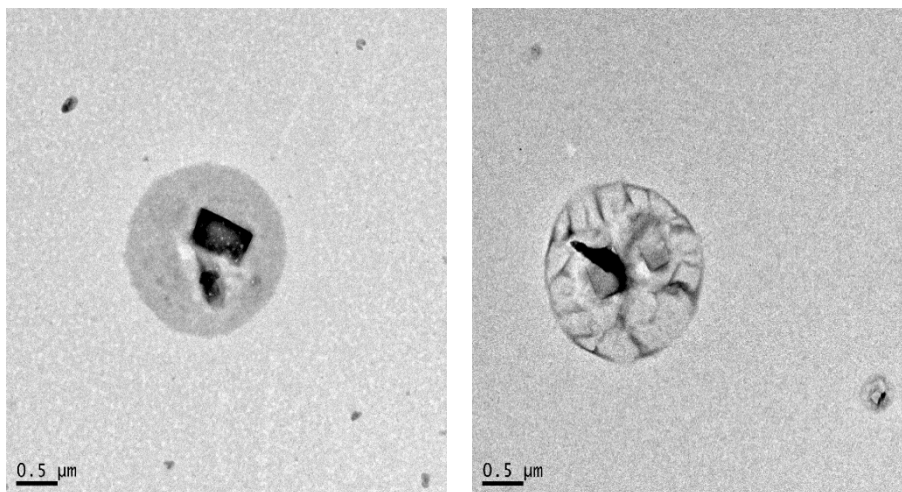

Figure 3.8. Representative TEM microphotographs of lipid droplets formed after emulsification of Gel 48 (right) and Gel 44 (left) fixed with phosphotungstic acid. The black spots are traces of staining with phosphotungstic.

The drug dissolution profiles of both the suppositories are shown in Figure 3.9. Gel 48 suppositories released more than 50% of tacrolimus within the first 60 min compared to Gel 44 suppositories, which required 90 min to reach the same percentage of drug released. A $f2$ similarity value of 21 was obtained, which indicates that Gel 44 and Gel 48 suppositories have different drug release profiles ($f2$ values between 50-100 indicate parity). Although Gel 44 showed a faster disintegration and emulsification, a delayed release was observed in comparison to Gel 48. It is hypothesised that the lower hydrophilic-lipophilic balance of Gel 44 (HLB=10.4) compared to Gel 48 (HLB=11.2) indicates a slightly higher lipophilicity of Gel 44, what would increase the retention of tacrolimus (lipophilic drug) and explain the longer duration of drug release (47). The experimental data was fitted to the Gompertz growth model (equation 1), because it is a sigmoid function which could describe the lag time and the slow growth at the beginning of a time period. The high correlation coefficients obtained with this fitting support the choice of this model, $(R^2) = 0.9996$ for Gel 48 and $(R^2) = 0.9747$ for Gel 44.
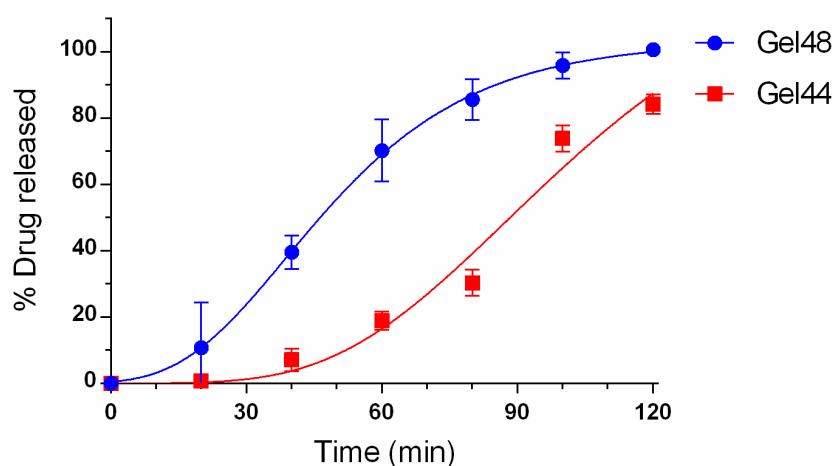
Figure 3.9. Drug release profile of Gel 44 and Gel 48 suppositories in phosphate buffer pH 8.

One important aspect of suppository formulations is that the suppository base materials should melt at body temperature to release drugs to the site of application (48, 49). Conventional rectal suppositories are formulated using polyethylene glycol (PEG), which possess various issues including a relatively high melting point, an inability for loaded drugs to absorb rapidly into mucous membranes and potential rectal irritation (50). SMEDDS could be used to overcome these problems. A study that compared SMEDDS suppositories with commonly used PEG suppositories found that SMEDDS suppositories showed a narrower melting point than PEG suppositories, which is important for maintaining the suppository shape during storage and insertion into the rectum. Moreover, SMEDDS suppositories released a lower amount of drug in the initial phase than PEG suppositories, displaying a more prolonged release of the drug in the rectum (51). The mixture of lipid excipients that have been selected in this study to prepare the suppositories results in a self-emulsifying system in which the tacrolimus is solubilized in the small droplets of oil (52). The materials displayed adequate viscosity for printing at low temperatures, which can make this formulation adequate for thermolabile compounds. Moreover, the rapid solidification of the suppositories precludes the need for post manufacturing time to allow the formulations to harden.

Previous studies have demonstrated the potential of 3DP to tailor oral medicines to individual patients (53-56), and the feasibility of this technology to prepare tailored medicines in a hospital setting (32). In the present study, we have investigated the potential of SSE 3DP for the development of customised lipid-based suppositories with different sizes and containing a specific dose of the drug. Although Gel 48 suppositories released drug at a faster rate, the better printing properties and better miscibility of Gelucire 44 provided by its lower melting point makes Gel 44 a more suitable formulation. Overall, we have demonstrated that with SSE 3DP it is possible to fabricate suppositories with the selected drug dose in a single step process, without the need for moulds. This approach represents a more rapid and cost-

efficient approach to prepare drug loaded suppositories tailored to each patient´s needs. This is of special interest for drugs with a narrow therapeutic index (57), such as tacrolimus (8), since dose requirements can be markedly different among patients of different age groups, for example, children and the elderly (58), which increases the risk of adverse effects (59).

CONCLUSIONS

This work demonstrates, for the first time, the use of a SSE 3D printer to fabricate self-supported lipid-based suppositories loaded with tacrolimus intended for the treatment of inflammatory bowel disease patients. Different sizes of 3D printed tacrolimus suppositories were produced with precise doses, giving rise to the possibility of manufacturing suppositories tailored to each patient´s needs without the need for moulds. The suppositories printed using combinations of two lipid excipients (Gelucire 44/14 or Gelucire 48/16) and coconut oil exhibited adequate viscosity for printing. The Gelucire 44/14 suppositories had a faster disintegration time but slower drug release rate than the Gelucire 48/16 suppositories. Although the drug release profiles were significantly different, both suppository types released more than 80% of tacrolimus within 120 minutes. The local delivery of precise doses of tacrolimus may reduce the risk of adverse effects without losing the immunosuppressive effect. The unprecedented flexibility of 3DP technologies could provide new manufacturing opportunities to produce personalized dosage forms on-demand.

CONFLIT OF INTEREST

The authors declare no conflit of interest.

REFERENCES

1.   Ng SC, Shi HY, Hamidi N, Underwood FE, Tang W, Benchimol EI, et al. Worldwide incidence and prevalence of inflammatory bowel disease in the 21st century: a systematic review of population-based studies. The Lancet. 2017;390(10114):2769-78.

2.   Kaplan GG. The global burden of IBD: from 2015 to 2025. Nature Reviews Gastroenterology & Hepatology. 2015;12(12):720-7.

3.   Ma C, Battat R, Dulai PS, Parker CE, Sandborn WJ, Feagan BG, et al. Innovations in Oral Therapies for Inflammatory Bowel Disease. Drugs. 2019;79(12):1321-35.

4.   Foppoli A, Maroni A, Moutaharrik S, Melocchi A, Zema L, Palugan L, et al. In vitro and human pharmacoscintigraphic evaluation of an oral 5-ASA delivery system for colonic release. International Journal of Pharmaceutics. 2019;572:118723.

5.   Jaeger SU, Klag T, Hoeger K, Klumpp S, Escher M, Malek N, et al. Tacrolimus Suppositories in Therapy-Resistant Ulcerative Proctitis. Inflammatory Intestinal Diseases. 2018;3(3):116-24.

6.   Smith R, Weekes H, Morgan L, Parkes M, Lee JC. P588 Tacrolimus suppositories: a safe and effective treatment for treatment-refractory proctitis. Journal of Crohn's and Colitis. 2019;13(Supplement_1):S408-S9.

7.   Kreijne JE, Lie MR, Dijkstra G, Löwenberg M, Van Assche GA, West R, et al. 818 - Tacrolimus Suppositories as Induction Therapy for Refractory Ulcerative Proctitis: A Randomized Controlled Trial. Gastroenterology. 2018;154(6):S-169.

8.   Berends SE, Strik AS, Löwenberg M, D'Haens GR, Mathôt RAA. Clinical Pharmacokinetic and Pharmacodynamic Considerations in the Treatment of Ulcerative Colitis. Clinical Pharmacokinetics. 2019;58(1):15-37.

9.   Talley NJ, Abreu MT, Achkar JP, Bernstein CN, Dubinsky MC, Hanauer SB, et al. An evidence-based systematic review on medical therapies for inflammatory bowel disease. Am J Gastroenterol. 2011;106 Suppl 1:S2-25; quiz S6.

10.   van Dieren JM, van Bodegraven AA, Kuipers EJ, Bakker EN, Poen AC, van Dekken H, et al. Local Application of Tacrolimus in Distal Colitis:Feasible and Safe. Inflammatory Bowel Diseases. 2008;15(2):193-8.

11.   Yanagi T, Ushijima K, Koga H, Tomomasa T, Tajiri H, Kunisaki R, et al. Tacrolimus for ulcerative colitis in children: a multicenter survey in Japan. Intest Res. 2019;17(4):476-85.

12.   Lawrance IC, Baird A, Lightower D, Radford-Smith G, Andrews JM, Connor S. Efficacy of Rectal Tacrolimus for Induction Therapy in Patients With Resistant Ulcerative Proctitis. Clin Gastroenterol Hepatol. 2017;15(8):1248-55.

13.   Kairuz TE, Gargiulo D, Bunt C, Garg S. Quality, safety and efficacy in the 'off-label' use of medicines. Curr Drug Saf. 2007;2(1):89-95.

14.   Trenfield SJ, Awad A, Goyanes A, Gaisford S, Basit AW. 3D Printing Pharmaceuticals: Drug Development to Frontline Care. Trends Pharmacol Sci. 2018;39(5):440-51.

15.   Ong JJ, Awad A, Martorana A, Gaisford S, Stoyanov E, Basit AW, et al. 3D printed opioid medicines with alcohol-resistant and abuse-deterrent properties. International Journal of Pharmaceutics. 2020;579:119169.

16.   Melocchi A, Uboldi M, Inverardi N, Briatico-Vangosa F, Baldi F, Pandini S, et al. Expandable drug delivery system for gastric retention based on shape memory polymers: Development via 4D printing and extrusion. International Journal of Pharmaceutics. 2019;571:118700.

17.   Melocchi A, Inverardi N, Uboldi M, Baldi F, Maroni A, Pandini S, et al. Retentive device for intravesical drug delivery based on water-induced shape memory response of poly(vinyl alcohol): design concept and 4D printing feasibility. International journal of pharmaceutics. 2019;559:299-311.

18.   Goyanes A, Wang J, Buanz A, Martínez-Pacheco R, Telford R, Gaisford S, et al. 3D Printing of Medicines: Engineering Novel Oral Devices with Unique Design and Drug Release Characteristics. Mol Pharm. 2015;12(11):4077-84.

19.   Khaled SA, Alexander MR, Irvine DJ, Wildman RD, Wallace MJ, Sharpe S, et al. Extrusion 3D Printing of Paracetamol Tablets from a Single Formulation with Tunable Release Profiles Through Control of Tablet Geometry. AAPS PharmSciTech. 2018;19(8):3403-13.

20.   Infanger S, Haemmerli A, Iliev S, Baier A, Stoyanov E, Quodbach J. Powder bed 3D-printing of highly loaded drug delivery devices with hydroxypropyl cellulose as solid binder. International Journal of Pharmaceutics. 2019;555:198-206.

21.   Goyanes A, Buanz AB, Basit AW, Gaisford S. Fused-filament 3D printing (3DP) for fabrication of tablets. Int J Pharm. 2014;476(1-2):88-92.

22.   Fina F, Goyanes A, Madla CM, Awad A, Trenfield SJ, Kuek JM, et al. 3D printing of drug-loaded gyroid lattices using selective laser sintering. Int J Pharm. 2018;547(1-2):44-52.

23.   Xu X, Robles-Martinez P, Madla CM, Joubert F, Goyanes A, Basit AW, et al. Stereolithography (SLA) 3D printing of an antihypertensive polyprintlet: Case study of an unexpected photopolymer-drug reaction. Additive Manufacturing. 2020;33:101071.

24.   Cui M, Li Y, Wang S, Chai Y, Lou J, Chen F, et al. Exploration and Preparation of a Dose-Flexible Regulation System for Levetiracetam Tablets via Novel Semi-Solid Extrusion Three-Dimensional Printing. J Pharm Sci. 2019;108(2):977-86.

25.   Farto-Vaamonde X, Auriemma G, Aquino RP, Concheiro A, Alvarez-Lorenzo C. Post-manufacture loading of filaments and 3D printed PLA scaffolds with prednisolone and dexamethasone for tissue regeneration applications. Eur J Pharm Biopharm. 2019;141:100-10.

26.   Vithani K, Goyanes A, Jannin V, Basit AW, Gaisford S, Boyd BJ. An Overview of 3D Printing Technologies for Soft Materials and Potential Opportunities for Lipid-based Drug Delivery Systems. Pharm Res. 2018;36(1):4.

27.   Tagami T, Ando M, Nagata N, Goto E, Yoshimura N, Takeuchi T, et al. Fabrication of Naftopidil-Loaded Tablets Using a Semisolid Extrusion-Type 3D Printer and the Characteristics of the Printed Hydrogel and Resulting Tablets. Journal of Pharmaceutical Sciences. 2019;108(2):907-13.

28.   Firth J, Basit AW, Gaisford S. The Role of Semi-Solid Extrusion Printing in Clinical Practice. In: Basit AW, Gaisford S, editors. 3D Printing of Pharmaceuticals: Springer International Publishing; 2018. p. 133-51.

29.   Goyanes A, Det-Amornrat U, Wang J, Basit AW, Gaisford S. 3D scanning and 3D printing as innovative technologies for fabricating personalized topical drug delivery systems. J Control Release. 2016;234:41-8.

30.   Khaled SA, Burley JC, Alexander MR, Yang J, Roberts CJ. 3D printing of five-in-one dose combination polypill with defined immediate and sustained release profiles. J Control Release. 2015;217:308-14.

31.   Khaled SA, Alexander MR, Wildman RD, Wallace MJ, Sharpe S, Yoo J, et al. 3D extrusion printing of high drug loading immediate release paracetamol tablets. Int J Pharm. 2018;538(1–2):223-30.

32.   Goyanes A, Madla CM, Umerji A, Piñeiro GD, Montero JMG, Diaz MJL, et al. Automated therapy preparation of isoleucine formulations using 3D printing for the treatment of MSUD: first single-centre, prospective, crossover study in patients. International Journal of Pharmaceutics. 2019:118497.

33.   Siepmann J, Faham A, Clas S-D, Boyd BJ, Jannin V, Bernkop-Schnürch A, et al. Lipids and polymers in pharmaceutical technology: Lifelong companions. International Journal of Pharmaceutics. 2019;558:128-42.

34.   Kang BK, Lee JS, Chon SK, Jeong SY, Yuk SH, Khang G, et al. Development of self-microemulsifying drug delivery systems (SMEDDS) for oral bioavailability enhancement of simvastatin in beagle dogs. Int J Pharm. 2004;274(1-2):65-73.

35.   Vithani K, Goyanes A, Jannin V, Basit AW, Gaisford S, Boyd BJ. A Proof of Concept for 3D Printing of Solid Lipid-Based Formulations of Poorly Water-Soluble Drugs to Control Formulation Dispersion Kinetics. Pharm Res. 2019;36(7):102.

36.   Testa A, Castiglione F, Nardone OM, Colombo GL. Adherence in ulcerative colitis: an overview. Patient Prefer Adherence. 2017;11:297-303.

37.   Sun Y, Ruan X, Li H, Kathuria H, Du G, Kang L. Fabrication of non-dissolving analgesic suppositories using 3D printed moulds. Int J Pharm. 2016;513(1):717-24.

38.   Tagami T, Hayashi N, Sakai N, Ozeki T. 3D printing of unique water-soluble polymer-based suppository shell for controlled drug release. Int J Pharm. 2019;568:118494.

39.   Persaud S, Eid S, Swiderski N, Serris I, Cho H. Preparations of Rectal Suppositories Containing Artesunate. Pharmaceutics. 2020;12(3).

40.   Patel P, Patel H, Panchal S, Mehta T. Formulation strategies for drug delivery of tacrolimus: An overview. Int J Pharm Investig. 2012;2(4):169-75.

41.   European Pharmacopoeia 8.0; Chapter 2.9.2; Disintegration of suppositories and pessaries.

42.   Moore JW, Flanner HH. Mathematical Comparison of Dissolution Profiles. Pharmaceutical Technology. 1996;20(6):64-75.

43.   Shah VP, Tsong Y, Sathe P, Liu JP. In vitro dissolution profile comparison--statistics and analysis of the similarity factor, f2. Pharm Res. 1998;15(6):889-96.

44.   Costa P, Manuel J, Lobo S. Modeling and comparison of dissolution profiles. Eur J Pharm Sci. 2001;13(2):123-33.

45.   Gattefossé. Gelucire 48/16 2020 [Available from: https://www.gattefosse.com/notre-histoire/pharmaceuticals-products/gelucire-4816/.

46.   Gattefossé. Gelucire 44/14 2020 [Available from: https://www.gattefosse.com/pharmaceuticals-products/gelucire-4414.

47.   Ali HH, Hussein AA. Oral nanoemulsions of candesartan cilexetil: formulation, characterization and in vitro drug release studies. AAPS Open. 2017;3(1):4.

48.   Yong CS, Xuan JJ, Paek SH, Oh YK, Woo JS, Lee MH, et al. Enhanced anti-tumor activity and alleviated hepatotoxicity of clotrimazole-loaded suppository using poloxamer-propylene glycol gel. Int J Pharm. 2006;321(1-2):56-61.

49.   Yarnykh T, Tolochko E, Chushenko V. Drug synthesis methods and manufacturing technology: Studying an assortment of suppository bases (Review). Pharmaceutical Chemistry Journal. 2011;44.

50.   Watanabe K, Yakou S, Takayama K, Isowa K, Nagai T. Rectal absorption and mucosal irritation of rectal gels containing buprenorphine hydrochloride prepared with water-soluble dietary fibers, xanthan gum and locust bean gum. Journal of Controlled Release. 1996;38(1):29-37.

51.   Gugulothu D, Pathak S, Suryavanshi S, Sharma S, Patravale V. Self-microemulsifiyng suppository formulation of β-artemether. AAPS PharmSciTech. 2010;11(3):1179-84.

52.   Huo T, Tao C, Zhang M, Liu Q, Lin B, Liu Z, et al. Preparation and comparison of tacrolimus-loaded solid dispersion and self-microemulsifying drug delivery system by in vitro/in vivo evaluation. Eur J Pharm Sci. 2018;114:74-83.

53.   Goyanes A, Allahham N, Trenfield SJ, Stoyanov E, Gaisford S, Basit AW. Direct powder extrusion 3D printing: Fabrication of drug products using a novel single-step process. Int J Pharm. 2019;567:118471.

54.   Xu X, Zhao J, Wang M, Wang L, Yang J. 3D Printed Polyvinyl Alcohol Tablets with Multiple Release Profiles. Scientific Reports. 2019;9(1):12487.

55.   Siyawamwaya M, du Toit LC, Kumar P, Choonara YE, Kondiah PPPD, Pillay V. 3D printed, controlled release, tritherapeutic tablet matrix for advanced anti-HIV-1 drug delivery. European Journal of Pharmaceutics and Biopharmaceutics. 2019;138:99-110.

56.   Awad A, Yao A, Trenfield SJ, Goyanes A, Gaisford S, Basit AW. 3D Printed Tablets (Printlets) with Braille and Moon Patterns for Visually Impaired Patients. Pharmaceutics. 2020;12(2):172.

57.   Din Fu, Choi JY, Kim DW, Mustapha O, Kim DS, Thapa RK, et al. Irinotecan-encapsulated double-reverse thermosensitive nanocarrier system for rectal administration. Drug Delivery. 2017;24(1):502-10.

58.   Breitkreutz J, Boos J. Paediatric and geriatric drug delivery. Expert Opin Drug Deliv. 2007;4(1):37-45.

59.   Florence AT, Lee VH. Personalised medicines: more tailored drugs, more tailored delivery. Int J Pharm. 2011;415(1-2):29-33.

Chapter IV.

Preclinical PET/CT evaluation of 3D printed tacrolimus rectal devices for the treatment of experimental Inflammatory Bowel Disease

CHAPTER IV

ABSTRACT

In this study, semisolid extrusion 3-dimensional printing technology was combined with preclinical medical imaging to prepare small suppositories loaded with tacrolimus and evaluate the feasibility of this approach to treat experimental inflammatory bowel disease in an animal model. Treatment with tacrolimus suppositories is often employed to treat patients with medication-resistant IBD, but the efficacy of this therapy has not yet been tested in animal models of the disease. Lipid based suppositories composed of Gelucire 44/14 and coconut oil were prepared with a suitable size for their rectal administration to rats. PET/CT scans were performed over time to assess disease activity in the animal model of TNBS (2, 4, 6-trinitrobenzenesulfonic acid) induced colitis. Maximum standardized uptake values (SUV_{max}), body weight changes and histological evaluation were used as inflammatory indices to measure the efficacy of the treatment. SUV_{max} values increased after induction of colitis, however, after the beginning of the treatment on day 3, a statistically significant decrease was observed on days 7 and 10 in transverse and descending colon sections compared to non-treated animals. Histological analysis using Nancy index as a reference score confirmed the remission of the disease. Moreover, statistical analysis showed a correlation (R^2 = 71.48 %) between SUV_{max} values and weight changes throughout the time. Overall, this study demonstrates the effectivity of the tacrolimus suppositories, the suitability of 3DP to prepare formulations for preclinical studies and highlights the usefulness of non-invasive PET/CT imaging to evaluate new therapies in the preclinical area

Keywords: 3D printing, PET/CT, tacrolimus, self-emulsifying system, suppository, rat.

149

INTRODUCTION

Inflammatory bowel disease (IBD) is a group of chronic disorders of unknown aetiology that cause prolonged inflammation of the gastrointestinal (GI) tract. The two main types of IBD are Crohn´s disease (CD) and ulcerative colitis (UC), being highly heterogenic with regard to activity, site and behaviour of the disease (1). Although the etiology of IBD remains to be fully elucidated, an interplay of luminal microflora, external environment and disturbances in the immune responses are hypothesized to trigger the onset of the disease in a genetically susceptible host (2). Conventional treatment of IBD is based on the topical and systemic use of 5-aminosalicylic acid, azathioprine and steroids. However, this first line of treatment does not always achieve remission of the disease. When this happens, biological treatments such as infliximab, tocilizumab or ustekinumab are used (3, 4). In cases where even these commercialized drugs are not sufficient to treat symptoms, pharmaceutical compounding is the last alternative to treat these patients (5).

Tacrolimus, a macrolide antibiotic with potent immunosuppressive properties (6), represent another treatment option for medication-resistant IBD, which can be administered orally, intravenously or rectally (7). This drug induces a rapid clinical response and mucosal healing in hospitalized patients with steroid-refractory UC and its use is also supported in CD refractory to conventional therapies (8). However, administration of oral or intravenous tacrolimus is related to toxicity and systemic adverse effects such as hypertension and renal impairment, limiting its use. These adverse effects are highly related to the trough serum levels of tacrolimus, which should be monitored (9). With the aim of reducing systemic side effects, topical therapy is often employed (10), mainly in the form of suppositories, but enemas and ointments are also used. Each type of formulation can reach different areas of the colon. Depending on the volume administered, enemas can reach the splenic flexure, while suppositories are more intended for local drug release into the rectum (11).

This rectal route of administration presents several advantages, such as the possibility to locally treat some conditions and the minimization of the first-pass effect if the drug is administered to the lower part of the rectum. In the case of tacrolimus therapy, although tacrolimus is absorbed through the rectal mucosa, the systemic levels of the drug are low and the number of adverse events is limited (12). However, tacrolimus suppositories are not commercially available, so they are often compounded in hospital pharmacy settings (6). Even though this therapy achieves excellent results in human therapy, to date there are no preclinical studies in animal models of the disease that investigate and demonstrate the efficacy of topical IBD therapy with tacrolimus suppositories.

Preclinical animal models of colitis, such as the TNBS (2, 4, 6 - trinitrobenzenesulfonic acid) (13) and dextran sodium sulfate (DSS) (14) induced colitis models could be used to demonstrate efficacy of treatments and the ability of pharmaceutical products to reach the area of interest for their therapeutic activity (15). The beneficial effect of tacrolimus in an animal model of DSS colitis was first proposed in 1995 (16). Since then, other studies have reported the therapeutic potential of tacrolimus in the treatment of IBD. For instance, a study using

tacrolimus entrapped into nanoparticles found that a more beneficial effect is obtained when the drug was subcutaneously, rather than orally, administered (17). Another study in a mouse DSS model showed that intrarectal administration of tacrolimus exerts a therapeutic effect through induction of apoptosis in activated macrophages (18). However, as mentioned above, there are still no studies in animal models of colitis that demonstrate the therapeutic activity of tacrolimus suppositories. Since this therapy is gaining more attention in clinical practice, a study of these characteristics would be of great interest.

Nevertheless, as with human suppositories, these formulations are not commercially available for preclinical studies, so researchers have to prepare them for each study. If suppositories are to be administered to small animals as rodents, it is necessary to prepare them in an appropriate size and shape. To avoid the need for a mould specifically designed to meet these requirements, three-dimensional printing (3DP) technology can offer an alternative for the manufacture of small batches of suppositories. This additive manufacturing technology enables the production of small devices with a size and dose adapted to the needs of the preclinical study (19). In particular, semisolid extrusion (SSE) 3DP technology is based on the deposition of semisolid materials (gel or pastes) in sequential layers through a syringe-based tool-head nozzle to create the 3D object, and it is highly relevant to print objects using soft materials (20-22). SSE was the first 3DP technology used for the preparation of personalised dose printlets (3D printed tablets) in a hospital setting for the treatment of a rare metabolic disease (23). Moreover, SSE was also used for printing lipid-based formulations, as solid self-microemulsifying drug delivery systems (S-SMEDDS) intended for oral administration (24). Self-emulsifying drug delivery systems (SEDDS) and self-microemulsifying drug delivery systems (S-SMEDDS) are lipid-based isotropic mixtures of oils, surfactants and co-surfactants that form kinetically stable oil-in-water (O/W) emulsions under mild agitation (25). This approach is especially useful for enhancing drug solubility of poorly water-soluble drugs, which are solubilized in the small drops of oil (26). The low oral bioavailability of tacrolimus and its poor water solubility made it a suitable candidate for inclusion in a 3D printed lipid-based suppository (27).

Medical imaging techniques commonly used in clinical practice (28) also represent a useful tool for noninvasively evaluating disease progression before and after treatment administration in preclinical animal studies (15, 29). In particular, PET/CT (Positron emission tomography/Computer Tomography) technology, allows repeated measurements using the same animal, thus reducing the number of animals needed (30), and has proven useful for the assessment of experimental colitis in rats (13, 28). Moreover, the maximum standardized uptake value (SUV_{max}), a common biomarker used in current clinical practice for the assessment of inflammatory processes, can be also used for evaluating disease progression and treatment response in the animal model of the IBD (31, 32).The aim of this study was to evaluate the therapeutic activity of 3D printed self-emulsifying suppositories (SES) loaded with tacrolimus for the treatment of experimental IBD in a previously developed and validated TNBS colitis animal model (13). Moreover, the *in vivo* disintegration time and distribution of the formulations was studied using barium sulphate as a contrast agent for computed

tomography (CT) imaging. Apart from using PET/CT imaging for monitoring disease progression and therapeutic response in the animal model, histological analyses were carried out to confirm the results obtained from the quantification of SUV_{max} values from PET images.

MATERIALS AND METHODS

Materials

Tacrolimus was purchased from Guinama S.L.U., Spain. Coconut oil was obtained from Acofarma, Spain. Barium sulphate Reagent Grade, 99%, was obtained from Honeywell, UK. Gelucire 44/14 was kindly donated by Gattefosse España SA, Spain. TNBS (2, 4, 6 - trinitrobenzenesulfonic acid) was purchased from Sigma-Aldrich Company Ltd, Madrid, Spain. Ethanol absolute was obtained from VWR International S.A.S., France. NaCl 0.9% B. Braun was purchased from Braun Medical Inc. Barcelona, Spain. Ultravist ® 300 mg / mL was purchased from Bayer Hispania S.L. Barcelona, Spain.

Methods

3D design

The software 123D Design (Autodesk Inc., USA) was used to design the templates of the suppositories, size 2.7mm diameter × 8.35mm height (Figure 4.1).
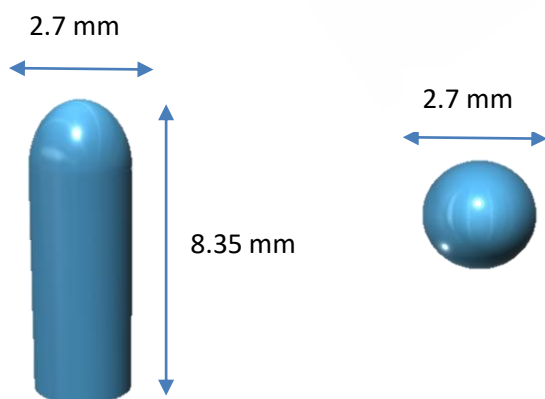

Figure 4.1. 3D model of the suppositories from different angles.

Semisolid extrusion 3D printing

The mixture of lipid excipients and drug composed of 79.55% of Gelucire 44/14, 19.55% of coconut oil and 0.9% of tacrolimus was mixed in a glass beaker and placed on a heating plate. The tacrolimus dose of 2 mg/kg body weight was selected according to published literature (33). The mixture was heated up to the melting point of the mixture (42 °C) under magnetic stirring until the complete solubilization of the drug in the lipid excipients. The mass was immediately transferred to a 5 mL extrusion syringe with a tapered extrusion tip (0.58 mm orifice) and allowed to solidify at room temperature. Then, the syringe was placed into the pharmaceutical 3D printer with the semisolid extrusion tool (M3DIMAKER, FabRx Ltd, UK). Using Ultimaker Cura software (v 15.04.6, Ultimaker), suppositories were designed as follows: 0.5mm layer height; 2.4mm shell thickness; 25 mm/s flow speed; 1.2 mm nozzle size, and printed in horizontal position. Finally, 3D printed suppositories were allowed to solidify at room temperature and subsequently stored in refrigeration at 4 °C.

Characterization of the 3D printed suppositories

Drug loading

The content uniformity of tacrolimus in the 3DP suppositories was determined in triplicate using high performance liquid chromatography (HPLC). Each suppository of approximately 50 mg was dissolved into 50 mL of ethanol absolute at room temperature with magnetic stirring to form a clear transparent solution. The amount of drug in solution was determined using an Agilent 1260 series HPLC system (Agilent Technologies, USA) equipped with Diode Array Detector HS, a solvent delivery quaternary pump system, maximum pressure of 400 bar and an autosampler with thermostat. The software model OpenLAB CDS 3D UV (PDA) was used for the data processing. The analysis was performed in an isocratic method. The column used was a Poroshell 120, EC-C18 (4,6x100 mm 4 μm) and at a temperature of 60ºC. The mobile phase was water-acetonitrile (35:65 v/v) using a flow rate of 1.5 mL.min-1. A wavelength of 210 nm was employed for the quantification of tacrolimus. The volume of the injected sample was 10 μL and the retention time was 3.3 minutes. Each sample was assayed in triplicate.

In vitro drug release

In order to obtain the *in vitro* drug release profiles, the 3DP suppositories were placed into glass vials with 10 mL phosphate buffer (0.1M) pH 8 under controlled conditions of agitation (100 rpm) and temperature (37 °C) using an orbital shaker (Heidolph Unimax 1010) to simulate conditions of the colon lumen. At appropriate time intervals, 1 mL aliquots were withdrawn and 1 mL of fresh medium was added to the vials. To solubilize the tacrolimus that could be trapped inside the lipid droplets, 0.5 mL of ethanol absolute were added to the

aliquots. Then, the samples were centrifuged for 30 min at 12500 rpm and the supernatant was collected. The samples were analysed by HPLC as described earlier.

Tacrolimus release profile from suppositories was fitted to the Gompertz growth model (equation (1))

$$\% \, released = \% \max \left(\frac{\%_{min}}{\%_{max}} \right)^{e^{-kt}} \tag{1}$$

where %max is the maximum percentage of drug released, %min is the minimum percentage of drug released and k is a constant. Gompertz growth model was fitted to drug release profile by non-linear regression analysis using the program GraphPad Prism (version 7.0). The Gompertz growth model is a logistic function useful for describing S-shaped curves composed of an induction phase, a linear increase and final saturation or depletion process.

In vivo disintegration time of 3D printed suppositories

The *in vivo* disintegration time of the 3D printed suppositories was investigated by CT imaging. Barium sulphate, used as a contrast agent, was dissolved in the mixture of lipid excipients and drug (30% w/w) and the printing process was carried out as described previously. The 3D printed suppositories were inserted intrarectally in the rats under anaesthesia (2% isoflurane) and CT scans were performed immediately after administration and 20 and 50 min post-administration.

Inflammatory Bowel Disease (IBD) animal model

These studies were carried out on male Sprague-Dawley rats (average weight of 250±25g) supplied by the animal facility at the University of Santiago de Compostela. During the experiments, animals were kept in individual cages under controlled temperature (22±1ºC) and humidity (60±5%) conditions, with day-night cycles regulated by artificial light (12/12 hours) and fed *ad libitum*. All animal experiments complied the ARRIVE guidelines (34) and were carried out in accordance with the Spanish and European Union (UE) directive for animal experiments RD53/2013 and 2010/63/EU. Experiments were approved by the University of Santiago de Compostela (USC) Bioethics Comitte, (Ref. 15007AE/12/FUN01FARM03/MRLF1), Xunta de Galicia. Experiments were performed at the Research Imaging Unit (UNIME) of the Health Research Institute of Santiago de Compostela (IDIS) (REGA number: ES1507802928 01) with the authorization of the research center management.

The TNBS-induced IBD animal model was obtained following the method previously described by Morris *et al.* (35). All animals were fasted for 18 h before rectal administration of TNBS in a dose of 50 mg/kg body weight dissolved in ethanol 50% (v/v), through a

catheter inserted rectally into the colon until reaching 8 cm proximal to the anus, under isoflurane anaesthesia (2%). Then, they were kept in a vertical position for 1 min to prevent leakage of the intracolonic instillation. Finally, animals were returned to their cages with free access to food and water

Experimental design

Assessment of the efficacy of tacrolimus treatment

Tacrolimus suppositories were inserted daily into the rectum of 6 rats at a dose of 2 mg/kg under isoflurane anaesthesia (2 %). The treatment was started 3 days after induction of colitis and was administered until day 15, when the animals were sacrificed. [^{18}F]FDG PET/CT scans were carried out before the IBD induction (basal condition) and 1, 3, 7, 10, 13 and 15 days post-TNBS administration and all the animals were daily weighted. Data from the control group were extracted from a previous work of this group (13), which were obtained following the same protocol as in the present study.

PET/CT acquisition and evaluation

PET/CT images were acquired using an Albira PET/CT Preclinical Imaging System (Bruker Biospin, Woodbridge, Connecticut, United States). The PET subsystem comprises three rings of eight compact modules based on monolithic crystals coupled to multi-anode photomultiplier tubes (MAPMTs), forming an octagon with an axial FOV of 8x14.8 cm (transaxial and axial directions respectively). This subsystem generates PET images with spatial resolution of 1.2 mm and a sensitivity of 10%. The CT subsystem consists of a microfocus x-ray tube of 50 kVp, a CsI scintillator 2D pixelated flat panel detector and a FOV of 5.2x5.2 cm, generating images of 90 µm spatial resolution.

The animals were anesthetized with 2% isoflurane until they were unconscious and 12±1 MBq of [^{18}F]FDG were injected in the tail vein of each animal. After 40 min, 2 mL of Iopromide Ultravist® 300 mg / mL (CT contrast agent) was administered intrarectally via a catheter inserted 8 cm proximal to the anus under isoflurane anaesthesia. Then, PET/CT static acquisitions were performed, consisting of 20 min PET scan followed by 20 min CT scan. PET images were reconstructed using the maximum likelihood expectation maximization (MLEM) algorithm with 12 iterations and image pixel size of $0.4{\times}0.4{\times}0.4$ mm^3, including scatter and random coincidences and no attenuation correction. The CT acquisition parameters were 35 kV for a tube current of 200 µA with 250 projections per bed. The FOV of PET scan focused from the upper part of the lungs to the lower extremities of the animal and the FOV of CT scan was focused on the abdominal region.

All images were analyzed using AMIDE software (amide.sourceforge.net). Fused [^{18}F]FDG PET/CT images were used to define three different regions of the rat colon

(ascending, transverse and descending regions). Then, quantitative analysis was carried out by using circularly delineated Regions of Interest (ROIs) on CT images following longitudinal colon sections at ascending, transverse and descending regions (Figure 4.5). The cylindrical ROIs dimensions ranged from 5 mm to 15 mm in diameter (fitting to the diameter of the colon section) and 1 mm in length. Subsequently, the ROIs were transferred to PET images in order to calculate the maximum [18F]FDG uptake value. Finally, Standardized Uptake Value (SUV_{max}) was calculated as the maximum [18F]FDG uptake value normalized by the injected activity and the body weight of the animal. The injected [18F]FDG activity was estimated by subtracting the extravasated activity in the tail.

Furthermore, Mean Rat Recovering Time (MRRT) was calculated using an equation similar to that used to calculate MRT (Mean Residence Time) in noncompartmental pharmacokinetic analysis. Like MRT, MRRT represents the average time it takes for a rat to regain the baseline SUVmax values, and therefore helps interpret the effect of the drugs in the colon. MRRT was calculated using the following equation:

$$MRRT = \frac{\int_0^\infty tSUV_{max}(t)dt}{\int_0^\infty SUV_{max}(t)dt} = \frac{AUMC}{AUC}$$

Where AUC is the area under the curve SUVmax versus time, and AUMC the area under the first moment curve SUVmax*time versus time.

Statistical analysis was carried out using a two-way analysis of the variance (ANOVA) including as factors time after induction of TNBS colitis and treatment. The data for non-treated animals were obtained from the previous work of this group (13) to compare the previous results with those obtained in the present study for animals treated with tacrolimus. Furthermore, Sidak's multiple comparisons test was carried out for comparing SUV_{max} values over time.

Macroscopic evaluation and histopathology

The animals were sacrificed by CO_2 inhalation (60-70%) in a euthanasia chamber on day 15 post-TNBS administration. Colons were removed, macroscopically examined and subsequently photographed. Afterwards, they were individually fixed in 10% formalin and dehydrated, paraffin embedded, sectioned in slices with 4 μm thickness and stained with H&E (haematoxylin and eosin). The samples were blindly evaluated by a digestive pathologist using a Zeiss® microscope.

Nancy histological index was used as a reference score for the histological disease activity (36, 37). The activity was scored in five grades as follows: (Grade 4) - Ulceration of colonic mucosa with inflamed granulation tissue. (Grade 3) - Presence of multiple clusters of neutrophils in lamina propria and epithelium and the acute inflammatory cells infiltrate is moderate to severe. (Grade 2) - Presence of few neutrophils in lamina propria and in epithelium and mild acute inflammatory cells infiltrate. (Grade 1) - Chronic inflammatory infiltrate with no acute inflammatory infiltrate. (Grade 0) - No increase in chronic inflammatory cell number or absence of histological significant disease.

Statistical analysis was carried out using the Mann-Whitney nonparametric test to evaluate the differences between Nancy scores obtained in the ascending, transverse and descending regions of tacrolimus group and non-treated group.

RESULTS AND DISCUSION

Characterization of 3D printed suppositories

Currently, tacrolimus suppositories are being widely used in clinical practice to treat patients with IBD refractory to other therapies, although there is no commercialized formulation yet. However, this formulation lacks preclinical animal studies demonstrating its efficacy. For this reason, in the study herein we have used semisolid extrusion 3DP to prepare 3D printed suppositories loaded with the drug tacrolimus to test its efficacy in the treatment of experimental colitis using a TNBS rat model. This technology enabled the preparation of small batches of suppositories for daily administration to rats in a single step process and without the need for suppository moulds adapted to small animals. The printed suppositories had an acceptable consistency for normal handing and were well-defined. No material slumping was observed during the printing process, although it was not necessary to use of a refrigerated build plate to help solidify the printed layers. During the printing process, the syringe temperature was set at 42 ºC being carefully controlled to avoid clogging of the nozzle by solidified material. The suppositories were printed horizontally and the printing time for each was 30s (Figure 4.2). The mean weight of the 3D printed suppositories was 54.5 ±4.2 mg. The final drug loading of the suppositories was 0.51±0.04 mg (theoretical amount was 0.50±0.02 mg), suggesting that drug did not undergo any degradation either during the mixture preparation or printing process.

Figure 4.2. 3D printed suppository in horizontal position.

Dissolution data is shown in Figure 4.3. The fitting of the experimental data to Equation (1) yielded a high correlation coefficient (R^2) = 0.9927. The maximum percentage of drug released was 99.80±2.43 and the minimum 4.41E-08±3.29E-07, with a k value of 0.065±0.007. The drug release from the suppositories showed a lag time of 15.5 min that could be explained by the time required for the disaggregation of the suppository and the beginning of emulsion formation. Afterwards, there was a continuous release of the drug with more than 50% of tacrolimus released within the first hour, achieving 100% release of the drug at 90 min. The complete release of the drug from the formulation corresponds to the asymptotic part of the curve.
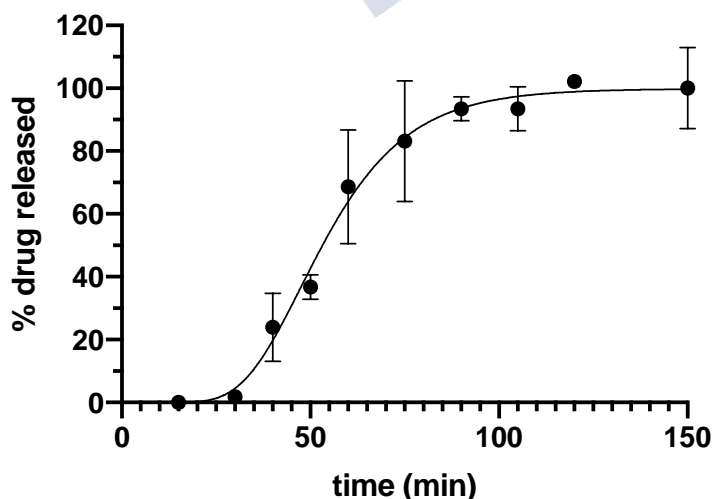

Figure 4.3. Drug release profile of Gel 44 suppositories in phosphate buffer pH 8.

The *in vivo* disintegration time of the 3D printed suppositories with barium sulphate was evaluated by inserting the suppository in the rectum of the animal under isoflurane anaesthesia. CT images showed that 20 min post-administration the formulation is still in the colon, whereas 50 min post-administration the suppository is no longer observed (Figure 4.4).
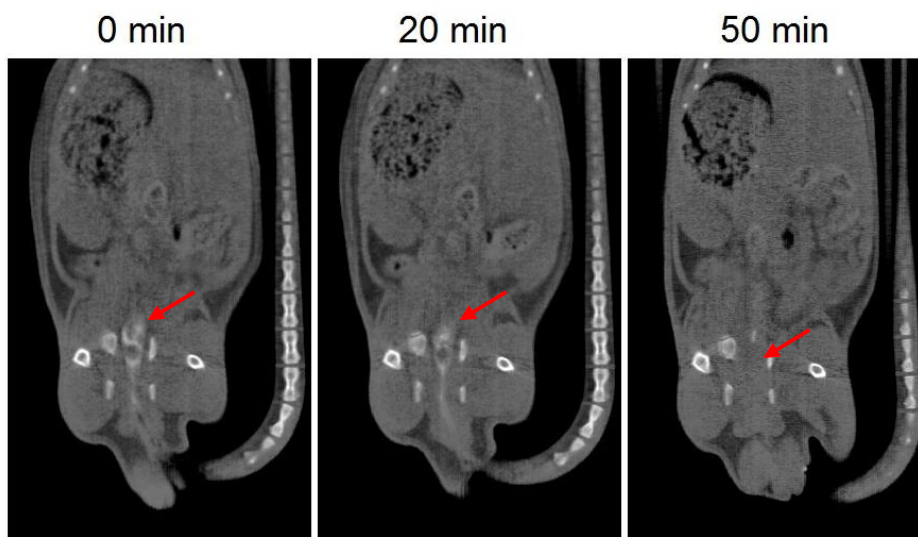

Figure 4.4. CT images of 3D printed suppositories with barium sulphate. The red arrow indicates the location of the suppository (white colour).

Assessment of the efficacy of tacrolimus treatment by PET/CT imaging and histopathological analysis

[18F]FDG PET/CT studies were conducted to assess the feasibility of treating experimental IBD with 3D printed suppositories loaded with tacrolimus. PET images were quantified in terms of SUVmax values, which are measures of relative [18F]FDG tissue uptake, providing data on the evolution of the disease throughout the days. Moreover, CT imaging allows anatomic localization of the colon area through the rectal administration of 1 mL of Iopromide (Ultravist 300 mg / mL), a contrast agent that facilitates the delineation of ROIs in fused PET/CT images (Figure 4.5). The administration of the suppositories and the performance of the [18F]FDG PET/CT studies were separated in time to avoid problems with the release of the drug.
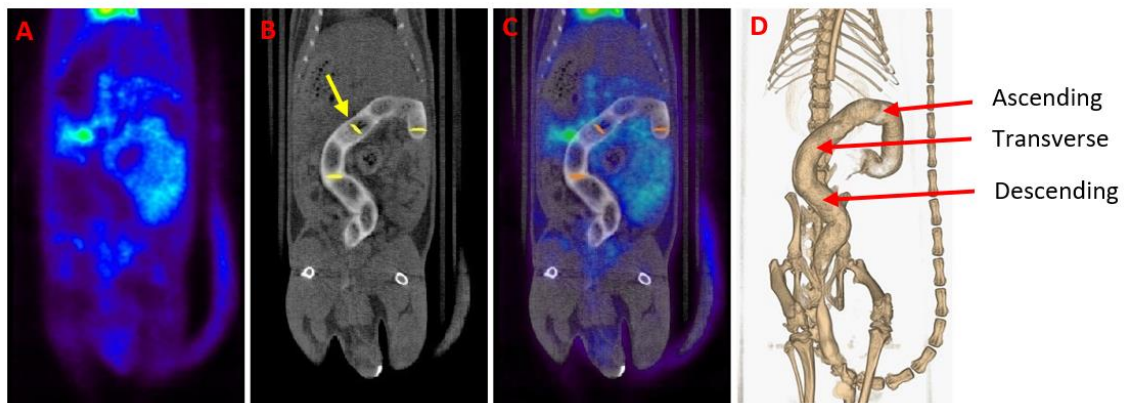
Figure 4.5. (A) Gastrointestinal PET image of a healthy animal. (B) CT scan of the same animal. A contrast agent was used for enhancing contrast in the colon of the animal (white colour). The yellow arrow indicates one of the circularly delineated Regions of Interest (ROIs). (C) [^{18}F]FDG PET/CT image obtained by the fusion of (A) and (B) images. Notice the normal [^{18}F]FDG uptake in the heart, bladder and kidneys. (D) Three-dimensional colon reconstruction from CT images with the three colonic sections indicated by the red arrow (ascending, transverse and descending).

SUV_{max} values of non-treated IBD animals were extracted from our previous work (13) and compared with the SUV_{max} values of IBD animals treated with the 3D printed tacrolimus suppositories. Figure 4.6 shows separately the SUV_{max} values obtained for ascending, transverse and descending colon sections of treated and non-treated animals. The effect of rectally administered tacrolimus begins to be noticed from the seventh day. The highest remission of inflammation was reached on days 10 and 13 mainly in the transverse and descending colon, with statistically significant differences between the treated and non-treated groups (13).
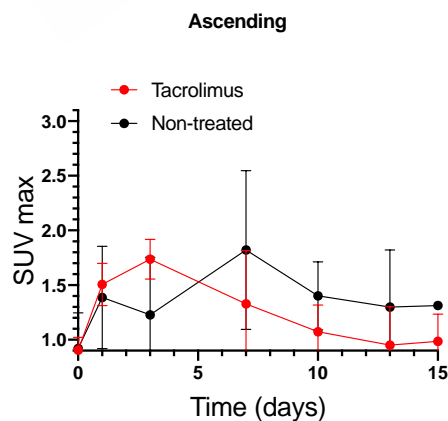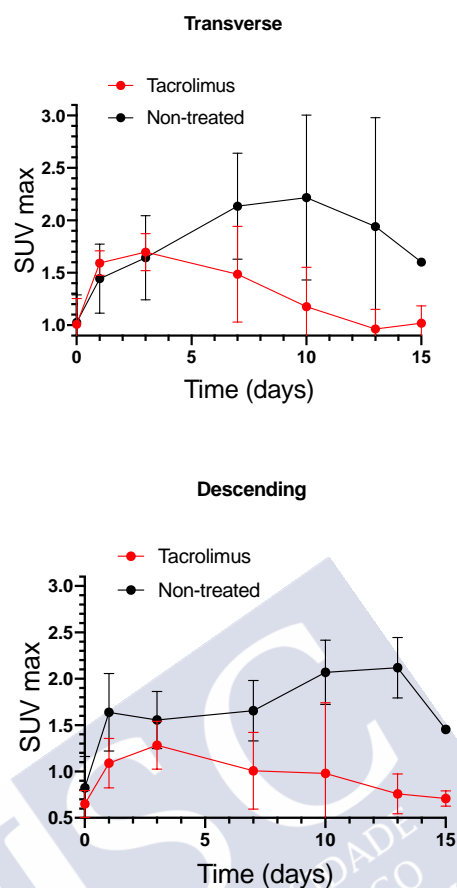
Figure 4.6. Longitudinal SUV$_{max}$ values for ascending, transverse and descending colonic segments over time for non-treated rats and animals treated with the 3D printed tacrolimus suppositories.
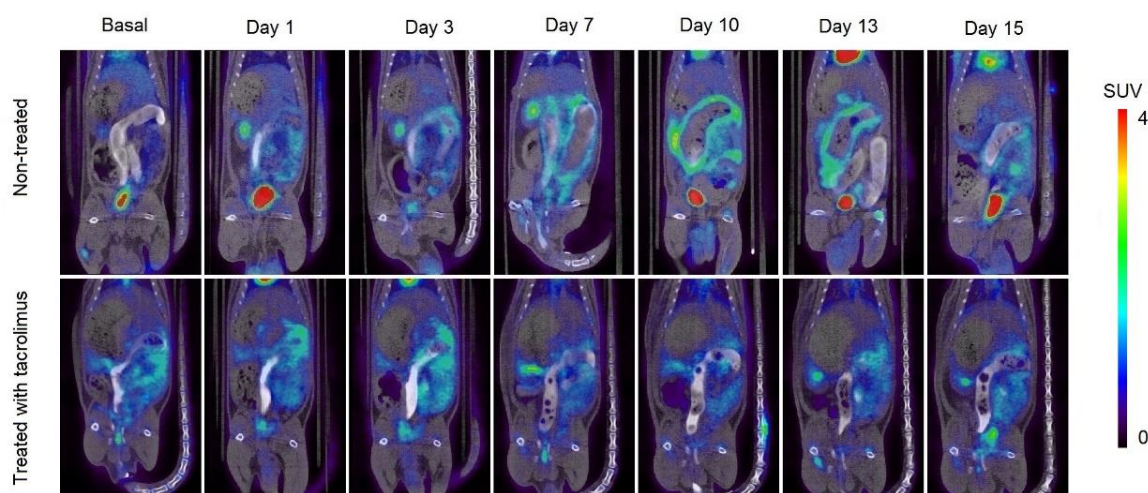
Figure 4.7. Longitudinal fused PET/CT images over time obtained from rats without treatment (13) after the colitis induction and treated with the 3D printed tacrolimus suppositories. The metabolic activity is coded on a colour scale ranging from blue (low [^{18}F]FDG uptake) to red (high [^{18}F]FDG uptake).

In Figure 4.7, it can be appreciated the increase in metabolic activity around the colon area due to inflammation caused by IBD, which corresponds to the increase in SUV_{max} values. In the treated group, there is a high [^{18}F]FDG uptake around the colon on days 1-3, which is subsequently reduced when the treatment administration begins on day 3. On days 7-13, only a slight [^{18}F]FDG accumulation can be appreciated in treated rats. On the contrary, the remission of inflammation in non-treated rats is only achieved on day 15, associated with the spontaneous remission of the TNBS-induced colitis.

Furthermore, a correlation (Pearson coefficient $R^2 = 71.48\%$) was found between the average SUVmax values for the ascending, transverse and descending regions of the colon with weight changes for each day on which PET/CT studies were performed. As can be seen in Figure 4.8, weight changes with respect to baseline are clearly associated with SUVmax values. Positive weight changes are linked to lower SUVmax values, which are mainly found in the group treated with tacrolimus suppositories. On the contrary, weight loss is related to the higher SUVmax values found in the non-treated group.
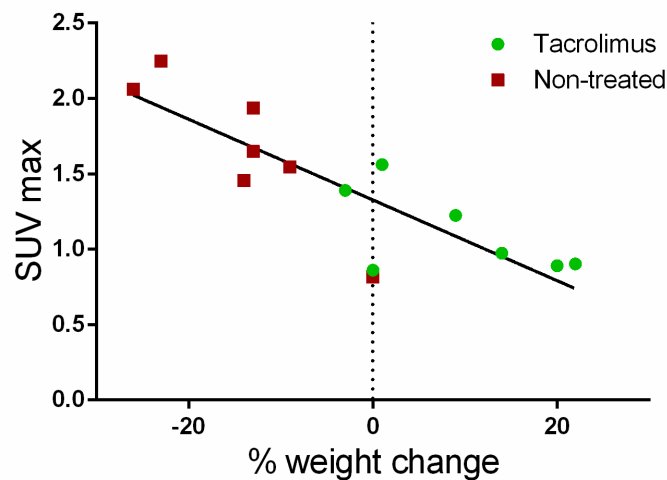
Figure 4.8. Correlation of average SUV$_{max}$ values with body weight changes from the baseline.

Macroscopic images of *ex-vivo* colons on day 15 after colitis induction are shown on Figure 4.9. Images of a non-treated and control animal extracted from our previous study (13) are also shown to be compared with the sample obtained from an animal treated with the tacrolimus 3D printed suppositories. Wall thickening and areas of necrosis are clearly seen in the colon of the non-treated animal, whereas the treated has clearly recovered, with no sign of damage visible to the naked eye.

Figure 4.9. Macroscopic images of *ex-vivo* colons on day 15 post-TNBS induction in A) control group (healthy animals), B) non-treated IBD rats and C) IBD rats treated with tacrolimus (13).

The histological evaluation of colon samples using the Nancy histological index (37) as a reference score showed improved values for the group treated with tacrolimus suppositories compared to the non-treated group. For transverse and descending colon samples, Mann-Whitney test gives a p value < 0.05 for differences between treated and non-treated animals (13). Figure 4.10 provides the results of the histological evaluation of each colon region on day 15 for non-treated and treated groups. The group treated with tacrolimus suppositories showed grade 0 in 5/5 descending colon, in 4/5 transverse colon and in 4/5 ascending colon samples. Moreover, grade 2 was only found in 1/5 ascending colon and 1/5 transverse colon samples. Figure 4.10 also shows representative images of different Nancy grades obtained from the histological examination of colon tissue samples from treated and non-treated rats. Different histological changes can be appreciated depending on the degree of colon damage, ranging from normal mucosal structures found in samples rated as grade 0, to relevant mucosal ulceration and granulation tissue found in samples rated as grade 4. In intermediate grades of colon damage, neutrophil infiltration with less or no sign of ulceration can be observed.

For transverse and descending colon, Mann-Whitney nonparametric test gives a p-value < 0.05 for differences between non-treated and treated animals.
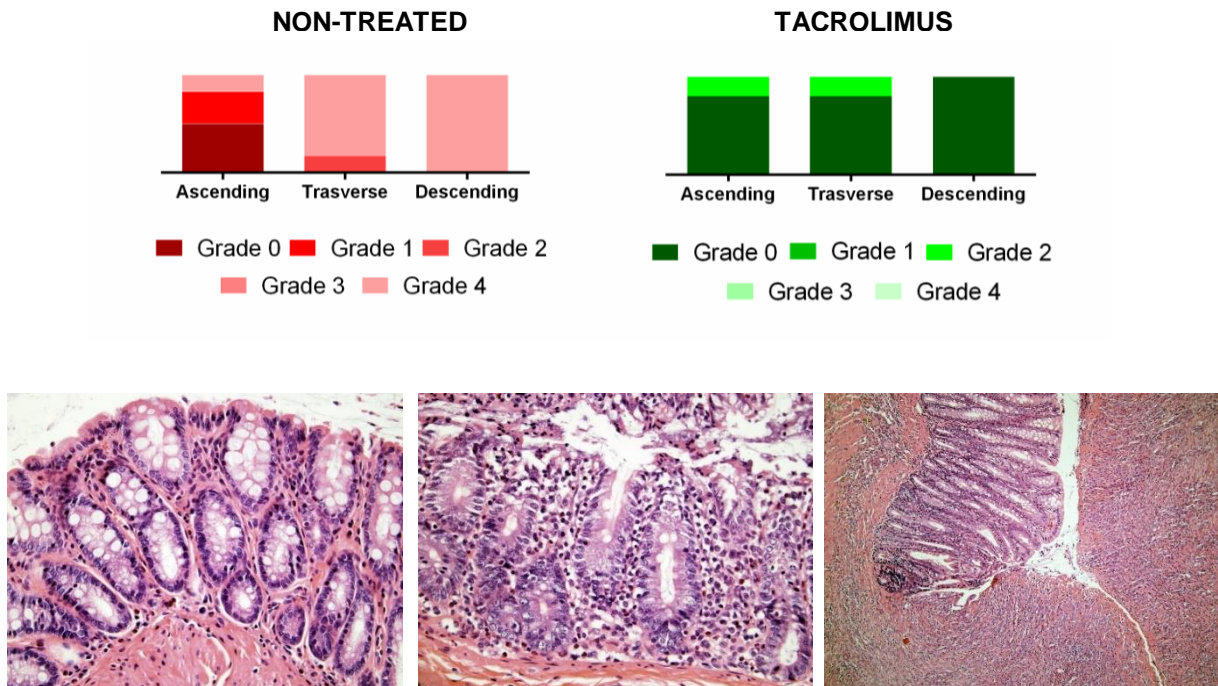
Figure 4.10. Above, graphical representation of Nancy grades for ascending, transverse and descending colon sections for non-treated and tacrolimus groups. Bellow, representative optical microscopy images at 40X (left and middle) and 10X magnification (right) of the Nancy index obtained from rats treated with tacrolimus suppositories. On the left, histologically normal mucosa corresponding to a grade 0 of Nancy index. On the middle, note the presence of occasional neutrophils in the lamina propria, with no signs of ulceration, corresponding to a grade 2 of Nancy index. On the right, ulcerated colonic mucosa, with loss of crypts replaced by granulation tissue, corresponding to a grade 4 of Nancy index.

Furthermore, the time it takes for an animal to regain baseline SUV_{max} values (MRRT) and the time at which the maximum value of SUV_{max} occurs (t_{max}) were calculated and the results are shown in Table 1. The statistical comparison (two-way ANOVA) indicates that for all colon sections, MRRT and t_{max} values are lower for rats treated with tacrolimus. The average time for a rat to recover baseline SUVmax values for the entire colon was 9.22 days for non-treated rats, which was reduced to 5 days after treatment with tacrolimus suppositories. In addition, the mean time required to reach the maximum SUVmax value and to begin to decrease was 10.50 days for non-treated animals compared to the 3.1 days for animals treated with tacrolimus. Consequently, the results indicate much faster recovery in animals treated with tacrolimus suppositories.

Table 1. Comparison of MRRT and t_{max} values of SUV_{max} vs time with and without tacrolimus treatment.

	Non-treated				Tacrolimus			
	MRRT		t_{max}		MRRT		T_{max}	
	Mean	SD	Mean	SD	Mean	SD	Mean	SD
Ascending	9.76	2.62	10.00	3.00	4.78	0.81	4.00	2.00
Transverse	8.37	1.01	10.75	2.87	4.68	1.37	3.50	2.52
Descending	9.54	1.06	10.75	1.50	5.74	1.86	1.80	1.10
Mean±SD	9.22±0.61		10.50±0.35		5.07±0.48		3.10±0.94	

To compare the efficacy of tacrolimus suppositories with other proposed treatments, MRRT and t_{max} were calculated from previously published data (13, 15). Results are shown in Table 2. No significant differences were obtained between rats treated with tacrolimus suppositories and rats treated with corticosteroid or resveratrol, but lower MRRT and t_{max} values were observed compared to melatonin.

Table 2. MRRT and t_{max} values of rats treated with the corticosteroid methylprednisolone, resveratrol and melatonin. The parameters were calculated from data from previously published works.

		Methylprednisolone		Resveratrol		Melatonin	
		Mean	SD	Mean	SD	Mean	SD
MRRT	Ascending	4.57	1.5	4.17	1.97	6.36	1.53
	Transverse	5.37	1.12	4.49	1.79	7.42	2.27
	Descending	4.29	1.53	3.72	2.49	6.37	1.5
	Mean±SD	4.74±0.56		4.13±0.39		6.72±0.61	
t_{max}	Ascending	3.00	2.83	1.83	1.03	5.92	4.10
	Transverse	3.25	1.26	1.92	1.00	4.75	3.49
	Descending	3.00	0.01	1.50	0.90	4.50	3.06
	Mean±SD	3.08±0.14		1.75±0.22		5.06±0.76	
Data obtained from		(13)		(15)			

On the whole, the decrease in disease activity assessed by PET/CT imaging and histological analysis confirmed the therapeutic effect of treatment with tacrolimus suppositories. This therapeutic effect was comparable to that obtained with the administration of an intraperitoneal corticosteroid or resveratrol in the form of an enema. The fact that treatment with tacrolimus has obtained a therapeutic effect similar to that of resveratrol can be explained by the antioxidant effect of the latter, since the TNBS animal model is specially aimed at testing chemical or natural compounds in terms of their antioxidant or anti-inflammatory properties (38, 39). It should be taken into account that animal models of IBD mimic the complex mechanisms involved in chronic intestinal inflammation, but only partially reflect the complexity of the human disease (40).

The therapeutic activity of tacrolimus has been previously described in other animal studies (41, 42), so the present study was focused on the development of a rectal dosage form that delivers the incorporate drug content directly to the colon. Tacrolimus rectal suppositories are commonly compounded in hospital pharmacy settings to treat IBD patients, but the efficacy of this therapy has not yet been investigated in preclinical studies with animal models of the disease. The capability of SSE 3DP to fabricate lipid-based printlets (24) was exploited to produce small suppository-shaped formulations loaded with the exact amount of drug needed for the animals. The selected mixture of lipid excipients, being Gelucire 44/14 the main component, has demonstrated adequate printability properties. The disaggregation time and the time required for emulsion formation from rectal devices prepared with this mixture were also acceptable. The local drug release was confirmed by CT images, which allowed the location of the suppositories after rectal administration and gave an approximate measure of the *in vivo* disintegration time. The self-emulsifying suppositories disintegrated in an acceptable amount of time, even with the lack of fluid in the colon. Since this drug delivery approach allows the release of the drug in the inflamed tissue area, a reduction of adverse effects of tacrolimus could be obtained due to a more local effect of the drug.

The manufacturing opportunities that 3DP could offer in preclinical research have not yet been fully exploited. This highly flexible technology allows the on demand manufacturing of devices containing the exact dosage of the drug and with sizes and geometries adapted to the animal model. To this date, few studies have reported the use of 3DP in preclinical research, with almost all focusing on oral drug delivery (43, 44). The study herein is the first that uses 3DP to manufacture dosage forms for rectal administration in rats. The results yielded by this work confirm the feasibility of this technique to prepare drug loaded lipid-based suppositories with self-emulsifying properties and adequate characteristics for its administration to rats. Moreover, the combination of lipid excipients investigated in this work has proved to be a suitable carrier for tacrolimus, which was successfully solubilized and released from the lipid droplets of the formed emulsion. The method described in the present work could also be applied to prepare drug-loaded suppositories for human administration. The affordable cost of 3D printers makes it possible to implement them in an hospital pharmacy setting, where pharmacists and technicians could take advantage of the versatility of this technology to prepare suppositories tailored to each patient's requirements. In particular, this drug delivery

strategy could benefit IBD patients who were prescribed rectal tacrolimus. The size and dose of tacrolimus could be adapted to adults or children, who can benefit from the immunosuppressive effect of tacrolimus while simultaneously reducing adverse effects.

CONCLUSIONS

The combination of 3DP with medical imaging offers a new approach for the development and assessment of novel IBD therapies in the preclinical area. The versatility of semisolid extrusion 3DP allowed the preparation of small self-emulsifying suppositories containing an exact dose of the drug with a size and shape adapted for their rectal administration in rats. The combination of Gelucire 44/14 and coconut oil showed adequate printability, and the disaggregation of the suppositories and subsequent release of the drug from the formed emulsion occurred within an acceptable period of time. Moreover, [^{18}F]FDG PET/CT imaging showed to be an useful tool for the assessment of the disease over time and CT imaging allowed to a better *in vivo* characterization of the suppositories. The quantification of inflammation using the SUV_{max} parameter, commonly used in clinical practice, helps the translation into humans of this new therapeutic approach.

ACKNOWLEDGEMENTS

CONFLIT OF INTEREST

The authors declare no conflict of interest.

REFERENCES

1.   Yadav V, Varum F, Bravo R, Furrer E, Bojic D, Basit AW. Inflammatory bowel disease: exploring gut pathophysiology for novel therapeutic targets. Translational Research. 2016;176:38-68.

2.   Ahmed FE. Role of genes, the environment and their interactions in the etiology of inflammatory bowel diseases. Expert Review of Molecular Diagnostics. 2006;6(3):345-63.

3.   Hazel K, O'Connor A. Emerging treatments for inflammatory bowel disease. Therapeutic Advances in Chronic Disease. 2020;11:2040622319899297.

4.   McConnell EL, Liu F, Basit AW. Colonic treatments and targets: issues and opportunities. Journal of Drug Targeting. 2009;17(5):335-63.

5.   Lawrance IC, Copeland TS. Rectal tacrolimus in the treatment of resistant ulcerative proctitis. Alimentary Pharmacology & Therapeutics. 2008;28(10):1214-20.

6.   Jaeger SU, Klag T, Hoeger K, Klumpp S, Escher M, Malek N, et al. Tacrolimus Suppositories in Therapy-Resistant Ulcerative Proctitis. Inflammatory Intestinal Diseases. 2018;3(3):116-24.

7.   Hoffmann P, Wehling C, Krisam J, Pfeiffenberger J, Belling N, Gauss A. Performance of tacrolimus in hospitalized patients with steroid-refractory acute severe ulcerative colitis. World J Gastroenterol. 2019;25(13):1603-17.

8.   Talley NJ, Abreu MT, Achkar JP, Bernstein CN, Dubinsky MC, Hanauer SB, et al. An evidence-based systematic review on medical therapies for inflammatory bowel disease. Am J Gastroenterol. 2011;106 Suppl 1:S2-25; quiz S6.

9.   Wu B, Tong J, Ran Z. Tacrolimus Therapy in Steroid-Refractory Ulcerative Colitis: A Review. Inflammatory Bowel Diseases. 2019;26(1):24-32.

10.   Matsuoka K, Saito E, Fujii T, Takenaka K, Kimura M, Nagahori M, et al. Tacrolimus for the Treatment of Ulcerative Colitis. Intestinal research. 2015;13(3):219-26.

11.   Hua S. Physiological and Pharmaceutical Considerations for Rectal Drug Formulations. Frontiers in Pharmacology. 2019;10:1196.

12.   Hart AL, Plamondon S, Kamm MA. Topical tacrolimus in the treatment of perianal Crohn's disease: exploratory randomized controlled trial. Inflamm Bowel Dis. 2007;13(3):245-53.

13.   Seoane-Viano I, Gomez-Lado N, Lazare-Iglesias H, Barreiro-de Acosta M, Silva-Rodriguez J, Luzardo-Alvarez A, et al. Longitudinal PET/CT evaluation of TNBS-induced inflammatory bowel disease rat model. Int J Pharm. 2018;549(1-2):335-42.

14.   Dmochowska N, Tieu W, Keller MD, Wardill HR, Mavrangelos C, Campaniello MA, et al. Immuno-PET of Innate Immune Markers CD11b and IL-1beta Detects Inflammation in Murine Colitis. J Nucl Med. 2019;60(6):858-63.

15.   Seoane-Viaño I, Gómez-Lado N, Lázare-Iglesias H, Rey-Bretal D, Lamela-Gómez I, Otero-Espinar F, et al. Evaluation of the therapeutic activity of Melatonin and Resveratrol in Inflammatory Bowel Disease: a longitudinal PET/CT study in an animal model. International Journal of Pharmaceutics. 2019:118713.

16.   Takizawa H, Shintani N, Natsui M, Sasakawa T, Nakakubo H, Nakajima T, et al. Activated Immunocompetent Cells in Rat Colitis Mucosa Induced by Dextran Sulfate Sodium and Not Complete but Partial Suppression of Colitis by FK506. Digestion. 1995;56(3):259-64.

17.   Lamprecht A, Yamamoto H, Takeuchi H, Kawashima Y. Nanoparticles enhance therapeutic efficiency by selectively increased local drug dose in experimental colitis in rats. J Pharmacol Exp Ther. 2005;315(1):196-202.

18.   Yoshino T, Nakase H, Honzawa Y, Matsumura K, Yamamoto S, Takeda Y, et al. Immunosuppressive effects of tacrolimus on macrophages ameliorate experimental colitis. Inflamm Bowel Dis. 2010;16(12):2022-33.

19.   Trenfield SJ, Awad A, Goyanes A, Gaisford S, Basit AW. 3D Printing Pharmaceuticals: Drug Development to Frontline Care. Trends Pharmacol Sci. 2018;39(5):440-51.

20.   Vithani K, Goyanes A, Jannin V, Basit AW, Gaisford S, Boyd BJ. An Overview of 3D Printing Technologies for Soft Materials and Potential Opportunities for Lipid-based Drug Delivery Systems. Pharm Res. 2018;36(1):4.

21.   Khaled SA, Burley JC, Alexander MR, Yang J, Roberts CJ. 3D printing of tablets containing multiple drugs with defined release profiles. Int J Pharm. 2015;494(2):643-50.

22.   Khaled SA, Burley JC, Alexander MR, Roberts CJ. Desktop 3D printing of controlled release pharmaceutical bilayer tablets. Int J Pharm. 2014;461(1-2):105-11.

23.   Goyanes A, Madla CM, Umerji A, Duran Piñeiro G, Giraldez Montero JM, Lamas Diaz MJ, et al. Automated therapy preparation of isoleucine formulations using 3D printing for the treatment of MSUD: First single-centre, prospective, crossover study in patients. Int J Pharm. 2019;567:118497.

24.   Vithani K, Goyanes A, Jannin V, Basit AW, Gaisford S, Boyd BJ. A Proof of Concept for 3D Printing of Solid Lipid-Based Formulations of Poorly Water-Soluble Drugs to Control Formulation Dispersion Kinetics. Pharm Res. 2019;36(7):102.

25.   Siepmann J, Faham A, Clas S-D, Boyd BJ, Jannin V, Bernkop-Schnürch A, et al. Lipids and polymers in pharmaceutical technology: Lifelong companions. International Journal of Pharmaceutics. 2019;558:128-42.

26.   Boyd BJ, Bergström CAS, Vinarov Z, Kuentz M, Brouwers J, Augustijns P, et al. Successful oral delivery of poorly water-soluble drugs both depends on the intraluminal behavior of drugs and of appropriate advanced drug delivery systems. European Journal of Pharmaceutical Sciences. 2019;137:104967.

27.   Lee DR, Ho MJ, Jung HJ, Cho HR, Park JS, Yoon S-H, et al. Enhanced dissolution and oral absorption of tacrolimus by supersaturable self-emulsifying drug delivery system. International journal of nanomedicine. 2016;11:1109-17.

28.   Bettenworth D, Reuter S, Hermann S, Weckesser M, Kerstiens L, Stratis A, et al. Translational 18F-FDG PET/CT imaging to monitor lesion activity in intestinal inflammation. J Nucl Med. 2013;54(5):748-55.

29.   Pio BS, Byrne FR, Aranda R, Boulay G, Spicher K, Song MH, et al. Noninvasive quantification of bowel inflammation through positron emission tomography imaging of 2-deoxy-2-[18F]fluoro-D-glucose-labeled white blood cells. Mol Imaging Biol. 2003;5(4):271-7.

30.   Gómez-Lado N, Seoane-Viaño I, Matiz S, Madla MC, Yadav V, Aguiar P, et al. Gastrointestinal Tracking and Gastric Emptying of Coated Capsules in Rats with or without Sedation Using CT imaging. Pharmaceutics. 2020;12(1).

31.   Du S, Sun H, Gao S, Xin J, Lu Z. Metabolic parameters with different thresholds for evaluating tumor recurrence and their correlations with hematological parameters in locally advanced squamous cell cervical carcinoma: an observational 18 F-FDG PET/CT study. Quantitative Imaging in Medicine and Surgery; Vol 9, No 3 (March 2019): Quantitative Imaging in Medicine and Surgery. 2019.

32.   Kaaru E, Bianchi A, Wunder A, Rasche V, Stiller D. Molecular Imaging in Preclinical Models of IBD with Nuclear Imaging Techniques: State-of-the-Art and Perspectives. Inflamm Bowel Dis. 2016;22(10):2491-8.

33.   Sakai M, Hobara N, Hokama N, Kameya H, Ohshiro S, Sakanashi M, et al. Increased bioavailability of tacrolimus after rectal administration in rats. Biol Pharm Bull. 2004;27(9):1480-2.

34.   Kilkenny C, Browne W, Cuthill IC, Emerson M, Altman DG. Animal research: reporting in vivo experiments: the ARRIVE guidelines. Br J Pharmacol. 2010;160(7):1577-9.

35.   Morris GP, Beck PL, Herridge MS, Depew WT, Szewczuk MR, Wallace JL. Hapten-induced model of chronic inflammation and ulceration in the rat colon. Gastroenterology. 1989;96(3):795-803.

36.   Marchal-Bressenot A, Scherl A, Salleron J, Peyrin-Biroulet L. A practical guide to assess the Nancy histological index for UC. Gut. 2016;65(11):1919.

37.   Marchal-Bressenot A, Salleron J, Boulagnon-Rombi C, Bastien C, Cahn V, Cadiot G, et al. Development and validation of the Nancy histological index for UC. Gut. 2017;66(1):43-9.

38.   Antoniou E, Margonis GA, Angelou A, Pikouli A, Argiri P, Karavokyros I, et al. The TNBS-induced colitis animal model: An overview. Annals of medicine and surgery (2012). 2016;11:9-15.

39.   Seoane-Viaño I, Gómez-Lado N, Otero-Espinar F, Fernández-Ferreiro A, Aguiar P, Ruibal A, et al. Preclinical Models of Inflammatory Bowel Disease and Colonic Treatments. 2019. p. http://openaccessebooks.com/inflammatory-bowel.

40.   Hatton GB, Yadav V, Basit AW, Merchant HA. Animal Farm: Considerations in Animal Gastrointestinal Physiology and Relevance to Drug Delivery in Humans. J Pharm Sci. 2015;104(9):2747-76.

41.   Hoshino H, Goto H, Sugiyama S, Hayakawa T, Ozawa T. Effects of FK506 on an experimental model of colitis in rats. Aliment Pharmacol Ther. 1995;9(3):301-7.

42.   Lamprecht A, Yamamoto H, Ubrich N, Takeuchi H, Maincent P, Kawashima Y. FK506 microparticles mitigate experimental colitis with minor renal calcineurin suppression. Pharm Res. 2005;22(2):193-9.

43.   Genina N, Boetker JP, Colombo S, Harmankaya N, Rantanen J, Bohr A. Anti-tuberculosis drug combination for controlled oral delivery using 3D printed compartmental dosage forms: From drug product design to in vivo testing. J Control Release. 2017;268:40-8.

44.   Arafat B, Qinna N, Cieszynska M, Forbes RT, Alhnan MA. Tailored on demand anti-coagulant dosing: An in vitro and in vivo evaluation of 3D printed purpose-designed oral dosage forms. European Journal of Pharmaceutics and Biopharmaceutics. 2018;128:282-9.

General discussion

GENERAL DISCUSSION

Inflammatory bowel disease (IBD) is an expanding global health problem of industrial-urbanized societies. Under a westernized lifestyle and certain environmental conditions, people who exhibit genetic predisposition are at increased risk of developing the disease. The main entities of IBD, Crohn's disease (CD) and ulcerative colitis (UC), can have a continuous clinical course with severe consequences, such as acute severe colitis, the need for surgical treatment or cancer development (1). Therefore, it is fundamental to limit the progression of the disease by the use of effective treatments with the least number of adverse effects. However, even with the great advances in the knowledge about the pathophysiology of the disease, there is still a need for new therapeutic alternatives that reconcile the most appropriate treatment for each patient and the cost.

The choice of treatment mainly depends on the grade and extent of the disease. Treatment options for UC vary from topical therapy in the form of enemas and suppositories for distal UC, to aminosalicylates (e.g., 5-ASA) in moderate disease progressing to immunomodulators (e.g., tacrolimus) for disease not controlled with aminosalicylates. Steroids are used to control acute flare-ups. In the case of CD, the mainstay of treatment is immunomodulatory drugs, such as tacrolimus. In severe disease, biological treatments such as monoclonal antibody therapy (e.g., anti-TNF therapy) is commonly prescribed (2). The cost of medications for IBD varies from inexpensive topical therapy and relatively cheap aminosalicylates to more expensive biological therapies. Despite the high costs of biologic agents, the use of these agents is increasing due to their efficacy, since it reduces hospitalization and need for surgery, which is one of the main goals of IBD treatment (3). Nevertheless, biological therapies as well as other oral treatments are not extent of side effects, some of them serious (4). The lack of safe, cost-effective treatments drives the search for alternative therapies that maintain remission for a longer period of time at an affordable cost.

In the last decades, novel mechanisms implicated in the pathogenesis of IBD have been elucidated. Among them, the contribution of oxidative stress to chronic intestinal inflammation is attracting the attention of the research community. Therefore, the inclusion of compounds with antioxidant and anti-inflammatory properties in the therapeutic arsenal could lead to better treatment responses with less side effects and lower costs (5). Furthermore, with the advent of digital technologies, significant opportunities have emerged either to improve the safety of current treatments or to assess the efficacy of new ones.

Medical imaging devices, such as PET/CT and MRI scanners, commonly used for the diagnosis and follow-up of patients, can also be used to evaluate new therapies in the preclinical area. In particular, the combination of structural with functional imaging

techniques, such as in PET/CT imaging, makes it possible to locate, characterize and quantify biological processes at the cellular level in living organisms. Apart from the additional information obtained in comparison with traditional techniques (e.g., histological analysis of tissues), another asset of medical imaging is the possibility of assessing the efficacy of new treatments in a non-invasive way. This allows to reduce the number of animals needed in each experiment since animals could be reused and their sacrifice is largely avoided (6).

Another advantage that comes with digital technology is the possibility to personalize the medical treatment according to the characteristics of each individual. In this regard, 3DP technology has represented a major breakthrough in the pharmaceutical sector since it constitutes an effective strategy to personalize drug products, from medical devices to dosage forms, that could be tailored to meet the individual needs of each patient (7). Moreover, the versatility of 3DP could also be exploited in the field of preclinical research. The drop in the price of 3D printers and their small size made 3DP an affordable technology that could be integrated into a laboratory setting. Thus, dosage forms with different sizes and geometries that contain the exact dose for the animal could be manufactured on demand in a rapid manner.

In the present work, the investigation of some therapeutic alternatives for the treatment of IBD based on compounds that are not currently included in the IBD therapeutic arsenal was carried out. Moreover, the improvement of current therapies through the use of 3DP technology was also explored. Specifically, three different approaches can be distinguished:

In the first one, two compounds with antioxidant and anti-inflammatory properties (melatonin and resveratrol) described in the literature have been tested in a rat model of experimental IBD. Longitudinal [^{18}F]FDG PET/CT scans were performed to assess the therapeutic activity of the compounds.

In the second one, tacrolimus suppositories commonly compounded in hospital pharmacy settings, were prepared using 3DP technology. In addition, the suitability of different lipid excipients with self-emulsifying properties for the printing process were evaluated.

In the third one, the most suitable combination of lipid excipients was selected, and the size of tacrolimus suppositories was reduced to meet the requirements for their administration to the rat model of the disease. Moreover, longitudinal [^{18}F]FDG PET/CT scans were performed to evaluate the viability of 3D printed suppositories to treat experimental IBD.

The final aims and the justification for this work is to provide evidence about the potential therapeutic activity of antioxidant compounds in the treatment of IBD, and to overcome some drawbacks of current therapy with tacrolimus suppositories. This last point is of special interest in drugs with narrow therapeutic index, such as tacrolimus, with which compounding errors and inaccurate dosing could lead to severe side effects.

Development of an animal model of IBD

The first part of the work focused on exploring the feasibility of the $[^{18}F]$FDG PET/CT imaging technique and the SUV_{max} parameter to monitor disease activity in an animal model of TNBS-induced colitis. PET/CT imaging integrates the physiological information obtained by PET with the anatomic information of CT. Moreover, SUV_{max} parameter is commonly used in clinical routine to quantify PET images. Consequently, their combination may be useful for the non-invasive quantification of inflammation in IBD.

Experimental colitis was chemically induced in Sprague Dawley rats by the use of 2,4,6-trinitrobenzenesulfonic acid (TNBS) (50 mg/kg body weight) dissolved in ethanol 50% (v/v) (8). These chemical reagents caused an acute inflammatory process with some histological features similar to those of human IBD, such as neutrophilic infiltration.

In this study, the animals were divided into three experimental groups. In the first one, TNBS colitis was induced in rats as described above and received no treatment. In the second one, TNBS colitis was also induced in rats, but after day 3 post-induction, the animals received a corticosteroid (methylprednisolone 0.5 mg / kg) as treatment. The third group was the control group and only received 0.9% saline solution.

To assess the evolution of inflammation from day 0 to 15, $[^{18}F]$FDG PET/CT scans were performed in basal condition and 1, 3, 7, 10, 13 and 15 days post-TNBS administration. The radiotracer $[^{18}F]$FDG was used to identify the areas with abnormally high glucose metabolism due to the inflammation caused by the TNBS and the SUV_{max} parameter was used to quantify $[^{18}F]$FDG uptake in those affected areas of the colon.

Fused PET/CT images showed extensive spatial patterns of inflammation in the animals with colitis, mainly affecting the transverse and descending colon. Spontaneous remission of TNBS colitis occurred on day 15 post-administration. However, in animals treated with the corticosteroid this remission was achieved on day 7, which was an expected positive response to corticosteroid treatment. Moreover, a good correlation ($R^2 = 0.82$) was found between SUV_{max} values and weight values of animals. Higher SUV_{max} values were related to higher weight loss, whereas lower SUV_{max} values were related to weight recovery and disease remission.

Histological analyzes were performed to confirm these results. The histological disease activity was scored using the Nancy index (9). As in the PET images, histological evaluation showed that the inflammation was clearly located in the descending and transverse colon. The obtained Nancy grades also correlate with SUV_{max} values, with a $R^2 = 0.61$. Higher SUV_{max} values were associated with higher Nancy grades, while lower Nancy grades were related to lower SUV_{max} values, mainly corresponding to treated rats.

At the light of these results, it could be concluded that the positive response showed to corticosteroid treatment validates this animal model for use in preclinical investigations of new compounds. Moreover, PET/CT technique and SUV_{max} parameter demonstrated to be

reliable tools to monitor disease progression and remission, showing high potential for use as a non-invasive method in the evaluation of therapeutic activity of new compounds.

<u>Evaluation of the therapeutic activity of melatonin and resveratrol</u>

The second part of this work focused on the evaluation of the therapeutic activity of two compounds with antioxidant and anti-inflammatory properties, melatonin and resveratrol. To this aim, the previously developed animal model was used in combination with PET/CT imaging to assess the progression of the inflammation after treatment administration.

Firstly, two different formulations intended for rectal administration, a water-based and a gel-based formulation, were prepared and their residence time *in vivo* in the colon was compared by the use of PET/CT. This was possible by the mixing of the radiotracer [^{18}F]FDG and a contras agent ((Iopromide Ultravist® 300 mg / mL) with the formulation. This experiment served to evaluate the spreadability of both vehicles in the colon in order to select the most suitable one as vehicle for the incorporation of the active substances. PET/CT images showed a better biodistribution and a longer residence time in the colon of the water-based enema compared to the gel. Therefore, melatonin and resveratrol were included in a water-based enema for their in *in vivo* therapeutic activity evaluation.

Then, animals were divided into two experimental groups; the first received melatonin as treatment and the second received resveratrol. The induction of TNBS colitis was performed as previously described in the first part of this discussion and [^{18}F]FDG PET/CT scans were performed in basal condition and 1, 3, 7, 10, 13 and 15 days post-TNBS administration. As in the case of corticosteroid treatment, treatment with melatonin or resveratrol begin on day 3 after the induction of colitis.

The results obtained in this study showed that a significant decrease in SUV$_{max}$ values after the beginning of the treatment with both compounds, being this decrease more remarkable in the resveratrol group. Histological analyzes using the Nancy index (9) confirmed these findings, obtaining improved scores for both treated groups in comparison with the non-treated one (10). Significant differences were found between the group treated with melatonin and the group treated with resveratrol, which highlights the positive outcome of resveratrol treatment.

In order to explain the better therapeutic activity of resveratrol compared to melatonin, the antioxidant capacities of both compounds were investigated using the ABTS assay (11). This method was based on the ability of an antioxidant to reduce ABTS radical cation (ABTS$^{\bullet+}$). Trolox was used as a reference antioxidant compound. Antioxidant capacity of melatonin and resveratrol was calculated comparing the concentrations of Trolox, melatonin and resveratrol that produce the same percentage of inhibition in ABTS$^{\bullet+}$ radical reduction. The results of this experiment showed that 1 µM of resveratrol provides the same antioxidant capacity of 2.36 µM of Trolox, being, therefore, the antioxidant capacity of resveratrol 2.36 times higher than that of Trolox. Contrarily, it has not been possible to calculate the

antioxidant capacity of melatonin using the ABTS method due to the insufficient inhibition of $ABTS^{•+}$ by melatonin. The results yielded by this experiment showed a limited antioxidant activity of melatonin compared to resveratrol, which is in general agreement with the differences in the therapeutic activity of both compounds.

On the whole, the results obtained in this work provide compelling evidence for the inclusion of melatonin and resveratrol in the therapeutic arsenal of IBD. Moreover, these results also suggest that the administration of compounds with antioxidant and anti-inflammatory properties appears to be effective in the treatment of gastrointestinal pathologies whose pathogenesis is in part due to oxidative stress, such as IBD.

<u>3D printing of tacrolimus suppositories</u>

In the third and final phase of this work, the attention was focused on the development of 3D printed tacrolimus suppositories for the treatment of UC. The rectal delivery of drugs with narrow therapeutic index, such as tacrolimus, is a promising strategy to maximise drug concentrations at the disease site whilst minimising systemic side effects. In current clinical practice, suppository formulations are not always available, so hospital pharmacists have to compound them from commercially available dosage forms, such as tablets for oral administration. This lead to a number of risks, such as compounding errors and inaccurate dosing (12). Moreover, suppositories are commonly prepared by moulding technique, which requires several steps and long periods of time for hardening.

To overcome these limitations and safety concerns, this work has explored the feasibility of semisolid extrusion 3DP to prepare lipid-based suppositories in a rapid and single-step process. Semisolid extrusion technology is highly relevant to print objects using soft materials (13). Moreover, the drug can be added directly to the lipid base without the need for intermediate steps.

In this third part of the work, two different approaches could be distinguished. The first one was based on testing different combinations of lipid excipients with self-emulsifying properties to prepare human-sized suppositories. In the second approach, the best combination has been selected and used to print suppositories in smaller size to carry out further studies in the previously developed TNBS animal model of colitis.

In the first approach, suppositories intended for human administration were printed in three different sizes using either Gelucire 44/14 (Gel 44) or Gelucire 48/16 (Gel 48). Coconut oil was added to both Gelucires as a plasticizing agent to improve printability of the final mixture. In addition, the suppositories were also printed both horizontally and vertically. Although suppositories were printed faster in horizontally, their quality was better when printed vertically, so the vertical position was selected as the best. This choice was supported by SEM images, which showed that the deposition of layers when printing vertically was better than when printing horizontally.

Extrusion force studies were carried out to evaluate the ease of extrusion of the mixtures at printing temperatures (42 ºC for Gel 44 and 48 ºC for Gel 48), being the energy required to extrude Gel 48 higher than that required for Gel 44 extrusion. FT-IR spectroscopy showed no detectable interactions between the drug and the lipid excipients. On the other hand, DSC and X-ray analysis indicated that the drug is in its amorphous form and is also forming a solid solution with the lipid excipients.

The disintegration time and self-emulsifying time of Gel 44 formulation were lower than those of Gel 48. Contrarily, Gel 48 suppositories displayed a faster rate of drug release. Gel 48 release more than 50% of tacrolimus within the first 60 min, whereas Gel 44 need 90 min to reach the same amount of drug released. Despite the faster release of Gel 48, both suppositories released more than 80% of drug load within 120 min. The longer onset of drug release of Gel 44 could be explained by its lower hydrophilic-lipophilic balance (HLB=10.4 for Gel 44 and HLB=11.2 for Gel 48), which leads to lower water solubility of Gel 44.

After self-emulsification, the formed system was characterized in terms of globule size and ζ potential. The globule size of both formulations was between 1-1.5 μm and the stability given by ζ potential was – 14 mV for Gel 44 and – 20 mV for Gel 48, which means that Gel 48 was the most stable. Moreover, the higher globule sizes obtained may be due to the inclusion of coconut oil, since it is described in literature that Gelucire 44/14 forms microemulsions and Gelucire 48/16 micellar systems in aqueous media (14,15). These sizes of lipid globules obtained by dynamic light scattering (DLS) measurements were consistent with those obtained by TEM images, confirming the results.

Finally, in light of the above, Gel 44 formulation was selected for further studies. Although Gel 48 suppositories released drug at a faster rate, the better printing properties and miscibility of Gel 44 mixture provided by its lower melting point and the lower extrusion energy required make Gel 44 a more adequate formulation.

In the second approach, the flexibility of 3DP was exploited to prepare small batches of 3D printed suppositories with the size and dosage adapted to the requirements of the rats employed in the study. The combination of lipid excipients used for printing the formulations was selected in base of the findings of the previous section (suppositories for humans), being Gel 44 the selected one. The aim of this study was to evaluate the therapeutic activity of 3D printed self-emulsifying suppositories loaded with tacrolimus for the treatment of experimental IBD. The rat model of experimental IBD was developed as described in the first part of this discussion (development of an animal model of IBD) and PET/CT imaging was used to monitor the evolution of disease.

The *in vivo* disintegration time of the suppositories was evaluated by including a 30% of barium sulphate (contrast agent) in the mixture. The suppositories were administered to the animals and the CT scans showed that 50 min after the administration the formulation was no longer observed. Moreover, the *in vitro* drug release showed a profile very similar to the that

obtained with the Gel 44 suppositories fabricated in human size, achieving 100% release of the drug at 90 min.

The induction of TNBS colitis was performed as previously described in the first part of this discussion and [^{18}F]FDG PET/CT scans were performed in basal condition and 1, 3, 7, 10, 13 and 15 days post-TNBS administration. The administration of tacrolimus begins on day 3 post-colitis induction. The obtained SUV$_{max}$ values were very similar for non-treated (10) and treated rats on days 0-7, but a significant decrease in SUVmax values can be noticed on days 10 and 13 in treated animals, especially in transverse and descending colon sections. Histological analyzes using the Nancy index (9) confirmed these findings, obtaining better scores for the treated group in comparison with the non-treated one (10). Furthermore, positive weight changes mainly found in the treated group were associated with lower SUV$_{max}$ values, which confirm the recovery of animals treated with tacrolimus suppositories.

The positive outcome of the treatment confirms that tacrolimus was efficiently released in the colon from the self-emulsifying suppositories. This local drug release was also confirmed by CT images, which allowed not only the location of the suppositories after administration, but also gave an approximate measure of the *in vivo* disintegration time. Even with the lack of fluid in the colon, the self-emulsifying suppositories disintegrated in an acceptable amount of time.

On the whole, it could be concluded from this final part of the work that semisolid extrusion 3DP represents an adequate tool for overcoming the problems of conventional suppository formulation (e.g., moulding technique). This manufacturing technology makes possible the printing of the exact dose of the drug mixed with lipid excipients in a single step process. Suppositories are prepared according to the patient's comfort, which can enhance adherence and consequently treatment outcomes. Moreover, the high flexibility of 3DP can be also exploited to produce small batches of suppositories adapted in dose and size for administration to small animals.

Overall assessment

In the light of the discussed in the three parts of this work, it could be concluded that the combination of animals models together with medical imaging give us a reliable tool to evaluate novel therapies in their preclinical stage. In particular, the animal model used in this work and its positive response to antioxidant therapy provide compelling evidence of the implication of oxidative stress in the pathogenesis of experimental IBD. Moreover, [^{18}F]FDG PET/CT imaging technique has proven to be a convenient method to monitor the evolution of inflammation in the GI tract. CT imaging has also proved to be a useful tool to investigate the *in vivo* biodistribution and disintegration time of rectal dosage forms.

On the other hand, semisolid extrusion 3DP provided a new opportunity to improve the safety of current IBD therapy with tacrolimus suppositories. This technology allows the manufacture of lipid-based suppositories with personalized sizes and doses in a single step

process. This approach represents a more efficient and cost-effective manner to prepare tacrolimus suppositories, while reducing the risk of adverse effects. Semisolid extrusion 3DP has also been shown to be capable of manufacturing small batches of suppositories with a size and a dose adapted for preclinical studies in rodents in a rapid and efficient manner.

REFERENCES

1.   M'Koma AE. Inflammatory bowel disease: an expanding global health problem. Clin Med Insights Gastroenterol. 2013;6:33-47.

2.   Ghosh N, Premchand P. A UK cost of care model for inflammatory bowel disease. Frontline Gastroenterol. julio de 2015;6(3):169-74.

3.   Sprakes MB, Ford AC, Suares NC, Warren L, Greer D, Donnellan CF, et al. Costs of care for Crohn's disease following the introduction of infliximab: a single-centre UK experience. Aliment Pharmacol Ther. diciembre de 2010;32(11-12):1357-63.

4.   Stallmach A, Hagel S, Bruns T. Adverse effects of biologics used for treating IBD. Best Pract Res Clin Gastroenterol. abril de 2010;24(2):167-82.

5.   Singh UP, Singh NP, Busbee B, Guan H, Singh B, Price RL, et al. Alternative Medicines as Emerging Therapies for Inflammatory Bowel Diseases. Int Rev Immunol. febrero de 2012;31(1):66-84.

6.   Kaaru E, Bianchi A, Wunder A, Rasche V, Stiller D. Molecular Imaging in Preclinical Models of IBD with Nuclear Imaging Techniques: State-of-the-Art and Perspectives. Inflamm Bowel Dis. 1 de octubre de 2016;22(10):2491-8.

7.   Goyanes A, Madla CM, Umerji A, Piñeiro GD, Montero JMG, Diaz MJL, et al. Automated therapy preparation of isoleucine formulations using 3D printing for the treatment of MSUD: first single-centre, prospective, crossover study in patients. Int J Pharm. 4 de julio de 2019;118497.

8.   Morris GP, Beck PL, Herridge MS, Depew WT, Szewczuk MR, Wallace JL. Hapten-Induced Model of Chronic Inflammation and Ulceration in the Rat Colon. Gastroenterology. 1 de febrero de 1989;96(2):795-803.

9.   Marchal-Bressenot A, Salleron J, Boulagnon-Rombi C, Bastien C, Cahn V, Cadiot G, et al. Development and validation of the Nancy histological index for UC. Gut. enero de 2017;66(1):43-9.

10.   Seoane-Viano I, Gomez-Lado N, Lazare-Iglesias H, Barreiro-de Acosta M, Silva-Rodriguez J, Luzardo-Alvarez A, et al. Longitudinal PET/CT evaluation of TNBS-induced inflammatory bowel disease rat model. Int J Pharm. 5 de octubre de 2018;549(1-2):335-42.

11.   Re R, Pellegrini N, Proteggente A, Pannala A, Yang M, Rice-Evans C. Antioxidant activity applying an improved ABTS radical cation decolorization assay. Free Radic Biol Med. mayo de 1999;26(9-10):1231-7.

12.   Kairuz TE, Gargiulo D, Bunt C, Garg S. Quality, safety and efficacy in the «off-label» use of medicines. Curr Drug Saf. enero de 2007;2(1):89-95.

13.   Vithani K, Goyanes A, Jannin V, Basit AW, Gaisford S, Boyd BJ. An Overview of 3D Printing Technologies for Soft Materials and Potential Opportunities for Lipid-based Drug Delivery Systems. Pharm Res. 7 de noviembre de 2018;36(1):4.

14.   Gelucire® 48/16 [Internet]. [citado 10 de marzo de 2020]. Disponible en: https://www.gattefosse.com/notre-histoire/pharmaceuticals-products/gelucire-4816/

15.   Gelucire® 44/14 [Internet]. [citado 10 de marzo de 2020]. Disponible en: https://www.gattefosse.com/pharmaceuticals-products/gelucire-4414.

Conclusions

CONCLUSIONS

The analysis of the results obtained in the evaluation of the therapeutic activity of antioxidant compounds for the treatment of inflammatory bowel disease (IBD) and the exploration of the feasibility of 3D printing to prepare rectal devices with sizes and doses adapted to meet the requirements of the study, enables us to draw the following conclusions:

1st - The [^{18}F]FDG PET/CT imaging technique have been found a suitable strategy to monitor disease activity in the rat model of TNBS colitis. Moreover, the SUV_{max} parameter allowed the quantification of [^{18}F]FDG uptake by the inflamed colonic tissue. On the other hand, the use of CT imaging together with a contrast agent gave an approximate measure of the residence time and biodistribution of the formulations in the colon. The Nancy histological index confirmed the results obtained from the analysis of PET images and showed a good correlation with SUV_{max} values.

2nd - The TNBS rat model of colitis proved to be a useful model for the investigation of the therapeutic activity of compounds with antioxidant and anti-inflammatory properties. The two substances evaluated in this work using [^{18}F]FDG PET/CT imaging, resveratrol, and melatonin in lower extent, displayed therapeutic effects when they were administered intrarectally to animals with the disease. The administration of the compounds included in a liquid enema showed improved retention time and biodistribution compared to their administration in a gel-based vehicle.

3rd - Semisolid extrusion 3D printing enabled the manufacture of human lipid-based suppositories with self-emulsifying properties in different sizes and containing the exact dose of tacrolimus. By the use of this technology, it was possible to print self-supporting suppositories in a single step process to suit the patient's comfort. The printed suppositories were well-defined and with an acceptable consistency for normal handling. The mixture formed by Gelucire 44/14 and coconut oil was uniform and suitable for printing, whereas the mixture formed by Gelucire 48/16 and coconut oil did not mix perfectly when melted, displaying worse properties for printing. Moreover, Gelucire 44/14 suppositories were found to have a faster disintegration time but slower rate of drug release than Gelucire 48/16 suppositories. Nevertheless, *in vitro* dissolution tests showed that both formulations released more than 80% of drug load within 120 min.

4th - The mixture of Gelucire 44/14 and coconut oil was selected for printing small rectal devices for the treatment of experimental IBD in the animal model of TNBS-induced colitis. Small batches of 3D printed suppositories with a size and dose adapted for administration to rats were successfully prepared. The therapeutic activity of the tacrolimus suppositories was

evaluated by [^{18}F]FDG PET/CT imaging and the analysis of PET images using the SUV$_{max}$ parameter confirmed the feasibility of treating experimental colitis with the tacrolimus-loaded suppositories.

Resumen

RESUMEN

La enfermedad inflamatoria intestinal es una afección inmunitaria crónica del intestino que alterna periodos de actividad o brotes con periodos de remisión o inactividad. La duración de los brotes y periodos de remisión es muy variable entre los pacientes, pudiendo presentar periodos de remisión de años o brotes de actividad de forma frecuente. Los dos tipos principales de enfermedad inflamatoria intestinal son la colitis ulcerosa y la enfermedad de Crohn. Debido al carácter crónico de estas patologías, a su tratamiento y los efectos adversos derivados de éste, estas enfermedades tienen un gran impacto en la calidad de vida y en la autoestima de los pacientes, causándoles en muchos casos un malestar psicológico general.

La frecuencia de aparición de la enfermedad inflamatoria intestinal varia con la zona geográfica, siendo mayor en Europa, Reino Unido y Norteamérica. En Europa, se estima que aproximadamente 1,1 millones de personas sufren de enfermedad de Crohn y 2,1 millones sufren de colitis ulcerosa. Además, las zonas urbanas tienen una prevalencia más elevada que las rurales. En una misma familia, si una persona padece de enfermedad inflamatoria intestinal, los familiares de primer grado tienen una probabilidad de padecerla a lo largo de sus vidas de casi un 10%. Los hijos de padres que padecen la enfermedad tienen un 36% de probabilidades de verse afectados. En el caso de la enfermedad de Crohn, el sitio anatómico y el tipo clínico concuerdan dentro de una misma familia.

Aunque la enfermedad inflamatoria intestinal es de origen desconocido, la principal hipótesis postula que, en individuos con predisposición genética, factores exógenos como la microflora luminal normal junto con otros factores relacionados con el hospedador, como puede ser la función inmune innata y adaptativa, producen un estado crónico de pérdida de la regulación inmunitaria. Esta pérdida de una respuesta inmune controlada se ve adicionalmente agravada por factores ambientales, como por ejemplo el tabaquismo. Por lo tanto, en la actualidad la enfermedad inflamatoria intestinal se considera una respuesta inmune local inapropiada frente a la microflora endógena intestinal, aunque los mecanismos implicados en esta pérdida de tolerancia todavía se desconocen.

A pesar de que la colitis ulcerosa y la enfermedad de Crohn comparten algunos de sus síntomas, como dolor abdominal, diarrea con o sin sangre y fiebre, son dos entidades completamente diferentes. La colitis ulcerosa afecta principalmente a la mucosa del recto, pudiendo extenderse en sentido proximal hasta abarcar todo o parte del colon. Histológicamente, la enfermedad se limita a la mucosa y la submucosa superficial, excepto en la enfermedad fulminante, en la cual las capas más profundas también se ven afectadas. Por su parte, la enfermedad de Crohn puede afectar a cualquier parte del tubo digestivo desde la boca hasta el ano. El recto, casi siempre afectado en la colitis ulcerosa, a menudo se encuentra

indemne en la enfermedad de Crohn. A diferencia de la colitis ulcerosa, la enfermedad de Crohn es un proceso transmural, pudiendo verse afectadas capas más profundas de la pared intestinal.

El tratamiento de la enfermedad inflamatoria intestinal dependerá de su gravedad y extensión. En la terapia convencional de la colitis de leve a moderada producida tanto por enfermedad de Crohn como por colitis ulcerosa se emplean los fármacos 5-ASA (ácido 5-aminosalicílico), como la mesalamina, que se administran tanto oral como rectalmente. En pacientes con enfermedad moderada a grave es común la administración de glucocorticoides por vía oral o parenteral, aunque estos fármacos no son eficaces en el tratamiento de sostén de ninguna de las dos enfermedades. En enfermedad dependiente o resistente a esteroides ha demostrado ser eficaz el tacrolimus, que es un antibiótico macrólido con actividad inmunosupresora. Otros agentes farmacológicos utilizados en la terapia de la enfermedad inflamatoria intestinal son la azatioprina, la 6-mercaptopurina y el metotrexato. Más recientemente, se han desarrollado nuevos tratamientos como son las terapias biológicas, que consisten en el uso de anticuerpos monoclonales como por ejemplo el infliximab, el tocilizumab y el ustekinumab.

Sin embargo, estos tratamientos convencionales son poco específicos, no siempre son efectivos y muy frecuentemente, están acompañados de serios efectos adversos, por lo que resultaría interesante encontrar alternativas y tratamientos más tolerables. Una alternativa es el empleo de moléculas naturales que permitan mejorar la sintomatología asociada a estas patologías. Diferentes trabajos en los que se realizan estudios *in vitro* e *in vivo* sugieren que los compuestos con propiedades antioxidantes y antiinflamatorias, como la melatonina (hormona endógena) y el resveratrol (polifenol de origen natural) podrían tener cierta efectividad en el tratamiento de patologías intestinales. En particular, se cree que una desregulación entre la producción de radicales libres y la de moléculas antioxidantes que neutralice un exceso de estas puede jugar un papel importante en la patogénesis de la enfermedad inflamatoria intestinal.

En etapas preclínicas de desarrollo de nuevos fármacos, es común el uso de animales de experimentación para estudiar la eficacia *in vivo* de nuevos compuestos. Actualmente, se encuentran descritos en la literatura científica numerosos modelos de enfermedad inflamatoria intestinal utilizando roedores, como por ejemplo los modificados genéticamente (ratones *knockout*) o los inducidos utilizando agentes químicos. Dentro de estos últimos, el modelo en rata de enfermedad inflamatoria intestinal obtenido mediante el empleo de un agente químico conocido como ácido 2,4,6-trinitrobenceno sulfónico (TNBS) disuelto en etanol y aplicado por vía rectal, ha demostrado ser un modelo de fácil inducción y gran reproducibilidad, el cual presenta un proceso inflamatorio de características histológicas muy similares a las de la enfermedad inflamatoria intestinal.

En las últimas décadas, las técnicas de imagen no invasivas habitualmente usadas en clínica para el diagnóstico y seguimiento de procesos inflamatorios e infecciosos, como la

Tomografía por Emisión de Positrones (PET), la Tomografía Computerizada (CT) y la Imagen por Resonancia Magnética (MRI), se han adaptado para su uso en el ámbito preclínico. Estas técnicas de imagen no invasivas permiten realizar la caracterización de los modelos animales, la evaluación de la actividad terapéutica de nuevos compuestos y el seguimiento de la enfermedad sin necesidad de sacrificar al animal, reduciendo en gran medida el número de animales necesarios en cada estudio. En particular, la combinación de una técnica de imagen molecular como el PET con una técnica de imagen anatómica como el CT, proporciona una localización anatómica adicional a la información fisiológica obtenida con el PET, lo que resulta de gran utilidad en estudios preclínicos ya que permite localizar la inflamación en el animal y evaluar su progresión o remisión después de ser administrado el tratamiento.

Por otra parte, la impresión 3D, una tecnología innovadora que ha revolucionado diversos sectores industriales, también ha demostrado su utilidad en la fabricación de medicamentos y dispositivos médicos. Diversos estudios han puesto de manifiesto la versatilidad de esta técnica para la fabricación de formas de dosificación con una dosis y unas características adaptadas a cada paciente, lo cual supone un gran avance hacia una medicina más personalizada en comparación con las técnicas convencionales de producción de medicamentos que se basan en la producción en masa de formas de dosificación con un rango limitado de dosis disponibles.

Una de las grandes limitaciones durante el desarrollo de un nuevo medicamento es la capacidad de solubilización del principio activo en el medio, un factor clave para su absorción y del cual depende en gran medida su biodisponibilidad. Entre los recursos tecnológicos disponibles para incrementar la solubilidad de fármacos poco solubles en medio acuoso, la utilización de sistemas autoemulsionables permite que una vez administrada la forma de dosificación vía oral, se formen emulsiones y microemulsiones solamente con la agitación proporcionada por los movimientos estomacales. De esta forma, el fármaco se encuentra solubilizado en la fase oleosa de la emulsión, lo que mejora su estabilidad en el medio acuoso intestinal e incrementa su absorción sistémica.

En este sentido, la administración oral de medicamentos, aun siendo la vía más recomendable y en general la que presenta una mayor aceptabilidad entre los pacientes, puede presentar algunas limitaciones. Como ya se ha mencionado, la biodisponibilidad de un fármaco se puede ver afectada cuando éste se administra por vía oral, la cual se puede ver aún más disminuida cuando el fármaco es susceptible de sufrir efecto de primer paso hepático. Además, las formas de dosificación se ven expuestas a cambios bruscos de pH así como a diferentes enzimas que pueden poner en riesgo su estabilidad. En el caso de formas de dosificación de liberación colónica, estas tienen que atravesar exitosamente todo el tracto gastrointestinal antes de llegar al colon y liberar allí el fármaco. Para ello se utilizan diversas estrategias como cubiertas entéricas que incluyen polisacáridos susceptibles de ser degradados por la microbiota colónica, pero dada la gran variabilidad interpersonal no en todos los pacientes resultan efectivas las mismas estrategias. Por este motivo, cuando las zonas

afectadas por la enfermedad inflamatoria intestinal se encuentran en zonas distales del colon o en el recto, la administración de los fármacos por vía rectal podría obtener mejores resultados terapéuticos.

La vía rectal permite la administración localizada del medicamento en la zona afectada, disminuyéndose así los efectos adversos derivados de una absorción sistémica. Además, el fármaco no se ve sometido a cambios de pH y se evita su degradación por parte de las enzimas intestinales. Por otra parte, si lo que se busca es un efecto sistémico, dependiendo de la zona en la que se administre el medicamento este no sufrirá efecto de primer paso, por lo que su biodisponibilidad apenas se verá afectada.

Con el fin último de evaluar alternativas terapéuticas para el tratamiento de la enfermedad inflamatoria intestinal, en el presente trabajo se validó un modelo animal de dicha enfermedad. Para ello, se utilizó un modelo de colitis experimental en ratas Sprague Dawley obtenido mediante la administración rectal del agente químico TNBS disuelto en etanol por vía rectal, causando una enfermedad aguda de características muy similares a la enfermedad inflamatoria intestinal humana. El seguimiento de la enfermedad se realizó utilizando la técnica de imagen PET/CT junto con el radiotrazador 18F-fluorodesoxiglucosa ($[^{18}F]FDG$) durante 15 días. La inflamación producida por la colitis causa un incremento del metabolismo celular que se traduce en una mayor captación del radiotrazador en las regiones inflamadas. Para cuantificar la captación de $[^{18}F]FDG$ se utilizó el parámetro SUV_{max} (valor estandarizado de captación máximo).

En primer lugar, se realizó un seguimiento a un primer grupo de animales con colitis experimental los cuales no recibieron ningún tratamiento. La progresión de la enfermedad en este grupo se comparó con otro grupo que fue tratado con un corticosteroide intraperitoneal (metilprednisolona) a partir del día 3 post inducción de la colitis. Los resultados obtenidos después de analizar las imágenes PET mostraron una mejoría significativa del grupo tratado con respecto al que no recibió ningún tratamiento. Estos hallazgos fueron confirmados mediante el análisis histológico de muestras de tejido colónico recogidas en diferentes días del estudio. La respuesta positiva de la enfermedad al tratamiento con metilprednisolona y el satisfactorio seguimiento de la misma mediante PET/CT validaron tanto el modelo animal como la técnica de imagen PET/CT para su uso posterior en la evaluación de la actividad terapéutica de nuevos compuestos.

En el segundo estudio, se evaluó el posible efecto beneficioso de la actividad antioxidante e antinflamatoria de la melatonina y el resveratrol en el tratamiento de la enfermedad. Para ello, se incluyeron los compuestos en un enema acuoso que se administró por vía rectal a los animales con colitis inducida por TNBS a partir del día 3 post inducción, y se realizó el seguimiento de la enfermedad mediante PET/CT como se describió anteriormente. El análisis de las imágenes PET mostraron una mejora significativa de la inflamación, siendo esta recuperación mayor en el grupo tratado con resveratrol. Estos resultados fueron confirmados mediante el análisis histológico de tejido colónico de los animales. Además, para tratar de

explicar el mejor resultado obtenido en el grupo que recibió resveratrol, se realizó una evaluación de la capacidad antioxidante de ambas moléculas, la cual confirmó el mayor poder antioxidante del resveratrol. En vista de los resultados obtenidos, se puede concluir que tanto la melatonina como el resveratrol poseen una actividad terapéutica beneficiosa en patologías intestinales que cursan con inflamación y en las cuales están implicados procesos oxidativos descontrolados, como es el caso de la enfermedad inflamatoria intestinal.

En la tercera parte de este trabajo, se exploró el potencial de la impresión 3D para la fabricación de supositorios lipídicos con el fármaco inmunosupresor tacrolimus destinados a su administración a pacientes con colitis ulcerosa. Dado que en la actualidad no está disponible ninguna forma comercial de supositorios con tacrolimus, estos son preparados en los servicios de farmacia hospitalaria. Este proceso suele ser lento, ya que se suelen utilizar moldes y se requieren periodos de tiempo para dejar que los supositorios se endurezcan, además de que se podrían producir errores en el pesado del fármaco que podrían derivar en severos efectos adversos en los pacientes.

Mediante el uso de una impresora 3D de semisólidos, los supositorios se pudieron imprimir en un solo paso sin necesidad de un molde o soporte, ya que las capas se solidificaban conforme eran depositadas una encima de otra hasta formar el supositorio. Los excipientes lipídicos seleccionados (Gelucire 44/14 y Gelucire 48/16) son capaces de autoemulsionarse en contacto con un medio acuoso. Dado el carácter hidrofóbico del tacrolimus, la utilización de estos sistemas autoemulsionables representa una estrategia efectiva para la solubilización del fármaco, ya que este se encontraría disuelto en la fase lipídica de la emulsión. Además, se empleó aceite de coco como agente plastificante para obtener una formulación final de características adecuadas para su impresión. Finalmente, se seleccionó la mezcla con Gelucire 44/14 como la más adecuada para la preparación de los supositorios y para su uso en posteriores estudios.

En la cuarta y última parte de este trabajo, la impresión 3D se combinó con la imagen médica por PET/CT para preparar supositorios de tacrolimus de pequeño tamaño y evaluar su potencial como forma de dosificación para el tratamiento de la colitis experimental en el modelo animal en rata anteriormente descrito. Es este estudio, se empleó la técnica de impresión 3D de semisólidos para preparar pequeños lotes de supositorios adaptados en tamaño y dosis para su administración rectal en ratas. Estos supositorios fueron administrados diariamente a los animales a partir del día 3 post inducción de la colitis. La mezcla de excipientes lipídicos utilizada fue extraída del estudio previo, siendo esta la que incluía Gelucire 44/14 en su formulación. El análisis de las imágenes PET mostraron una clara mejoría de los animales tratados con los supositorios de tacrolimus respecto al grupo que no recibió tratamiento, hallazgos que fueron además confirmados mediante el análisis histológico de muestras de tejido colónico de los animales. En vista de los resultados obtenidos, se pudo concluir que la impresión 3D resultó ser una estrategia útil para la preparación de formulaciones en el ámbito preclínico. Esta técnica permitió la preparación de supositorios con el tamaño deseado de forma rápida y efectiva y con la dosis de fármaco exacta sin

necesidad de emplear moldes con un tamaño definido. Por otra parte, la mezcla de excipientes seleccionada liberó el fármaco *in vivo* de manera efectiva, lo cual se demuestra por la remisión de la enfermedad observada mediante el análisis de las imágenes PET.

A modo de conclusión general, se puede concluir que tanto la impresión 3D de medicamentos como la imagen médica por PET/CT son dos herramientas útiles para la preparación y evaluación de nuevas terapias tanto en el ámbito clínico como preclínico. Por su parte, los sistemas autoemulsionantes han probado su utilidad para la solubilización de fármacos poco solubles en medio acuoso y su posterior liberación en el lugar de acción del medicamento. Finalmente, los dos compuestos antioxidantes evaluados en este trabajo, la melatonina y el resveratrol, han demostrado ser beneficiosos en la terapia de la enfermedad inflamatoria intestinal, en la cual es muy probable que un desequilibrio en la producción de radicales libres juegue un papel importante en su patogénesis.

Publications

LIST OF PUBLICATIONS

Introduction

Seoane-Viaño, I., Gómez-Lado, N., Otero-Espinar, F.J., Fernández-Ferreiro, A., Aguiar, P., Luzardo-Álvarez, A., & Ruibal Morell, Á. (2019). "Preclinical Models of Inflammatory Bowel Disease and Colonic Treatments." In Roy et al. (Ed.), Inflammatory Bowel Disease, (Volume 2, Chaper 1). Open Access eBooks. Available in: http://openaccessebooks.com/inflammatory-bowel-disease-volume-2.html

Seoane-Viaño, I., Otero-Espinar, F.J. & Goyanes, Á. (2020). "3D printing of Pharmaceutical Products." In Riveiro Rodriguez et al. (Ed.), Handbook in Additive Manufacturing and Surface Treatment, (Chapter 24). Elsevier. (*In Press*).

Chapter I

Seoane-Viano, I., Gomez-Lado, N., Lazare-Iglesias, H., Barreiro-de Acosta, M., Silva-Rodriguez, J., Luzardo-Alvarez, A., Herranz, M., Otero-Espinar, F.J., Antunez-Lopez, J.R., Lamas, M.J., Aguiar, P., Fernandez-Ferreiro, A. & Ruibal A. (2018). "Longitudinal PET/CT evaluation of TNBS-induced inflammatory bowel disease rat model." International Journal of Pharmaceutics, 549, 335-342.

Chapter II

Seoane-Viaño, I., Gómez-Lado, N., Lázare-Iglesias, H., Rey-Bretal, D., Lamela-Gómez, I., Otero-Espinar, F.J., Blanco-Méndez, J., Ramón Antúnez-López, J.R., Pombo-Pasín, M., Aguiar, P., Ruibal, Á., Luzardo-Álvarez A. & Fernández-Ferreiro, A. (2019). "Evaluation of the therapeutic activity of Melatonin and Resveratrol in Inflammatory Bowel Disease: a longitudinal PET/CT study in an animal model." International Journal of Pharmaceutics, 118713.

Chaper III

Seoane-Viaño, I., Ong, J.J., Luzardo-Álvarez, A., González-Barcia, M., Basit, A.W., Otero-Espinar, F.J. & Goyanes, Á. (2020). "3D printed tacrolimus suppositories for the treatment of ulcerative colitis." Asian Journal of Pharmaceutical Sciences, (*Under review*).